nagra.

Arbeitsbericht NAB 22-02

TBO Stadel-2-1: Data Report

Dossier VIII
Rock Properties, Porewater Characterisation and Natural Tracer Profiles

September 2022

C. Zwahlen, L. Aschwanden, E. Gaucher, T. Gimmi, A. Jenni, M. Kiczka, U. Mäder, M. Mazurek, D. Ross, D. Rufer, H.N. Waber, P. Wersin & D. Traber

National Cooperative for the Disposal of Radioactive Waste

Hardstrasse 73
P.O. Box
5430 Wettingen
Switzerland
Tel. +41 56 437 11 11

nagra.ch

nagra.

Arbeitsbericht NAB 22-02

TBO Stadel-2-1: Data Report

Dossier VIII Rock Properties, Porewater Characterisation and Natural Tracer Profiles

September 2022

C. Zwahlen[1], L. Aschwanden[1], E. Gaucher[1], T. Gimmi[1], A. Jenni[1], M. Kiczka[1], U. Mäder[1,2], M. Mazurek[1], D. Ross[1], D. Rufer[1], H.N. Waber[1], P. Wersin[1] & D. Traber[3]

[1] Rock-Water Interaction, University of Bern

[2] Rock-Water Consulting, Boll

[3] Nagra

Keywords:
STA2-1, Nördlich Lägern, TBO, deep drilling campaign, rock properties, petrophysical parameters, water content, porosity, mineralogy, clay mineral content, clay mineral composition, sulphate minerals, porewater chemistry, natural tracer profiles

National Cooperative for the Disposal of Radioactive Waste

Hardstrasse 73
P.O. Box
5430 Wettingen
Switzerland
Tel. +41 56 437 11 11

nagra.ch

Nagra Arbeitsberichte ("Working Reports") present the results of work in progress that have not necessarily been subject to a comprehensive review. They are intended to provide rapid dissemination of current information.

This NAB aims at reporting drilling results at an early stage. Additional borehole-specific data will be published elsewhere.

In the event of inconsistencies between dossiers of this NAB, the dossier addressing the specific topic takes priority. In the event of discrepancies between Nagra reports, the chronologically later report is generally considered to be correct. Data sets and interpretations laid out in this NAB may be revised in subsequent reports. The reasoning leading to these revisions will be detailed there.

This report was finalised in June 2023.

This Dossier was prepared by the Rock-Water Interaction Group of the University of Bern (authors are listed in the individual chapters). D. Traber was the responsible Nagra project manager.

The authors warmly acknowledge the laboratory work of:
P. Bähler and C. Pichler efficiently produced a substantial part of the data presented in this report.
U. Eggenberger, J. Krbanjevic, M. Wolffers, W. Zucha, A. Zappatini and F. Gfeller provided data for mineralogical and BET analyses as well as evaluation tools.
J. Richards and L. de Doliwa Zielinski performed the core sampling and cores processing.
Th. Siegenthaler expertly machined core samples for advective displacement experiments.
T. Oyama (CRIEPI, Japan) kindly collaborated in the context of porewater squeezing.
N. Schwendener from IRM University of Berne provided X-ray CT scans of a substantial number of core samples.

We are also grateful for the excellent work of the drill-site team who successfully provided sealed core samples according to our specifications.

We thank P. Blaser and M. Unger for editorial work.

Text, clarity and discussions were improved by a thorough review by A. Gautschi.

Table of Contents

List of Tables

List of Figures

Electronic Appendices

App. A Comprehensive data base with results of laboratory analyses (xls format)

App. B Detailed documentation of advective displacement experiments (xls format)

App. C HI report

Note: Appendices are available upon request.

1 Introduction

1.1 Context

To provide input for site selection and the safety case for deep geological repositories for radioactive waste, Nagra has drilled a series of deep boreholes ("Tiefbohrungen", TBO) in Northern Switzerland. The aim of the drilling campaign is to characterise the deep underground of the three remaining siting regions located at the edge of the Northern Alpine Molasse Basin (Fig. 1-1).

In this report, we present the results from the Stadel-2-1 borehole.

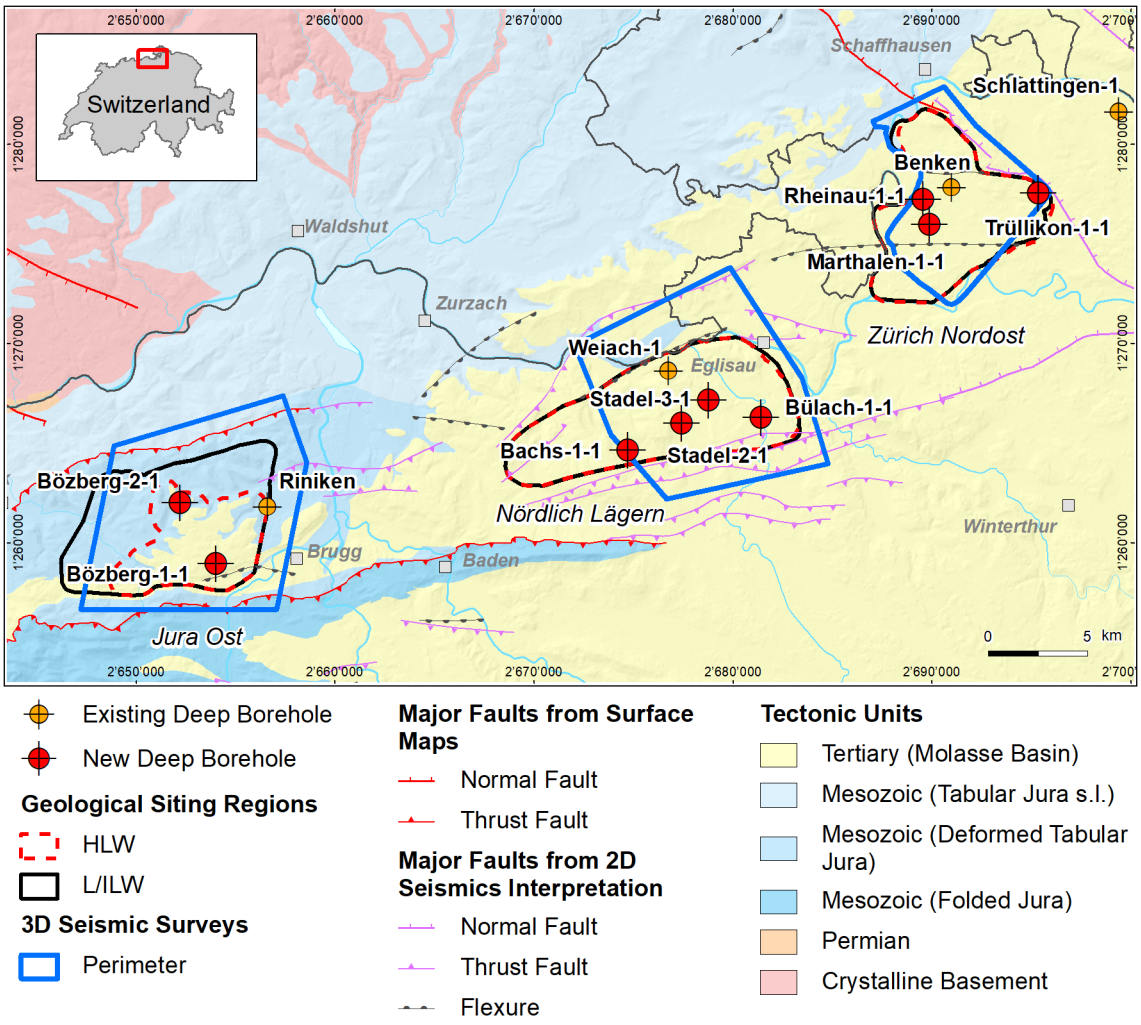

Fig. 1-1: Tectonic overview map with the three siting regions under investigation

1.2 Location and specifications of the borehole

The Stadel-2-1 (STA2-1) exploratory borehole is the seventh borehole drilled within the framework of the TBO project. The drill site is located in the central part of the Nördlich Lägern siting region (Fig. 1-2). The vertical borehole reached a final depth of 1'288.12 m (MD)[1]. The borehole specifications are provided in Tab. 1-1.

Tab. 1-1: General information about the STA2-1 borehole

Siting region	Nördlich Lägern
Municipality	Stadel (Canton Zürich / ZH), Switzerland
Drill site	Stadel-2 (STA2)
Borehole	Stadel-2-1 (STA2-1)
Coordinates	LV95: 2'677'447.617 / 1'265'987.019
Elevation	Ground level = top of rig cellar: 417.977 m above sea level (asl)
Borehole depth	1'288.12 m measured depth (MD) below ground level (bgl)
Drilling period	25th January – 8th July 2021 (spud date to end of rig release)
Drilling company	Daldrup & Söhne AG
Drilling rig	Wirth B 152t
Drilling fluid	Water-based mud with various amounts of different components such as[2]: 0 – 670 m: Bentonite & polymers 670 – 1'051 m: Potassium silicate & polymers 1'051 – 1'117 m: Water & polymers 1'117 – 1'288.12 m: Sodium chloride brine & polymers

The lithostratigraphic profile and the casing scheme are shown in Fig. 1-3. The comparison of the core versus log depth[3] of the main lithostratigraphic boundaries in the STA2-1 borehole is shown in Tab. 1-2.

[1] Measured depth (MD) refers to the position along the borehole trajectory, starting at ground level, which for this borehole is the top of the rig cellar. For a perfectly vertical borehole, MD below ground level (bgl) and true vertical depth (TVD) are the same. In all Dossiers depth refers to MD unless stated otherwise.

[2] For detailed information see Dossier I.

[3] Core depth refers to the depth marked on the drill cores. Log depth results from the depth observed during geophysical wireline logging. Note that the petrophysical logs have not been shifted to core depth, hence log depth differs from core depth.

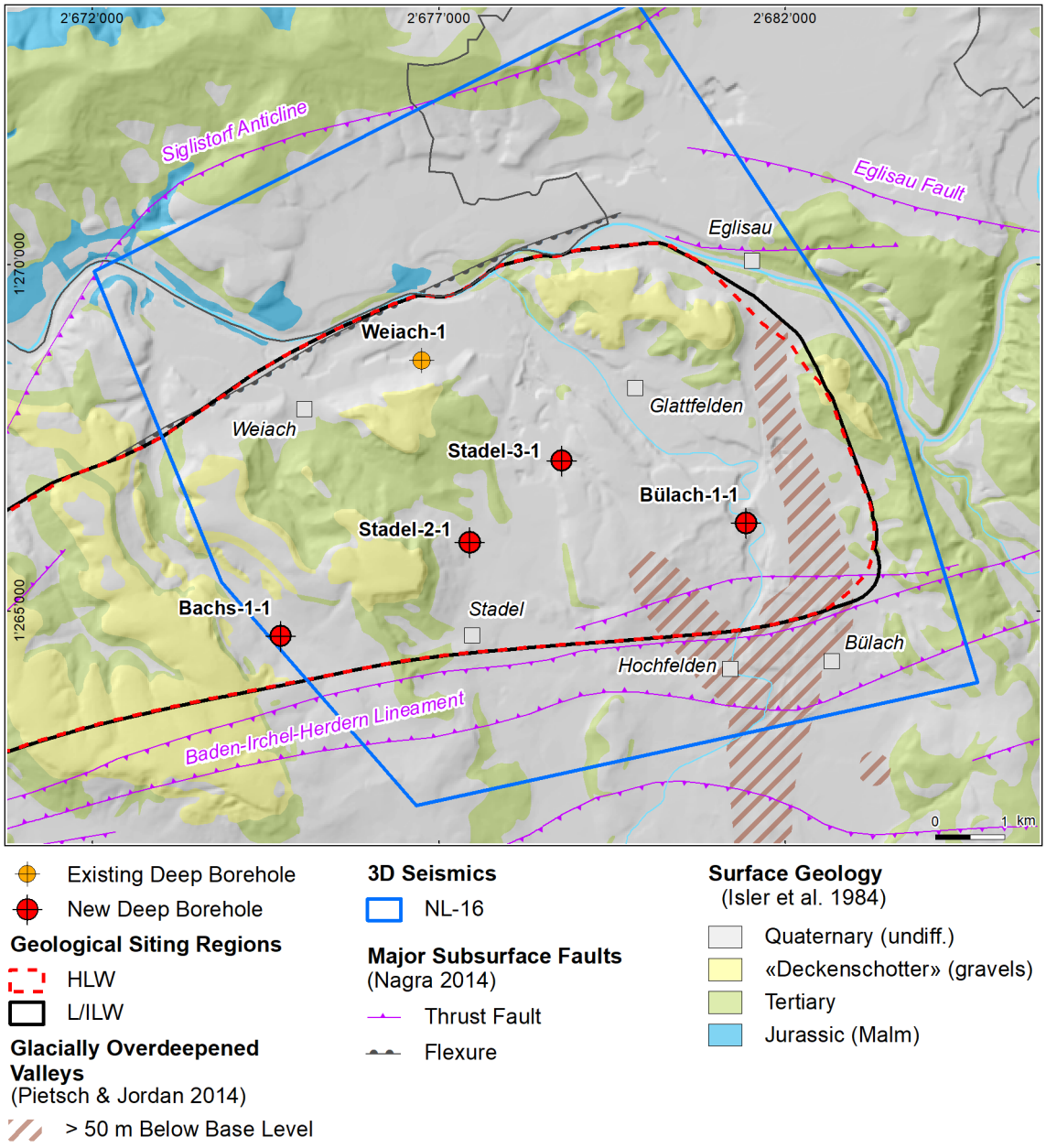

Fig. 1-2: Overview map of the investigation area in the Nördlich Lägern siting region with the location of the STA2-1 borehole in relation to the boreholes Weiach-1, BUL1-1, STA3-1 and BAC1-1

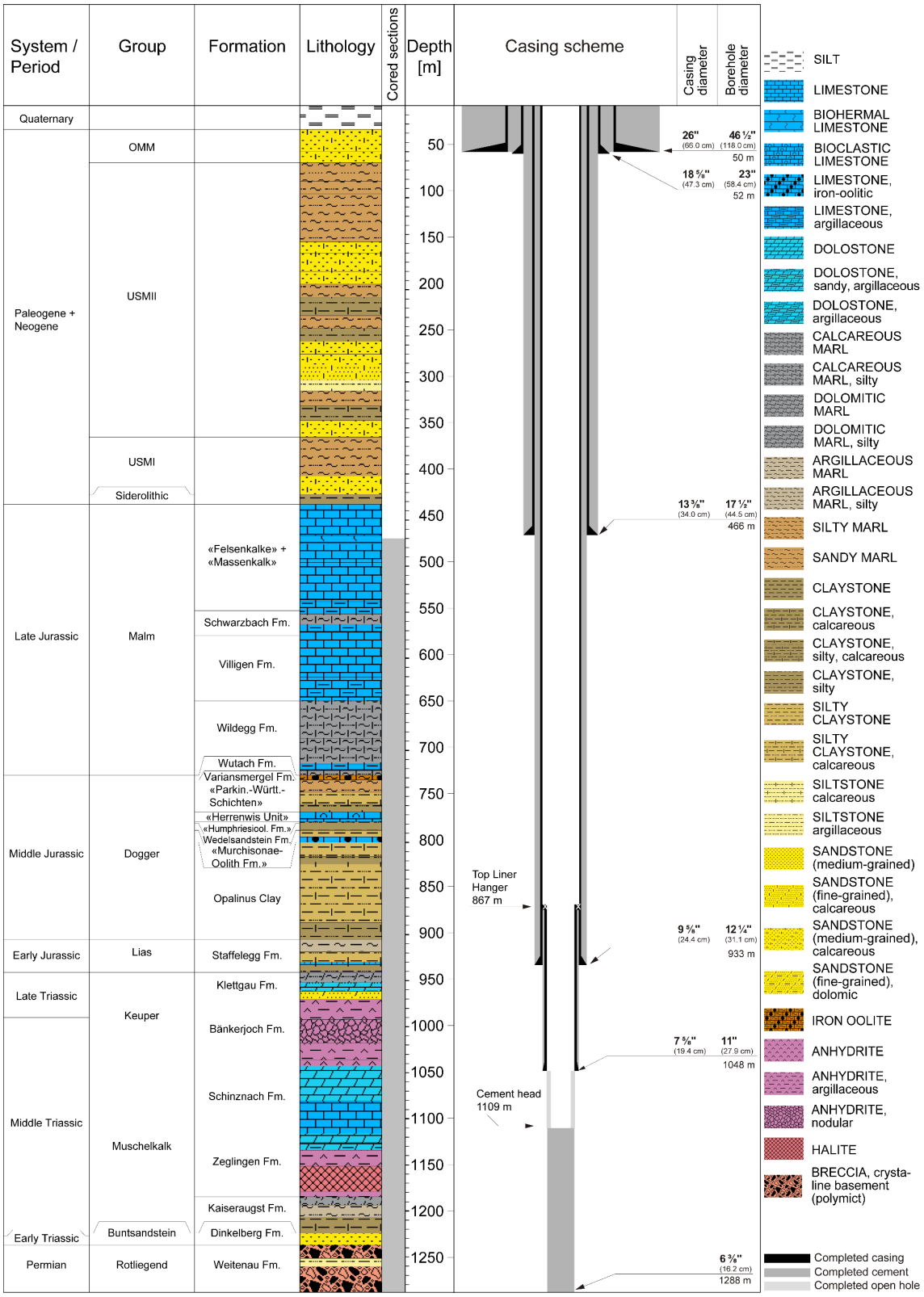

Fig. 1-3: Lithostratigraphic profile and casing scheme for the STA2-1 borehole[4]

[4] For detailed information see Dossier I and III.

Tab. 1-2: Core and log depth for the main lithostratigraphic boundaries in the STA2-1 borehole[5]

System / Period	Group	Formation		Core depth in m (MD)	Log depth in m (MD)	
Quaternary					**26.0**	—
Paleogene + Neogene	OMM				62.0	—
	USM				422.0	—
	Siderolithic				**433.0**	—
Jurassic	Malm	«Felsenkalke» + «Massenkalk»		548.35	548.62	—
		Schwarzbach Formation		575.08	575.45	—
		Villigen Formation		646.23	646.63	—
		Wildegg Formation		727.18	728.20	—
	Dogger	Wutach Formation		732.16	733.25	—
		Variansmergel Formation		734.92	735.95	—
		«Parkinsoni-Württembergica-Schichten»		767.02	768.05	—
		«Herrenwis Unit»		777.54	778.47	—
		«Humphriesioolith Formation»		779.34	780.27	—
		Wedelsandstein Formation		786.85	787.79	—
		«Murchisonae-Oolith Formation»		799.67	800.67	—
		Opalinus Clay		905.20	906.87	—
	Lias	Staffelegg Formation		**940.89**	**941.42**	—
Triassic	Keuper	Klettgau Formation		969.87	970.52	—
		Bänkerjoch Formation		1043.07	1043.62	—
	Muschelkalk	Schinznach Formation		1116.01	1116.69	—
		Zeglingen Formation		1184.72	1185.42	—
		Kaiseraugst Formation		1224.20	1225.07	—
	Buntsandstein	Dinkelberg Formation		**1237.01**	**1237.94**	—
Permian	Rotliegend	Weitenau Formation	final depth	1288.12	1288.87	

[5] For details regarding lithostratigraphic boundaries see Dossier III and IV; for details about depth shifts (core goniometry) see Dossier V.

1.3 Documentation structure for the STA2-1 borehole

NAB 22-02 documents the majority of the investigations carried out in the STA2-1 borehole, including laboratory investigations on core material. The NAB comprises a series of stand-alone dossiers addressing individual topics and a final dossier with a summary composite plot (Tab. 1-3).

This documentation aims at early publication of the data collected in the STA2-1 borehole. It includes most of the data available approximately one year after completion of the borehole. Some analyses are still ongoing (e.g. diffusion experiments, analysis of veins, hydrochemical interpretation of water samples) and results will be published in separate reports.

The current borehole report will provide an important basis for the integration of datasets from different boreholes. The integration and interpretation of the results in the wider geological context will be documented later in separate geoscientific reports.

Tab. 1-3: List of dossiers included in NAB 22-02
Black indicates the dossier at hand.

Dossier	Title	Authors
I	TBO Stadel-2-1: Drilling	P. Hinterholzer-Reisegger
II	TBO Stadel-2-1: Core Photography	D. Kaehr & M. Gysi
III	TBO Stadel-2-1: Lithostratigraphy	P. Jordan, P. Schürch, H. Naef, M. Schwarz, R. Felber, T. Ibele & H.P. Weber
IV	TBO Stadel-2-1: Microfacies, Bio- and Chemostratigraphic Analysis	S. Wohlwend, H.R. Bläsi, S. Feist-Burkhardt, B. Hostettler, U. Menkveld-Gfeller, V. Dietze & G. Deplazes
V	TBO Stadel-2-1: Structural Geology	A. Ebert, S. Cioldi, E. Hägerstedt & H.P. Weber
VI	TBO Stadel-2-1: Wireline Logging, Micro-hydraulic Fracturing and Pressure-meter Testing	J. Gonus, E. Bailey, J. Desroches & R. Garrard
VII	TBO Stadel-2-1: Hydraulic Packer Testing	R. Schwarz, R. Beauheim, S.M.L. Hardie & A. Pechstein
VIII	TBO Stadel-2-1: Rock Properties, Porewater Characterisation and Natural Tracer Profiles	C. Zwahlen, L. Aschwanden, E. Gaucher, T. Gimmi, A. Jenni, M. Kiczka, U. Mäder, M. Mazurek, D. Roos, D. Rufer, H.N. Waber, P. Wersin & D. Traber
IX	TBO Stadel-2-1: Rock-mechanical and Geomechanical Laboratory Testing	E. Crisci, L. Laloui & S. Giger
X	TBO Stadel-2-1: Petrophysical Log Analysis	S. Marnat & J.K. Becker
	TBO Stadel-2-1: Summary Plot	Nagra

1.4 Scope and objectives of this dossier

The dossier at hand summarises the laboratory work of the Rock-Water Interaction Group (RWI) of the University of Bern, Institute of Geological Sciences, dedicated to rock and porewater characterisation of core materials obtained from the STA2-1 borehole. The level of ambition is to document observations and measurements and to provide a quality-assured dataset. Closely related data obtained by other laboratories (e.g. CEC data by PSI) are integrated into our data.

Data are evaluated and discussed to some degree, including consistency and plausibility checks. An in-depth discussion, sophisticated modelling efforts and regional comparisons with data from other sites are beyond the scope of this report. Additional data obtained by other groups (e.g. hydraulic tests, groundwater sampling, geophysical borehole and core logging, structural logging) are considered in several cases but not in a comprehensive way. An integrated interpretation of all available data is deferred to a later stage of the TBO programme, when results from several boreholes can be synthesised for a siting region.

Throughout this report, rock samples used for analysis are identified by their mid-sample depth in m.

Note that «Brauner Dogger» is used for the Dogger units overlying the Opalinus Clay. In the Sectoral Plan Stages 1 and 2, «Brauner Dogger» is referred to the clay-rich rock sequence east of the lower Aare valley only (Nagra 2008).

2 Geoscientific data of interest and drilling conditions

Carmen Zwahlen, Martin Mazurek, Eric Gaucher

2.1 Geological information

The STA2-1 borehole is located in the eastern part of the siting region Nördlich Lägern south-west of the village of Glattfelden (Canton Zürich; Fig. 1-1). Nördlich Lägern lies in the Deformed Eastern Tabular Jura between the autochtonous Tabular Jura in the north and the Folded Jura in the SW. The siting area is delineated by some major tectonic structures, the Siglistorf Anticline and the Eglisau Fault in the north and the Baden – Irchel – Herdern Lineament and the Jura Main Thrust to the south. Tectonically, the Deformed Tabular Jura is compressively overprinted by the alpine forefront. This is for example manifested by the thrust of the Mesozoic sediments about 200 m to the north assumed to have occurred in the Triassic salt layers of the Zeglingen Formation (Nagra 2014).

According to seismic interpretations, no relevant faults were identified in the Mesozoic sediment stack at the borehole location. The regional dip of the bedding is subhorizontal towards SE.

2.2 Structural logging

The results of structural core logging are documented in Dossier V, where the following types of structural features are distinguished:

- Fault planes and fault zones (shear structures); mainly oriented bedding-subparallel and S-dipping (average at 163/05).
- Brittle extensional fractures (structures without shear or slip indication; e.g., joints, veins, tension gashes); these exhibit large variations in orientation and dip (2 – 90°), however, a poorly defined cluster showing mean orientations of 290/81 is identified.
- Stylolites; three classes with different orientation and dipping trend: 1) parallel or subparallel to bedding, SE- dipping (169/05) and 2&3) subvertical, NNE & SSW dipping (7/78 & 191/72).
- Larger open pores

The interpreted structures are unevenly distributed among the stratigraphic units. Highest frequencies of structures are observed in the carbonates of the Malm and the Schinznach Formation but also in the Bänkerjoch Formation. The Dogger and the Liassic show distinctly less structures, especially the Opalinus Clay shows only few. However, a prominent deformed interval (883.78 – 890.19 m log depth) was identified in the Opalinus Clay, characterised by disturbed bedding, numerous fault planes and tension gashes (Fig. 2-1). All fault planes are mineralised (i.e. closed) with synkinematic calcite and thicknesses of generally < 2 mm. Most fault planes dip towards the WNW and a few towards ESE with dip angles from 16° to 72°. A second deformation interval is documented in the Zeglingen Formation (1'152.02 – 1'179.58 m log depth). In this interval, several halite layers appear as fine-grained halite with elongated grains alternating with partly recrystallised layers with sigma-clasts. Anhydrite-rich layers with thin dolomitic intercalations occur between the salt intervals and are often characterised by boudin-like fabrics or by networks of tension gashes in an en-echelon arrangement.

A compilation of all fault zones, mirror-like fault planes and shear bands encountered at STA2-1 is provided in Tab. 2-1.

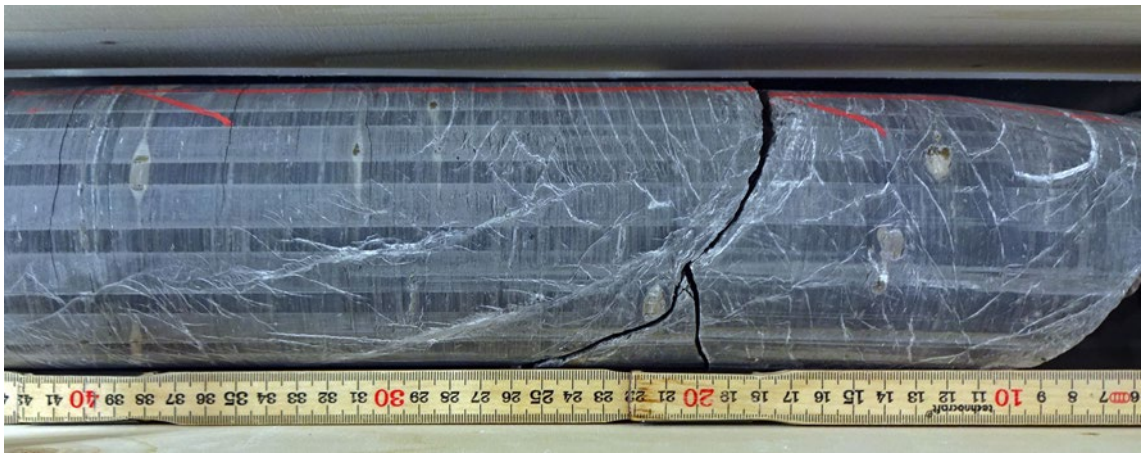

Fig. 2-1: Fault planes and tension gashes in the interval from 885.93 m to 886.33 m MD (log depth)

Tab. 2-1: List of interpreted fault zones, mirror-like fault planes (MirFP) and shear bands (SB) From Dossier V.

Top [m MD log depth]	**Bottom** [m MD log depth]	**Thickness** [m]	**Formation**	**Type**
504.98	505.14	0.16	«Felsenkalke» + «Massenkalk»	MirFP zone
516.06	516.24	0.18	«Felsenkalke» + «Massenkalk»	Fault zone
517.17	517.25	0.08	«Felsenkalke» + «Massenkalk»	MirFP zone
535.46	535.71	0.25	«Felsenkalke» + «Massenkalk»	Fault zone
538.14	542.21	4.07	«Felsenkalke» + «Massenkalk»	FP zone
692.90	693.09	0.19	Wildegg Fm.	FP zone
885.80	886.48	0.68	Opalinus Clay	Fault zone
941.94	942.37	0.43	Klettgau Fm.	MirFP zone
958.60	958.70	0.10	Klettgau Fm.	MirFP zone
958.88	959.10	0.22	Klettgau Fm.	MirFP zone
962.13	962.55	0.42	Klettgau Fm.	MirFP zone
971.18	971.38	0.20	Bänkerjoch Fm.	MirFP zone
999.83	1'000.34	0.51	Bänkerjoch Fm.	MirFP zone
1'008.07	1'008.26	0.19	Bänkerjoch Fm.	MirFP zone
1'014.11	1'014.14	0.03	Bänkerjoch Fm.	Fault zone
1'154.06	1'154.26	0.20	Zeglingen Fm.	Salt SB zone
1'154.51	1'154.90	0.39	Zeglingen Fm.	Salt SB zone
1'157.13	1'159.27	2.14	Zeglingen Fm.	Salt SB zone
1'162.52	1'166.70	4.20	Zeglingen Fm.	Salt SB zone
1'166.70	1'168.69	1.99	Zeglingen Fm.	Salt SB zone
1'168.73	1'170.07	0,62	Zeglingen Fm.	Salt SB zone
1'173.83	1'174.68	0.87	Zeglingen Fm.	Salt SB zone
1'219.07	1'219.09	0.02	Kaiseraugst Fm.	MirFP zone
1'220.55	1'220.63	0.08	Kaiseraugst Fm.	MirFP zone
1'255.41	1'255.48	0.07	Weitenau Fm.	MirFP zone

2.3 Hydrogeological conditions

Thirteen hydraulic packer tests were conducted in the STA2-1 borehole (Dossier VII), and selected results for the more permeable Malm, Keuper and Muschelkalk aquifer sections are summarised in Tab. 2-2. Hydraulic conductivities for the clay-rich section «Brauner Dogger» to Staffelegg Formation range from 3×10^{-15} to 3×10^{-11} m/s (best estimates).

Tab. 2-2: Selected results from hydraulic packer tests for the more permeable sections of the STA2-1 borehole

The best estimates for transmissivity T, hydraulic conductivity K and hydraulic head are indicated. Data are from Dossier VII.

Top [m MD]	**Bottom** [m MD]	**Length** [m]	**Geological units**	**T** [m^2/s]	**K** [m/s]	**Head** [m asl]
473.50	542.67	69.17	«Felsenkalke» + «Massenkalk» (Malm aquifer)	2×10^{-07}	3×10^{-09}	368
951.00	973.00	22.00	Klettgau Fm. (Keuper aquifer)	1×10^{-06}	6×10^{-8}	345
1'058.80	1'117.00	58.20	Schinznach Fm. (Muschelkalk aquifer)	2×10^{-06}	3×10^{-08}	354

2.4 Groundwater samples

Groundwater samples with variable degrees of drilling-fluid contamination were obtained from the Malm, Keuper and Muschelkalk aquifers. For the present report, values for the chemically conservative parameters Cl and Br and the water-isotope ratios $\delta^{18}O$ and $\delta^{2}H$ are of major interest, as these serve as boundary conditions for the porewater data. These values are not corrected for (minor) drilling-fluid contamination, and the raw data are presented in Tab. 2-3 along with the information on the chemical water type and mineralisation of the groundwaters.

Tab. 2-3: Conservative parameters for groundwater from the Malm and Muschelkalk aquifer in borehole STA2-1 not corrected for drilling-fluid contamination

Parameter	**Unit**	**Malm aquifer**	**Keuper aquifer**	**Muschelkalk aquifer**
Chemical type		Na-Cl	Na-(Ca)-SO_4-Cl	Ca-Na-(Mg)-SO_4-(Cl)
Mineralisation (TDS)	[g/L]	11.5	15.1	3.6
Chloride (Cl^-)	[mg/L]	6'330	3'900	370
Bromide (Br^-)	[mg/L]	21.9	3.0	0.09
1'000*Br/Cl	[mol/mol]	1.54	0.34	0.11
$\delta^{18}O$ of water	[‰$_{VSMOW}$]	–1.79	–7.33	–11.66
$\delta^{2}H$ of water	[‰$_{VSMOW}$]	–52.1	–55.2	–83.7
Test interval	[m MD]	473.50 – 542.67	951.00 – 973.00	1'058.80 – 1'117.00

2.5 Drilling conditions and drilling muds

During drilling of STA2-1 four different drilling muds were used: bentonite-polymer, potassium-silicate-polymer, water-polymer and sodium-chloride-polymer (Dossier I). Key information is listed in Tab. 2-4. No major mud losses were observed during the drilling operations.

The composition of the K silicate polymer mud is listed in Tab. 2-5. Besides K silicate, the mud contains various conditioners (Flowzan, soda ash and others) for achieving the desired density and viscosity/rheology. The groundwater sample in the Malm was taken in the Bentonite plus polymer section, the sample in the Keuper in the K-Si plus polymer section and the Muschelkalk sample was taken in the water plus polymer section.

Tab. 2-4: Drilling muds
Based on Dossier I.

Depth interval [m]	**Geological unit**	**Drilling mud**	**Comments**
0 – 467	Quaternary – «Felsenkalke» + «Massenkalk»	Bentonite + polymer	Destructive drilling
467 – 670	«Felsenkalke» + «Massenkalk» – Wildegg Fm.	Bentonite + polymer	cored
670 – 936	Wildegg – Staffelegg Fm.	K-Si + polymer	cored
936 – 1'051	Staffelegg –Schinznach Fm.	K-Si + polymer	cored
1'051 – 1'117	Schinznach – Zeglingen Fm.	Water + polymer	cored
1'117 – 1'288	Zeglingen – Weitenau Fm.	NaCl + polymer	cored

Tab. 2-5: Composition of three drilling muds
From Lorenz et al. (2023).

Parameter	**Units**	**Bentonite mud**	**K silicate mud**	**NaCl mud**
Depth	[m]	473 – 660	943 – 973	1'058 – 1'115
pH		8	12.4	11
EC	[µS/cm]	7'883	73'888	16'055
uranine	[ppb]	1'052	1'265	Not measured
tritium	[TU]	5.9	12.0	5.2
Alk (pH 8.2)	[meq/l]	3	1'104	46
DOC	[mg/L]	4'195	Not measured	4'490
Na	[mg/L]	2'566	2'898	3'763
K	[mg/L]	64	56'638	1'601
NH_4	[mg/L]	< 1	< 1	< 1
Ca	[mg/L]	89	52	36
Mg	[mg/L]	21	2	2
Si	[mg/L]	20	28'288	406
Cl	[mg/L]	830	519	2'261
SO_4	[mg/L]	190	861	503
NO_3	[mg/L]	< 1	18	19
Br	[mg/L]	0.20	0.19	0.44
F	[mg/L]	1.4	0.7	7
Sr	[mg/L]	3.8	1.0	0.8
Ba	[mg/L]	0.33	0.11	0.51

The values are the mean of 8 analyses of samples taken in the suction pit and in the shaker for the mud monitoring. First sample 06/02/2021, last sample 14/02/2021 for the Bentonite drilling mud; First sample 13/05/2021, last sample 15/05/2021 for the K silicate drilling mud; First sample 11/06/2021, last sample 15/06/2021 for the NaCl drilling mud.

3 Sampling and applied methods

3.1 Sampling strategy

Carmen Zwahlen, Martin Mazurek

A suite of 6 different sample types were investigated (Tab. 3-1). Sample types and the general procedures of core sampling, sample conditioning and storage are described by Rufer & Stockhecke (2019).

Tab. 3-1: Sample types and sampling strategy
This table includes on-site conditioned samples relevant for the present report.

Sample type	**Main study targets**	**Sampling (by on-site team)**
RP (various rock properties), PW (porewater chemistry)	Characterisation of rock and porewater chemistry	Sample lithology representative of the current lithofacies and the sampled core section (usually 3 m). Sampling with a regular spacing in order to obtain a representative data set
SQ (squeezing)	Characterisation of porewater chemistry	Focussed on clay-rich lithologies due to methodological constraints
AD (advective displacement)	Characterisation of porewater chemistry	Focussed on clay-rich lithologies due to methodological constraints
DI (diffusion experiments)	Diffusion coefficients, cation exchange & sorption parameters at PSI	Coverage of a wide range of lithologies (in particular clay-mineral contents)
NG (noble gas analysis)	Concentrations and isotopic compositions of dissolved noble and reactive gases	Sampling with a regular spacing, with situational tightening of the sampling interval close to potentially water-conducting features
GM (geomechanics)	Mineralogy and grain density of samples studied for their geomechanical properties by other laboratories	Representative sampling of the most relevant lithologies within the Opalinus Clay

3.2 Laboratory programme

Carmen Zwahlen

A total of 147 core segments were prepared on-site and designated for our studies, including samples for geomechanical tests (4 GM samples) and diffusion experiments (18 DI samples) for which the main studies were performed by other laboratories (see Tab. 3-3) but some supporting measurements were performed in our laboratories (e.g. mineralogy, water content, density).

A substantial subset of theses 147 samples was analysed for geochemical and petrophysical characterisation (porewater: PW, RP), squeezing (SQ), advective displacement (AD) and diffusion (DI). These 143 samples were investigated in the RWI laboratories as part of the standard programme, and Tab. 3-2 provides an overview. In Tab. 3-3, the analytical programme for the various sample types is shown in more detail.

Tab. 3-2: Number of samples analysed for the different geological units

Unit	**PW (RWI)**	**RP (HI)**	**SQ**	**AD**	**DI**	**GM**	**Total**
Malm	24				4		28
«Brauner Dogger»	15	10	2	1	6		34
Opalinus Clay	17	19	1	2		1	40
Staffelegg Fm.	6	4	1	1	3		15
Klettgau Fm.	5				5	3	13
Bänkerjoch Fm.	6						6
Schinznach Fm.	7						7
All	**92**	**23**	**4**	**4**	**18**	**4**	**143**

Tab. 3-3: Analytical programme performed for the different sample types
×× = standard programme, × = selected samples only, calc. = calculated.

Method	**PW (RWI)**	**RP (HI)**	**SQ**	**AD**	**DI**	**GM**
Bulk mineralogical composition including CNS analysis	×		××	××	××	××
Clay mineralogy	×			××	×	
Bulk wet density	××			calc.	××	
Grain density	××			calc.	×	××
Water content	××	××	××	××	××	
BET surface area					×	
Cation-exchange properties (Ni-en method)	×*			×		
Aqueous extraction	××		××	××		
Pore-water squeezing			××			
Advective displacement of porewater				××		
Stable water isotopes	××	××	××	××		

* Subsamples collected during sample preparation, re-packed and sent to PSI for analysis

3.3 Analytical methods and methods of raw-data processing

Martin Mazurek

Experimental procedures, analytical methods and data processing, including error calculations, are documented in Waber (ed.) (2020) and are not repeated here. Any deviations or more details are given in the respective Chapter 4 sections.

3.4 Methods of raw-data processing

Thomas Gimmi & Martin Mazurek

Approaches and formalisms to evaluate and process measured data are also documented in Waber (ed.) (2020), including formalisms for the quantification of propagated errors. This information is not repeated here, but additional information is provided for situations where the current practice is not documented or deviates from that described in Waber (ed.) (2020).

Corrections for high salinities were not required for this dataset. Such corrections were developed for saline samples from the BUL1-1 dataset and are documented in Mazurek et al. (2021).

The evaluation of diffusive-exchange experiments for obtaining the ratios of stable isotopes of water was slightly adjusted compared to the documentation in Waber (ed.) (2020). This revised procedure is documented in Chapter 3 of the BUL1-1 data report by Mazurek et al. (2021).

4 Results

4.1 Documentation of measured and calculated data

Martin Mazurek & Carmen Zwahlen

Raw data collected in the framework of the analytical programme of STA2-1 are organised in a FileMaker data base, including raw-data files (e.g. XRD quantification not corrected for C/N/S analysis), graphics (e.g. XRD patterns) and photographs. The main purpose of this data base is to ensure the full documentation and traceability of original and derived data presented in this report. From this data base, the relevant data were exported into a comprehensive Excel sheet, which is attached as Appendix A (Excel file). The full dataset for advective displacement experiments are provided as Appendix B (Excel file).

The objective of the Excel summary sheet is not to fully document all analyses made but, per parameter and sample, to indicate the best or most representative value in case multiple measurements were made, and to list parameters calculated from the original measurements. For example, only one composition is given for squeezed and advectively displaced porewaters in a sample, even though multiple aliquots were collected and analysed. Explanatory notes for this sheet follow here.

Measurements on cation exchange capacity and selectivity were mostly performed by PSI. This data is partially integrated into Section 5.7, with reference to a stand-alone data report issued by PSI, and along with our own measurements on few selected samples. These data are also integrated in the Excel summary sheet in Appendix A.

Bulk mineralogy (X-ray diffraction and CNS analysis)

- Contents of minerals not detected by X-ray diffraction are set to 0, as the actual detection limits are difficult to quantify. 'tr' = present in trace amounts.
- Clay-mineral content is not measured directly but is calculated by difference to 100%.
- Pyrite content is calculated from the measured S content, assuming that pyrite is the main S reservoir in the rock. This is not the case in anhydrite-bearing rocks, which are typically free of pyrite. Here, the S is used to calculate the content of anhydrite.
- Column 'Füchtbauer name' refers to the nomenclature of clastic rocks as defined in Naef et al. (2019). Names are listed only for rock compositions that have < 10 wt.-% minerals not represented in the Füchtbauer triangle (i.e. minerals other than clays, calcite, dolomite/ ankerite, siderite, quartz, K-feldspar, plagioclase). In particular, this means that evaporitic rocks are not given a Füchtbauer name. If a rock contains ≥ 90 wt.-% minerals represented in the Füchtbauer triangle but also contains anhydrite, this is stated in brackets.

Clay mineral groups

- All data refer to wt.-% of the total rock.
- Illite/smectite ML (85-90) refers to a mixed-layer phase with 85 – 90% illite layers, Chl/Sm ML (85-95) designates a chlorite-smectite mixed-layer phase with 85 – 95% chlorite (analogous for the other listed mixed-layer phases).

End-member clays

- All data refer to wt.-% of the total rock.
- Illite, smectite and chlorite partially occur in mixed-layer phases. Here, the respective total contents of the end-members are calculated. For example, if a sample contains 10 wt.-% illite and 8 wt.-% illite/smectite mixed layers containing 75% illite, the end-member illite content would be 16 wt.-%.

Petrophysical parameters

- Bulk wet density was measured, and bulk dry density was calculated using equation 5-14 in Waber (ed.) (2020).
- Pycnometer porosity was calculated from densities using equation 5-16 in Waber (ed.) (2020).
- Water content (dry) was calculated from water content (wet) using $w_d = w_w/(1-w_w)$.
- Water-loss porosity was calculated using bulk wet density (equation 5-9 in Waber ed. 2020) or grain density (equation 5-7 in Waber ed. 2020).
- The formalisms to calculate water content from isotope diffusive-exchange experiments are detailed in Mazurek et al. (2021).

Chloride and bromide from aqueous extracts recalculated to porewater concentrations using water content

- Concentrations are given relative to bulk porewater as well as relative to various assumptions regarding anion accessibility in the pore space. The calculation is made using equation 6-1 in Waber (ed.) (2020). The variants pertaining to the dependence of anion accessibility on the clay-mineral content are discussed in Chapter 5.

Errors

- The error columns refer to analytical uncertainty or instrument precision for measured parameters and to propagated errors for calculated parameters, following the formalisms documented in Waber (ed.) (2020).

4.2 Mineralogical composition

Martin Mazurek

4.2.1 Whole rock data

A total of 89 mineralogical analyses by XRD and CNS were performed in the section Villigen Formation (Malm) – Schinznach Formation (Triassic), plus another 16 samples for which only CNS data were obtained (contents of S, C(org) and C(inorg)). The full dataset is documented in Appendix A, and Tab. 4.2-1 provides formation-specific summaries. Plots against depth for the most relevant minerals are shown in Fig. 4.2-1, and a representation in the Füchtbauer triangle is given in Fig. 4.2-3.

The Triassic section is lithologically heterogeneous, mainly due to the variable contents of dolomite, calcite and anhydrite. Particularly high contents of quartz are identified in the Frick Member of the Staffelegg Formation and in the Ergolz Member of the Klettgau Formation. In the latter, feldspar contents are also high. Systematic depth trends cannot be resolved. The overlying

Dogger – Lias section is discussed in detail further below. In the lower part of the Wildegg Formation, an upward trend of decreasing clay-mineral and increasing calcite contents is seen, which is similar to the trend in borehole BUL1-1 but opposite to STA3-1.

Infrequent occurrences of some phases, mostly in minor or trace amounts, have been identified:

- Abundant goethite (39 wt.-%) and minor maghemite (3 wt.-%) in an intensely brown sample from the Wutach Formation
- Minor amounts of goethite and traces of haematite in the Ergolz Member of the Klettgau Formation
- Traces of marcasite in the Rietheim Member of the Staffelegg Formation
- Traces of fluorite in a sample from the Leutschenberg/Kienberg Members of the Schinznach Formation

The depth profiles of the contents of S and N (based on CNS analysis) are shown in Fig. 4.2-2. Variable but often high S contents, mostly related to the presence of pyrite, are seen in the Dogger – Lias section. In the Triassic, high S contents are related to anhydrite. N contents above the quantification limit of 0.01 wt.-% are found almost exclusively in the Dogger and Lias. The highest N content is observed in the Staffelegg Formation, likely related to the presence of abundant organic matter in the Rietheim Member.

Tab. 4.2-1: Bulk-rock mineralogy: formation-specific means, medians, standard deviations and ranges [wt.-%]

For the calculation of statistical parameters, values below the limit of quantification were set to 0. The sample from the Wutach Formation contains 3 – 4 wt.-% maghemite, and two samples from the Rietheim Member of the Staffelegg Formation contain 1 wt.-% marcasite (not listed). Numbers of analyses are indicated below the formation name (analyses of S, N, C(inorg), C(org) / analyses of minerals).

Formation (number of analyses)	**Member**		**S** [wt.-%]	**N** [wt.-%]	**C(inorg)** [wt.-%]	**C(org)** [wt.-%]	**Quartz** [wt.-%]	**K-feldspar** [wt.-%]	**Plagioclase** [wt.-%]	**Calcite** [wt.-%]	**Dolomite / Ank.** [wt.-%]	**Siderite** [wt.-%]	**Anhydrite** [wt.-%]	**Goethite** [wt.-%]	**Haematite** [wt.-%]	**Pyrite** [wt.-%]	**Clay minerals** [wt.-%]
«Felsenkalke» + «Massenkalk» (7/0)		Mean	0.00	0.00	11.48	0.12											
		Median	0.00	0.00	11.78	0.11											
		Stdev	0.00	0.00	0.92	0.05											
		Min	0.00	0.00	9.41	0.06											
		Max	0.00	0.00	11.93	0.21											
Schwarzbach Fm. (2/0)		Mean	0.00	0.00	9.78	0.29											
		Median	0.00	0.00	9.78	0.29											
		Stdev	0.00	0.00	0.67	0.08											
		Min	0.00	0.00	9.30	0.24											
		Max	0.00	0.00	10.25	0.35											
Villigen Fm. (8/2)		Mean	0.04	0.00	11.17	0.24	2.5	0.9	0.0	84.2	0.5	0.0	0.0	0.0	0.0	0.2	11.4
		Median	0.00	0.00	11.45	0.21	2.5	0.9	0.0	84.2	0.5	0.0	0.0	0.0	0.0	0.2	11.4
		Stdev	0.08	0.00	0.64	0.11	0.8	1.3	0.0	2.2	0.7	0.0	0.0	0.0	0.0	0.3	1.2
		Min	0.00	0.00	9.91	0.16	1.9	0.0	0.0	82.6	0.0	0.0	0.0	0.0	0.0	0.0	10.5
		Max	0.22	0.00	11.61	0.45	3.0	1.8	0.0	85.8	1.0	0.0	0.0	0.0	0.0	0.4	12.2

Tab. 4.2-1: (continued)

Formation (number of analyses)	**Member**		**S** [wt.-%]	**N** [wt.-%]	**C(inorg)** [wt.-%]	**C(org)** [wt.-%]	**Quartz** [wt.-%]	**K-feldspar** [wt.-%]	**Plagioclase** [wt.-%]	**Calcite** [wt.-%]	**Dolomite / Ank.** [wt.-%]	**Siderite** [wt.-%]	**Anhydrite** [wt.-%]	**Goethite** [wt.-%]	**Haematite** [wt.-%]	**Pyrite** [wt.-%]	**Clay minerals** [wt.-%]
Wildegg Fm. (10/10)	Effingen Mb.	Mean	0.10	0.00	7.63	0.38	7.6	3.3	0.8	61.3	2.1	0.0	0.0	0.0	0.0	0.2	24.3
		Median	0.08	0.00	7.20	0.37	7.3	3.6	1.2	57.8	2.0	0.0	0.0	0.0	0.0	0.1	26.9
		Stdev	0.09	0.01	1.33	0.05	2.7	1.3	0.7	11.5	1.7	0.0	0.0	0.0	0.0	0.2	7.2
		Min	0.00	0.00	6.14	0.31	2.3	0.0	0.0	49.2	0.0	0.0	0.0	0.0	0.0	0.0	10.5
		Max	0.24	0.03	10.38	0.45	11.1	4.6	1.6	85.6	5.7	0.0	0.0	0.0	0.0	0.4	32.8
Wutach Fm. (1/1)		Mean	0.03	0.00	1.02	0.35	5.6	0.0	0.0	8.5	0.0	0.0	0.0	38.6	0.0	0.1	43.9
Variansmergel Fm. (2/2)		Mean	0.74	0.04	1.90	0.55	16.2	3.5	2.0	13.2	2.4	0.0	0.0	0.0	0.0	1.4	60.8
		Median	0.74	0.04	1.90	0.55	16.2	3.5	2.0	13.2	2.4	0.0	0.0	0.0	0.0	1.4	60.8
		Stdev	0.23	0.00	0.56	0.07	1.1	2.7	0.0	8.3	3.3	0.0	0.0	0.0	0.0	0.4	6.1
		Min	0.57	0.04	1.50	0.51	15.4	1.6	1.9	7.4	0.0	0.0	0.0	0.0	0.0	1.1	56.5
		Max	0.90	0.04	2.29	0.60	17.0	5.4	2.0	19.1	4.7	0.0	0.0	0.0	0.0	1.7	65.1
«Parkinsoni-Württembergica-Sch.» (9/9)		Mean	0.47	0.03	3.00	0.63	20.3	6.2	3.7	23.2	1.7	0.0	0.0	0.0	0.0	0.9	43.4
		Median	0.54	0.04	2.78	0.65	20.7	6.3	3.8	23.2	2.4	0.0	0.0	0.0	0.0	1.0	42.9
		Stdev	0.20	0.02	0.52	0.11	3.3	0.4	0.6	3.8	1.6	0.0	0.0	0.0	0.0	0.4	6.8
		Min	0.13	0.00	2.37	0.40	14.9	5.3	2.8	17.2	0.0	0.0	0.0	0.0	0.0	0.2	32.5
		Max	0.78	0.05	3.87	0.73	24.8	6.6	4.6	28.9	3.5	0.0	0.0	0.0	0.0	1.5	53.6
«Herrenwis Unit» (3/2)		Mean	0.29	0.01	6.50	0.47	20.1	5.0	2.2	36.4	0.0	0.0	0.0	0.0	0.0	0.8	35.0
		Median	0.16	0.00	5.99	0.47	20.1	5.0	2.2	36.4	0.0	0.0	0.0	0.0	0.0	0.8	35.0
		Stdev	0.32	0.02	4.03	0.29	4.9	0.5	0.3	19.1	0.0	0.0	0.0	0.0	0.0	0.7	12.5
		Min	0.05	0.00	2.75	0.18	16.6	4.6	2.0	22.9	0.0	0.0	0.0	0.0	0.0	0.3	26.1
		Max	0.66	0.04	10.77	0.75	23.5	5.3	2.4	49.9	0.0	0.0	0.0	0.0	0.0	1.2	43.9
«Humphriesi-oolith Fm.» (2/2)		Mean	0.47	0.04	2.38	0.73	18.6	4.8	2.7	19.0	0.7	0.0	0.0	0.0	0.0	0.9	52.6
		Median	0.47	0.04	2.38	0.73	18.6	4.8	2.7	19.0	0.7	0.0	0.0	0.0	0.0	0.9	52.6
		Stdev	0.14	0.00	0.15	0.08	0.1	0.3	0.1	2.4	1.0	0.0	0.0	0.0	0.0	0.3	2.0
		Min	0.37	0.04	2.27	0.67	18.5	4.6	2.6	17.3	0.0	0.0	0.0	0.0	0.0	0.7	51.2
		Max	0.57	0.05	2.49	0.78	18.6	5.0	2.8	20.7	1.5	0.0	0.0	0.0	0.0	1.1	54.0
Wedelsandstein Fm. (3/3)		Mean	0.31	0.04	1.15	0.70	22.9	5.7	3.0	9.6	0.0	0.0	0.0	0.0	0.0	0.6	57.6
		Median	0.28	0.05	1.19	0.73	21.5	5.7	3.0	9.9	0.0	0.0	0.0	0.0	0.0	0.5	59.5
		Stdev	0.07	0.03	0.10	0.16	3.7	0.3	0.3	0.9	0.0	0.0	0.0	0.0	0.0	0.1	4.1
		Min	0.26	0.00	1.03	0.53	20.1	5.4	2.7	8.6	0.0	0.0	0.0	0.0	0.0	0.5	52.9
		Max	0.39	0.05	1.22	0.85	27.1	5.9	3.3	10.2	0.0	0.0	0.0	0.0	0.0	0.7	60.4
«Murchisonae-Oolith Fm.» (3/3)		Mean	0.63	0.04	1.31	0.66	23.1	4.8	3.2	10.9	0.0	0.0	0.0	0.0	0.0	1.2	56.1
		Median	0.60	0.04	0.60	0.59	22.8	5.7	3.1	5.0	0.0	0.0	0.0	0.0	0.0	1.1	62.3
		Stdev	0.17	0.01	1.44	0.21	1.3	2.2	0.9	12.0	0.0	0.0	0.0	0.0	0.0	0.3	13.6
		Min	0.47	0.04	0.35	0.49	22.0	2.4	2.4	2.9	0.0	0.0	0.0	0.0	0.0	0.9	40.6
		Max	0.82	0.05	2.97	0.90	24.5	6.4	4.2	24.7	0.0	0.0	0.0	0.0	0.0	1.5	65.6

Tab. 4.2-1: (continued)

Formation (number of analyses)	**Member**		**S** [wt.-%]	**N** [wt.-%]	**C(inorg)** [wt.-%]	**C(org)** [wt.-%]	**Quartz** [wt.-%]	**K-feldspar** [wt.-%]	**Plagioclase** [wt.-%]	**Calcite** [wt.-%]	**Dolomite / Ank.** [wt.-%]	**Siderite** [wt.-%]	**Anhydrite** [wt.-%]	**Goethite** [wt.-%]	**Haematite** [wt.-%]	**Pyrite** [wt.-%]	**Clay minerals** [wt.-%]
Opalinus Clay (20/20)	All	Mean	0.44	0.06	1.48	0.91	21.6	4.8	3.0	9.3	0.0	3.5	0.0	0.0	0.0	0.8	56.0
		Median	0.35	0.06	1.31	0.91	20.6	5.2	3.1	7.2	0.0	3.1	0.0	0.0	0.0	0.6	58.4
		Stdev	0.35	0.02	0.86	0.15	5.6	1.0	0.6	7.5	0.0	1.8	0.0	0.0	0.0	0.7	9.8
		Min	0.04	0.00	0.90	0.54	12.4	1.8	2.0	4.6	0.0	0.0	0.0	0.0	0.0	0.1	26.3
		Max	1.49	0.08	5.03	1.17	39.2	5.7	3.8	40.2	0.0	7.8	0.0	0.0	0.0	2.8	69.4
Opalinus Clay (4/4)	Sub-unit with silty calc. beds	Mean	0.65	0.04	2.27	0.89	26.0	4.9	3.0	16.9	0.0	2.3	0.0	0.0	0.0	1.2	44.8
		Median	0.51	0.05	1.57	0.93	22.8	5.1	3.2	10.8	0.0	2.1	0.0	0.0	0.0	0.9	46.4
		Stdev	0.60	0.03	1.87	0.31	9.2	0.8	0.7	15.7	0.0	0.6	0.0	0.0	0.0	1.1	15.9
		Min	0.10	0.00	0.90	0.54	19.1	3.8	2.0	6.0	0.0	1.7	0.0	0.0	0.0	0.2	26.3
		Max	1.49	0.07	5.03	1.17	39.2	5.7	3.6	40.2	0.0	3.2	0.0	0.0	0.0	2.8	59.9
Opalinus Clay (3/3)	Upper silty sub-unit	Mean	0.57	0.05	1.44	0.89	26.3	5.1	3.4	9.6	0.0	2.8	0.0	0.0	0.0	1.1	50.8
		Median	0.77	0.05	1.46	0.86	25.6	5.1	3.4	9.5	0.0	2.8	0.0	0.0	0.0	1.4	50.0
		Stdev	0.42	0.00	0.17	0.06	2.9	0.1	0.2	1.4	0.0	0.2	0.0	0.0	0.0	0.8	3.0
		Min	0.09	0.05	1.27	0.85	23.8	5.0	3.3	8.2	0.0	2.7	0.0	0.0	0.0	0.2	48.3
		Max	0.86	0.05	1.61	0.95	29.4	5.2	3.6	11.0	0.0	3.0	0.0	0.0	0.0	1.6	54.1
Opalinus Clay (8/8)	Mixed clay-silt-carbonate sub-unit	Mean	0.20	0.07	1.28	0.90	21.1	4.9	3.2	6.3	0.0	5.1	0.0	0.0	0.0	0.4	58.2
		Median	0.21	0.07	1.31	0.91	20.9	5.2	3.1	6.2	0.0	4.9	0.0	0.0	0.0	0.4	58.4
		Stdev	0.08	0.00	0.18	0.06	1.0	1.0	0.4	1.2	0.0	1.4	0.0	0.0	0.0	0.2	2.2
		Min	0.04	0.06	0.93	0.81	19.5	2.6	2.7	4.6	0.0	3.1	0.0	0.0	0.0	0.1	54.3
		Max	0.30	0.07	1.53	1.00	22.7	5.6	3.8	8.5	0.0	7.8	0.0	0.0	0.0	0.6	61.5
Opalinus Clay (5/5)	Clay-rich sub-unit	Mean	0.55	0.07	1.20	0.97	16.2	4.5	2.4	8.0	0.0	2.3	0.0	0.0	0.0	1.0	64.5
		Median	0.50	0.06	1.19	1.04	17.1	5.2	2.4	7.1	0.0	2.8	0.0	0.0	0.0	0.9	62.9
		Stdev	0.20	0.01	0.18	0.14	2.1	1.5	0.5	1.8	0.0	1.5	0.0	0.0	0.0	0.4	3.3
		Min	0.39	0.06	0.95	0.80	12.4	1.8	2.0	6.6	0.0	0.0	0.0	0.0	0.0	0.7	61.2
		Max	0.91	0.08	1.43	1.10	17.7	5.3	3.2	10.8	0.0	3.8	0.0	0.0	0.0	1.7	69.4
Staffelegg Fm. (11/11)		Mean	0.72	0.05	3.12	2.05	23.5	4.3	2.9	24.9	1.0	0.0	0.0	0.0	0.0	1.2	40.0
		Median	0.52	0.04	1.27	0.75	20.7	5.1	3.1	9.6	0.0	0.0	0.0	0.0	0.0	1.0	40.0
		Stdev	0.67	0.06	3.13	2.06	15.8	2.1	1.1	26.8	1.3	0.0	0.0	0.0	0.0	0.9	12.7
		Min	0.10	0.00	0.81	0.26	1.5	0.0	0.0	5.0	0.0	0.0	0.0	0.0	0.0	0.2	7.5
		Max	2.04	0.17	10.86	5.37	43.7	6.1	4.1	90.5	3.5	0.0	0.0	0.0	0.0	2.6	59.5
Klettgau Fm. (11/11)		Mean	0.55	0.00	4.43	0.07	25.4	7.0	5.9	3.0	31.1	0.0	2.3	0.6	0.2	0.6	23.8
		Median	0.05	0.00	6.80	0.09	23.4	6.1	4.3	0.0	47.4	0.0	0.0	0.0	0.0	0.1	26.0
		Stdev	0.67	0.00	4.41	0.04	14.5	3.5	5.0	3.8	31.8	0.0	2.9	0.8	0.5	1.1	12.1
		Min	0.00	0.00	0.00	0.00	3.0	1.4	0.0	0.0	0.0	0.0	0.0	0.0	0.0	0.0	0.4
		Max	1.80	0.00	11.65	0.12	43.3	13.9	13.0	10.3	88.5	0.0	7.6	1.9	1.3	3.4	45.5

Tab. 4.2-1: (continued)

Formation (number of analyses)	**Member**		**S** [wt.-%]	**N** [wt.-%]	**C(inorg)** [wt.-%]	**C(org)** [wt.-%]	**Quartz** [wt.-%]	**K-feldspar** [wt.-%]	**Plagioclase** [wt.-%]	**Calcite** [wt.-%]	**Dolomite / Ank.** [wt.-%]	**Siderite** [wt.-%]	**Anhydrite** [wt.-%]	**Goethite** [wt.-%]	**Haematite** [wt.-%]	**Pyrite** [wt.-%]	**Clay minerals** [wt.-%]
Bänker-joch Fm. (6/6)		Mean	11.83	0.01	2.00	0.17	3.4	2.3	0.8	3.9	11.8	0.0	50.2	0.0	0.0	0.0	27.5
		Median	16.50	0.00	0.76	0.13	1.6	0.9	0.0	0.0	5.4	0.0	70.1	0.0	0.0	0.0	25.4
		Stdev	9.26	0.02	2.26	0.13	4.3	3.0	1.2	8.0	16.7	0.0	39.3	0.0	0.0	0.0	16.6
		Min	0.00	0.00	0.47	0.07	0.0	0.0	0.0	0.0	1.6	0.0	0.0	0.0	0.0	0.0	9.9
		Max	20.00	0.04	5.92	0.42	11.0	7.2	2.3	19.9	45.5	0.0	84.9	0.0	0.0	0.0	54.9
Schinz-nach Fm. (7/7)	All	Mean	0.09	0.00	10.88	0.71	1.5	1.8	0.0	16.2	68.6	0.0	0.4	0.0	0.0	0.0	10.8
		Median	0.00	0.00	10.81	0.42	1.5	1.6	0.0	0.0	72.2	0.0	0.0	0.0	0.0	0.0	12.2
		Stdev	0.24	0.00	1.15	0.73	1.3	1.6	0.0	22.7	20.3	0.0	1.0	0.0	0.0	0.0	7.4
		Min	0.00	0.00	8.96	0.13	0.0	0.0	0.0	0.0	36.7	0.0	0.0	0.0	0.0	0.0	2.1
		Max	0.64	0.00	12.10	2.06	3.6	4.0	0.0	57.4	92.5	0.0	2.7	0.0	0.0	0.0	23.2
Schinz-nach Fm. (4/4)	Stamberg Mb.	Mean	0.16	0.00	10.59	1.13	1.3	1.5	0.0	0.0	81.3	0.0	0.7	0.0	0.0	0.0	14.2
		Median	0.00	0.00	10.68	1.03	0.7	1.1	0.0	0.0	82.0	0.0	0.0	0.0	0.0	0.0	13.2
		Stdev	0.32	0.00	1.27	0.72	1.7	1.8	0.0	0.0	9.8	0.0	1.4	0.0	0.0	0.0	6.7
		Min	0.00	0.00	8.96	0.42	0.0	0.0	0.0	0.0	68.8	0.0	0.0	0.0	0.0	0.0	7.1
		Max	0.64	0.00	12.05	2.06	3.6	3.7	0.0	0.0	92.5	0.0	2.7	0.0	0.0	0.0	23.2
Schinz-nach Fm. (3/3)	Lied. + Leu-tschenb. + Kienb. Mb.	Mean	0.01	0.00	11.27	0.14	1.8	2.3	0.0	37.8	51.7	0.0	0.0	0.0	0.0	0.0	6.2
		Median	0.00	0.00	11.66	0.14	1.5	1.6	0.0	33.6	46.3	0.0	0.0	0.0	0.0	0.0	3.0
		Stdev	0.01	0.00	1.07	0.02	0.5	1.4	0.0	17.8	18.4	0.0	0.0	0.0	0.0	0.0	6.4
		Min	0.00	0.00	10.06	0.13	1.5	1.4	0.0	22.5	36.7	0.0	0.0	0.0	0.0	0.0	2.1
		Max	0.02	0.00	12.10	0.16	2.4	4.0	0.0	57.4	72.2	0.0	0.0	0.0	0.0	0.0	13.5

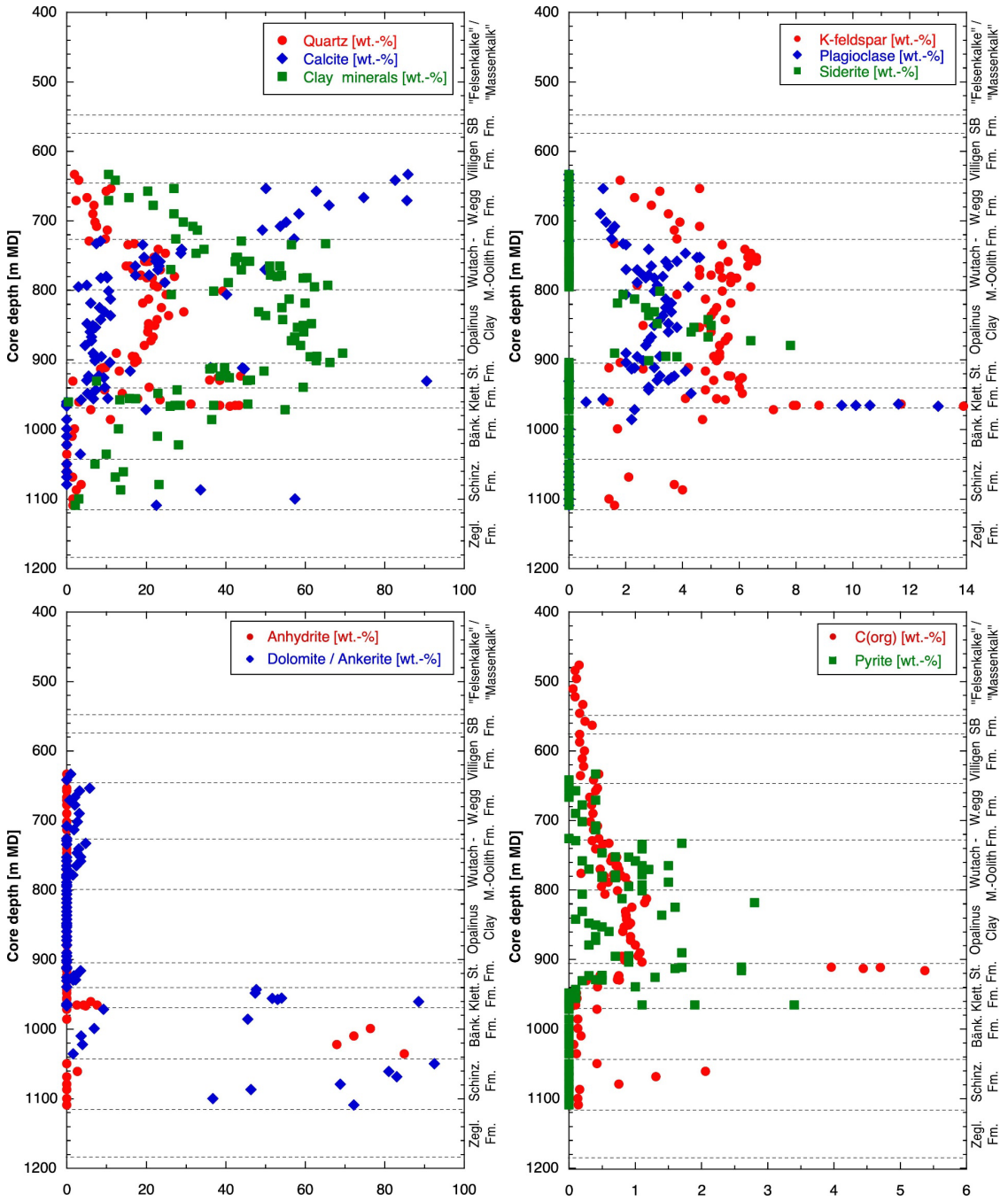

Fig. 4.2-1: Mineral contents in the bulk rock as a function of depth

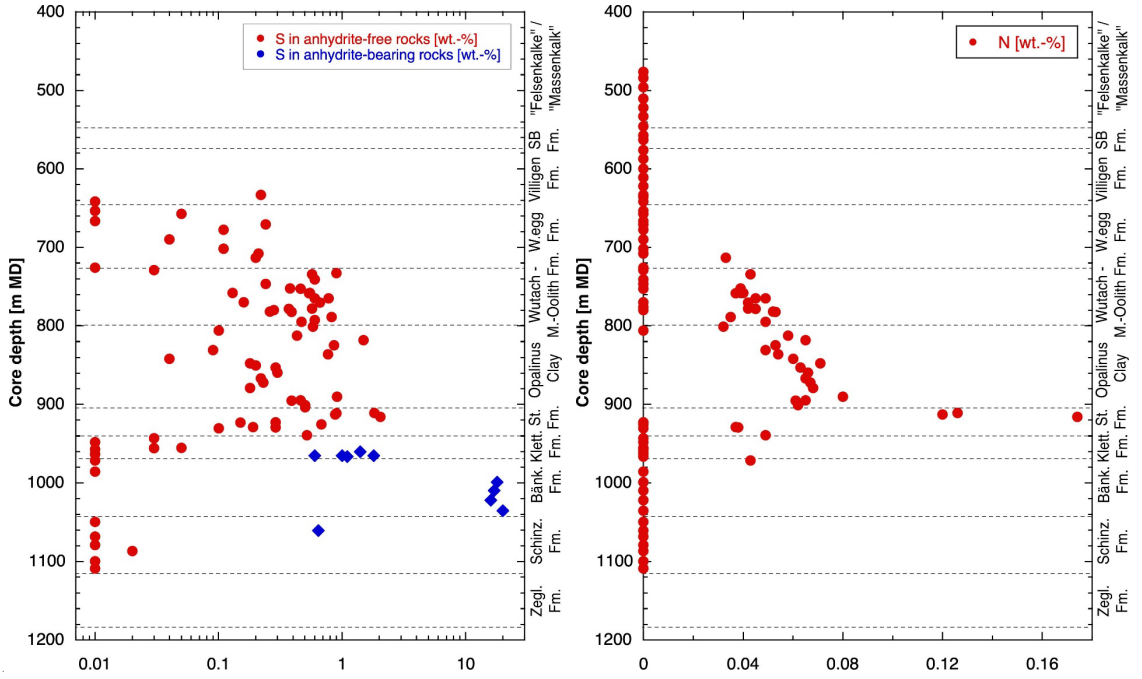

Fig. 4.2-2: Contents of S and N in the bulk rock as a function of depth

S contents below the detection limit of 0.05 wt.-% are represented by data points shown at 0.01 wt.-%. N contents below the detection limit of 0.01 wt.-% are represented by data points shown at 0 wt.-%.

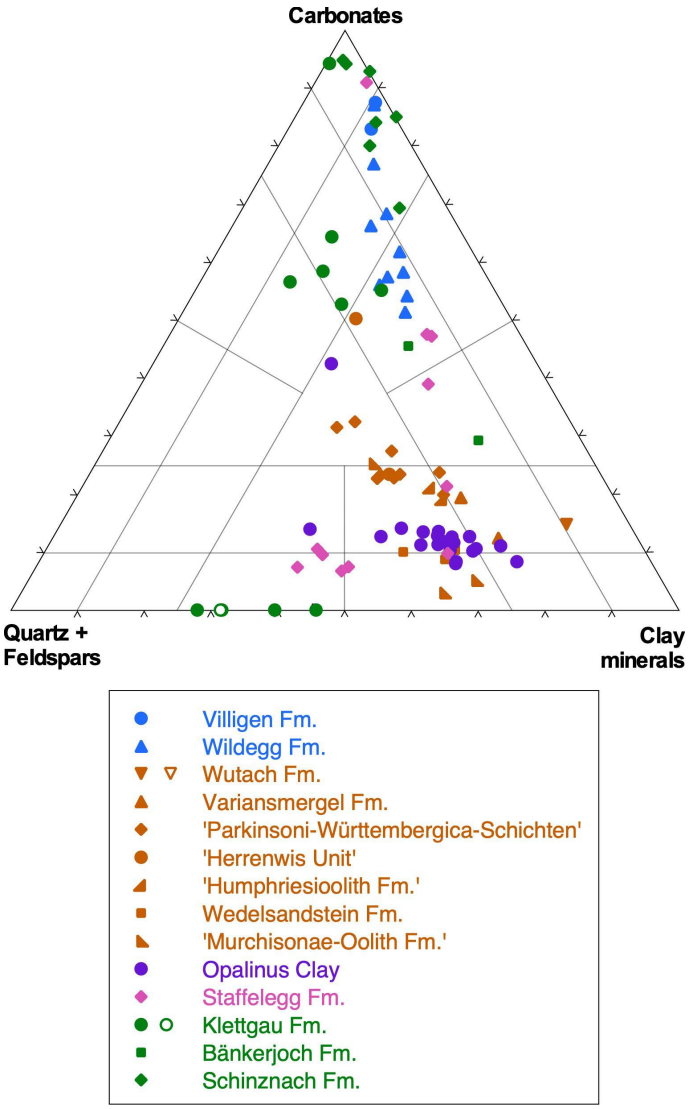

Fig. 4.2-3: Mineralogical composition of studied samples in the Füchtbauer triangle

Open symbols indicate samples containing 10 – 50 wt.-% minerals other than those represented by the Füchtbauer triangle (which are clays, calcite, dolomite/ankerite, siderite, magnesite, quartz, K-feldspar, plagioclase). Samples with > 50 wt.-% of such minerals are excluded. In the Wutach Formation, the additional phase is goethite, and in the Klettgau Formation, it is anhydrite.

A closer look at the section Staffelegg Formation – Opalinus Clay – «Brauner Dogger»

The graphs shown in Fig. 4.2-4 indicate systematic depth trends of the contents of quartz, clay minerals and calcite, whereas other minerals show no evident systematic variability.

Staffelegg Formation

Lithological heterogeneity is a characteristic in the Staffelegg Formation, which, according to the Füchtbauer nomenclature, contains claystone, marl, limestone and sandstone/siltstone. Within the Frick Member (918.46 – 930.24 m), clay-mineral contents decrease towards the top, while quartz contents (and therefore the quartz/clay ratio) increase. High contents of pyrite and C(org) are observed in samples from the Rietheim Member (909.98 – 916.14 m).

Opalinus Clay

Informal sub-units within the Opalinus Clay were defined by Mazurek & Aschwanden (2020) on a regional basis, and this scheme was successfully applied to several TBO boreholes. In borehole STA2-1 (as in STA3-1), however, mineralogical trends are less well expressed, in particular when compared to the findings from the BUL1-1 profile (Mazurek et al. 2021). The subdivision of the 'Mixed clay-silt-carbonate sub-unit' into two sections with distinct trends is not evident. Some other minor trends are indicated in Fig. 4.2-4; in several cases, they do not end at the boundaries of the sub-units as defined in Dossier III.

«Murchisonae-Oolith Formation»

No distinct trends can be identified, possibly also due to the small number of studied samples.

Wedelsandstein Formation – «Herrenwis Unit»

A trend of upwards decreasing clay-mineral contents is seen.

«Parkinsoni-Württembergica-Schichten»

Clay-mineral contents decrease and quartz contents increase upwards, resulting in a sharply increasing ratio of quartz to clay minerals. Plagioclase shows a conspicuous maximum in the centre of the unit.

Conclusion

There are less systematic depth trends in the STA2-1 profile when compared to STA3-1 or, even more so, BUL1-1. This is particularly the case in the Opalinus Clay where the few trends can extend beyond the boundaries of the sub-units as defined in Dossier III.

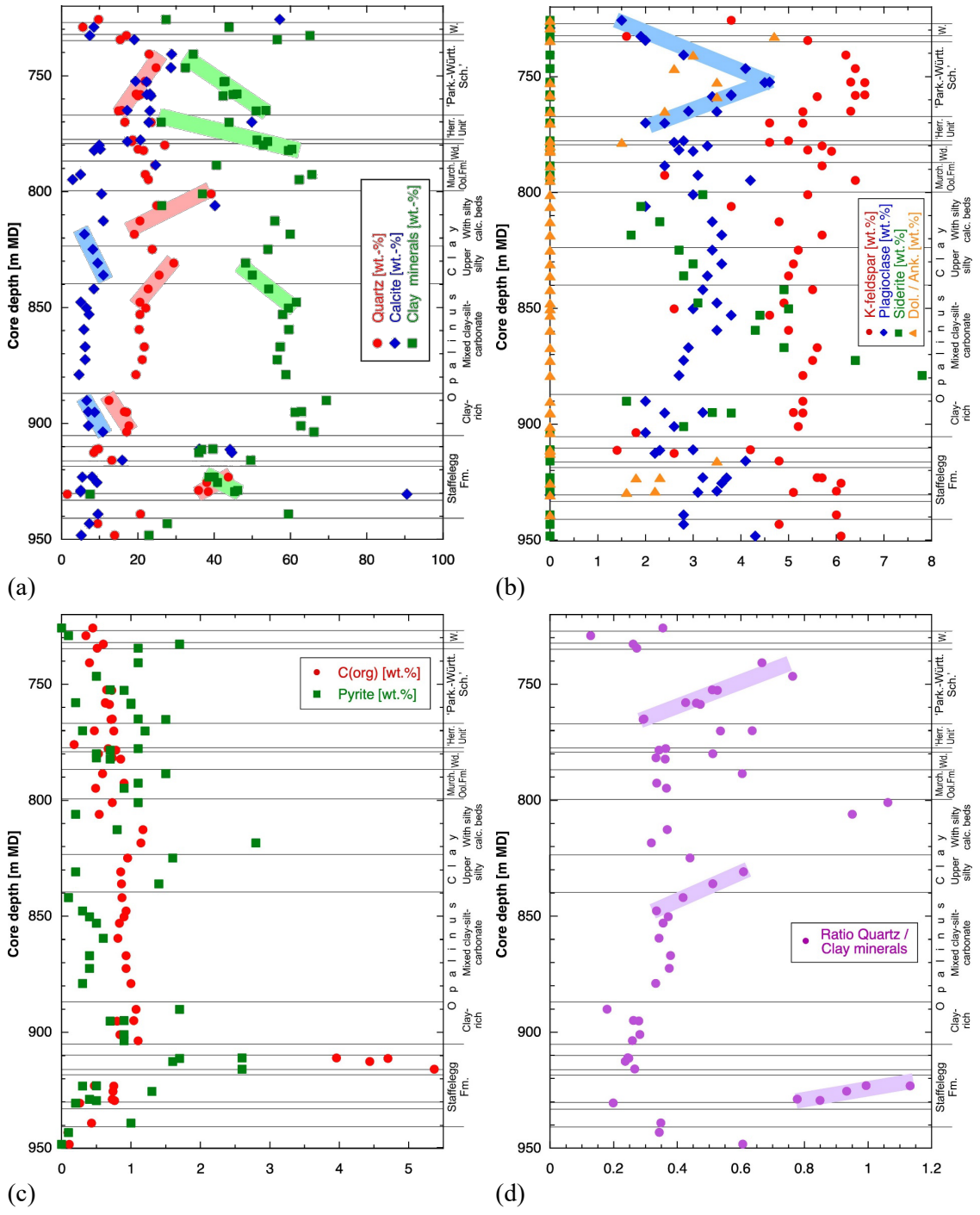

Fig. 4.2-4: Depth trends of mineral contents in the bulk rock in the Lias – Dogger interval

Coloured bars highlight systematic trends. Dolomite contents of 47 – 48 wt.-% in 2 samples from the Gruhalde Member of the Klettgau Formation are out of the range shown in (b).

4.2.2 Clay minerals

A total of 27 mineralogical analyses of the clay fraction were performed in the section Villigen Formation – Klettgau Formation. The full dataset is documented in Appendix A, and Tab. 4.2-2 provides formation-specific summaries, normalising the contents of individual clay phases to the sum of all clay minerals.

The identified clay-mineral species include illite, smectite, illite/smectite mixed layers, kaolinite, chlorite and chlorite/smectite mixed layers. The identification of chlorite/smectite mixed layers in all samples is in contrast with older data from northern Switzerland where this mineral was rarely reported (Mazurek 2017). However, this is not a real difference but due to the improved methodology of the evaluation of X-ray patterns that was applied for the TBO campaign (details in Waber ed. 2020). Because the chlorite/smectite mixed-layer phase contains 85 – 95 % chlorite layers, its XRD reflections are close to those of pure chlorite. The new methodology also allows to better resolve the fraction of smectite layers in the illite/smectite mixed-layer phase. As seen in Tab. 4.2-2, illite-rich mixed layers dominate, but minor amounts of illite-poorer mixed layers also occur. Given the fact that the contents of mixed-layer phases and the smectite fractions in these are known, the end-member compositions of illite, smectite, chlorite and kaolinite (whether in mixed layers or as a discrete phase) can be calculated and are also listed in Tab. 4.2-2.

Depth trends of the relative proportions of clay minerals are shown graphically in Fig. 4.2-5 for individual clay phases (a) and end-member clays (b). The depth plot of the latter is less noisy than that of the individual clay minerals. Smectite as a discrete phase occurs only infrequently and is quantitatively subordinate. Most smectite is found in illite/smectite mixed-layer minerals. Variability of the smectite end-member is limited, and chlorite also varies only weakly. In contrast, the relative proportions of the two main end-member clays, namely illite and kaolinite, vary substantially over the profile (Figs. 4.2-5 and 4.2-6). The Klettgau Formation is characterised by the dominance of the illite end member, while the proportions of kaolinite are low (illite/kaolinite ratios are in the range 2.5 – 37). The overlying Dogger – Lias interval will be explored in more detail below.

Tab. 4.2-2: Mineralogical composition of the clay fraction: formation-specific means, medians, standard deviations and ranges

Formation (number of analyses)	**Mem-ber**		**Individual clay phases** [wt.-% of clay fraction]										**End-member clays** [wt.-% of clay fraction]			
			Illite	**Ill/Sm ML (85-90)**	**Ill/Sm ML (75-80)**	**Ill/Sm ML (50-70)**	**Ill/Sm ML (20-40)**	**Total Ill/Sm**	**Smectite**	**Kaolinite**	**Chlorite**	**Chl/Sm ML (85-95)**	**Illite**	**Smectite**	**Kaolinite**	**Chlorite**
Villigen Fm. (1)		Mean	28.7	36.7	1.4	15.1	0.0	53.2	1.0	7.0	1.8	8.3	70.1	13.7	7.0	9.2
«Parkinsoni-Württem-bergica-Sch.» (4)		Mean	30.4	28.1	5.7	6.3	0.0	40.0	0.0	20.7	1.6	7.4	62.6	8.6	20.7	8.3
		Median	30.1	28.7	4.7	6.7	0.0	40.9	0.0	20.0	1.4	7.8	62.8	8.6	20.0	8.6
		Stdev	1.1	3.3	6.1	2.2	0.0	2.8	0.0	2.6	0.7	1.4	2.9	0.6	2.6	1.0
		Min	29.4	23.5	0.0	3.5	0.0	35.9	0.0	18.4	1.0	5.6	58.8	8.0	18.4	6.8
		Max	32.0	31.4	13.2	8.2	0.0	42.3	0.0	24.3	2.5	8.6	65.9	9.1	24.3	9.0
«Humphriesi-oolith Fm.» (2)		Mean	33.2	15.5	7.4	8.9	0.0	31.7	0.1	21.0	2.8	11.3	57.6	8.4	21.0	13.1
		Median	33.2	15.5	7.4	8.9	0.0	31.7	0.1	21.0	2.8	11.3	57.6	8.4	21.0	13.1
		Stdev	0.3	3.6	10.5	3.6	0.0	3.3	0.1	0.3	0.2	2.3	2.8	0.1	0.3	2.3
		Min	33.0	12.9	0.0	6.3	0.0	29.4	0.0	20.8	2.6	9.6	55.6	8.3	20.8	11.5
		Max	33.4	18.0	14.8	11.4	0.0	34.0	0.1	21.2	2.9	12.9	59.5	8.5	21.2	14.7
Wedelsandstein Fm. (1)		Mean	24.6	25.9	0.0	6.3	0.0	32.2	0.0	30.0	3.3	9.9	50.3	7.2	30.0	12.4
«Murchisonae-Ool. Fm.» (1)		Mean	31.3	21.5	4.4	1.0	0.0	26.9	0.0	25.9	5.3	10.7	53.3	5.6	25.9	15.2
Opalinus Clay (10)	All	Mean	27.6	13.0	11.6	3.3	0.0	27.9	0.0	32.4	1.9	10.1	50.0	6.6	32.4	11.0
		Median	27.2	12.0	12.0	3.0	0.0	25.4	0.0	33.2	2.0	10.1	49.0	6.5	33.2	11.3
		Stdev	1.9	9.0	7.5	2.3	0.0	6.5	0.0	6.0	0.9	0.7	5.7	0.8	6.0	1.1
		Min	25.9	0.0	0.0	0.0	0.0	22.0	0.0	21.2	0.0	8.6	44.4	5.3	21.2	9.5
		Max	31.4	28.0	25.5	6.8	0.0	42.7	0.0	38.8	3.5	11.1	61.0	8.3	38.8	12.5
Opalinus Clay (2)	Sub-unit with silty calcareous beds	Mean	26.9	21.5	16.1	1.2	0.0	38.7	0.0	23.3	1.9	9.4	58.7	7.7	23.3	10.5
		Median	26.9	21.5	16.1	1.2	0.0	38.7	0.0	23.3	1.9	9.4	58.7	7.7	23.3	10.5
		Stdev	1.3	6.0	13.3	1.6	0.0	5.7	0.0	2.9	0.4	1.1	3.3	0.8	2.9	1.2
		Min	25.9	17.2	6.7	0.0	0.0	34.7	0.0	21.2	1.6	8.6	56.3	7.1	21.2	9.6
		Max	27.8	25.7	25.5	2.3	0.0	42.7	0.0	25.3	2.1	10.1	61.0	8.3	25.3	11.3
Opalinus Clay (2)	Upper silty sub-unit	Mean	28.5	20.5	6.3	2.4	0.0	29.1	0.0	29.8	2.0	10.7	52.3	6.1	29.8	11.8
		Median	28.5	20.5	6.3	2.4	0.0	29.1	0.0	29.8	2.0	10.7	52.3	6.1	29.8	11.8
		Stdev	2.8	10.6	8.8	0.9	0.0	2.7	0.0	0.5	0.0	0.6	0.3	0.1	0.5	0.6
		Min	26.5	13.0	0.0	1.7	0.0	27.2	0.0	29.4	2.0	10.3	52.1	6.0	29.4	11.4
		Max	30.5	28.0	12.5	3.0	0.0	31.0	0.0	30.1	2.0	11.1	52.5	6.2	30.1	12.2

Tab. 4.2-2: (continued)

Formation (number of analyses)	**Mem-ber**		**Individual clay phases** [wt.-% of clay fraction]										**End-member clays** [wt.-% of clay fraction]			
			Illite	**Ill/Sm ML (85-90)**	**Ill/Sm ML (75-80)**	**Ill/Sm ML (50-70)**	**Ill/Sm ML (20-40)**	**Total Ill/Sm**	**Smectite**	**Kaolinite**	**Chlorite**	**Chl/Sm ML (85-95)**	**Illite**	**Smectite**	**Kaolinite**	**Chlorite**
Opalinus Clay (3)	Mixed clay-silt-carbonate sub-unit	Mean	28.1	9.2	11.3	4.5	0.0	25.1	0.0	35.0	1.7	10.1	47.8	6.5	35.0	10.7
		Median	26.7	8.7	15.5	5.9	0.0	24.7	0.0	35.8	1.9	10.1	45.9	6.7	35.8	11.1
		Stdev	2.9	6.4	8.1	3.2	0.0	0.8	0.0	4.1	0.5	0.6	3.9	0.4	4.1	1.1
		Min	26.1	3.1	2.0	0.8	0.0	24.5	0.0	30.6	1.1	9.5	45.1	6.0	30.6	9.5
		Max	31.4	15.9	16.5	6.8	0.0	26.0	0.0	38.7	2.1	10.7	52.3	6.8	38.7	11.5
Opalinus Clay (3)	Clay-rich sub-unit	Mean	27.1	6.2	12.5	4.1	0.0	22.8	0.0	37.6	2.0	10.2	45.0	6.1	37.6	11.2
		Median	27.6	7.6	11.4	3.4	0.0	22.0	0.0	37.3	2.4	10.0	45.2	6.1	37.3	11.3
		Stdev	1.0	5.6	3.1	1.6	0.0	1.3	0.0	1.0	1.8	0.4	0.6	0.9	1.0	1.4
		Min	25.9	0.0	10.0	3.0	0.0	22.0	0.0	36.8	0.0	9.9	44.4	5.3	36.8	9.8
		Max	27.8	10.9	16.0	6.0	0.0	24.3	0.0	38.8	3.5	10.7	45.5	7.0	38.8	12.5
Staffelegg Fm. (5)		Mean	38.1	16.0	4.4	7.1	0.0	20.7	0.7	19.5	3.5	10.5	59.6	7.6	19.5	13.2
		Median	32.7	19.2	3.2	5.6	0.0	27.9	0.0	20.9	3.0	9.6	60.0	7.8	20.9	14.0
		Stdev	11.9	12.2	6.5	3.1	0.0	14.8	1.5	4.6	1.8	1.8	4.3	0.3	4.6	2.1
		Min	28.0	0.0	0.0	4.0	0.0	0.0	0.0	12.2	1.8	8.8	55.1	7.1	12.2	10.2
		Max	57.3	28.3	15.7	10.6	0.0	35.5	3.3	23.3	5.9	13.0	64.3	7.9	23.3	15.7
Klettgau Fm. (3)		Mean	57.6	20.6	0.0	4.3	0.0	24.9	0.0	9.4	1.9	6.2	77.7	5.3	9.4	7.6
		Median	64.6	20.4	0.0	5.9	0.0	26.3	0.0	3.2	0.8	5.9	85.5	6.1	3.2	6.1
		Stdev	26.1	8.3	0.0	2.9	0.0	10.8	0.1	11.5	1.9	3.3	18.1	2.5	11.5	4.8
		Min	28.8	12.4	0.0	1.0	0.0	13.4	0.0	2.3	0.7	3.1	57.0	2.5	2.3	3.7
		Max	79.5	28.9	0.0	6.0	0.0	34.9	0.1	22.6	4.1	9.6	90.6	7.4	22.6	13.0

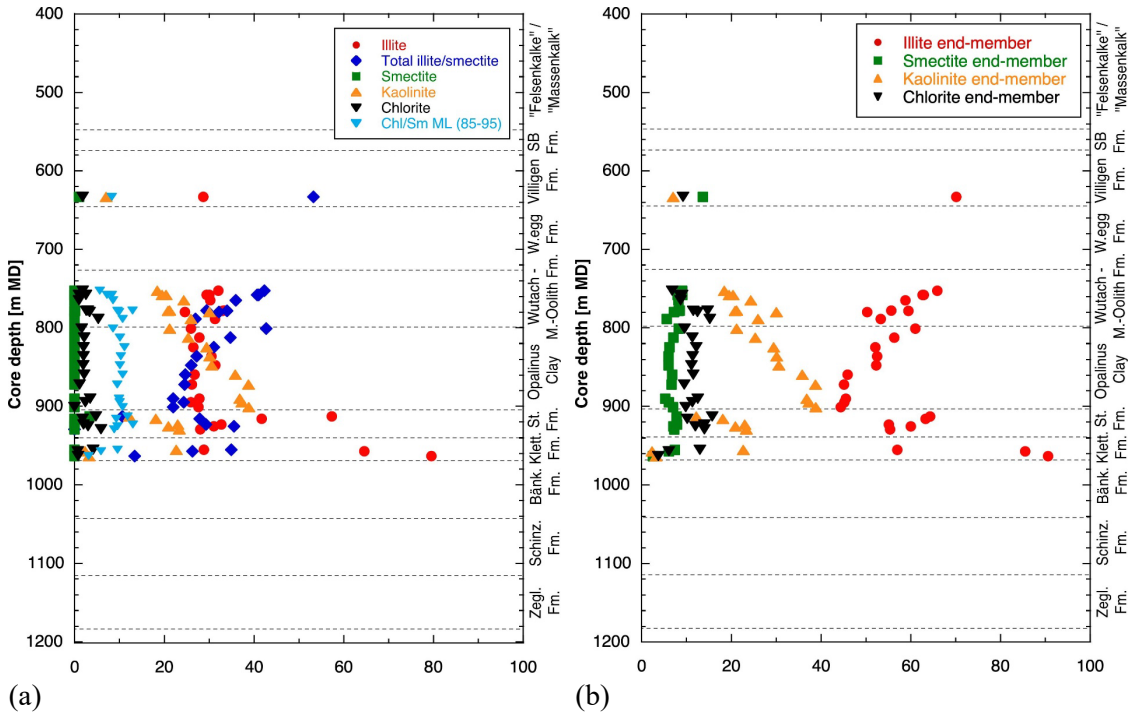

Fig. 4.2-5: Mineralogical composition of the clay fraction as a function of depth; (a) individual clay minerals, (b) end-member clays

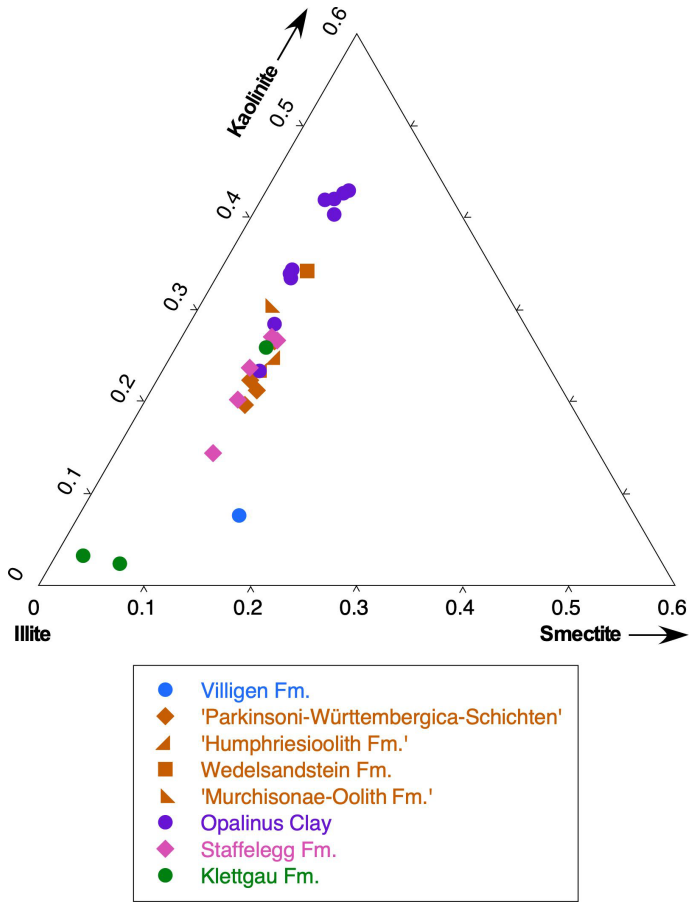

Fig. 4.2-6: Relative mass proportions of illite, smectite and kaolinite end-member clays

A closer look at the section Staffelegg Formation – Opalinus Clay – «Brauner Dogger»

The composition of the clay fraction in this interval shows some distinct depth trends (Figs. 4.2-7 and 4.2-8). In comparison to the overlying clay-rich sub-unit of the Opalinus Clay, the Staffelegg Formation has low kaolinite and high illite contents, and the ratio illite/kaolinite increases to values > 5 towards the top – a feature not observed equally clearly (if at all) in the STA3-1 and BUL1-1 profiles. The composition of the clay fraction changes abruptly at the base of the Opalinus Clay, which begins with about equal proportions of illite and kaolinite. The ratio illite/kaolinite then evolves continuously to values around 3 at the top of the Opalinus Clay. In the «Parkinsoni-Württembergica-Schichten», another systematic trend of increasing illite and decreasing kaolinite contents can be identifed towards the top of the formation.

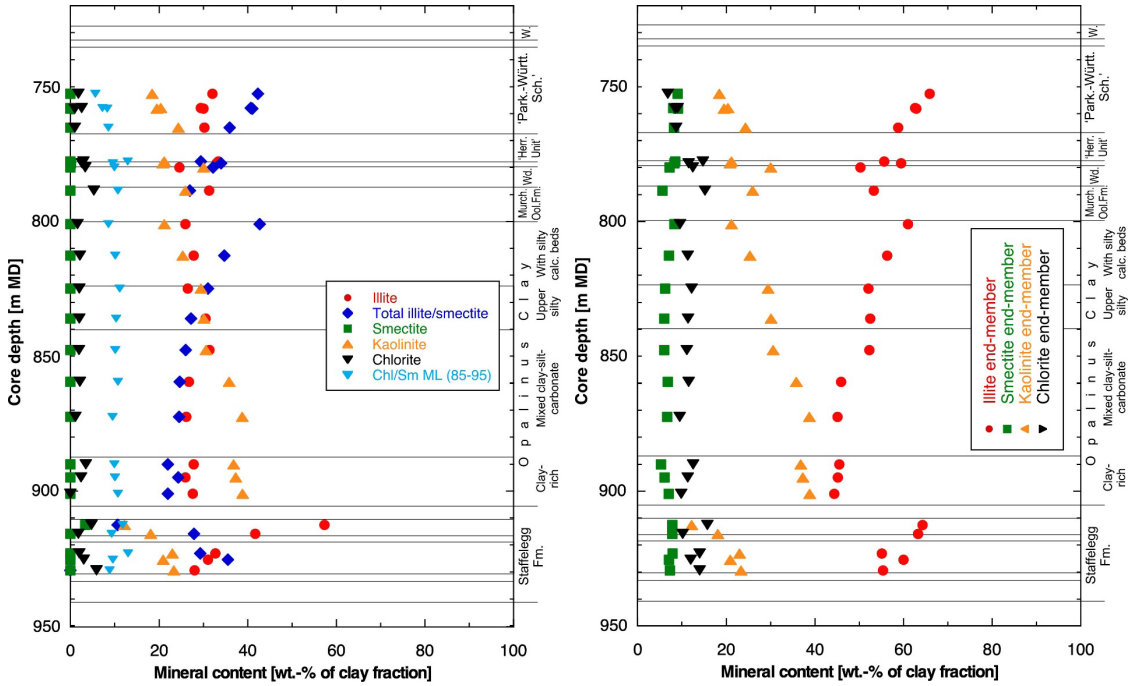

Fig. 4.2-7: Mineralogical composition of the clay fraction as a function of depth in the Lias – Dogger interval; (a) individual clay minerals, (b) end-member clays

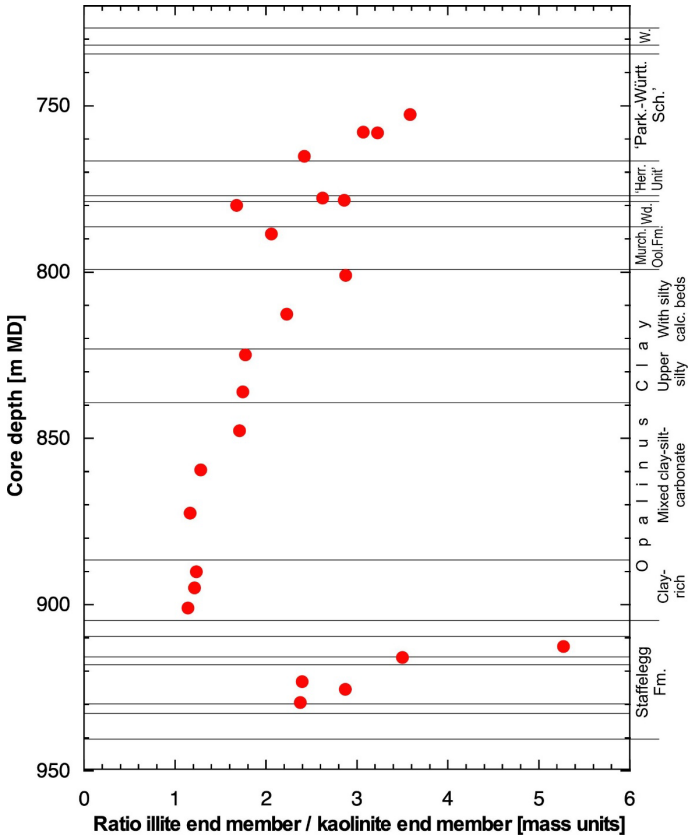

Fig. 4.2-8: Ratio of the illite to kaolinite end-member clays as a function of depth

4.3 Petrophysical parameters

Martin Mazurek & Lukas Aschwanden

All petrophysical measurements were performed at the University of Bern, except for 30 samples for which gravimetric water contents and water contents from diffusive isotope exchange experiments were obtained at Hydroisotop GmbH. The acquired parameters are listed in Tab. 4.3-1. The formalisms to calculate additional parameters from measured data (such as porosity) are detailed in Waber (ed.) (2020). Formation-specific statistical data are summarised in Tab. 4.3-2, and the full data set is documented in Appendix A. In cases where gravimetric water content was available but density data were missing, water-loss porosity was calculated assuming a grain density of 2.7 g/cm^3. The uncertainty related to this assumption is small.

Acceptance criteria for diffusive isotope exchange experiments are discussed at length in Section 4.8.1, where the results for a number of experiments (both isotope values and water contents based on mass balance) were excluded if they failed to meet the criteria. What is considered here are the water contents based on experiments classified as "good" and "less reliable" – the latter show some deviations, but these are considered to be minor and may result in a somewhat larger error band. This is the same procedure as pursued for all boreholes studied to date. However, a new phenomenon in the data set obtained by Hydroisotop GmbH was identified for STA2, resulting in a slightly segmented, curly pattern in part of the isotope data (see Fig. 4.8-3). As argued in Section 4.8.1.2, three samples representing the minima of the segments were excluded and deemed to be affected by artefacts. The respective water contents based on mass balance are therefore also excluded and not considered here.

Tab. 4.3-1: Analytical programme for petrophysical measurements

Gravimetric water content and water content from isotope mass balance for additional 8 samples were analysed at late stages of reporting and are not included here.

	Number of samples
Bulk wet density	98
Grain density	92
Gravimetric water content	139
Water content from isotope mass balance	75
N_2 adsorption (BET external surface + full isotherm)	17

Tab. 4.3-2: Summary of measured and calculated petrophysical data

Listed water contents (wet) are averages of measurements performed on typically 3 sub-samples. n = number of samples per geological unit.

Formation	Member / Sub-unit		Bulk wet density [g/cm³]	Bulk dry density, calculated [g/cm³]	Grain density [g/cm³]	Pycnometer porosity [–]	Gravimetry: Water content (wet) (105 °C) [wt.-%]	Gravimetry: Water content (dry) (105 °C) [wt.-%]	Gravimetry: Water-loss porosity using bulk wet density [–]	Gravimetry: Water-loss porosity using grain density [–]	Isotope mass balance: Water content (wet) based on isotope diff. exch. [wt.-%]	Isotope mass balance: Porosity based on isotope diff. exch. using bulk wet density [–]	Isotope mass balance: Porosity based on isotope diff. exch. using grain density [–]	External surface area (BET) [m²/g dry rock]
«Felsenkalke» + «Massenkalk»		Mean	2.687	2.671	2.712	0.015	0.607	0.613	0.016	0.016	0.822	0.022	0.022	
		Median	2.695	2.683	2.713	0.011	0.373	0.374	0.010	0.010	0.422	0.011	0.011	
		Stdev	0.018	0.031	0.003	0.011	0.488	0.497	0.013	0.013	0.765	0.020	0.020	
		Min	2.659	2.617	2.709	0.007	0.252	0.253	0.007	0.007	0.366	0.010	0.010	
		Max	2.703	2.696	2.715	0.034	1.578	1.603	0.042	0.042	2.284	0.061	0.060	
		n	7	7	7	7	7	7	7	7	6	6	6	0
Schwarzbach Fm.	All	Mean	2.635	2.586	2.707	0.045	1.875	1.913	0.049	0.049	2.214	0.058	0.057	
		Median	2.635	2.586	2.707	0.045	1.875	1.913	0.049	0.049	2.214	0.058	0.057	
		Stdev	0.035	0.050	0.000	0.019	0.595	0.618	0.015	0.015	1.113	0.029	0.028	
		Min	2.610	2.550	2.707	0.032	1.454	1.475	0.039	0.038	1.427	0.038	0.038	
		Max	2.660	2.621	2.707	0.058	2.296	2.350	0.060	0.060	3.001	0.078	0.077	
		n	2	2	2	2	2	2	2	2	2	2	2	0
Villigen Fm.		Mean	2.665	2.639	2.710	0.026	0.962	0.975	0.025	0.025	1.082	0.029	0.029	10.47
		Median	2.672	2.652	2.711	0.024	0.726	0.731	0.019	0.019	0.845	0.023	0.023	
		Stdev	0.030	0.045	0.006	0.016	0.611	0.625	0.016	0.016	0.681	0.018	0.018	
		Min	2.625	2.581	2.697	0.006	0.332	0.333	0.009	0.009	0.413	0.011	0.011	
		Max	2.703	2.692	2.718	0.046	1.845	1.880	0.049	0.048	2.191	0.058	0.057	
		n	8	8	8	8	8	8	8	8	6	6	6	1
Wildegg Fm.	Effingen Mb.	Mean	2.590	2.511	2.709	0.074	3.035	3.136	0.078	0.078	3.499	0.091	0.089	
		Median	2.592	2.506	2.707	0.079	3.236	3.344	0.084	0.083	3.627	0.094	0.093	
		Stdev	0.029	0.048	0.010	0.014	0.794	0.840	0.020	0.020	0.657	0.016	0.016	
		Min	2.542	2.445	2.701	0.052	1.381	1.400	0.036	0.036	2.547	0.067	0.066	
		Max	2.635	2.599	2.734	0.091	3.990	4.156	0.102	0.101	4.601	0.118	0.115	
		n	10	10	8	8	10	10	10	10	8	8	8	0
Wutach Fm.		Mean	2.605	2.309	3.278	0.295	8.616	9.526	0.296	0.220				43.71
		n	1	1	1	1	2	2	1	2	0	0	0	1
Variansmergel Fm.		Mean	2.483	2.328	2.725	0.146	6.038	6.427	0.155	0.148				40.77
		n	1	1	1	1	2	2	1	2	0	0	0	1
«Parkinsoni-Württembergica-Sch.»		Mean	2.516	2.398	2.704	0.113	4.650	4.882	0.118	0.116	4.883		0.121	35.44
		Median	2.515	2.397	2.705	0.113	4.640	4.866	0.118	0.116	4.947		0.123	34.99
		Stdev	0.036	0.045	0.010	0.018	0.709	0.779	0.014	0.017	1.083		0.025	2.20
		Min	2.448	2.315	2.693	0.090	3.320	3.434	0.098	0.085	3.267		0.084	33.30
		Max	2.574	2.472	2.718	0.144	5.820	6.180	0.135	0.143	6.168		0.151	38.49
		n	11	11	9	9	17	17	11	17	6	0	6	4
«Herrenwis Unit»		Mean	2.554	2.451	2.724	0.100	4.058	4.248	0.103	0.103	4.020	0.102	0.101	
		Median	2.540	2.420	2.715	0.108	4.705	4.937	0.120	0.118	4.020	0.102	0.101	
		Stdev	0.061	0.098	0.020	0.030	1.567	1.689	0.038	0.037	2.506	0.061	0.059	
		Min	2.501	2.371	2.710	0.068	2.271	2.324	0.060	0.060	2.248	0.059	0.059	
		Max	2.620	2.560	2.747	0.125	5.199	5.484	0.130	0.129	5.792	0.145	0.143	
		n	3	3	3	3	3	3	3	3	2	2	2	0

Tab. 4.3-2: (continued)

Formation	Member / Sub-unit		Bulk wet density [g/cm³]	Bulk dry density, calculated [g/cm³]	Grain density [g/cm³]	Pycnometer porosity [–]	Gravimetry: Water content (wet) (105 °C) [wt.-%]	Gravimetry: Water content (dry) (105 °C) [wt.-%]	Gravimetry: Water-loss porosity using bulk wet density [–]	Gravimetry: Water-loss porosity using grain density [–]	Isotope mass bal.: Water content (wet) based on isotope diff. exch. [wt.-%]	Isotope mass bal.: Porosity based on isotope diff. exch. using bulk wet density [–]	Isotope mass bal.: Porosity based on isotope diff. exch. using grain density [–]	External surface area (BET) [m²/g dry rock]
«Humphriesioolith Fm.»		Mean	2.509	2.373	2.717	0.127	5.507	5.828	0.136	0.136				
		n	1	1	1	1	2	2	1	2	0	0	0	0
Wedel-sandstein Fm.		Mean	2.490	2.351	2.692	0.127	5.310	5.611	0.139	0.131	5.435	0.147	0.134	13.46
		Median	2.487	2.348	2.689	0.127	5.550	5.876	0.139	0.136	5.435		0.134	
		Stdev	0.012	0.013	0.007	0.007	0.563	0.625	0.001	0.013	0.590		0.013	
		Min	2.480	2.339	2.687	0.120	4.470	4.679	0.138	0.112	5.018		0.125	
		Max	2.504	2.366	2.700	0.133	5.672	6.013	0.141	0.140	5.852		0.143	
		n	3	3	3	3	4	4	3	4	2	1	2	1
«Murchi-sonae-Oolith Fm.»		Mean	2.510	2.381	2.725	0.126	5.599	5.939	0.129	0.138	6.430		0.156	33.86
		Median	2.510	2.381	2.725	0.126	5.550	5.877	0.129	0.137	6.430		0.156	
		Stdev	0.028	0.059	0.030	0.012	0.888	0.993	0.031	0.020	0.659		0.014	
		Min	2.490	2.339	2.704	0.118	4.251	4.440	0.108	0.109	5.964		0.146	
		Max	2.530	2.422	2.746	0.135	6.650	7.124	0.151	0.161	6.896		0.167	
		n	2	2	2	2	5	5	2	5	2	0	2	1
Opalinus Clay	All	Mean	2.535	2.424	2.698	0.102	4.524	4.742	0.112	0.113	5.041		0.125	
		Median	2.526	2.409	2.702	0.106	4.660	4.888	0.117	0.117	5.182		0.129	
		Stdev	0.034	0.048	0.013	0.016	0.541	0.586	0.016	0.013	0.531		0.012	
		Min	2.499	2.376	2.669	0.048	2.193	2.242	0.058	0.057	3.986		0.101	
		Max	2.640	2.582	2.713	0.116	5.170	5.452	0.129	0.128	5.739		0.141	
		n	17	17	17	17	39	39	17	39	17	0	17	0
Opalinus Clay	Sub-unit with silty calc. beds	Mean	2.550	2.451	2.698	0.092	4.129	4.315	0.099	0.104	5.091		0.126	
		Median	2.531	2.423	2.705	0.101	4.310	4.506	0.107	0.108	5.344		0.132	
		Stdev	0.065	0.094	0.020	0.031	0.907	0.976	0.029	0.022	0.537		0.012	
		Min	2.499	2.376	2.669	0.048	2.193	2.242	0.058	0.057	4.475		0.112	
		Max	2.640	2.582	2.713	0.116	4.930	5.186	0.123	0.123	5.455		0.135	
		n	4	4	4	4	8	8	4	8	3	0	3	0
Opalinus Clay	Upper silty sub-unit	Mean	2.532	2.429	2.695	0.099	4.086	4.261	0.103	0.103	4.156		0.105	
		Median	2.532	2.427	2.696	0.102	4.209	4.394	0.105	0.106	4.068		0.103	
		Stdev	0.013	0.018	0.008	0.009	0.282	0.306	0.005	0.007	0.227		0.005	
		Min	2.520	2.412	2.687	0.089	3.650	3.788	0.097	0.093	3.986		0.101	
		Max	2.545	2.448	2.702	0.105	4.340	4.537	0.108	0.109	4.414		0.111	
		n	3	3	3	3	6	6	3	6	3	0	3	0
Opalinus Clay	Mixed clay-silt-carbonate sub-unit	Mean	2.534	2.416	2.702	0.106	4.680	4.910	0.118	0.117	5.258		0.130	
		Median	2.525	2.406	2.706	0.109	4.654	4.881	0.117	0.117	5.264		0.130	
		Stdev	0.025	0.025	0.011	0.008	0.197	0.217	0.003	0.005	0.335		0.008	
		Min	2.503	2.388	2.679	0.093	4.250	4.439	0.115	0.107	4.720		0.118	
		Max	2.570	2.454	2.710	0.114	5.086	5.359	0.124	0.126	5.739		0.141	
		n	7	7	7	7	16	16	7	16	7	0	7	0

Tab. 4.3-2: (continued)

Formation	Member / Sub-unit		Bulk wet density [g/cm³]	Bulk dry density, calculated [g/cm³]	Grain density [g/cm³]	Pycnometer porosity [–]	Gravimetry: Water content (wet) (105 °C) [wt.-%]	Gravimetry: Water content (dry) (105 °C) [wt.-%]	Gravimetry: Water-loss porosity using bulk wet density [–]	Gravimetry: Water-loss porosity using grain density [–]	Isotope mass bal.: Water content (wet) based on isotope diff. exch. [wt.-%]	Isotope mass bal.: Porosity based on isotope diff. exch. using bulk wet density [–]	Isotope mass bal.: Porosity based on isotope diff. exch. using grain density [–]	External surface area (BET) [m²/g dry rock]
Opalinus Clay	Clay-rich sub-unit	Mean	2.524	2.400	2.689	0.107	4.890	5.142	0.123	0.122	5.288		0.131	
		Median	2.527	2.404	2.687	0.106	4.864	5.113	0.123	0.121	5.264		0.130	
		Stdev	0.012	0.017	0.011	0.003	0.222	0.245	0.005	0.005	0.272		0.006	
		Min	2.510	2.381	2.678	0.105	4.610	4.833	0.119	0.115	5.005		0.125	
		Max	2.534	2.415	2.700	0.111	5.170	5.452	0.129	0.128	5.618		0.138	
		n	3	3	3	3	9	9	3	9	4	0	4	0
Staffelegg Fm.		Mean	2.504	2.406	2.648	0.092	3.894	4.062	0.099	0.097	4.289	0.123	0.108	19.33
		Median	2.530	2.433	2.684	0.092	3.950	4.112	0.101	0.099	4.088	0.123	0.103	21.65
		Stdev	0.077	0.099	0.081	0.018	0.965	1.030	0.028	0.022	0.894	0.027	0.021	11.58
		Min	2.392	2.273	2.505	0.052	1.127	1.140	0.030	0.030	3.005	0.104	0.077	2.75
		Max	2.629	2.599	2.742	0.120	5.260	5.552	0.132	0.130	5.678	0.142	0.140	33.74
		n	9	9	9	9	15	15	9	15	6	2	6	5
Klettgau Fm.		Mean	2.524	2.398	2.759	0.134	5.027	5.314	0.126	0.126	5.800	0.144	0.145	18.58
		Median	2.577	2.452	2.766	0.104	4.835	5.082	0.125	0.122	4.899	0.126	0.124	15.64
		Stdev	0.103	0.130	0.054	0.049	1.430	1.596	0.031	0.033	1.883	0.040	0.043	5.69
		Min	2.339	2.171	2.681	0.093	3.385	3.504	0.088	0.089	3.959	0.103	0.103	14.97
		Max	2.609	2.514	2.855	0.213	7.202	7.761	0.173	0.180	8.082	0.196	0.201	25.15
		n	10	10	8	8	10	10	10	10	5	5	5	3
Bänkerjoch Fm.		Mean	2.782	2.733	2.861	0.046	1.871	1.946	0.049	0.049	2.178	0.057	0.056	
		Median	2.853	2.823	2.910	0.030	1.028	1.040	0.029	0.029	1.358	0.039	0.038	
		Stdev	0.170	0.222	0.103	0.045	2.104	2.227	0.053	0.052	2.382	0.060	0.058	
		Min	2.514	2.375	2.696	0.005	0.207	0.207	0.006	0.006	0.219	0.006	0.006	
		Max	2.942	2.936	2.952	0.119	5.510	5.831	0.139	0.136	6.375	0.160	0.155	
		n	6	6	6	6	6	6	6	6	6	6	6	0
Schinznach Fm.	All	Mean	2.671	2.591	2.809	0.077	3.098	3.272	0.080	0.080	3.316	0.086	0.085	
		Median	2.716	2.648	2.809	0.057	2.440	2.501	0.066	0.066	2.358	0.064	0.064	
		Stdev	0.097	0.164	0.038	0.067	2.792	3.061	0.069	0.068	2.975	0.073	0.072	
		Min	2.473	2.267	2.755	0.015	0.320	0.321	0.009	0.009	0.342	0.009	0.009	
		Max	2.750	2.717	2.854	0.201	8.349	9.110	0.206	0.205	8.955	0.221	0.218	
		n	7	7	7	7	7	7	7	7	7	7	7	0
Schinznach Fm.	Stamberg Mb.	Mean	2.627	2.507	2.834	0.115	4.644	4.939	0.120	0.119	4.902	0.126	0.125	
		Median	2.659	2.556	2.837	0.101	3.894	4.073	0.103	0.102	4.148	0.110	0.109	
		Stdev	0.112	0.179	0.019	0.066	2.805	3.131	0.067	0.067	3.062	0.073	0.072	
		Min	2.473	2.267	2.809	0.057	2.440	2.501	0.066	0.066	2.358	0.064	0.064	
		Max	2.716	2.648	2.854	0.201	8.349	9.110	0.206	0.205	8.955	0.221	0.218	
		n	4	4	4	4	4	4	4	4	4	4	4	0
Schinznach Fm.	Lied. + Leu-tschenb. + Kienb. Mb.	Mean	2.730	2.702	2.775	0.026	1.036	1.050	0.028	0.028	1.202	0.033	0.032	
		Median	2.723	2.714	2.764	0.031	1.182	1.196	0.033	0.032	1.178	0.032	0.032	
		Stdev	0.017	0.024	0.026	0.010	0.656	0.668	0.018	0.018	0.872	0.024	0.023	
		Min	2.718	2.674	2.755	0.015	0.320	0.321	0.009	0.009	0.342	0.009	0.009	
		Max	2.750	2.717	2.805	0.033	1.607	1.633	0.044	0.043	2.086	0.057	0.056	
		n	3	3	3	3	3	3	3	3	3	3	3	0

4.3.1 Water content

The distribution of gravimetric water content in the studied section Malm – Triassic is shown in Fig. 4.3-1. Note that the error bars on gravimetric water content reflect the variability among 3 aliquots of the samples, i.e. they are a measure of the lithological heterogeneity of the sample on the cm-scale. The following systematics of the water contents can be observed in the Triassic and in the Malm (the Dogger – Lias section is detailed further below):

- In the Schinznach Formation, an upwards increasing trend is identified. It is more clearly defined than in the STA3-1 borehole.
- A similarly well-defined trend is seen in the Bänkerjoch Formation, whereas no such trend exists in STA3-1.
- The Klettgau Formation also shows a clear trend of upward increase, again in contrast to STA3-1.
- The section Wildegg Formation – Villigen Formation indicates a general decrease of the water contents towards the top. A similar but less well-defined trend is seen in STA3-1.
- A sharp upwards decrease is identified in the overlying Schwarzbach Formation, even though defined only by a limited number of data points.

The described trends likely indicate sedimentological cycles. They are more clearly defined than the trends observed in the mineralogy data (Section 4.2.1, Fig. 4.2-1). Water contents from gravimetry and from isotope diffusive exchange correlate well (Fig. 4.3-2), but the latter shows values that are consistently higher, about 6%$_{rel}$ on average. The sample at 960.43 m falls off the general trend, and this can be explained by heterogeneity on the cm-scale (dolostone with macro-porous domains, see photo in Fig. 4.3-9).

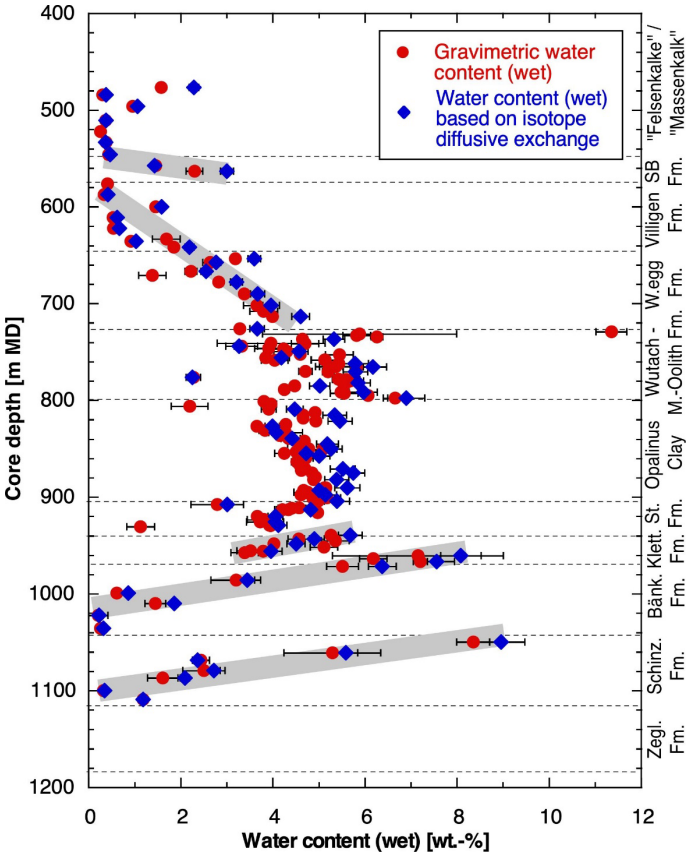

Fig. 4.3-1: Water content as a function of depth

Trends are only indicated for the Malm and Triassic sections (thick grey bars), the Dogger and Lias are detailed in Fig. 4.3-3. Black bars for gravimetric water content indicate 1σ variability among 3 aliquots of the same sample. Black bars for water content from isotope diffusive exchange represent the propagated analytical error.

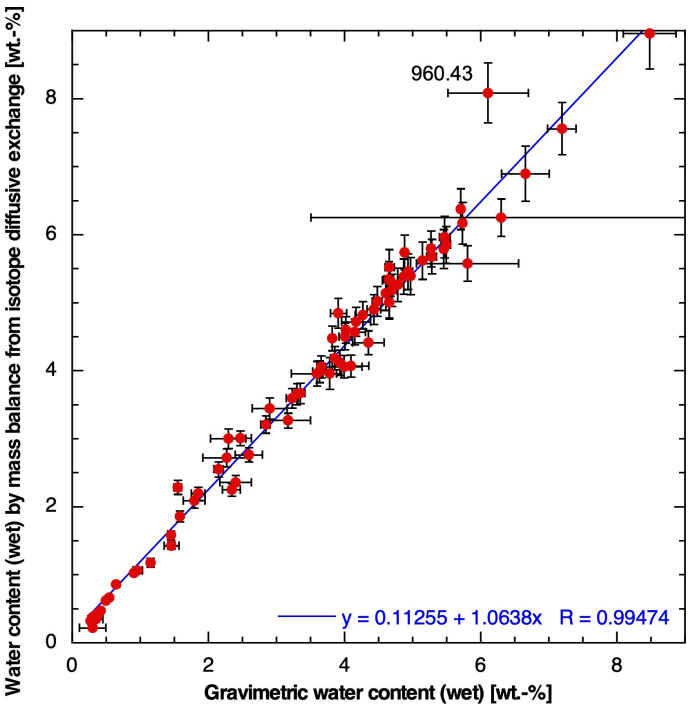

Fig. 4.3-2: Correlation of water contents based on gravimetry and on isotope diffusive exchange

Black bars of gravimetric water content indicate 1σ variability among 2 aliquots of the same sample. Black bars for water content from isotope diffusive exchange represent the propagated analytical error. Note that only the 2 gravimetric water contents obtained from the aliquots used for the isotope diffusive exchange experiments were considered in this graph, so the correlation refers to identical sample materials. This is particularly important for anhydrite-bearing samples, given the fact that only the anhydrite-poorest portions of such samples were used for diffusive-exchange experiments. The marked sample was not considered in the linear regression.

A closer look at the clay-rich Lias – Dogger section

As shown in Fig. 4.3-3, water contents in the Lias – Dogger section show several systematic trends with depth. These are similar for gravimetric water content and that obtained from isotope mass balance:

- In the Frick Member section (918.46 – 930.24 m) of the Staffelegg Formation, a clear upward trend towards lower values is evident, similar to STA3.
- In the overlying Rietheim and Gross Wolf Members (905.20 – 916.14 m), a distinct cycle of strongly decreasing water content is observed, same as in STA3.
- A sharp discontinuity towards higher values is observed at the base of the Opalinus Clay. Systematic trends are not well defined in the lower part of the formation, except for a decrease in the lower part of the 'Mixed clay-silt-carbonate sub-unit' (only seen in gravimetric water content).
- A cycle of decreasing water content starts in the uppermost 'Mixed clay-silt-carbonate sub-unit' and extends to the top of the 'Silty sub-unit'. The overlying 'Sub-unit with silty calcareous beds' represents a cycle starting with high values that decrease upwards.

- A similar cycle of decreasing water content is observed in the «Murchisonae-Oolith Formation».
- The «Parkinsoni-Württembergica-Schichten» can be subdivided into two cycles, with a minimum at about 745 m.

Overall, water contents tend to indicate clearer trends than mineralogy (Section 4.2.1, Fig. 4.2-4).

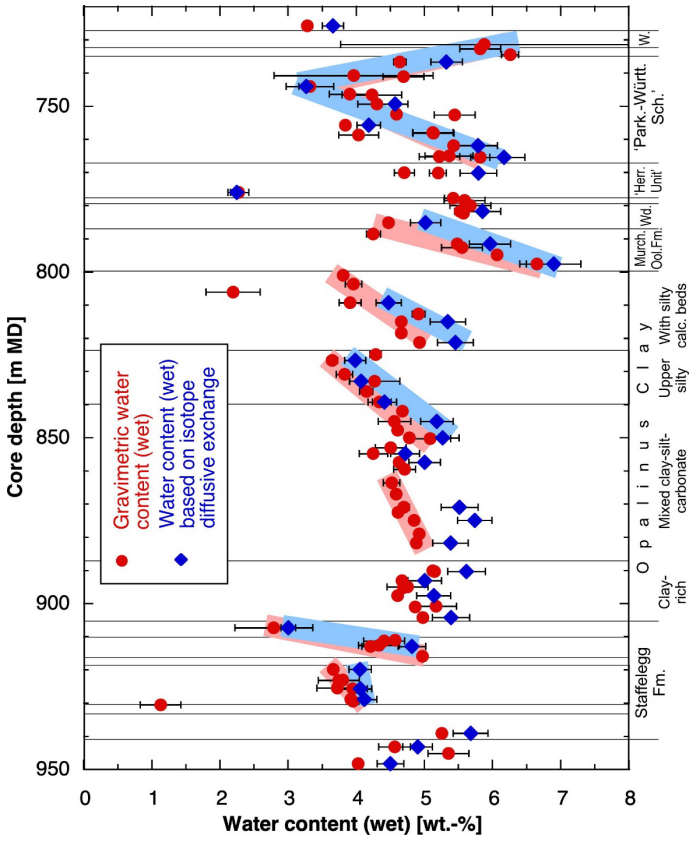

Fig. 4.3-3: Water content (wet) as a function of depth in the Lias-Dogger interval

Black bars of gravimetric water content indicate 1σ variability among 3 aliquots of the same sample. Black bars of water content from isotope diffusive exchange represent the propagated analytical error. Gravimetric water content of sample 729.13 from the Wutach Formation (11.35 wt.-%) is outside the plotted range.

4.3.2 Grain density

The grain-density profile is shown in Fig. 4.3-4. Throughout the Malm, Dogger and Lias units, values are around 2.7 g/cm^3, with only limited scatter. Outliers towards higher values typically correlate with elevated contents of pyrite or goethite. The only other conspicuous excursion is identified in the Rietheim Member of the Staffelegg Formation («Posidonienschiefer»), where high contents of organic matter (C_{org} = 2.4 – 5.4 wt.-%) lead to markedly lower grain-density values.

In the underlying Triassic section, values become higher, as does variability. This reflects the lithological heterogeneity, in particular the variable contents of dolomite and anhydrite with their high mineral densities (2.85 and 2.97 g/cm^3, respectively). Fig. 4.3-5 shows the correlation between grain density and dolomite/ankerite contents. Grain density increases linearly with dolomite content, and outliers are due to the presence of anhydrite or organic carbon.

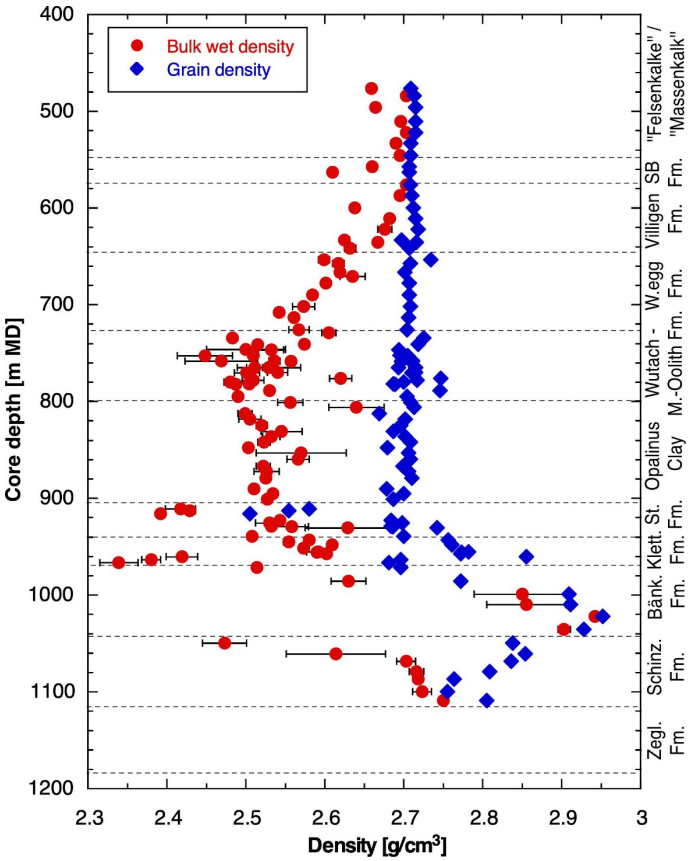

Fig. 4.3-4: Depth profile of bulk wet and grain densities

Black bars of bulk wet density indicate 1σ variability among 3 pieces of the same sample. Analytical error bars of grain density are smaller than the symbol size. Sample 729.13 from the Wutach Formation, containing 39 wt.-% goethite and 3 wt.-% maghemite, has a grain density of 3.278 g/cm^3, which is outside the plotted range.

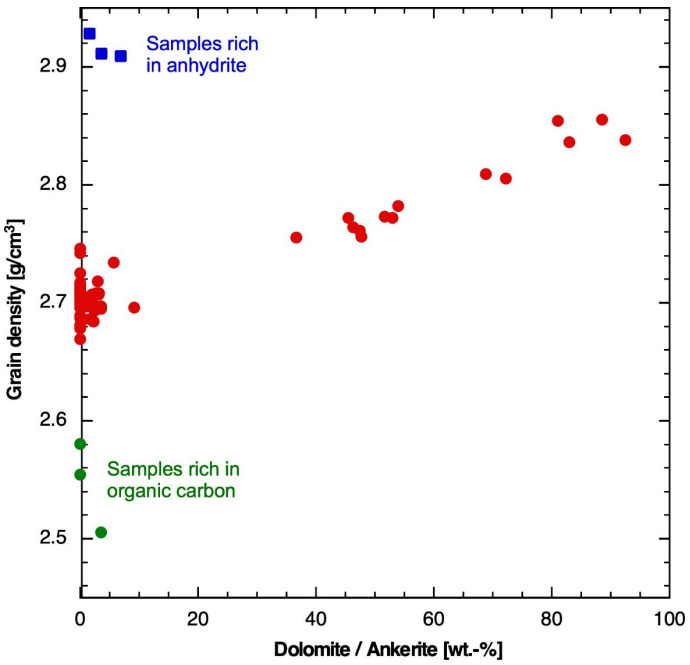

Fig. 4.3-5: Grain density as a function of the contents of dolomite/ankerite

Blue points are from the Bänkerjoch Formation and indicate anhydrite contents > 67 wt.-%. Some other samples with low anhydrite content (< 8 wt.-%) are not separated from the bulk data. Green points (≥ 4 wt.-% organic carbon) are from the Rietheim Member of the Staffelegg Formation.

4.3.3 Bulk wet density

Data are shown in Fig. 4.3-4 as a function of depth. Large error bars for some samples reflect heterogeneity on the cm scale.

4.3.4 Porosity

Three different approaches were used to constrain rock porosity (for details see Waber ed. 2020):

- *Water-loss porosity:* calculation from the gravimetric water content using either bulk wet or grain density.
- *Porosity from isotope diffusive exchange:* calculation from the water content obtained by mass balance using either bulk wet or grain density.
- *Pycnometer porosity:* calculation from bulk dry and grain densities; bulk dry density is calculated from bulk wet density and water content.

Water-loss porosity and porosity from isotope diffusive exchange were calculated using bulk wet density by default. If the latter was not available, grain density was used, by which full water saturation of the pore space was assumed. The graphic in Fig. 4.3-6 shows that the two densities yield near-identical porosities, so the choice of the type of density for the calculation incurs no additional uncertainty.

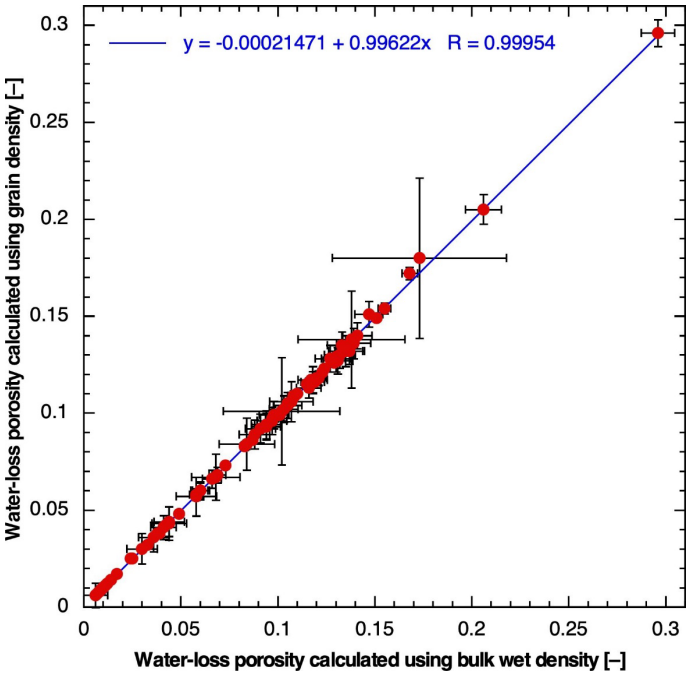

Fig. 4.3-6: Water-loss porosity calculated from gravimetric water content using either bulk wet or grain density

Bars indicate propagated errors, which are dominated by local heterogeneity of water content.

Comparison of porosities obtained by different methods

An excellent linear correlation is observed between water-loss porosity and porosity from isotope diffusive exchange (Fig. 4.3-7). The latter yields about 7% higher values.

A good linear correlation is also found between pycnometer porosity and porosity from isotope diffusive exchange (Fig. 4.3-8). The latter yields about 13%$_{rel}$ higher values. Two outliers are explained by sample heterogeneity (see illustrations in Fig. 4.3-9). Outlier 960.43 m (Klettgau Formation, Gansingen Member) is a porous dolostone with macroporous domains (dissolution vugs) and evident textural heterogeneity on the cm-scale. Outlier 966.63 m (Klettgau Formation, Ergolz Member) is an anhydrite-bearing sandstone with laminae of contrasting grain sizes.

The correlation between water-loss and pycnometer porosity is shown in Fig. 4.3-10. Again, some samples from the Klettgau Formation fall off the trend. Excluding these outliers yields a slope of the regression line of about 0.92.

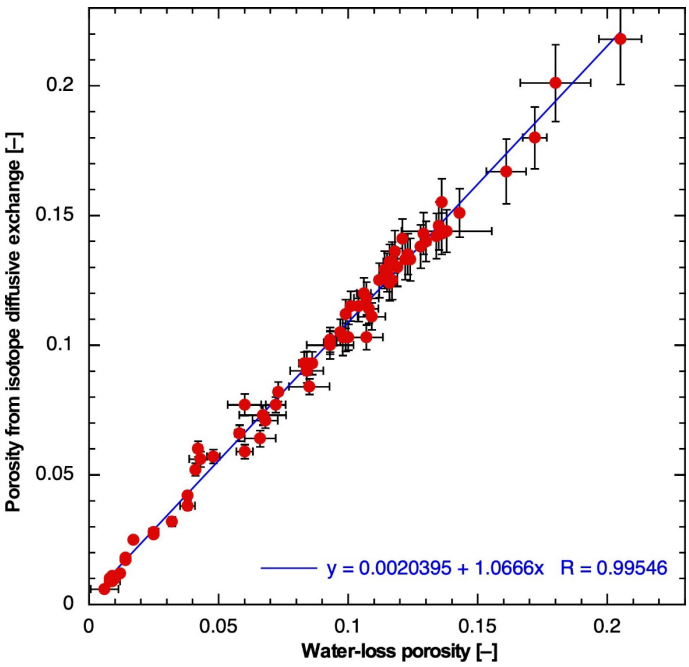

Fig. 4.3-7: Correlation of water-loss porosity and porosity from isotope diffusive exchange
Bars indicate propagated errors. Note that only the gravimetric water contents obtained from the aliquots used for the isotope diffusive exchange experiments were considered for the x-axis of this graph, so the correlation refers to identical sample materials.

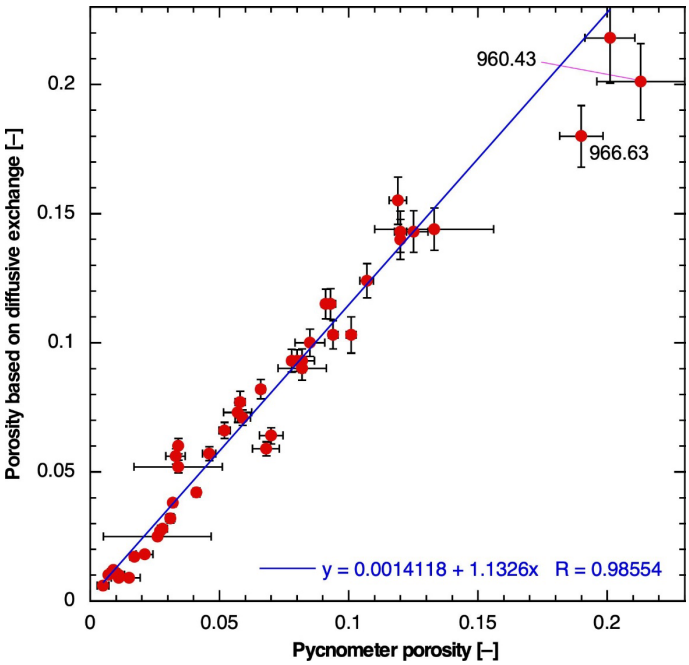

Fig. 4.3-8: Correlation of pycnometer porosity and porosity from isotope diffusive exchange
Bars indicate propagated errors. Marked outliers were excluded from the regression.

960.43 m
(Klettgau Formation,
Gansingen Member)

966.63 m
(Klettgau Formation,
Ergolz Member)

Fig. 4.3-9: Illustrations of heterogeneous samples
Width of photographs is 10 cm.

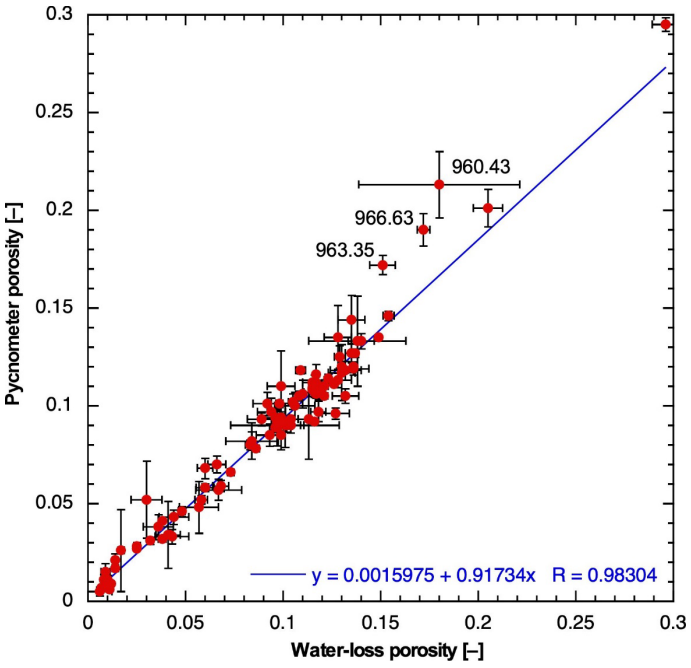

Fig. 4.3-10: Correlation of water-loss and pycnometer porosity
Bars indicate propagated errors. The indicated outliers were excluded from the regression.

Depth trends

In Fig. 4.3-11, porosity is shown as a function of depth. The shape of the profile is similar to that of water content (Fig. 4.3-1 and 4.3-3), including the systematic trends. The comments made on the distribution of water content with depth (Section 4.3.1) also apply to porosity.

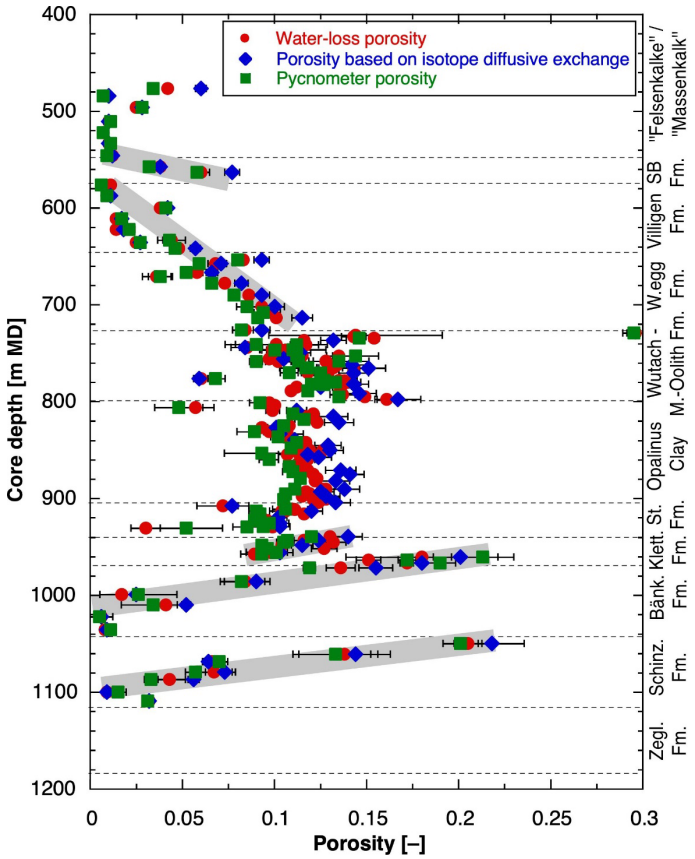

Fig. 4.3-11: Depth trends of porosities obtained by different methods

Trends are indicated for the Malm and Triassic sections (thick grey bars). Trends in the Dogger-Lias section are analogous to those shown for water content in Fig. 4.3-3.

Porosity as a function of mineralogical composition

The correlation of porosity with clay-mineral content is shown in Fig 4.3-12. When considering all available data (Fig. 4.3-12a), a general positive correlation can be identified, but scatter is substantial. Marked outliers towards high porosity at comparatively low clay-mineral content are dolostones of the Klettgau and Schinznach Formations and sandstones of the Klettgau Formation. The dolostones were affected by diagenetic dissolution to some degree, and so their porosity is not the result of compaction and cementation alone. The sandstones have a grain-supported fabric, which limits the compaction of the intergranular space. Sample 729.13 from the Wutach Formation is from a goethite-rich Fe-oolite. Sample 1'022.28, an outlier towards low porosity, contains 67 wt.-% anhydrite. When only samples from the Malm – Dogger – Lias section are considered, i.e. when the mineralogically and texturally more heterogeneous samples from the Triassic are excluded, a more systematic correlation is obtained (Fig. 4.3-12b).

The slope of the correlation in Fig. 4.3-12 is steeper for clay-mineral contents in the range of 0 – 30 wt.-% and becomes flatter at higher clay-mineral contents. The presence of anhydrite tends to reduce porosity for a given clay-mineral content. Fig. 4.3-13 illustrates that porosity approaches 0 for anhydrite-rich samples.

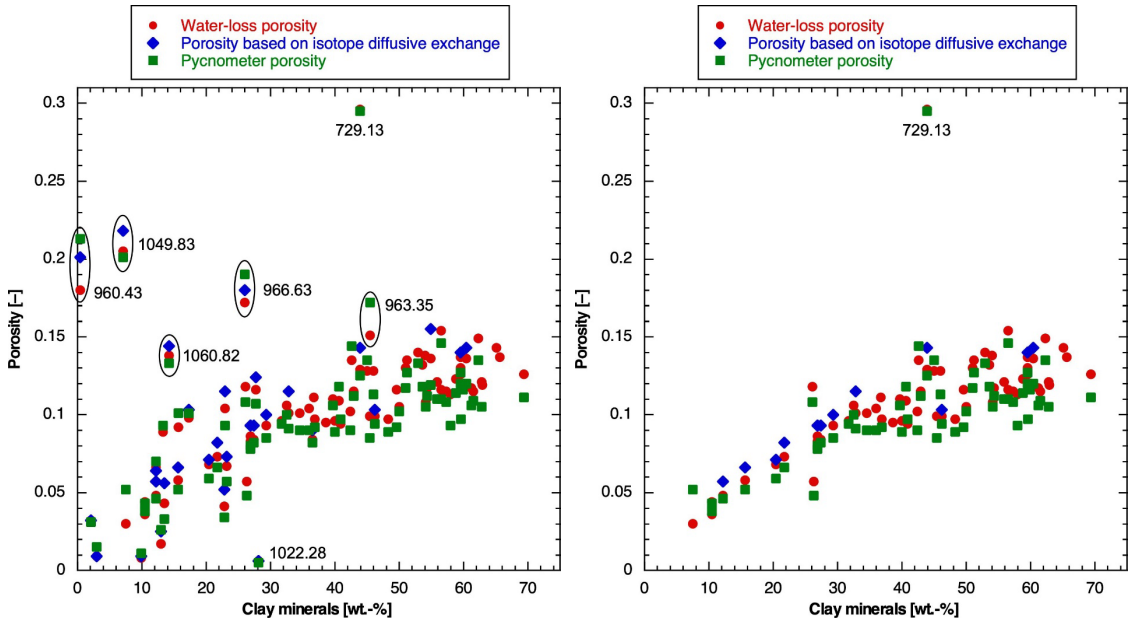

Fig. 4.3-12: Porosity as a function of clay-mineral content. a) all data, b) data from the section Malm – Dogger – Lias

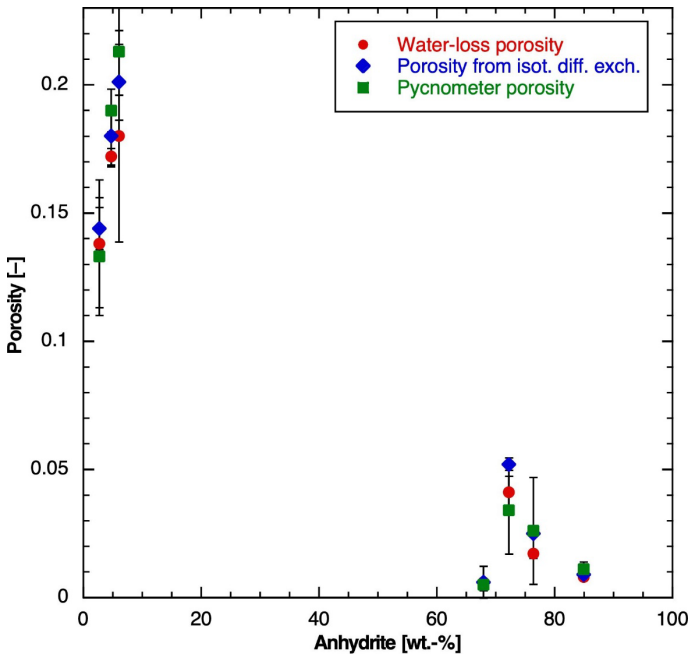

Fig. 4.3-13: Porosity of anhydrite-bearing samples
Bars indicate propagated errors.

4.3.5 Specific surface area and pore size distributions from N_2 ad-/desorption

Thomas Gimmi

Depth trends

Nitrogen adsorption data were obtained for 17 samples from the upper and lower confining units of the Opalinus Clay, comprising very different lithologies (Tab. 4.3-2). These included samples on which through-diffusion experiments (PSI, Van Loon & Glaus, 2023), squeezing experiments, or regular porewater investigations were performed[6]. One sample each was from the Villigen Formation (633.23 m), the Wutach Formation (729.13 m), the Variansmergel Formation (732.784 m), the Wedelsandstein Formation (779.96 m), and the «Murchisonae-Oolith Formation» (792.72 m), four from the «Parkinsoni-Württembergica-Schichten» (752.73 m, 758.02 m, 758.23 m and 765.21 m), five from the Staffelegg Formation (at 911.28 m, 912.69 m and 915.94 m from the Rietheim Member, at 925.51 m from the Frick Member, at 930.53 m from the Beggingen Member), and three from the Klettgau Formation (at 955.40 m and 957.28 m from the Seebi Member, at 963.35 m from the Ergolz Member).

Because of the comparably small number of samples and the lack of data from the Opalinus Clay, the depth trends of the specific surface area S_{BET} are not very clear (Fig. 4.3-14). However, a comparison with the data obtained from the Stadel-3-1 and the Bülach-1-1 boreholes (right plot in Fig. 4.3-14) shows that the variation with the rock formation is similar in all these boreholes. Note that the samples from Bülach-1-1 with low S_{BET} values in the upper part of the Wutach Formation to «Murchisonae-Oolith Formation» originate from the «Herrenwis Unit». In Stadel-2-1, this unit is thinner and located closer to the Opalinus Clay, and no nitrogen adsorption data are available.

As N_2 cannot reach interlayer pores of smectites, S_{BET} represents surfaces of external (non-interlayer) pores. The largest values of about 44 and 41 m^2/g were found for the Wutach sample (729.13 m) and the Variansmergel sample (732.74 m), respectively, in the uppermost part of the zone denoted as Wutach Formation – «Murchisonae-Oolith Formation». The first one is a goethite- and clay-rich iron-oolith, the second a claystone with 65 wt.-% of clay minerals. Lowest values of 2.75 m^2/g and 10.5 m^2/g were determined for limestone samples from the Staffelegg Formation (Beggingen Member, 930.53 m) and from the Villigen Formation (633.23 m), respectively. The samples from the «Murchisonae-Oolith Formation» to the overlying «Parkinsoni-Württembergica-Schichten» have values between ~ 34 – 38 m^2/g). As observed in other boreholes, the S_{BET} values in the Staffelegg Formation span a considerable range (~ 3 – 34 m^2/g), due to heterogeneities regarding depositional environment and diagenesis.

The variation of the specific surface area S_{BET} with depth is generally related to trends observed in other physical and mineralogical properties of samples from the Stadel-2-1 borehole, such as the bulk dry density, the gravimetric water content, the water-loss porosity, or the clay-mineral content.

---

6 This batch of sample was intentionally focussed on the confining units.

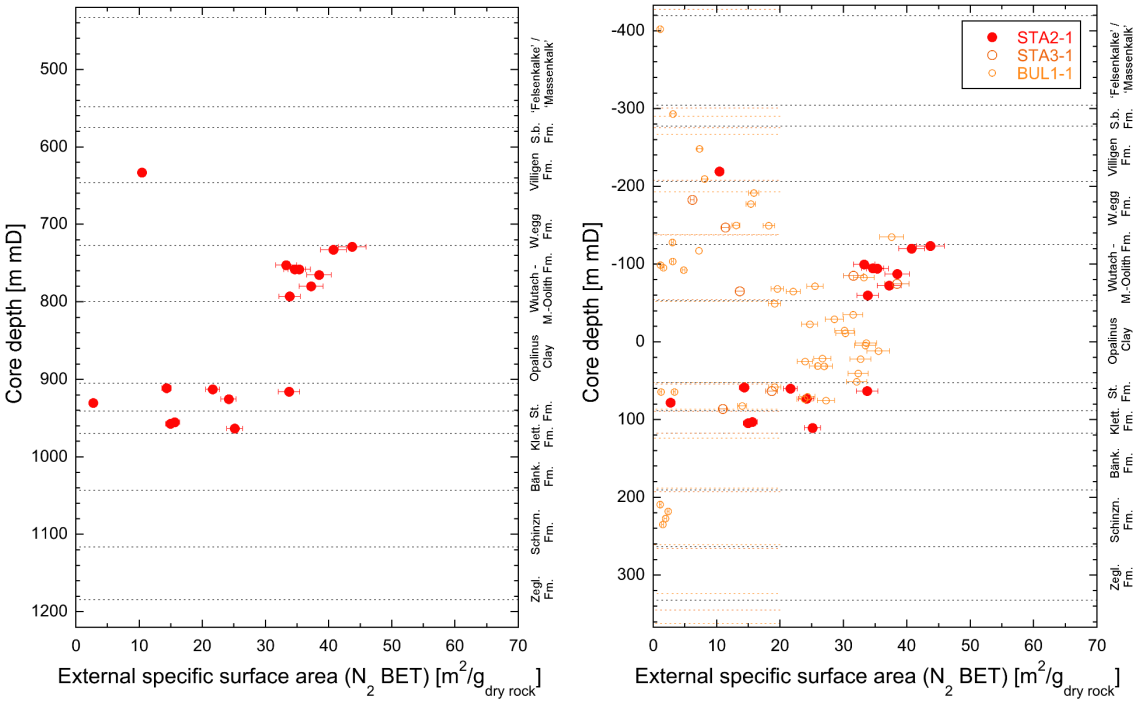

Fig. 4.3-14: Specific surface area (S_{BET}) derived from N_2 adsorption as a function of depth; left: Data from the Stadel-2-1 borehole, right: Comparison of data from the Stadel-2-1 borehole with those from the Stadel-3-1 and Bülach-1-1 boreholes, with depth relative to the center of Opalinus Clay

S_{BET} represents external surfaces only. The total specific surface area, including interlayer surfaces, would be larger depending on the smectite content of the sample. Errors resulting from sample preparation and handling are estimated to be ± 5% in general and ± 10% for $S_{BET} < 2$ m^2 g^{-1}, as given by the error bars. In the right plot, the orange dashed lines show formation boundaries for the Stadel-3-1 and the Bülach-1-1 borehole.

Correlation of S_{BET} with water content and clay-mineral content

The specific surface area S_{BET} tends to increase with the gravimetric water content (Fig. 4.3-15). The correlation is, however, very weak, which is also related to the small number and the lithological differences between the chosen samples from the confining units. The sample from the Wutach Formation (729.13 m) with the largest S_{BET} value has an over proportionally large water content of 13 wt.-%, such that this data point lies far to the right of the weak correlation seen for the other points from the Stadel-2-1 borehole or for the data points from the Bülach-1-1 borehole. Note that this sample has a goethite content of 39 wt.-%, so it is also exotic from a mineralogical perspective. One sample from the Klettgau Formation (963.35 m, Ergolz Member) and one from the Staffelegg Formation (911.28 m, Rietheim Member) also have comparably large water contents and thus tend to lie to the right of the general trend line. The lowest S_{BET} value of 2.75 m^2/g for the limestone sample from the lower Staffelegg Formation (930.53 m, Beggingen Member) is associated with a very small water content.

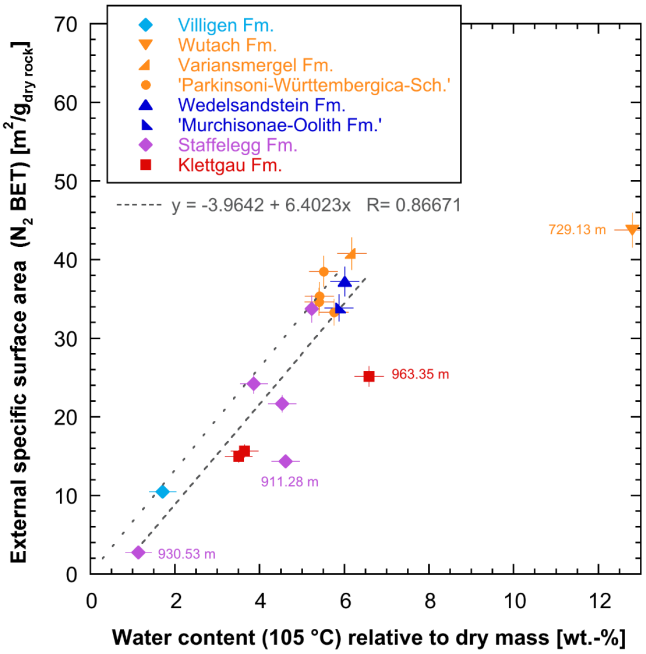

Fig. 4.3-15: Specific surface area (S_{BET}) derived from N_2 adsorption plotted against the gravimetric water content relative to the dry mass of the samples

Error bars show estimated errors for the water content (based on standard deviations of other samples) and estimated errors for S_{BET}. The dotted line shows the regression obtained for the Bülach-1-1 data set which includes samples from all formations. The slope is similar to a regression for the STA2-1 data when excluding the sample at 729.13 m (dashed line; a regression for all speficially chosen samples from STA3-1 is considered to be less meaningful).

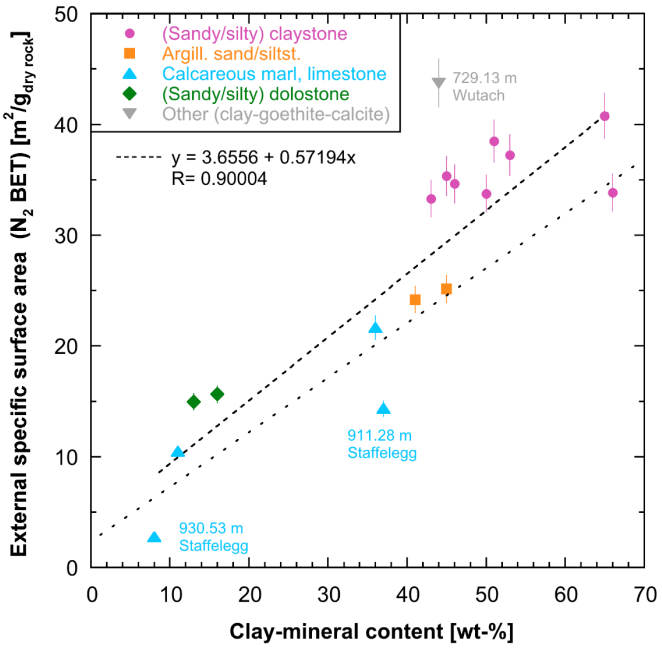

Fig. 4.3-16: Relation between external specific surface area (S_{BET}) derived from N_2 adsorption and content of clay minerals

The samples are assigned to three classes according to their positions in the Füchtbauer diagram (i.e., according to lithological rock types). The dashed line is a regression on the Stadel-2-1 data excluding the sample at 729.13 m; the dotted line shows the regression obtained for the Bülach-1-1 data including samples from all formations.

The specific surface area S_{BET} also tends to increase with the clay-mineral content (Fig. 4.3-16), but the correlation is again weak for the specifically chosen samples from the Stadel-2-1 borehole. While the Wutach sample (729.13 m) lies below the general trend of S_{BET} with the water content (Fig. 4.3-15), it lies above the general trend of S_{BET} with the clay-mineral content (Fig. 4.3-16) because its water content or porosity is very large compared to its clay-mineral content (cf. Fig. 4.3-12). The argillaceous sandstone/siltstone sample from the Klettgau Formation (963.35 m) does no longer appear as an outlier when plotting S_{BET} against the clay-mineral content (Fig. 4.3-16); it has also a comparably large water content (*cf.* Fig. 4.3-12).

When plotting S_{BET} against individual clay end-member contents (Fig. 4.3-17), positive correlations exist with the illite and the smectite end-member contents, similarly as reported for the Bülach-1-1 and the Stadel-3-1 data. The Klettgau sample (963.35 m) and the Staffelegg sample (911.28 m) represent outliers (no individual clay-mineral contents are available for the other previous outlier from the Wutach Formation). When excluding these outliers, the slope of S_{BET} vs. illite end-member content (1.0 $m^2\ g^{-1}$ wt.-$\%^{-1}$) is similar to that for the Bülach-1-1 data (1.1 $m^2\ g^{-1}$ wt.-$\%^{-1}$). Only very vague trends exist between S_{BET} and kaolinite or chlorite end-member contents, like for the Bülach-1-1 data.

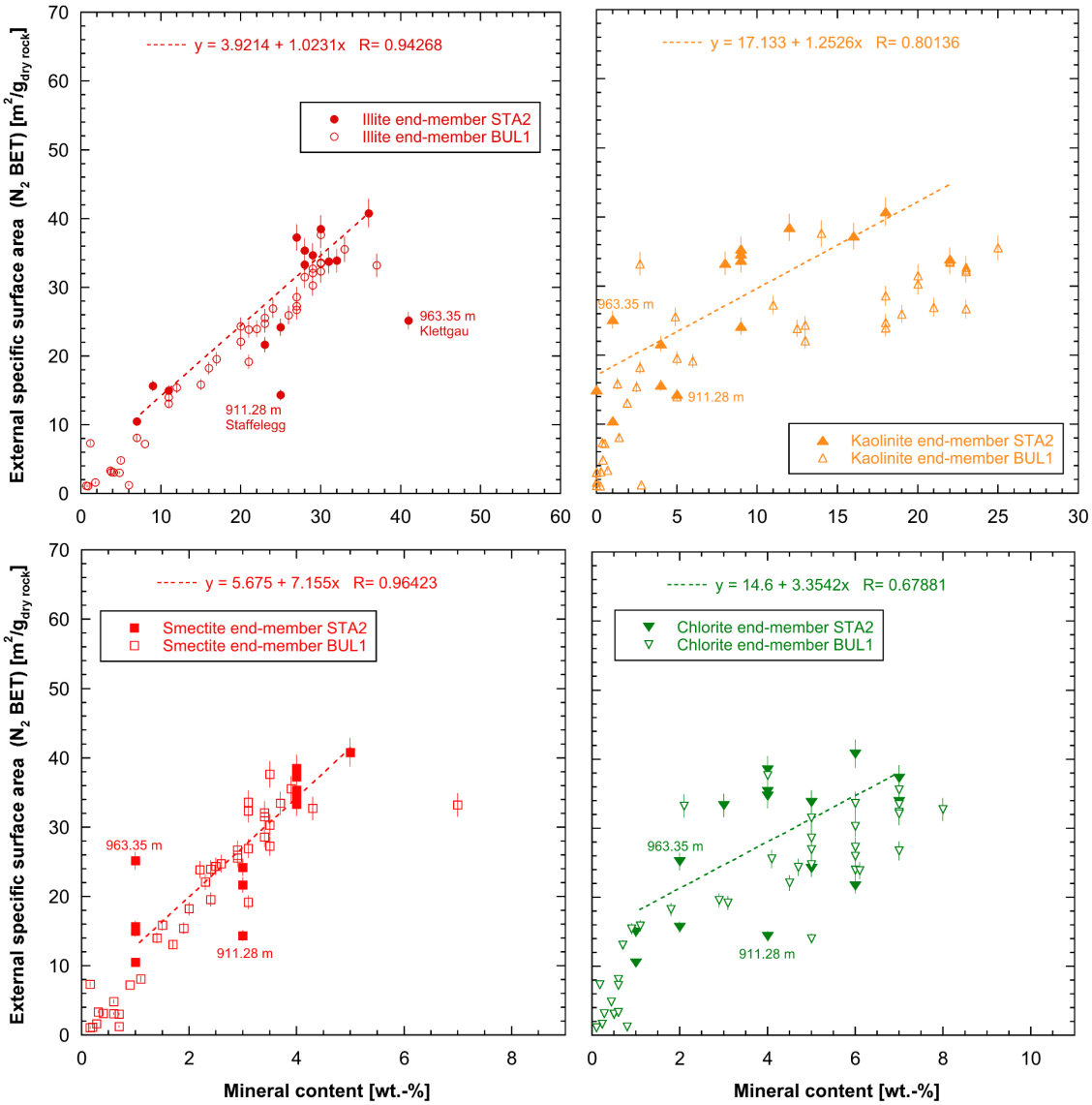

Fig. 4.3-17: Relation between external specific surface area (S_{BET}) derived from N_2 adsorption and contents of specific clay mineral end-members

The solid symbols and the regression line represent the Stadel-2-1 data which do not include any samples from the Opalinus Clay (the three marked samples are excluded from the regression); the open symbols show Bülach-1-1 data including samples from all formations.

Average sizes of external pores derived from S_{BET}

Average sizes of external pores were estimated from the specific surface area S_{BET} and the water content per dry mass WC_d as:

$$\overline{r_{ext}} = WC_d/(\rho_w\, S_{BET})$$

with ρ_w the water density taken to be 1 g mL^{-1}. This calculation assumes negligible pore volumes in interlayer pores, i.e., it attributes the measured water content to external pores only (which is not appropriate for samples with relevant smectite end-member contents).

The slope of the linear relation in Fig. 4.3-15 represents S_{BET}/WC_d. From the inverse of this slope (6.40 m^2 g^{-1} wt.-%$^{-1}$ when excluding the mentioned outliers), we obtain an overall average layer thickness (or radius) of external pores of 1.6 nm, which corresponds to about 5 to 6 water layers. A similar average value was obtained for the samples from Bülach-1-1, which included many claystone samples.

Instead of calculating an overall average from the linear regression, it is more interesting to derive an average layer thickness for each sample. Fig. 4.3-18 plots average external pore radii (attributing all water to external surfaces) for each sample as a function of the gravimetric water content per dry solid mass (a) and as a function of the total clay-mineral content (b). The values range between radii of 1.4 and 4.1 nm (diameter of 2.9 – 8.3 nm). Comparably large values were obtained for two Staffelegg samples (Beggingen Member, 930.53 m; Rietheim Member, 911.28 m), the Wutach Formation sample (729.13 m), and a Klettgau Formation sample (963.35 m), that is, samples with comparably small S_{BET} values or large water contents. The five samples from the Staffelegg formation show rather variable values with radii between 1.6 and 4.1 nm (diameters 3.1 – 8.3 nm). The two dolostone samples show intermediate radii of ~ 2.3 nm (diameters ~ 4.7 nm). The four (very sandy/silty) claystone samples from the «Parkinsoni-Württembergica-Schichten» show only a small range (radii of 1.4 – 1.7 nm, diameters 2.9 – 3.5 nm). These samples, as well as those with similar mineralogy from the Variansmergel, the Wedelsandstein, the «Murchisonae-Oolith Formation», and one from the Staffelegg Formation (Rietheim Member, 915.94 m, radius 1.6 nm, diameter 3.1 nm) have 4 – 5 wt.-% smectite end-member contents, so average pore radii considering also interlayer pores would tend to be slightly smaller than the calculated average external pore radii.

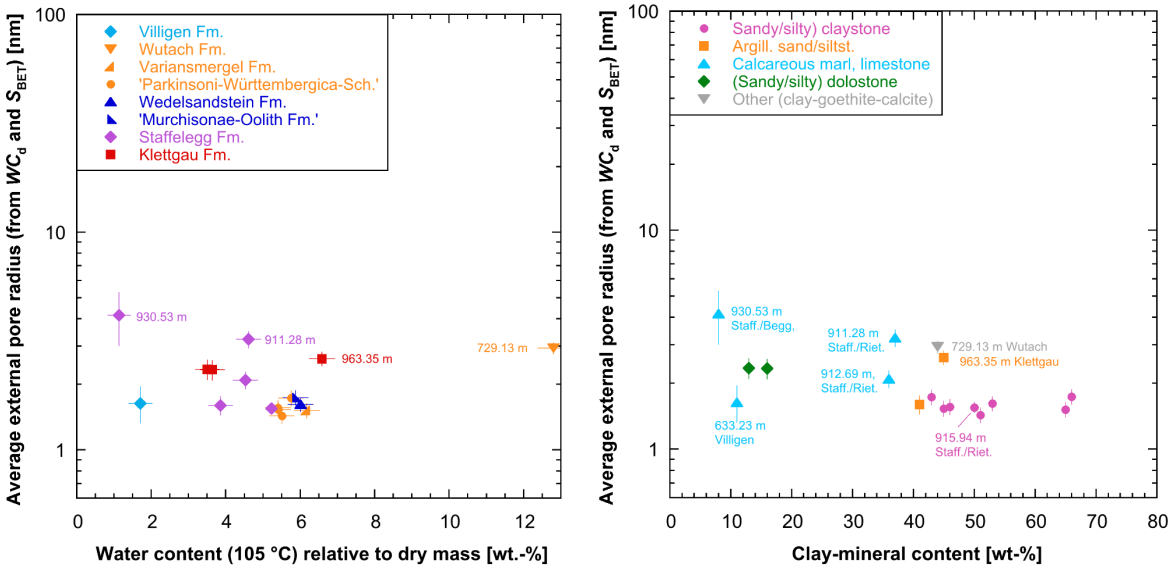

Fig. 4.3-18: Average external pore radius calculated from S_{BET} and the gravimetric water content (assuming insignificant interlayer pore volume) plotted against the gravimetric water content per dry mass of the samples (a) and against the total clay-mineral content (b)

Samples are grouped according to geological units (a) or according to rock lithology (b). Error bars show estimated errors for the water content (based on standard deviations of other samples) and propagated errors for the average external pore radius.

Distribution of external pore sizes derived from N_2 isotherms

Size distributions (diameters) of external pores were derived from N_2 ad- and desorption isotherms (using the standard BJH algorithm). Results from N_2 desorption for all samples are shown in Fig. 4.3-19, grouped according to rock lithology. Most samples show a clear, partly prominent peak at a diameter of about 4 nm in these curves. These peaks are typically related to the closure of the hysteresis of the isotherm and are thus attributed to liquid instabilities (instability of the configuration of liquid nitrogen during desorption) rather than to a distinct pore volume in this size range. The pore volume drained at this point is in reality very likely distributed over a range of (mostly) larger pore sizes. Hysteresis and thus a clear closure peak is generally interpreted as indicating a relatively complex pore architecture (e.g., Thommes et al. 2015), as especially found in clay-rich samples.

The two samples classified as limestones according to the Füchtbauer nomenclature (633.23 m, Villigen Formation; 930.53 m, Staffelegg Formation, Beggingen Member) show a major, comparably narrow peak at a diameter of ~ 100 nm besides the medium or small hysteresis peak. The sample from 633.23 m shows also a second, broader peak near diameters of 10 – 20 nm. The size distributions of the two calcareous marls (911.28 m and 912.69 m; Staffelegg Formation, Rietheim Member) are distinctly different from those of the limestones, with important and broad peaks at a diameter of ~ 6 nm, and secondary peaks near ~ 60 nm. They both also show a large hysteresis peak, which indicates a more complex pore network compared to the limestone samples. This is probably related to their considerable clay-mineral content of 36 – 37 wt.-% and their comparably high content of organic matter (4.44 – 4.70 wt.-%).

The very argillaceous sandstone/siltstone sample at 925.51 m (Staffelegg Formation, Frick Member, clay-mineral content of 41 wt.-%; Fig. 4.3-19b) exhibits a typical distribution for this class of samples, with a strong hysteresis peak besides two comparably weak, but broad peaks around ~ 10 nm and ~ 60 nm. The other very argillaceous sandstone/siltstone sample (963.35 m, Klettgau Formation, Ergolz Member, clay-mineral content of 45 wt.-%) shows a less typical size distribution for this class, with only a medium hysteresis peak followed by a single, broad peak between ~4 – 60 nm (peak at ~10 nm).

The very sandy/silty claystone samples (752.73 m, 758.02 m, 758.23 m, 779.96 m, 792.72 m; Fig. 4.3-19c) and two of the claystone samples (732.74 m, 765.21 m) exhibit similar diameter size distributions, with an important peak at ~ 6 – 10 nm and a secondary peak at ~ 60 – 100 nm, in addition to the strong hysteresis peak. The peaks of the sample at 732.74 m tend to appear at the lower diameter range within this group of samples. The diameter distribution of the claystone sample at 915.94 m (Staffelegg Formation, Rietheim Member) is clearly shifted to smaller pores: It has a very strong hysteresis peak that appears to overlap with an important peak at a diameter of ~ 4 nm (with a shoulder up to ~ 10 nm) and only a very weak secondary peak at ~ 60 nm.

The diameter size distribution of samples classified as (very sandy/silty) dolostones (955.40 m and 957.28 m) are shown in Fig. 4.3-19d. They are both characterised by a small hysteresis peak followed by a very extended peak with diameters ranging from ~ 4 – 200 nm (peak at ~ 10 nm), consistent with their low clay-mineral contents of 13 – 16 wt.-%.

Finally, the diameter size distribution of the sample from the Wutach Formation that contains considerable amounts of clay minerals, goethite and calcite (no classification according to the Füchtbauer scheme) is presented in Fig. 4.3-19e. It is similar to that of the very sandy/silty claystone sample from the «Murchisonae-Oolith Formation» (792.72 m), with a strong hysteresis peak, an important peak around ~6 nm and a weak second peak around 100 nm.

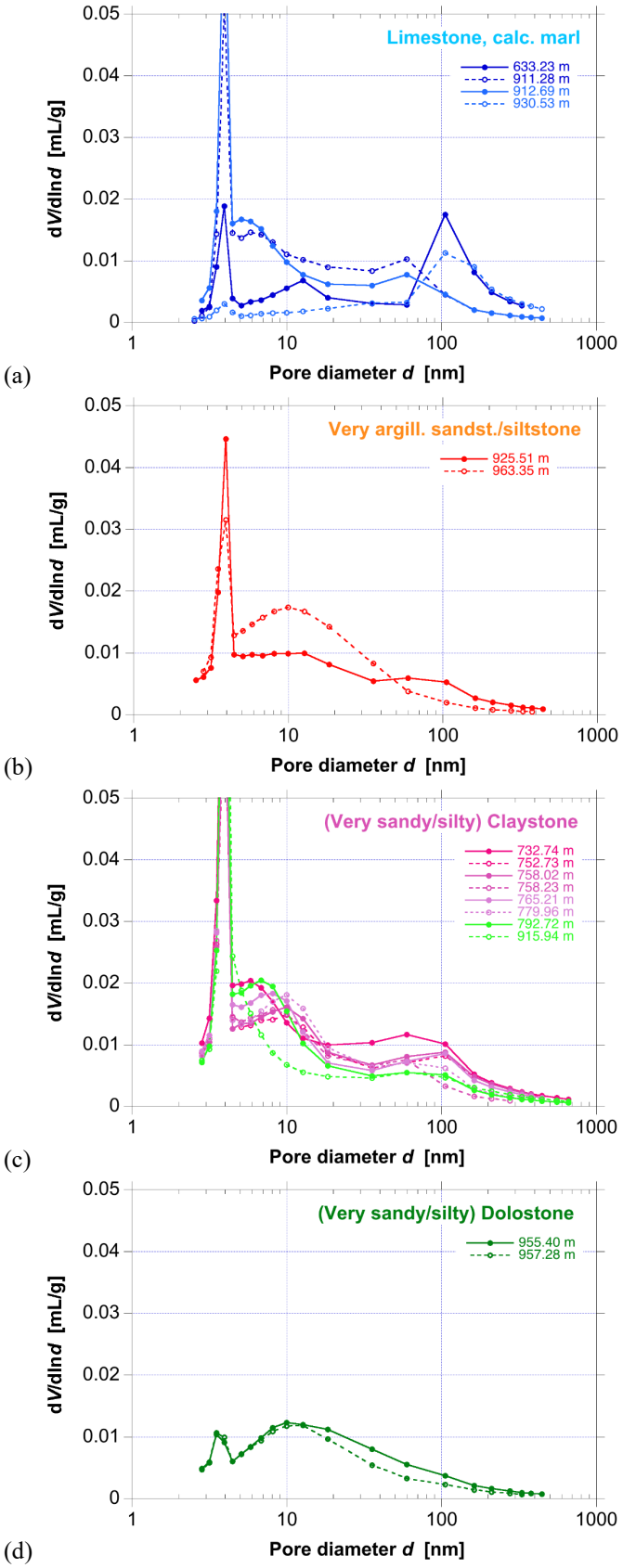

Fig. 4.3-19: (see opposite site)

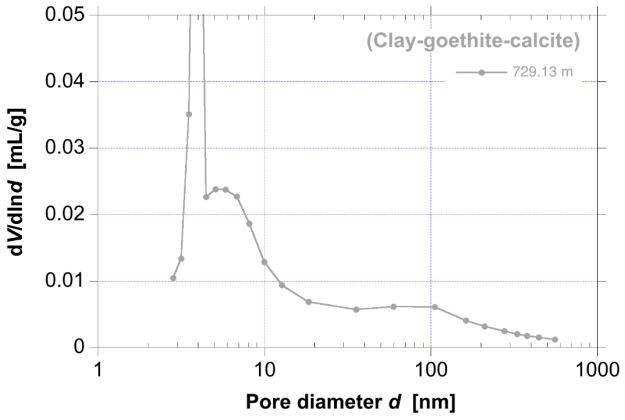

(e)

Fig. 4.3-19: Distribution of (external) pore diameters derived from N_2 desorption

(a) Limestones (633.23 m, 930.53 m) and calcareous marls (911.28 m, 912.69 m), (b) very argillaceous sandstone/siltstones (925.51 m, 963.35 m), (c) very sandy/silty claystones (752.73 m, 758.02 m, 758.23 m, 779.96 m, 792.72 m) and claystones (732.74 m, 765.21 m, 915.94 m), (d) very sandy/silty dolostone (957.28 m) and dolostone (955.40 m), (e) sample 729.13 m with important amounts of clay minerals, goethite, and calcite (no Füchtbauer name)

The reliability of the pore size distribution results was tested by comparing maximum adsorbed amounts of N_2 at highest N_2 pressures, expressed as wt.-% H_2O, with the samples' water contents (Fig. 4.3-20). Many values are near the 1:1 line, lending generally confidence to the derived size distributions. For the two limestone samples from the Villigen Formation (633.23 m) and the Staffelegg Formation (930.53 m, Beggingen Member) with low water contents (1.7 and 1.1 wt.-%, respectively), the total amount of adsorbed N_2 clearly exceeds the water contents, meaning that either some cm-scale heterogeneity exists, or that the frequency of some (probably larger) pores was overestimated by N_2 adsorption. The comparably large relative standard deviations of the water content of 18% and 27% for these two samples, respectively, indicate important heterogeneity or uncertainty, but the differences seen in Fig. 4.3-20 are clearly above what can be expected just by this uncertainty. For the two samples from the Ergolz Member in the Klettgau Formation (963.35 m) and from the Wutach Formation (729.13 m), the total adsorbed amount of N_2 is clearly smaller than their water content (sample from Klettgau Formation: ~ 4.0 mL/g, water content ~ 6.6 mL/g; sample from Wutach Formation: ~ 6.4 mL/g, water content ~ 12.8 mL/g). The sample from the Wutach Formation is a goethite- and clay-rich Fe-oolith with a very large water content (*cf.* Figs. 4-3.3, 4-3.12). In both cases, it seems unlikely that the discrepancy between amount of adsorbed N_2 and water content is related to small-scale heterogeneity (the reported relative standard deviations of the water content for these samples are 6% or below only), so it may indicate incomplete adsorption of N_2 and thus an underestimation of the frequency of some (probably micro-) pores.

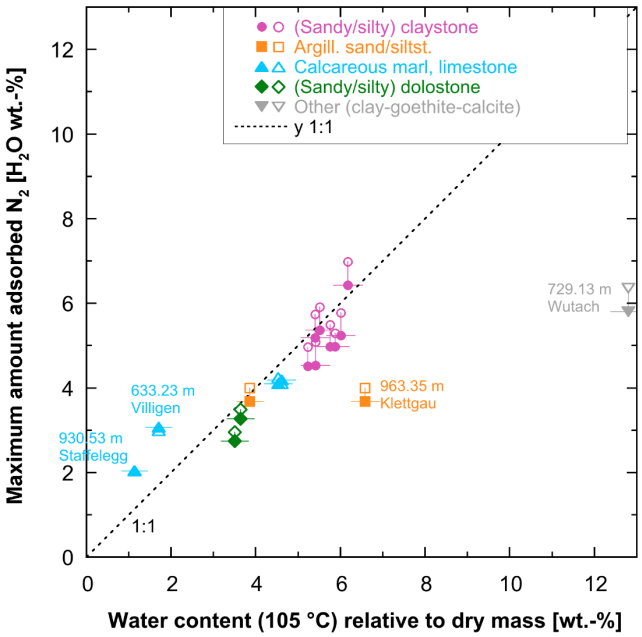

Fig. 4.3-20: Comparison of maximum amount of adsorbed N_2 (recalculated to H_2O wt.-%) with water content per dry sample mass

Open symbols: adsorption, closed symbols: desorption

Average sizes of external pores based on pore size distributions calculated from the N_2 isotherms

Average sizes of external pores cannot only be obtained from S_{BET} and the water content as shown above but also from the pore size distribution derived from N_2 isotherms. In both cases, it is assumed that interlayer pore volumes (which are not probed by N_2 adsorption) are insignificant. Radii directly derived by averaging the BJH pore size distributions (Fig. 4.3-21) are similar to those estimated from S_{BET} and the gravimetric water content (Fig. 4.3-18) for the Wutach Formation sample (729.13 m), and larger by a factor of 1.3 – 3.9 for all other samples. They tend to be smallest for the (sandy/silty) claystone samples and the argillaceous sandstone/siltstone samples (radii of 2.5 – 4.0 nm and diameter of ~ 5 – 8.1 nm), intermediate for the calcareous marl and the dolostone samples (radii of 3.3 – 5.3 nm, diameter of 6.6 – 10.7 nm), and largest for the limestone samples at 633.23 m and 930.5 m (radii of 5.1 – 14.5 nm, diameter of 10.3 – 29 nm, the latter value for the sample from the Beggingen Member in the Staffelegg Formation). These trends are similar as those observed in the Bülach-1-1 borehole.

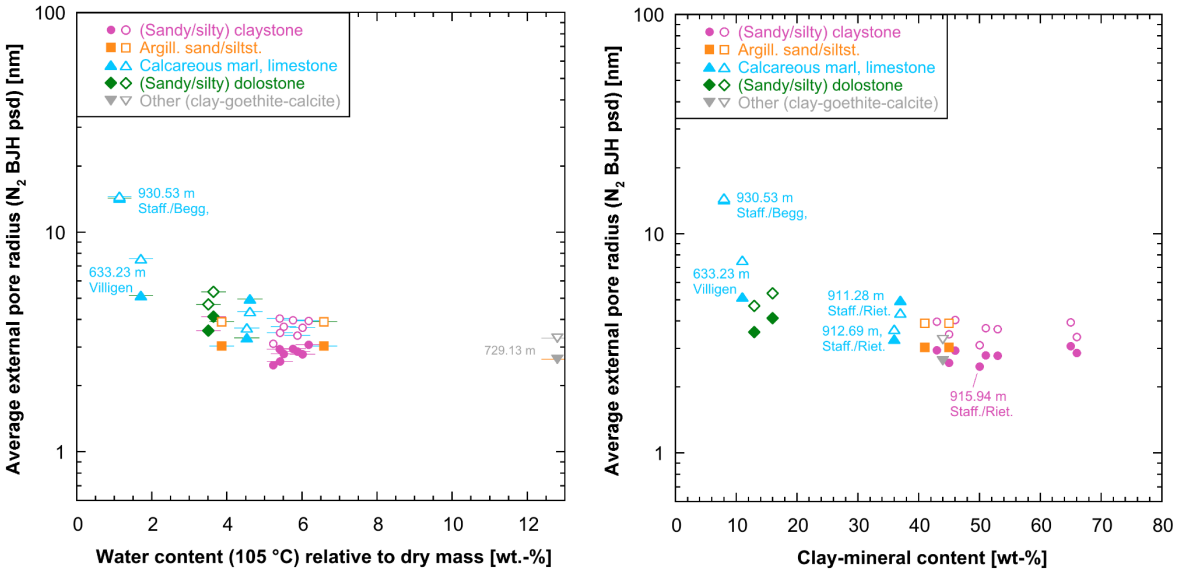

Fig. 4.3-21: Average external pore radius (assuming insignificant interlayer pore volume) based on the BJH pore size distribution from the N_2 isotherms (closed symbols: adsorption; open symbols: desorption) plotted against the gravimetric water content per dry mass of the samples (a) and against the total clay-mineral content (b)

Samples are grouped according to rock lithology. Error bars show estimated errors for the water content per dry mass (based on standard deviations of other samples)

4.4 Data from aqueous extraction tests

Carmen Zwahlen

Aqueous extraction (AqEx) tests are a simple but useful method to improve the understanding of the porewater – rock system across a sequence of sedimentary rocks if carried out at regular intervals. In this section, we present the data from aqueous extraction tests performed at a solid to liquid ratio of approximately 1. The data are discussed further in Chapter 5. The full dataset can be found in Appendix A, and details about the method are given in Waber (ed.) (2020).

4.4.1 Sample material and overview of analytical work

A total of 88 moisture-preserved drill core samples (PW, AD, SQ) from the Malm to the Schinznach Formation were subjected to aqueous extraction tests. Additionally, unsqueezed parts of the four SQ samples were also extracted after drying in order to compare the Cl and Br inventories of wet material ("pre") and dried material ("post"). The samples from the Schinznach Formation were extracted from coarser subsamples (2 cm pieces) and compared to additional extracts at normal sample size (1 cm pieces) and also after milling (100 µm grains). The coarser subsamples were left to react for 48h instead of 24h to allow a complete exchange with the porewater.

Additionally, the data of the wet extracted solutions that include analysis of cations were used to model the mineral saturation states and the partial pressure of CO_2. These parameters were calculated with the PHREEQC Version 3 code (Parkhurst & Appelo 2013) and the PSI/Nagra thermodynamic database (Thoenen et al. 2014) assuming a temperature of 25 °C.

Tab. 4.4-1: Summary of analytical work performed on samples for aqueous extraction tests from the different geological formations (excluding duplicate and post-mortem extracts of AD and SQ experiments*; cf.* Sections 4.7.4 and 4.6.5)

Sample type: PW: porewater sample, AD: advective displacement sample, SQ: squeezing sample, AqEx: aqueous extraction tests, *S/L*: solid to liquid ratio.

Group	**Formation**	**Sample type**	**LAB**	**AqEx at *S/L* 1, pH, Alkalinity, Anions only**	**AqEx at *S/L* 1, pH, Alkalinity, Anions & Cations**
Malm	«Felsenkalke» + «Massenkalk»	PW	RWI	7	
Malm	Schwarzbach Fm.	PW	RWI	2	
Malm	Villigen Fm.	PW	RWI	7	
Malm	Wildegg Fm.	PW	RWI	8	
Dogger	Wutach Fm.	PW	RWI	1	
Dogger	Variansmergel Fm.	PW, SQ	RWI	2	
Dogger	«Parkinsoni-Württembergica-Sch.»	PW	RWI	5	
Dogger	«Herrenwis Unit»	PW	RWI	3	
Dogger	«Humphriesioolith Fm.»	PW, AD	RWI	1	1
Dogger	Wedelsandstein Fm.	PW	RWI	2	
Dogger	«Murchisonae-Oolith Fm.»	PW, SQ	RWI	3	
Dogger	Opalinus Clay	PW, AD, SQ	RWI	18	2
Lias	Staffelegg Fm.	PW, AD, SQ	RWI	5	3
Keuper	Klettgau Fm.	PW	RWI		5
Keuper	Bänkerjoch Fm.	PW	RWI		6
Muschelkalk	Schinznach Fm.	PW	RWI		7
Total		PW, AD, SQ	RWI	64	24

4.4.2 Aqueous extraction tests at a *S/L* of ~ 1

Ion concentrations in aqueous extracts have a limited significance if they are not recalculated to porewater concentrations. For cations possibly involved in reactions (ion exchange/sorption, dissolution/precipitation), this is not feasible. For conservative anions, it can be based on the measured water content (leading to bulk porewater concentrations) or additionally corrected for anion exclusion (leading to concentrations in the anion-accessible porewater, here called 'free' porewater concentrations). For chemically conservative components, this recalculation is established in Chapter 5. Thus, in this section only ion ratios are presented that are independent of the recalculation formalisms, as well as bulk porewater concentrations for Cl and Br.

4.4.2.1 Contamination by drilling fluid

During sample preparation, approximately 1.5 cm of rim material is removed from the drill core samples to avoid contamination by the drilling fluid. However, in porous and permeable rocks such as e.g. dolostones or sandstones, the drilling fluid might reach the central parts of a drill core. This was already observed in a few samples from the Bülach-1-1, Trüllikon-1-1, Marthalen-1-1, Bözberg-1-1 and Stadel-3-1 boreholes (Mazurek et al. 2021; Aschwanden et al. 2021 & 2022; Mäder et al. 2021; Wersin et al. 2022).

The drilling fluid was a potassium silicate mud down to the upper part of the Schinznach Formation, a water based polymer drilling mud until the bottom of the Schinznach Formation and a NaCl drilling mud below (Tab. 2-4). The K-silicate drilling mud is highly alkaline, characterised by a high Si and K concentration (approx. 40 g/L Si, 70 g/L K, mostly balanced by OH) and only a small portion is required to affect an entire aqueous extract. The K-silicate drilling mud contains SO_4, Cl and Na concentrations that do not differ much or are lower than porewater concentrations and thus bear much less potential to contaminate the aqueous extracts (drilling mud approx. 0.9 g/L SO_4, 0.5 g/L Cl and 3 g/L Na; Tab. 2-5).

In this borehole, we identified three samples from the Klettgau and Schinznach Formation that show evidence for contamination by the K-Si-drilling fluid for selective components (Tab. 4.4-2). All three samples exhibit a high K concentration and two of them also a Na/K ratio below 1 (Fig. 4.4-5), which is difficult to reach through an evolving marine porewater in the corresponding formations, or by later processes. Additionally, two of the contaminated samples have elevated alkalinity values and in case of the sample at 1'049.83m depth also a high pH value that points towards contamination by the drilling fluid (Tab. 4.4-2). These contaminated samples are argillaceous sandstones or dolostones with a high porosity and likely elevated permeability allowing percolation of the drilling fluid to central parts of the drill core sample.

The extent of contamination can be estimated based on the K concentration of the drilling mud and the assumption that all measured K in the aqueous extracts derives from the drilling mud. For the sample at 960.43 m depth the maximum estimated proportion of contamination exceeds the analytical error for Cl and Na. The sample at 966.63 m depth shows little contamination and the estimated proportion of contamination lies within the analytical uncertainty. In contrast, the sample at 1'049.83 m depth shows an estimated proportion of contamination that exceeds the analytical uncertainty in all presented components (Cl, Na, SO_4, Br). All samples that show indications for contamination by the drilling fluid in the presented ion concentration are highlighted with red circles in the following figures.

Tab. 4.4-2: List of 3 samples and their geochemical characteristics which classify them as contaminated by the drilling fluid

The K-Si drilling fluid is characterised by a high pH, alkalinity and a high K concentration.

Depth [m]	**Formation**	**Member**	**WC_{wet}** [%]	**K** [mg/L]	**Na/K** [mol/mol]	**pH**	**Alk** [meq/L]
960.43	Klettgau Fm.	Gansingen Mb.	7.2	2'080	0.2	8.0	22.0
966.63	Klettgau Fm.	Ergolz Mb.	7.2	155	5.5	8.0	0.7
1'049.83	Schinznach Fm.	Stamberg Mb.	9.1	3'219	0.1	10.8	69.1

4.4.2.2 Anions

The Cl concentrations in the aqueous extracts range from 1.3 to 211 mg/L or 0.04 to 5.95 mmol/L reaching maximum values in the Rietheim Member of the Staffelegg Formation, excluding two outliers from oolithic samples in the Wutach Formation (735 mg/L) and «Murchisonae-Oolith Formation» (203 mg/L). The Br concentrations vary from 0.01 to 0.6 mg/L or 2×10^{-4} to 8×10^{-3} mmol/L with maximum values in the Staffelegg Formation, excluding the sample from the Wutach Formation (2.1 mg/L) (Fig. 4.4-1).

The depth profile of the Br/Cl ratio (Fig. 4.4-2) displays values close to seawater in the Malm. In the top of the «Brauner Dogger» section the Br/Cl ratios decrease to constant values of around 1.3E-3 down to the bottom of the Opalinus Clay. The ratios decrease throughout the Staffelegg

and Klettgau Formations to a local minimum in the top of the Bänkerjoch Formation. Subsequently, the ratios increase in the Bänkerjoch Formation before decreasing in the Schinznach Formation (coarse samples) towards minimum values in the rock salt of the Zeglingen Formation. The samples from the Schinznach Formation were extracted from coarser subsamples (2 cm pieces) and compared to additional extracts at normal (1 cm pieces) and milled (100 µm grains) size, respectively (Tab. 4.4-3). The first two samples, which were extracted with different subsample sizes are dolostones and show a small variation in the Br/Cl ratio between the different grain sizes. The lower two samples are limestones and show a clear increase in the Br/Cl with decreasing grain sizes of the extracts. These limestones are expected to contain a large amount of fluid inclusions, which break on the edge of the aqueous extract grains. It is likely that the fluid inclusions increase the Br/Cl ratio substantially in this limestone formation depending on the sample size (Fig. 4.4-2). These additional samples are further discussed in Section 4.4.3.

All aqueous extracts from dry material (SQ) have systematically lower ratios compared to extracts on wet material (SQ) due to their lower Br concentrations (dry: 1.25, 1.11, 1.07, 0.67 vs. wet: 1.32, 1.24, 1.32, 1.32). This suggests that Br is not behaving conservatively after drying and that some Br is retained during subsequent extraction (e.g. binding to solid organic matter).

Tab. 4.4-3: Aqueous extract of coarse, normal and milled samples of the Schinznach Formation

The coarse, normal and milled sample pieces are approximately 2 cm, 1 cm and 100 µm in size, respectively.

Depth [m]	**Sub-sample**	**Wet Rock** [g]	**H_2O** [g]	**Cl** [mg/L]	**Br** [mg/L]	**1'000*Br/Cl** [molal]	**SO_4** [mg/L]	**Ca** [mg/L]
1'050	coarse	30.6	30.5	95.9	< 0.16		923	2
1'050	normal	30.3	30.5	104.0	0.23	2.2	1'096	7
1'050	milled	30.1	30.4	111.0	0.25	2.3	2'749	7
1'061	coarse	22.5	20.0	40.3	0.14	3.4	1'608	575
1'061	normal	30.7	30.4	50.5	0.35	7.0	1'747	538
1'061	milled	30.0	30.5	64.3	0.39	6.0	2'014	597
1'087	coarse	21.9	20.1	11.5	0.03	2.6	107	23
1'087	normal	30.3	30.4	16.4	0.14	8.7	87	14
1'087	milled	30.1	30.5	48.3	0.47	9.7	118	18
1'109	coarse	22.0	20.1	55.5	0.05	0.9	67	17
1'109	normal	30.1	30.4	74.4	0.28	3.7	84	7
1'109	milled	30.1	30.5	126.0	0.81	6.4	83	10

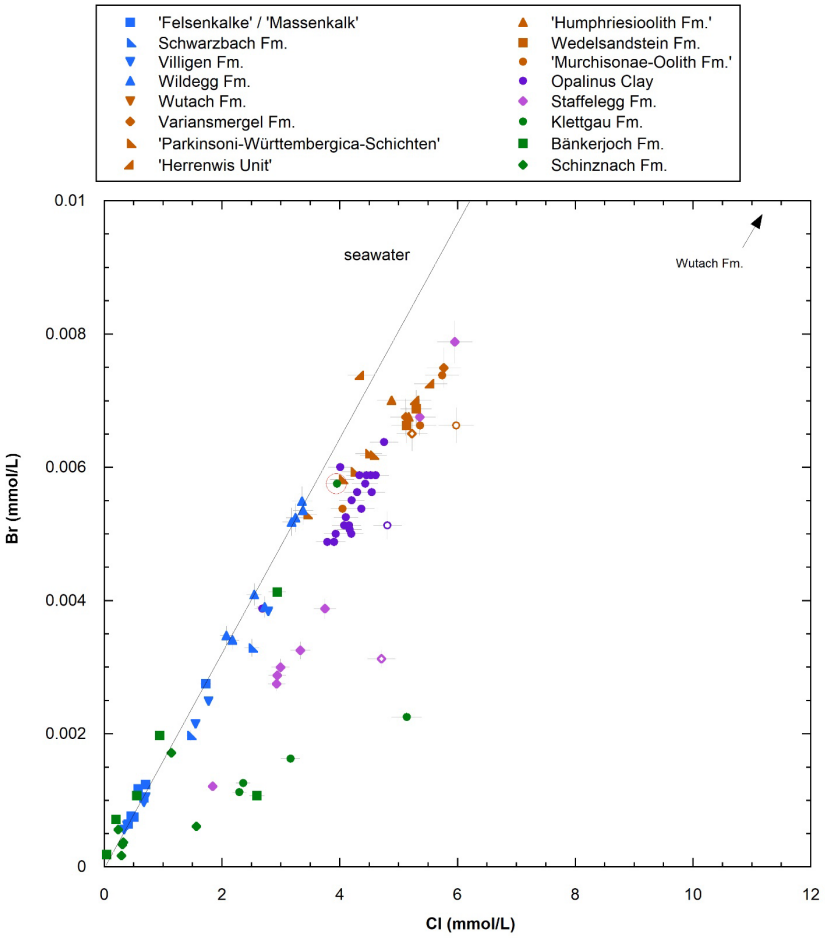

Fig. 4.4-1: Molar Br versus Cl concentrations in aqueous extracts at a *S/L* ratio of about 1

Empty symbols mark aqueous extracts from dry material. The sample with contamination by the drilling fluid is circled in red.

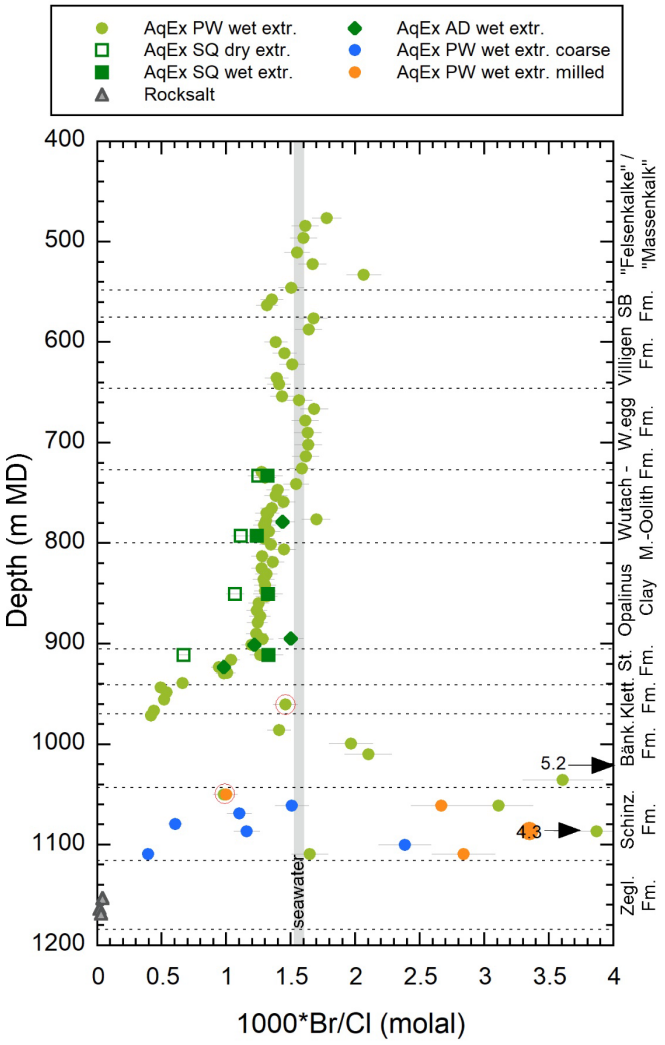

Fig. 4.4-2: Depth profile of the molar Br/Cl ratio in aqueous extracts at a *S/L* ratio of about 1
The samples with contamination by the drilling fluid are circled in red. The blue samples in the Schinznach Formation are considered the least affected by fluid inclusions.

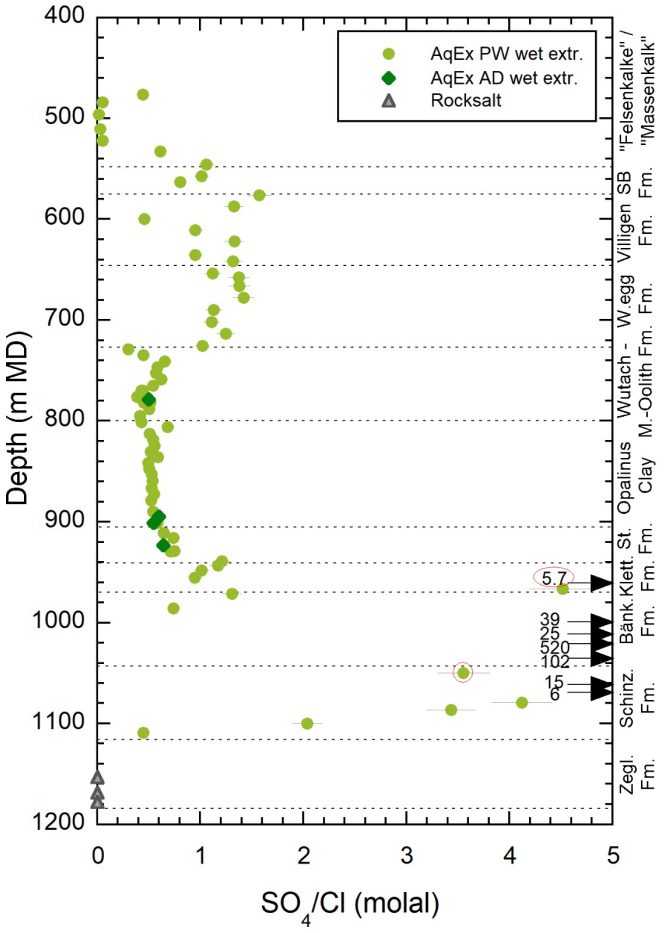

Fig. 4.4-3: Depth profile of SO_4/Cl molar concentration ratio in aqueous extracts at a *S/L* ratio of about 1

The samples with contamination by the drilling fluid are circled in red.

The SO_4 concentrations vary between 2.0 and 923 mg/L with the exception of 7 anhydrite bearing samples in the Klettgau, Bänkerjoch and Schinznach Formations where concentrations of 1'608 to 2'227 mg/L are reached. The SO_4/Cl ratio in aqueous extract solutions generally do not reflect porewater ratios due to potential dissolution of sulphate minerals and other processes during the extraction. There is remarkably little scatter in the SO_4/Cl ratio throughout the Dogger and Lias section of the profile, which might indicate that the sulphate contributions from mineral dissolution are minimal in this part of the profile. The multiple aqueous extracts in the Schinznach Formation show an increasing sulphate concentration with decreasing sample size in the dolomite samples and almost no variation in the limestone samples (Tab. 4.4-3). The additional sulphate in the milled dolomite samples might derive from pyrite oxidation.

The F concentrations in aqueous extracts range between 0.4 and 7.7 mg/L across the entire depth profile (not shown) with the highest values being in the Schwarzbach and Wildegg Formation, and «Felsenkalke» + «Massenkalk». The NO_3 concentrations vary between 0.09 and 4.2 mg/L with the maximum value reached in the Staffelegg Formation. The alkalinity varies between 0.2 and 8.2 meq/L, disregarding the highly contaminated samples (22 and 69.1 meq/L). The pH (not

shown) scatters from the «Felsenkalke» + «Massenkalk» to the top part of the Bänkerjoch Formation between 8 and 9.5 with a few outliers. In the Bänkerjoch and Schinznach Formations the pH values shift to lower values between 7.2 and 8.2 with one outlier of 6.2 in the Bänkerjoch Formation.

4.4.2.3 Cations

Cation concentrations were solely measured in the four AD aqueous extract samples as well as in most of the PW samples below the Staffelegg Formation.

The Na concentrations in the aqueous extracts vary between 3 and 497 mg/L with maximum values reached in the Klettgau Formation. The Na/Cl ratios of the depth profile show little variability from the Dogger to the top of the Bänkerjoch Formation (Fig. 4.4-4). The ratios reach a maximum in the middle and lower part of the Bänkerjoch Formation before dropping down to ratios around 1 in the Schinznach Formation, which is in agreement with the presence of rock salt in the lower Zeglingen Formation.

The K concentrations range from 2.4 mg/L up to maximum values of 27.9 mg/L in the Bänkerjoch Formation, disregarding the contaminated samples with 155 to 3'219 mg/L. The Na/K ratios are nearly constant throughout the Dogger and reach maximum values in the Klettgau Formation and top of the Bänkerjoch Formation (Fig. 4.4-5). The lowermost AD sample plots close to the neighbouring PW sample. The ratios decrease in the Bänkerjoch Formation and reach lower values in the Schinznach Formation. The lower most sample in the Schinznach Formation displays a higher ratio in agreement with high expected rock salt ratios.

The Sr concentrations range from 0.05 to 15.3 mg/L with maximum values reached in the Bänkerjoch Formation. The Sr/Cl ratios have low values in the Dogger with higher values reached in the Bänkerjoch Formation and the upper part of the Schinznach Formation (Fig. 4.4-6). These high values can be explained by the release of Sr from the dissolution of anhydrite or celestite during aqueous extraction. Celestite was not detected by XRD in any of the anhydrite-bearing samples in the Bänkerjoch Formation, which could mean that either celestite was present below XRD detection and did partially dissolve (in agreement with the saturation indices of 0, see below), and/or that all Sr is derived from anhydrite dissolution.

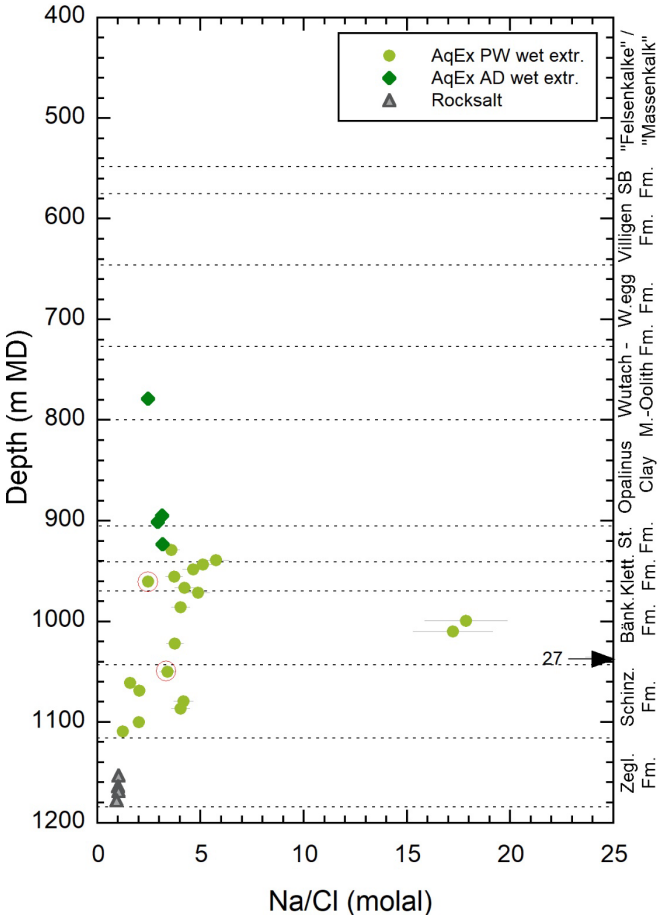

Fig. 4.4-4: Depth profile of the Na/Cl molar concentration ratio in aqueous extracts at a *S/L* ratio of about 1

The samples with contamination by the drilling fluid are circled in red.

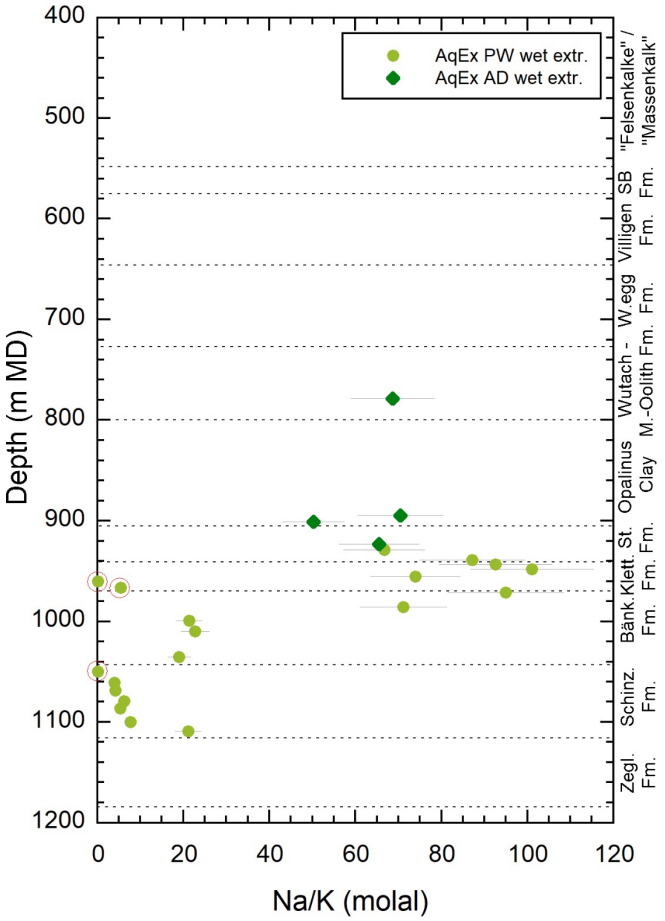

Fig. 4.4-5: Depth profile of the Na/K molar concentration ratio in aqueous extracts at a *S/L* ratio of about 1

The samples with contamination by the drilling fluid are circled in red.

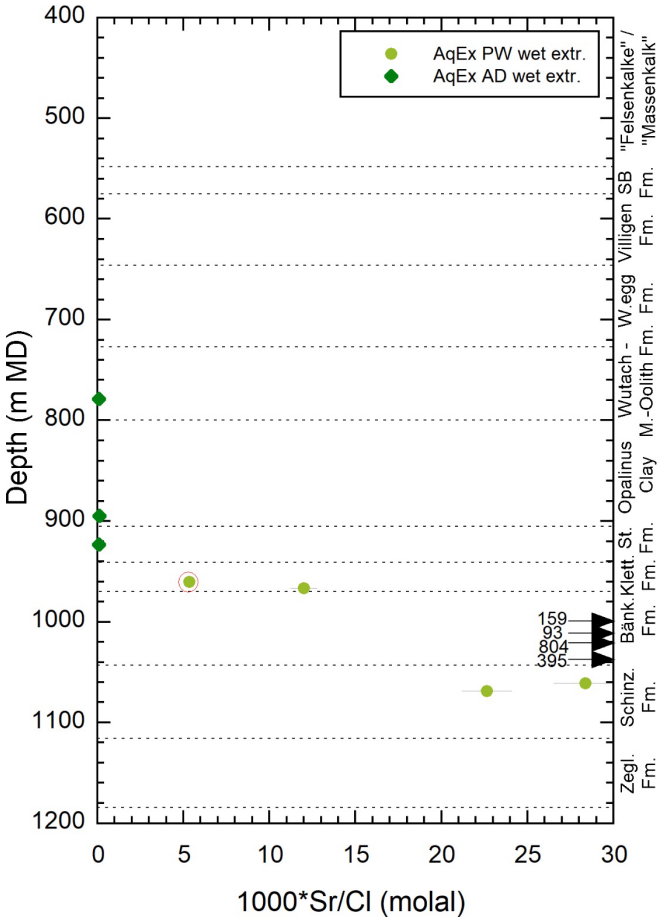

Fig. 4.4-6: Depth profile of the Sr/Cl molar concentration ratio in aqueous extracts at a *S/L* ratio of about 1

The sample with contamination by the drilling fluid is circled in red.

4.4.2.4 Saturation indices

The saturation indices of calcite and dolomite of the aqueous extract solutions vary across the different formations (Tab. 4.4-4). From the «Humphriesioolith Formation» to the Klettgau Formation the solutions are saturated or close to saturation with respect to calcite but mostly undersaturated with respect to dolomite (one sample in the Klettgau Formation is saturated with respect to dolomite). The samples at 778.4 and 923.3 m depth are undersaturated with respect to dolomite (ord) despite containing a few percent of dolomite. The samples from the Bänkerjoch and the Schinznach Formations are more diverse with half of the samples reaching saturation or oversaturation with respect to calcite (SI -1.1 to 0.64) but only a couple of those are also saturated with respect to dolomite (SI -2.9 to 0.87). Note that the sample at 1'022.3 m depth has a low pH of 6.23 and is extremely (-5.3) undersaturated with respect to dolomite despite containing 4 wt.-% of dolomite. This might be related to the extraction time (24 h) that is too short to reach equilibrium with dolomite. The sample at 1'035.6 m depth and the lowermost four Schinznach Formation samples are all undersaturated with respect to calcite despite containing 3, 34, 57 and 22 wt.-% calcite. The lowermost three Bänkerjoch Formation and all Schinznach Formation

samples contain dolomite but are calculated to be undersaturated with respect to dolomite. Calcite oversaturation in the anhydrite-bearing sample at 999.1 m depth can be explained by the dissolution of Ca-sulphate producing excess Ca that cannot be precipitated as calcite sufficiently fast.

The sulphate minerals gypsum, anhydrite and celestite are undersaturated by 1 to 3 orders of magnitude in all extract solutions with the exception of 4 samples from the Bänkerjoch Formation and one sample from the Schinznach Formation. These samples contain 3 to 85 wt.-% anhydrite, are saturated with respect to gypsum and celestite (not the sample at 1'060.8 m depth) and not far from saturation with respect to anhydrite, however, no celestite has been detected by XRD (detection limit of 1 wt.-%). Dolomite and celestite saturation indices are missing for some samples because the Mg and Sr concentrations are below the limit of detection, respectively.

Tab. 4.4-4: Saturation indices for calcite, dolomite (disordered and ordered), gypsum, anhydrite and celestite at a *S/L* ~ 1, pH and partial pressure of CO_2

Mineral saturation indices were calculated with the PHREEQC Version 3 code (Parkhurst & Appelo 2013) and the PSI/Nagra thermodynamic database (Thoenen et al. 2014) assuming a temperature of 25° C. Fm. stands for Formation, Ho for «Humphriesioolith Formation», Opa for Opalinus Clay, Sta for Staffelegg, Kl for Klettgau, Bä for Bänkerjoch, Sch for Schinznach Formation, *S/L* for solid/liquid, Cc for Calcite, Do for Dolomite ordered or disordered, Gy for gypsum, An for Anhydrite and Ce for Celestite. Empty cells in the SI Do and SI Ce columns are due to concentrations below the limit of detection in Mg or Sr, respectively. Note that the sample *in italics* (1'022.3 m depth) has a suspiciously low measured pH of 6.23 and a very low SI of Dolomite despite containing 4% Dolomite. There are no analytical indications which would discard this analysis as unreliable.

Fm.	**Depth** [m]	***S/L***	**SI Cc**	**SI Do (dis)**	**SI Do (ord)**	**SI Gy**	**SI An**	**SI Ce**	**pH**	**$\log_{10}$ pCO_2** [bar]
Ho	778.4	0.88	-0.11	-1.10	-0.55	-2.65	-2.87	-2.55	8.76	-3.57
Opa	895.0	0.91	0.06	-0.81	-0.26	-2.63	-2.85	-2.51	8.76	-3.44
Opa	900.8	0.89	-0.12	-1.15	-0.60	-2.67	-2.90		8.63	-3.33
Sta	923.3	0.92	-0.03	-1.06	-0.51	-2.95	-3.17	-2.79	9.12	-3.96
Sta	928.9	0.93	-0.03			-2.86	-3.09		8.97	-3.73
Sta	939.2	0.90	0.07			-2.91	-3.14		9.03	-3.70
Kl	943.2	0.92	0.01			-2.77	-2.99		8.91	-3.59
Kl	948.3	0.92	0.17			-2.90	-3.13		9.20	-3.93
Kl	955.6	0.95	0.09	-0.27	0.28	-2.61	-2.84		9.03	-3.86
Bä	971.6	0.90	-0.03			-2.59	-2.81		8.87	-3.63
Bä	985.7	0.94	0.54	0.32	0.87	-2.67	-2.89		9.20	-3.84
Bä	999.1	0.99	0.64	-0.38	0.17	0.09	-0.13	0.11	8.11	-3.63
Bä	1'009.9	0.98	0.26	-1.02	-0.47	0.09	-0.13	0.14	7.76	-3.27
Bä	*1'022.3*	*0.99*	*-1.69*	*-5.87*	*-5.32*	*0.09*	*-0.13*	*-0.02*	*6.23*	*-2.25*
Bä	1'035.6	0.98	-0.14	-2.40	-1.85	0.10	-0.12	0.06	7.46	-3.15
Sch	1'060.8	1.01	0.39	-0.67	-0.12	-0.04	-0.27	-0.34	8.00	-3.59
Sch	1'068.6	0.95	-0.60	-2.20	-1.65	-1.42	-1.64	-1.40	7.60	-3.08
Sch	1'079.2	1.05	-1.09	-2.92	-2.37	-1.80	-2.03		7.23	-2.61
Sch	1'086.7	1.05	-0.73	-2.13	-1.58	-1.97	-2.19		7.84	-3.31
Sch	1'100.0	1.04	-0.69	-2.18	-1.63	-2.41	-2.64		8.07	-3.60
Sch	1'109.2	1.07	-0.75	-2.07	-1.52	-2.27	-2.49		7.99	-3.53

4.4.3 Chloride and bromide concentrations in bulk porewater

The formalisms to recalculate Cl and Br concentrations in aqueous extracts to concentrations in bulk porewater are given in Waber (ed.) (2020). In clay-free rocks, this recalculation to bulk water content delivers the transport relevant porewater concentrations of Cl and Br directly. In clay-bearing rocks, the anion-exclusion effect has to be considered in order to result in 'free' porewater concentrations. The derivation of the Cl and Br accessible porosity proportion and calculation of 'free' porewater concentrations is established in Chapter 5.

The recalculation of Cl and Br concentrations in aqueous extracts to concentrations in bulk porewater (Figs. 4.4-7 and 4.4-8) requires the knowledge of the water content of the rocks, which is obtained by calculating the average of three gravimetric water contents (one regular sample and two subsamples used for diffusive-exchange experiments). Additional aqueous extraction tests were carried out on 4 dried water content subsamples from the Dogger to the Lias in order to compare the concentration between extracts from dry and wet material. In the Schinznach Formation the aqueous extracts with different sample sizes (coarse, normal, milled) highlight the contribution from fluid inclusions.

The depth profiles of Cl and Br concentrations in bulk porewater cover large ranges of 480 to 39'553 mg/L and 1.9 to 42 mg/L, respectively (Figs. 4.4-7 and 4.4-8). In the Br profile, the four aqueous extracts conducted on dried rock material show lower concentrations compared to the extracts from wet material (Fig. 4.4-9). Such differences between extracts from dry and wet material are also seen in the Cl data in the sample from the Rietheim Member of the Staffelegg Formation (Fig. 4.4-9). These differences may be related to the drying process (e.g., attachment to organic matter), but this issue is not yet resolved. The large organic carbon content of the Rietheim Member sample combined with the pronounced difference in Br and even Cl concentrations is in agreement with this hypothesis.

Both, the Cl and Br concentrations, show considerable scatter in the «Felsenkalke» + «Massenkalk» and down to the Villigen Formation. The Villigen Formation forms a sharp positive excursion between almost constant concentrations in the Schwarzbach and Wildegg Formation. There is a general decreasing trend from the Wutach Formation down to the bottom of the Opalinus Clay, followed by a sharp jump to higher concentrations in the Staffelegg Formation and a subsequent decrease to values slightly lower than at the base of the Opalinus Clay (Figs. 4.4-7 and 4.4-8). At the top of the Klettgau Formation there is a sharp decrease in values and a slight positive excursion throughout the Klettgau Formation. In the Bänkerjoch Formation the Br and Cl values scatter at higher concentrations before dropping to minimum values of the profile in the Schinznach Formation. There is a large difference in concentrations between the different sample sizes in the limestone (lower) part of the Schinznach Formation. The coarse samples are considered to be least effected by contribution of fluid inclusions and hence give the lowest values. The inferred contribution from fluid inclusions increases with depth and is largest at the base of the Schinznach Formation. The Cl concentration increases more than the Br concentration in the lowermost Schinznach Formation samples. This indicates that there is a real increase in Cl despite the contribution from fluid inclusions.

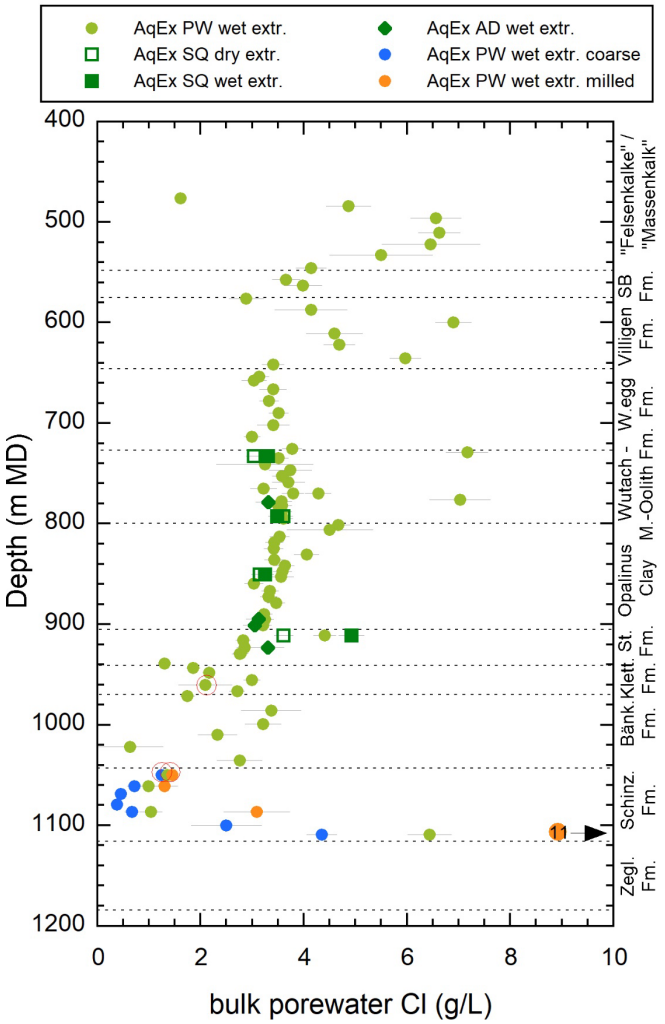

Fig. 4.4-7: Bulk porewater Cl concentrations versus depth from aqueous extracts of PW, AD and SQ samples

The samples with contamination by the drilling fluid are circled in red.

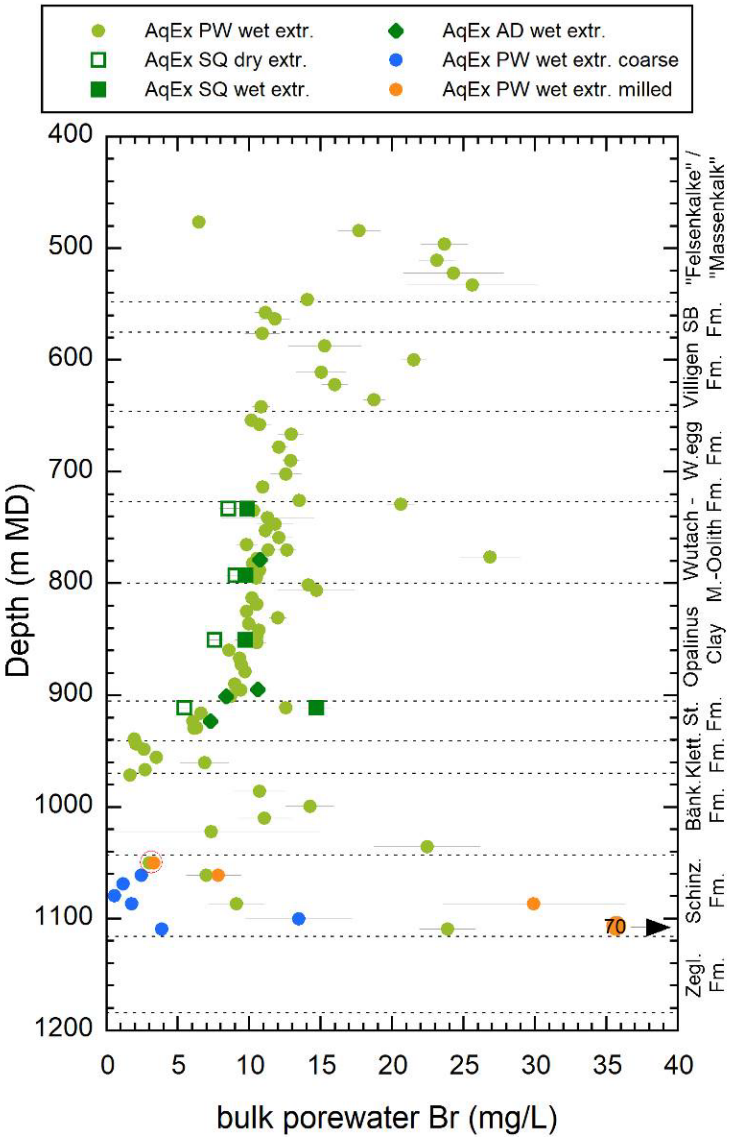

Fig. 4.4-8: Bulk porewater Br concentrations versus depth from aqueous extracts of PW, AD and SQ samples

The samples with contamination by the drilling fluid are circled in red.

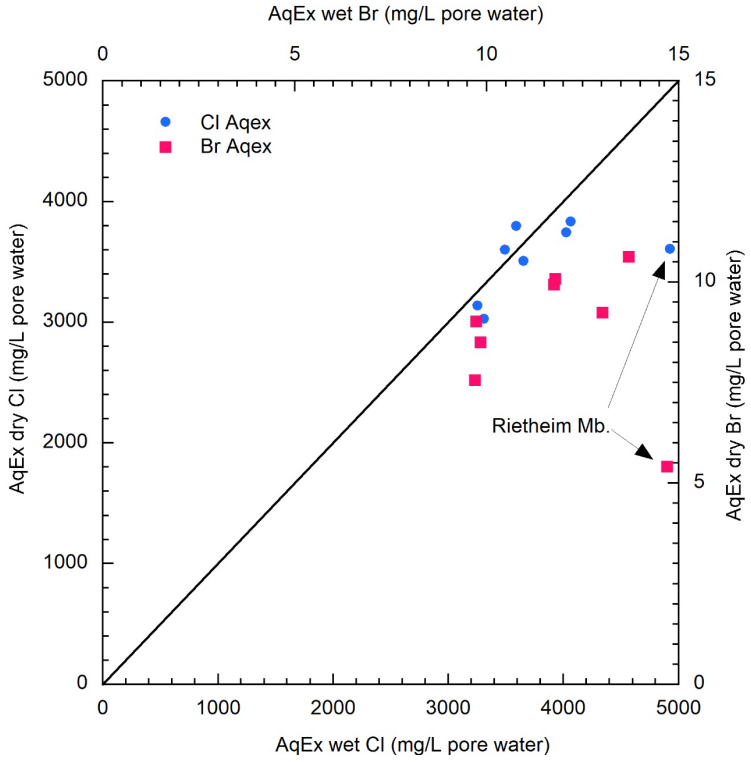

Fig. 4.4-9: Bulk porewater Br and Cl concentrations in aqueous extracts on wet versus dry material of SQ samples from STA2-1 and STA3-1

Note that the sample from the Rietheim Member (Staffelegg Formation) is exceptionally low in Br and Cl concentrations in the aqueous extract conducted on dry material.

4.5 Cation-exchange extraction data

Paul Wersin

Three samples used for advective displacement experiments (AD samples) were analysed at Uni Bern with the nickel ethylenediamine (Ni-en) extraction method to determine the cation exchange capacity (CEC) and the composition of the clay exchanger (for methodology see Waber ed. 2020). Material from end pieces above and below the AD core was mixed to obtain a representative sample for Ni-en extraction. For the Opalinus Clay sample only material from above the core was used. A larger number of samples were studied by the team at PSI using the CsCl extraction method (see Section 5.6 and Marques Fernandes & Baeyens 2023). The objective of the Ni-en extraction study was (i) to help to analyse the AD data (Section 4.7) and (ii) to compare and verify the PSI study with an alternative method.

The CEC can be derived in two ways: (1) From the consumption of the index cation (Ni in this case) during extraction and (2) from the sum of extracted cations (ΣCAT). Note that the latter includes (i) the exchangeable cations, (ii) cations dissolved in the porewater and (iii) cations released from potentially dissolving minerals (e.g. carbonates, sulphates) during extraction. Thus, in principle, the CEC derived from the sum of cations requires correction from contributions of (ii) and (iii). Corrected CEC and exchangeable cation data are discussed in Section 5.6, where the data from Uni Bern is also compared with that of PSI. The analysis does not include ammonium, NH_4^+, known to be present in small but usually measurable amounts (1 – 1.5 mg/L in aqueous extracts, at $S/L \approx 1$, Appendix A).

Tab. 4.5-1 shows the Ni consumption and extracted cation data (Na, K, Ca, Mg, Sr, Ba) for solid/liquid ratios (*S/L*) around 1[7]. Anion data (F, Cl, Br, SO_4, NO_3) is depicted in Tab. 4.5-2. Note that Ni nitrate was added to the samples, which explains the high NO_3 contents.

Tab. 4.5-1: Cation data from Ni-en extracts at a *S/L* ratio around 1 (Uni Bern data)
Fe content in extract: < 0.001 mg/kg

Type	**Depth** [m]	**Formation**	***S/L*** [g/g]	**Na** meq/kg	**K** meq/kg	**Ca** meq/kg	**Mg** meq/kg	**Sr** meq/kg	**Ba** meq/kg	**ΣCAT** meq/kg	**Ni cons.** meq/kg
AD	778.43	«Humphriesi-oolith Fm.»	0.88	64.0	6.6	44.4	17.2	0.7	0.002	132.9	137.2
AD	895.02	Opalinus Clay	0.91	57.6	5.3	40.9	13.0	0.6	0.012	117.5	131.8
AD	923.27	Staffelegg Fm.	0.92	42.1	5.0	23.6	7.4	0.4	0.007	78.5	86.9

Tab. 4.5-2: Anion data from Ni-en extracts at a *S/L* ratio around 1 (Uni Bern data)

Type	**Depth** [m]	**Formation**	***S/L*** [g/g]	**F** meq/kg	**Cl** meq/kg	**Br** meq/kg	**NO_3** [a] meq/kg	**SO_4** meq/kg
AD	778.43	«Humphriesioolith Fm.»	0.88	0.013	4.9	0.007	222.4	3.7
AD	895.02	Opalinus Clay	0.91	< 0.01	4.0	0.006	220.7	3.3
AD	923.27	Staffelegg Fm.	0.92	0.012	3.4	0.003	219.9	3.2

[a] Nitrate is part of the added Ni-en stock solution

The CEC derived from Ni consumption of the three AD samples lies in the range of 87 – 137 meq/kg_{rock} and is similar to the uncorrected sum of cations (79 – 133 meq/kg_{rock}).

The depth profiles of Ni consumption and ΣCAT data show similar values for the «Brauner Dogger» and Opalinus Clay sample, but a lower one for the sample in the Staffelegg Formation (Fig. 4.5-1). This sample also has a lower clay-content than the other two samples (Fig. 4.5-2). The relationship between clay-mineral content and CEC data is further discussed in Section 5.6.

Na and Ca are the main extracted cations, followed by Mg and K (Tab. 4.5-1). Note that at this point the extractable cations have not been corrected for the contribution of dissolved cations and mineral dissolution (see Section 5.6). The molar Ca/Na ratio is about 1 for the two upper samples from the «Brauner Dogger» and Opalinus Clay and slightly lower for the Staffelegg Formation sample (0.7). Mg correlates with Ca, thus the same trend is noted for the (Ca+Mg)/Na ratios (Fig. 4.5-3).

[7] A solution mass equal to the mass of the wet rock was added, leading to *S/L* (mass of dry rock / [mass of added solution + porewater]) slightly below 1.

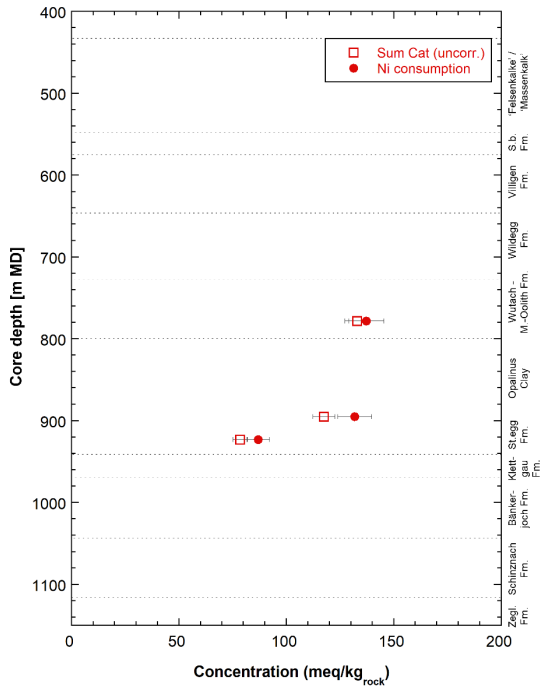

Fig. 4.5-1: Depth profile of Ni consumption and sum of cations (uncorrected, Uni Bern data)
Errors reflect propagated analytical uncertainties.

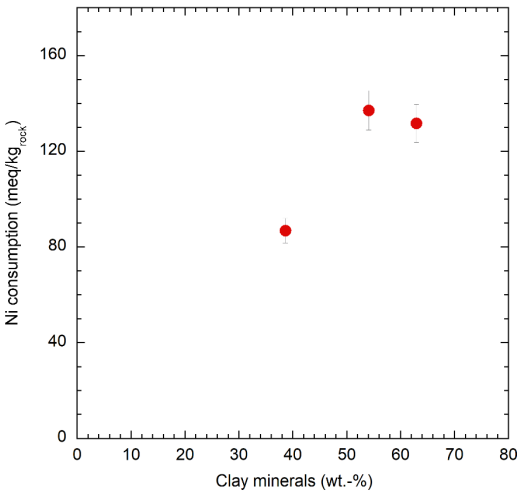

Fig. 4.5-2: Ni consumption vs. clay-mineral content (Uni Bern data)

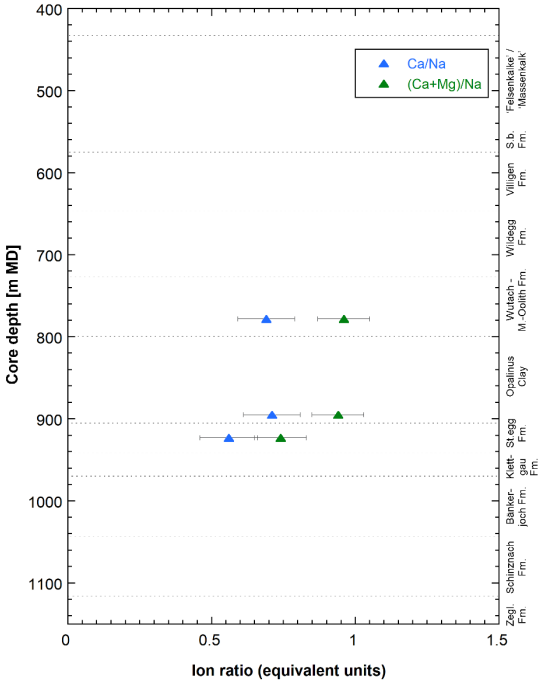

Fig. 4.5-3: Depth profiles of Ca/Na and (Ca+Mg)/Na ratios in Ni-en extracts (Uni Bern data)
Errors reflect propagated analytical uncertainties.

Speciation calculations on the Ni-en extracts were carried out with the PHREEQC Version 3 code (Parkhurst & Appelo 2013) and the PSI/Nagra thermodynamic database (Thoenen et al. 2014) assuming a temperature of 25 °C. The ethylene diamine complexes were taken from the MINTEC database (Allison et al. 1991) and included in the calculations. The concentration of ethylene diamine in the extracts, which was not analysed, was constrained by charge balance. The dissolved carbonate concentration (not measured) was constrained by assuming calcite equilibrium. The calculated TIC values are low, in the range of 0.09 – 0.13 mM (Tab. 4.5-4). The calculated partial pressures of CO_2 (pCO_2) and saturation indices for selected minerals are depicted in Tab. 4.5-4. The Ni-en extracts are clearly undersaturated with regard to the carbonate minerals dolomite and strontianite. They are also undersaturated with regard to the sulphate minerals gypsum and celestite, but either close to saturation or oversaturated with regard to barite.

Tab. 4.5-4: Calculated saturation indices of selected minerals, TIC, and log pCO_2 for Ni-en extract solutions
Calcite saturation was enforced in the calculations.

Type	Depth [m]	Formation	log pCO_2 [bar]	TIC [mol/kg_w]	Gypsum	Celestite	Barite	Dolomite (ord)	Dolomite (dis)	Strontianite
AD	778.43	«Humphriesi-oolith Fm.»	-4.78	0.13	-1.24	-0.99	-0.14	-0.28	-0.83	-1.02
AD	895.02	Opalinus Clay	-4.90	0.09	-1.22	-0.98	0.62	-0.37	-0.92	-0.99
AD	923.27	Staffelegg Fm.	-4.86	0.11	-1.39	-1.12	0.46	-0.38	-0.93	-0.96

4.6 Data from squeezing experiments

Martin Mazurek

A small set of 4 samples from the interval Variansmergel Formation – Staffelegg Formation were subjected to porewater squeezing. Photographs of the core samples are shown in Fig. 4.6-1. The mineralogical composition of the samples is listed in Tab. 4.6-1. Clay mineral contents are ≥ 60 wt.-%, except for the calcareous marl sample from the Rietheim Member of the Staffelegg Formation. The latter sample also has a particularly high content of organic carbon.

Tab. 4.6-1: Mineralogical composition of samples subjected to squeezing experiments
Empty field = mineral not identified. "tr" = trace.

Depth [m]	**Formation**	**Member**	**S** [wt.-%]	**C(inorg)** [wt.-%]	**C(org)** [wt.-%]	**Quartz** [wt.-%]	**K-feldspar** [wt.-%]	**Plagioclase** [wt.-%]	**Calcite** [wt.-%]	**Dolomite / Ank.** [wt.-%]	**Siderite** [wt.-%]	**Magnesite** [wt.-%]	**Anhydrite** [wt.-%]	**Pyrite** [wt.-%]	**Clay minerals** [wt.-%]
732.74	Variansmergel Fm.		0.90	1.50	0.60	17	2	2	7	5				1.7	65
792.72	«Murchisonae-Oolith Fm.»		0.60	0.60	0.90	22	2	3	5					1.1	66
850.29	Opalinus Clay	'Mixed clay-silt-carbonate sub-unit'	0.20	1.30	0.90	22	3	3	6		5			0.4	60
911.28	Staffelegg Fm.	Rietheim Mb.	0.90	5.30	4.70	9	1	2	44		tr			1.7	37

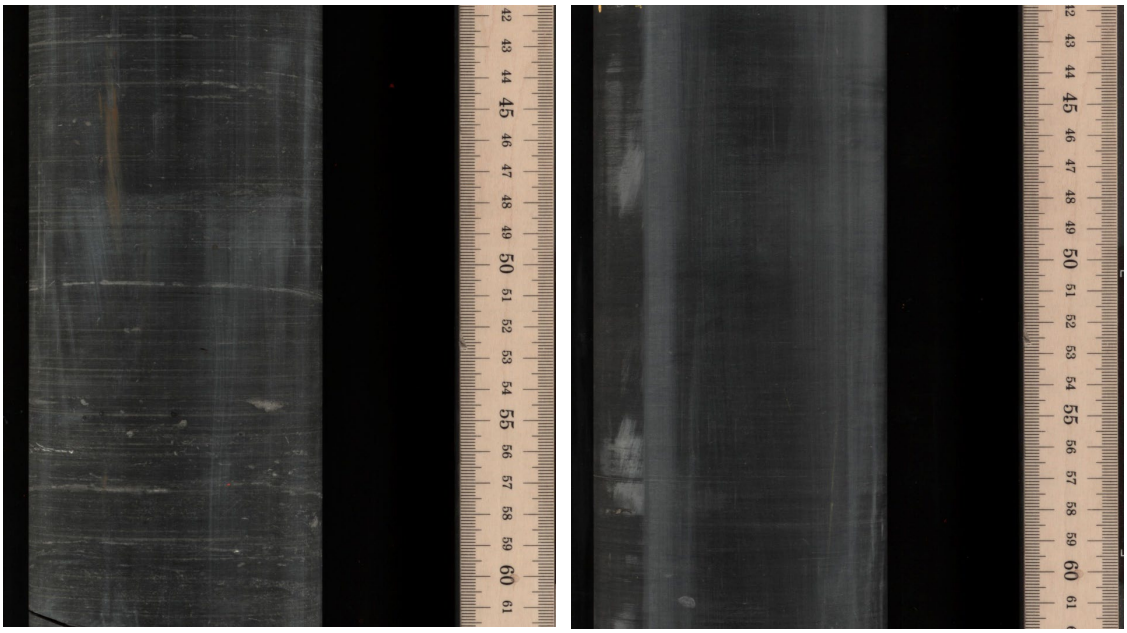

STA2-1 732.74 STA2-1 792.72

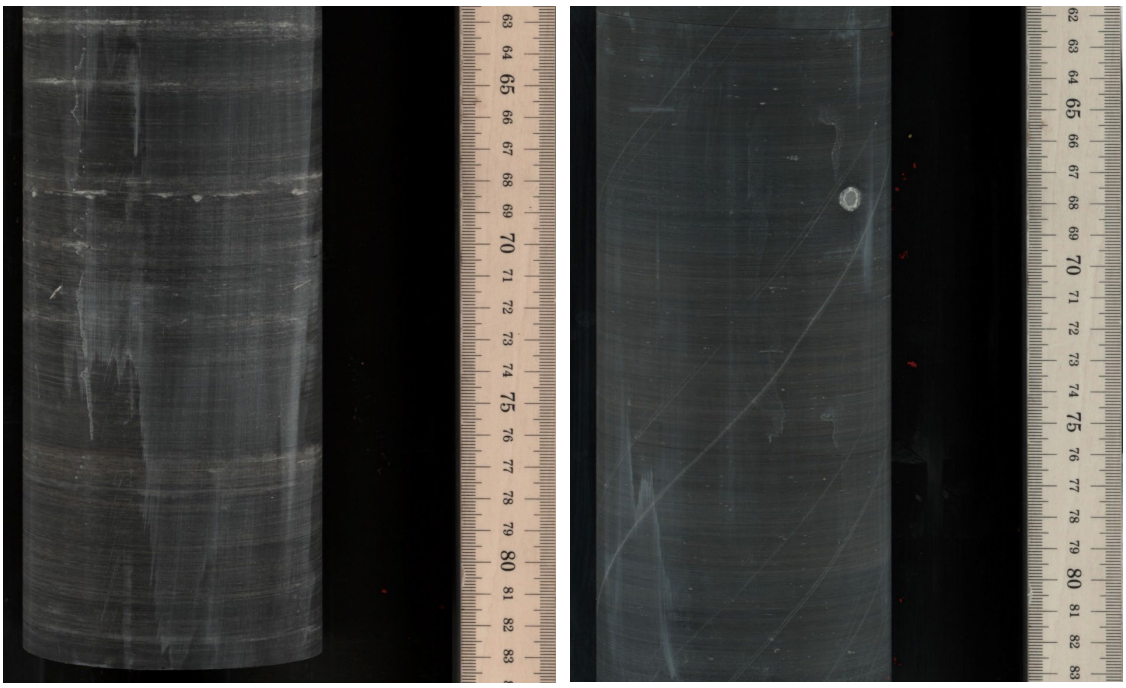

STA2-1 850.29 STA2-1 911.28

Fig. 4.6-1: Photographs of core samples subjected to squeezing

4.6.1 Mass recovery

The water masses obtained by squeezing are listed in Tab. 4.6-2 and shown graphically in Fig. 4.6-2 as a function of the squeezing pressure. Given the small number of samples, a correlation between the initial water content of the sample and the total mass recovery, as observed in other squeezing campaigns, is not well established (Fig. 4.6-3). Samples yielded first water aliquots at 200 MPa, except for the sample from the Staffelegg Formation where 300 MPa

were required to extract porewater. For 3 samples, a sufficient water mass was obtained in the pressure range 200 – 300 MPa. Therefore, the experiments were terminated at 300 MPa, i.e. no waters were squeezed at higher pressures. For the sample from the Staffelegg Formation, the experiment was terminated after squeezing water at 400 MPa.

Tab. 4.6-2: Water masses squeezed at different pressure steps

The initial water content was reconstructed on the basis of the measured water content of the squeezed sample and the squeezed water mass (see Section 4.6.5), and this value was then used to calculate the initial mass of porewater in the sample. "-": pressure step not applied.

Depth [m]	**Formation**	**Initial sample mass (CRIEPI)** [g]	**Initial wet water content** [wt.-%]	**Mass of porewater prior to squeezing** [g]	**Mass squeezed at P =**						**Total mass squeezed** [g]
					100 MPa [g]	**150 MPa** [g]	**200 MPa** [g]	**300 MPa** [g]	**400 MPa** [g]	**500 MPa** [g]	
732.74	Variansmergel Fm.	386.88	5.651	21.86	0	-	1.96	1.88	-	-	3.84
792.72	«Murch.-Oolith Fm.»	386.58	5.365	20.74	0	-	2.10	1.66	-	-	3.76
850.29	Opalinus Clay	387.67	4.476	17.35	0	-	0.70	1.59	-	-	2.29
911.28	Staffelegg Fm.	357.59	4.078	14.58	0	-	0	1.09	1.16	-	2.25

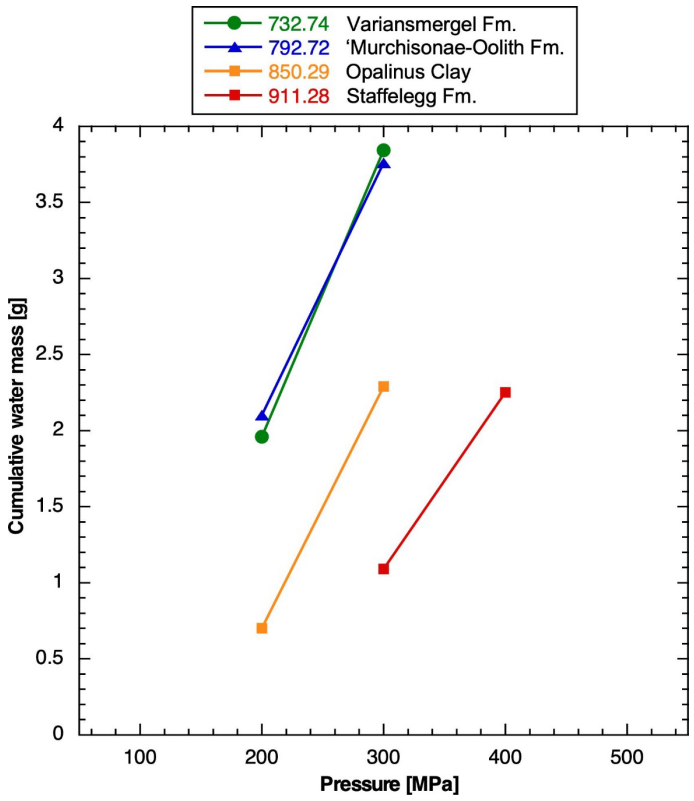

Fig. 4.6-2: Cumulative water masses obtained by squeezing as a function of the squeezing pressure

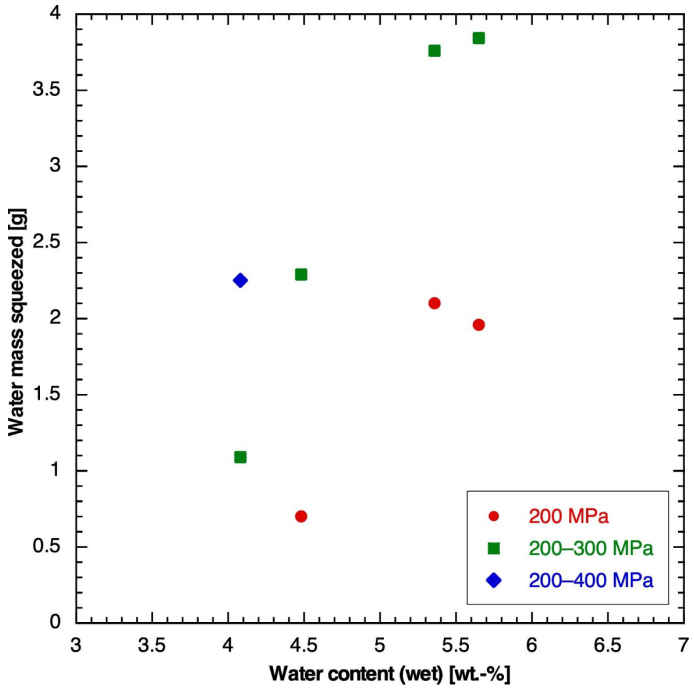

Fig. 4.6-3: Correlation of the original water content and the cumulative water mass obtained by squeeezing

4.6.2 Chemical composition of squeezed waters

The first squeezed aliquots yielded ≥ 0.7 g water in all cases, from which a complete data set (major-ion composition, TIC/TOC, pH, water isotopes) could be obtained. The chemical compositions of squeezed waters are listed in Tab. 4.6-3 and shown graphically as a function of squeezing pressure in Fig. 4.6-4. Na is by far the most abundant cation, and Cl dominates the anions, followed by SO_4.

The concentrations of the monovalent ions Na, K, Cl and Br decrease with squeezing pressure, likely due to ion-filtration effects that become important at higher pressures (Mazurek et al. 2015). Ca and Mg evolve slightly towards higher concentrations. As discussed in Mazurek et al. (2015) and Rufer & Mazurek (2018), the composition of the first water aliquot recovered from a sample is considered to be closest to that of the porewater, and these analyses are highlighted by bold print in Tab. 4.6-3. Fluoride concentrations, in particular in the first squeezed aliquots, are contaminated by F leached from the fiberglass filters and so are not representative of the porewater. For clarity, a subset of the data considered to be useful for further interpretation is summarised in Tab. 4.6-4.

The chemical compositions are similar to those obtained for squeezed waters from the STA-3 core (Aschwanden et al. 2022), with some minor differences. Na, Cl, Br and TDS show slightly lower concentrations in STA-2. In contrast, Ca and Mg yield somewhat higher concentrations.

Tab. 4.6-3: Chemical composition of squeezed waters: full data set

Bold print indicates the selected ("best") aliquots. F concentrations, in particular in the first squeezed aliquots, are contaminated by F leached from the fiberglass filters and so are not representative of the porewater.

Depth [m]	**Pressure** [MPa]	**Squeezing time** [d]	**Mass squeezed** [g]	**Na** [mg/L]	**NH_4** [mg/L]	**K** [mg/L]	**Ca** [mg/L]	**Mg** [mg/L]	**Sr** [mg/L]	**F** [mg/L]	**Cl** [mg/L]	**Br** [mg/L]	**NO_3** [mg/L]	**SO_4** [mg/L]	**pH**	**TIC** [mg/L]	**TOC** [mg/L]	**TDS** [mg/L]	**Charge balance** [%]
732.74	**200**	**3**	**1.96**	**4'329**	**< 10**	**87.3**	**812**	**238**	**21.4**	**8.5**	**6'480**	**18.8**	**13.21**	**2'634**	**8.61**	**25.2**	**150.9**	**14'924**	**2.6**
	300	3	1.88	3'391	< 10	44.7	809	245	21.3	5.0	5'057	15.5	4.37	2'474	8.51	20.8	81.7	12'255	-1.8
792.72	**200**	**4**	**2.10**	**4'227**	**< 10**	**91.9**	**722**	**200**	**20.5**	**8.0**	**6'260**	**18.7**	**8.26**	**2'299**	**8.38**	**23.0**	**185.0**	**14'160**	**-1.2**
	300	3	1.66	3'606	< 10	55.9	757	216	18.0	4.9	5'357	15.1	5.45	2'343	8.26	31.1	99.0	12'637	-1.4
850.29	**200**	**4**	**0.70**	**4'104**	**< 10**	**74.6**	**774**	**174**	**17.3**	**12.1**	**6'057**	**16.8**	**10.10**	**2'139**	**8.33**	**24.3**	**232.9**	**13'737**	**0.2**
	300	3	1.59	4'000	< 10	55.6	839	204	29.0	5.8	5'891	17.4	4.46	2'310	8.49	20.8	153.7	13'617	0.2
911.28	**300**	**3**	**1.09**	**5'138**	**< 10**	**89.0**	**936**	**227**	**20.2**	**10.7**	**7'044**	**19.3**	**11.60**	**3'306**	**8.55**	**22.3**	**226.2**	**17'144**	**0.3**
	400	3	1.16	4'751	< 10	59.9	993	251	25.8	4.7	6'853	19.1	5.45	3'504	8.53	25.7	149.0	16'749	-2.0

Tab. 4.6-4: Chemical composition of squeezed waters: summary of selected analyses to be used for interpretation

Depth [m]	**Formation**	**Pressure** [MPa]	**Squeezing time** [d]	**Mass squeezed** [g]	**Na** [mg/L]	**K** [mg/L]	**Ca** [mg/L]	**Mg** [mg/L]	**Sr** [mg/L]	**Cl** [mg/L]	**Br** [mg/L]	**NO_3** [mg/L]	**SO_4** [mg/L]	**pH**	**TIC** [mg/L]	**TOC** [mg/L]
732.74	Variansm. Fm.	200	3	1.96	4'329	87.3	812	238	21.4	6'480	18.8	13.21	2'634	8.61	25.2	150.9
792.72	«Murch.-O. Fm.»	200	4	2.10	4'227	91.9	722	200	20.5	6'260	18.7	8.26	2'299	8.38	23.0	185.0
850.29	Opalinus Clay	200	4	0.70	4'104	74.6	774	174	17.3	6'057	16.8	10.10	2'139	8.33	24.3	232.9
911.28	Staffelegg Fm.	300	3	1.09	5'138	89.0	936	227	20.2	7'044	19.3	11.60	3'306	8.55	22.3	226.2

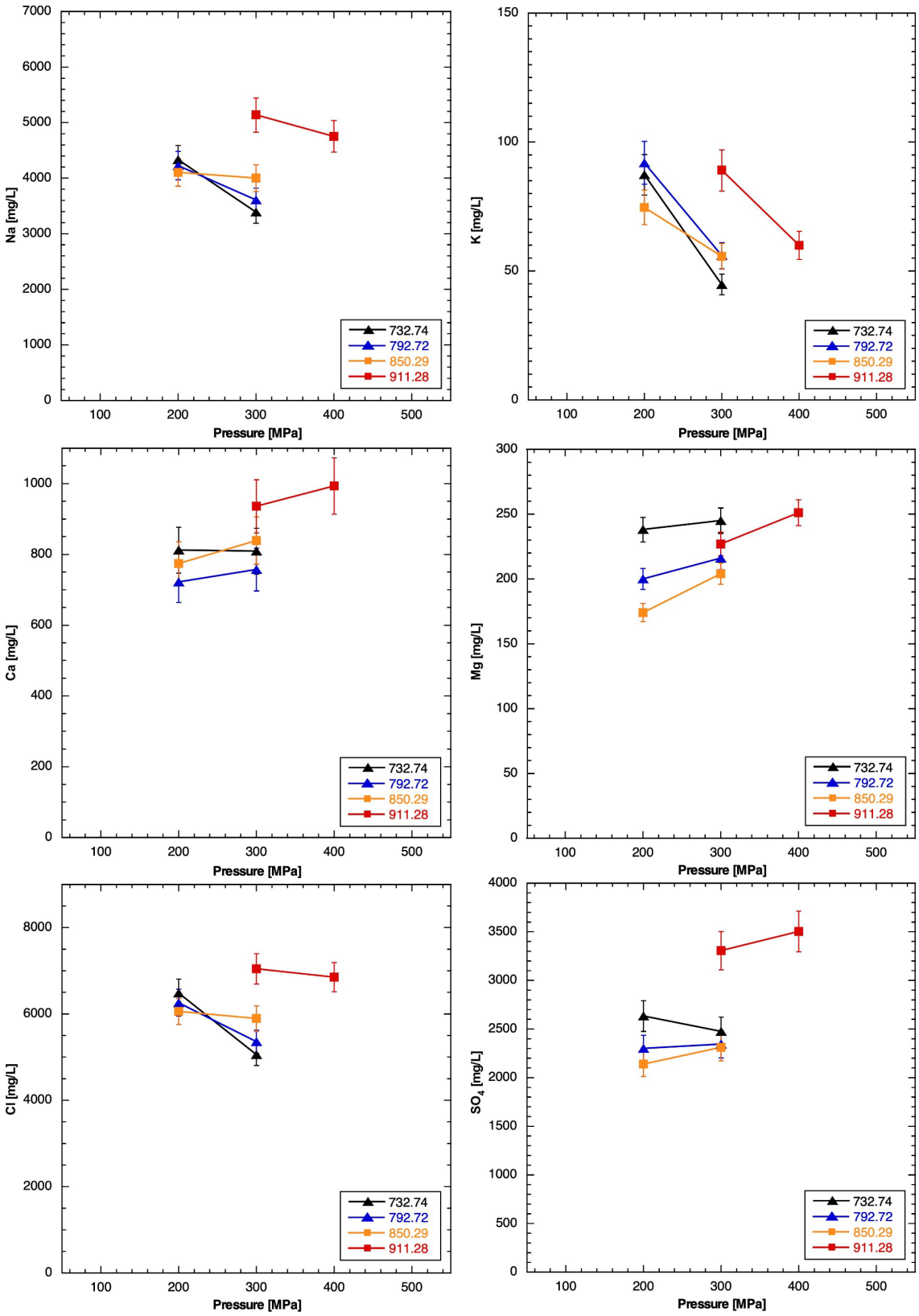

Fig. 4.6-4: Ion concentrations in squeezed waters as a function of squeezing pressure
Bars indicate analytical errors of ion-chromatography analysis.

4.6.3 Depth trends

Profiles with depth for various porewater constituents are shown in Fig. 4.6-5. Given the fact that only 4 samples were studied, trends should preferably be studied in conjunction with data from other methods. Nevertheless, the following observations can be made:

- Na, Cl and SO_4 show a weak decreasing trend with depth in the Dogger but distinctly higher concentrations in the Staffelegg Formation (the latter was also observed in STA-3). For Mg, the same trend is observed and is even more strongly expressed.
- In the Staffelegg Formation, Na/Cl, SO_4/Cl and salinity increase slightly.
- Ca contents are constant in the Dogger but increase in the Staffelegg Formation, similar to the trend in STA-3. In contrast, the depth trend for Mg differs markedly from that of STA-3.
- The Br/Cl ratio is slightly below that of current seawater and does not evolve with depth. It is similar to that of STA-3 but markedly higher than in the BUL-1 profile.
- The SO_4/Cl ratio is higher than in seawater. It is similar to that of porewater from STA-3 but higher than in the BUL-1 core at the same stratigraphic level.

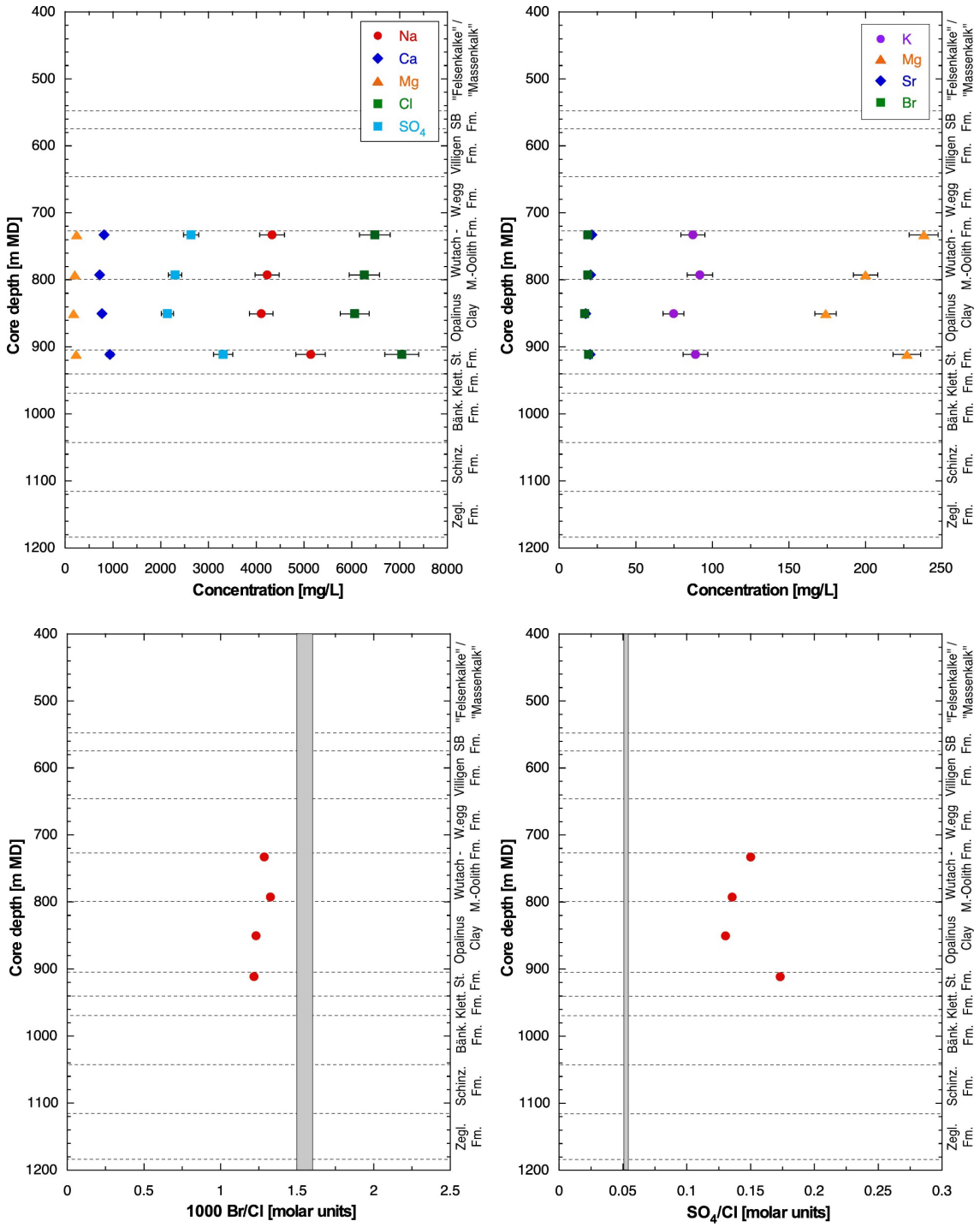

Fig. 4.6-5: Depth trends of ion concentrations and ion ratios in squeezed waters

Only the selected aliquots are shown for each sample. Bars indicate analytical errors of ion-chromatography analysis. Grey bars represent current seawater ratios.

4.6.4 Geochemical modelling and mineral saturation states

Mineral saturation indices for squeezed waters were calculated using PHREEQC V3 and the PSI/Nagra thermodynamic data base at 25 °C (Thoenen et al. 2014) and are shown in Tab. 4.6-5.

- Squeezed waters are strongly oversaturated with respect to calcite, dolomite and magnesite, a feature already known from previous studies (e.g. Mazurek et al. 2015). The oversaturation is possibly due to the fact that mineral solubility at high pressures during squeezing is higher than at atmospheric pressure. Further, outgassing of CO_2 during the squeezing process increases the pH and the saturation indices of calcite and dolomite (Tournassat et al. 2015). Further outgassing my take place in the headspace of the sample vials during sample storage. The comparatively low calculated pCO_2 suggest that some outgassing may have taken place, which also affects pH. However, this nevertheless does not markedly affect the obtained major-ion composition due to the large buffering capacity of the rock-water system in clay-rich lithologies. Last, lattice defects in carbonate minerals induced by deformation during squeezing might increase the solubility of these minerals. On the other hand, outgassing into the external atmosphere during sample storage in glass vessels is not considered to contribute to the low pCO_2) Such a process should also be seen by higher δ-values of water isotopes, which is not the case (see Section 4.8), but this depends on the mode of water loss (via a gas phase, or via a liquid film). In Section 5.5.1 below, an attempt is made to restore the out-gassing by model calculations assuming equilibrium with calcite.
- A more limited oversaturation is seen for strontianite.
- The waters are close to saturation with respect to celestite and only marginally undersaturated with respect to gypsum (except for the sample from the Staffelegg Formation that is at gypsum saturation).
- Using the data from Tab. 4.6-3, squeezed waters are strongly oversaturated with respect to fluorite, which is a consequence of the contamination of F by the filter material. Therefore, no F data are listed in Tab. 4.6-4.

Tab. 4.6-5: Mineral saturation indices for squeezed waters

Bold print indicates the selected ("best") aliquots.

Depth [m]	Formation	Pressure [MPa]	pH	TIC [M]	log pCO_2	SI Calcite	SI Aragonite	SI Dolomite (ordered)	SI Dolomite (disordered)	SI Strontianite	SI Magnesite	SI Gypsum	SI Anhydrite	SI Celestite	SI Fluorite
732.74	Variansmergel Fm.	**200**	**8.61**	**2.13E-03**	**-3.73**	**1.48**	**1.34**	**2.76**	**2.21**	**0.36**	**0.96**	**-0.08**	**-0.29**	**0.07**	**1.13**
		300	8.51	1.75E-03	-3.69	1.33	1.19	2.48	1.93	0.21	0.82	-0.07	-0.29	0.07	0.68
792.72	«Murchisonae-Oolith Fm.»	**200**	**8.38**	**1.94E-03**	**-3.51**	**1.21**	**1.07**	**2.20**	**1.65**	**0.12**	**0.66**	**-0.16**	**-0.38**	**0.01**	**1.05**
		300	8.26	2.62E-03	-3.24	1.26	1.11	2.30	1.75	0.09	0.72	-0.12	-0.34	-0.02	0.65
850.29	Opalinus Clay	**200**	**8.33**	**2.05E-03**	**-3.43**	**1.23**	**1.08**	**2.14**	**1.59**	**0.03**	**0.59**	**-0.15**	**-0.37**	**-0.08**	**1.46**
		300	8.49	1.76E-03	-3.68	1.33	1.18	2.37	1.82	0.32	0.72	-0.10	-0.31	0.16	0.84
911.28	Staffelegg Fm.	**300**	**8.55**	**1.89E-03**	**-3.73**	**1.41**	**1.27**	**2.53**	**1.98**	**0.20**	**0.80**	**0.04**	**-0.17**	**0.10**	**1.37**
		400	8.53	2.18E-03	-3.64	1.47	1.33	2.68	2.13	0.34	0.88	0.09	-0.13	0.22	0.66

4.6.5 Water content and aqueous extraction of squeezed and adjacent unsqueezed core material

For the calculation of the Cl-accessible porosity fraction f_{Cl} (see below), the inventories of water and Cl in the rock prior to squeezing must be known. These data can be obtained by two alternative methods:

1. Measure the water content (by drying) and then the Cl content (by aqueous extraction) of the squeezed material (so-called POST data). From these data, the masses of water and Cl remaining in the sample after squeezing can be calculated. By adding the masses of squeezed water and Cl to these data, the respective contents prior to squeezing can be reconstructed.
2. Measure the water content (by drying) and Cl content (by aqueous extraction of wet material) of adjacent unsqueezed material some 10 cm away (so-called PRE data).

Note that in method 1) aqueous extraction is performed on dry material, while wet material is used in method 2). Both approaches have advantages and disadvantages:

- Method 1) has the advantage that all measurements are performed on the same material, so potential heterogeneity is not an issue. On the other hand, the reconstruction of the water and Cl inventories is less direct and assumes that the dead volume of the system is negligible (which is likely the case[8]). The results are listed in Tab. 4.6-6.
- Method 2) directly yields the desired data – no addition of two measurements is needed – but relies on the assumption that the measurement performed on adjacent material is also representative for the squeezed material itself. The assumption of homogeneity incurs some degree of uncertainty. Moreover, the material used for the PRE measurements (typically a 8 – 10 cm long piece of core) has been exposed to the atmosphere for a few minutes during sample preparation (dry sawing) prior to being re-sealed again. While this was the case for the squeezed material as well, the exposed surface area of the adjacent cutoff material is much larger. Results are shown in Tab. 4.6-7.

[8] A sensitivity calculation was performed on the impact of dead volume. Assuming a dead volume of 1 mL results in an anion-accessible porosity fraction that is 0.01 – 0.04 higher than the value without the consideration of a dead volume. The most strongly expressed shift is found in samples where only a small water volume was squeezed, while it becomes insignificant for samples with a good water yield.

Tab. 4.6-6: Water contents and results of aqueous-extraction tests on previously squeezed samples (method 1, POST data)

Depth [m]	**Formation**	**Water content (wet) of squeezed sample** [wt.-%]	**Reconstructed initial water content (wet)** [wt.-%]	**Mass of porewater in squeezed sample** [g]	**Aqueous extraction of squeezed sample**				
					Mass of dry rock [g]	**Mass of added water** [g]	***S/L*** [g/g]	**Cl** [mg/$L_{extract\ solution}$]	**Br** [mg/$L_{extract\ solution}$]
732.74	Variansm. Fm.	4.705	5.651	18.02	30.13	30.08	1.002	132	0.36
792.72	«Murch.-Ool. Fm.»	4.435	5.365	16.98	30.04	30.09	0.998	126	0.35
850.29	Opalinus Clay	3.909	4.476	15.06	30.39	30.29	1.003	111	0.30
911.28	Staffelegg Fm.	3.471	4.078	12.33	30.18	30.19	1.000	120	0.17

Tab. 4.6-7: Water contents and results of aqueous-extraction tests on material adjacent to squeezed samples (method 2, PRE data)

Depth [m]	**Formation**	**Water content (wet)** [wt.-%]	**Aqueous extraction of virgin material adjacent to squeezed sample**				
			Mass of dry rock [g]	**Mass of added water** [g]	***S/L*** [g/g]	**Cl** [mg/$L_{extract\ solution}$]	**Br** [mg/$L_{extract\ solution}$]
732.74	Variansm. Fm.	5.820	28.64	30.48	0.888	181	0.54
792.72	«Murch.-Ool. Fm.»	5.550	29.79	30.37	0.927	190	0.53
850.29	Opalinus Clay	5.086	28.95	30.44	0.905	158	0.47
911.28	Staffelegg Fm.	4.409	29.51	30.40	0.929	211	0.63

4.6.6 Chloride-accessible porosity

The Cl-accessible porosity fraction f_{Cl} can be estimated from:

$$f_{Cl} = \frac{C_{Cl\ in\ bulk\ porewater}}{C_{Cl\ in\ squeezed\ water}}$$

$C_{Cl\ in\ squeezed\ water}$ is taken from Tab. 4.6-4, assuming that these data represent the concentrations in the anion-accessible pore space. $C_{Cl\ in\ bulk\ porewater}$ can be obtained using the two alternative methods described in Section 4.6.5. According to method 1, the masses of Cl and water obtained by squeezing and by drying/aqueous extraction of the squeezed material are added. The formalism is documented in more detail in Mazurek et al. (2021), and the results are listed in Tab. 4.6-8.

Alternatively, applying method 2, $C_{Cl\ in\ bulk\ porewater}$ can be obtained directly by drying/aqueous extraction of adjacent, unsqueezed rock according to:

$$C_{Cl\ in\ bulk\ porewater} = \frac{C_{Cl\ in\ extract\ solution}}{S/_L\ w_d}$$

using the data listed in Tab. 4.6-7 (w_d = water content relative to dry rock). The results are shown in Tab. 4.6-9.

The resulting Cl-accessible porosity fractions obtained by the two methods are also listed in Tabs. 4.6-8 and 4.6-9. They are shown as a function of the clay-mineral content in Fig. 4.6-6. The clay-rich samples from the Dogger yield consistent results with values for f_{Cl} in the narrow range 0.50 – 0.56. The results obtained by the two methods agree closely, with marginally higher values for method 2.

The sample from the Staffelegg Formation shows a major discrepancy between the two methods, with the lowest f_{Cl} for method 1 and an aberrantly high f_{Cl} for method 2. Macroscopically, the sample appears to be homogeneous (Fig. 4.6-1), so heterogeneity is not an obvious explanation. The following arguments can be put forward:

- The Rietheim Member of the Staffelegg Formation has a high content of organic material (Tab. 4.6-1) and contains abundant macroporous fossils in specific horizons. The architecture of the pore space may therefore show particular characteristics.
- A high f_{Cl} is suspected on the basis of aqueous extraction data, as discussed in Section 5.2.
- Recent data have shown systematic differences between Br concentrations from aqueous extracts performed on wet sample materials (=standard procedure) and extracts performed on samples that were dried at 105 °C under atmospheric conditions prior to extraction (Section 4.4). In order to explore this observation, unsqueezed portions of squeezing samples from STA-3 and STA-2 were subjected to both wet and dry extraction. Br concentrations from dry extracts were systematically lower, and the largest discrepancy was observed for the sample from the Rietheim Member from STA-2. Cl concentrations based on the two extraction methods were consistent, with the exception of the sample from the Rietheim Member from STA-2 where the value from the dry extract was 27% lower when compared to the wet extract. Note that f_{Cl} data listed for method 2 (Tab. 4.6-9) are based on wet extracts (Section 4.6.5). When using data from dry extracts, a value for f_{Cl} of 0.51 is obtained, compared to 0.70 when using wet extracts.
- The processes leading to the observed discrepancies are not well known at this stage. For Cl, the organic-rich sample from the Rietheim Member is the only one showing a discrepancy for Cl, while for all other samples the differences are minor and do not markedly affect the calculation of f_{Cl}. In general, a value around 0.7 better fits independent data (e.g. those from diffusion experiments, or the larger mean pore diameters obtained from N_2 ad-/desorption isotherms, see Section 4.3.5).
- At this stage, it is difficult to judge which of the two f_{Cl} values obtained for the Rietheim Member is closer to reality, and both should be used with caution.

Tab. 4.6-8: Cl-accessible porosity fractions derived from squeezing and aqueous-extraction experiments using method 1 to obtain $C_{Cl\ in\ bulk\ porewater}$

Depth [m]	**Formation**	**Total mass of squeezed Cl** [mg]	**Mass of Cl in aq. extract of squeezed core** [mg]	**Porewater mass squeezed** [g]	**Water mass remaining in squeezed core** [g]	**Cl in bulk pore-water** [mg/L]	**Cl-accessible porosity fraction f_{Cl}** [-]
732.74	Variansm. Fm.	22.21	48.1	3.84	18.02	3'215	0.50
792.72	«Murch.-Ool. Fm.»	22.04	46.0	3.76	16.98	3'281	0.52
850.29	Opalinus Clay	13.61	40.9	2.29	15.06	3'141	0.52
911.28	Staffelegg Fm.	7.47	41.0	2.25	12.33	3'327	0.47

Tab. 4.6-9: Cl-accessible porosity fractions derived from squeezing and aqueous-extraction experiments, using method 2 to obtain $C_{Cl\ in\ bulk\ porewater}$

Depth [m]	**Formation**	**Cl concentration in bulk porewater (in adjacent unsqueezed rock)** [mg/L]	**Cl-accessible porosity fraction f_{Cl}** [-]
732.74	Variansm. Fm.	3'307	0.51
792.72	«Murch.-Ool. Fm.»	3'490	0.56
850.29	Opalinus Clay	3'253	0.54
911.28	Staffelegg Fm.	4'925	0.70

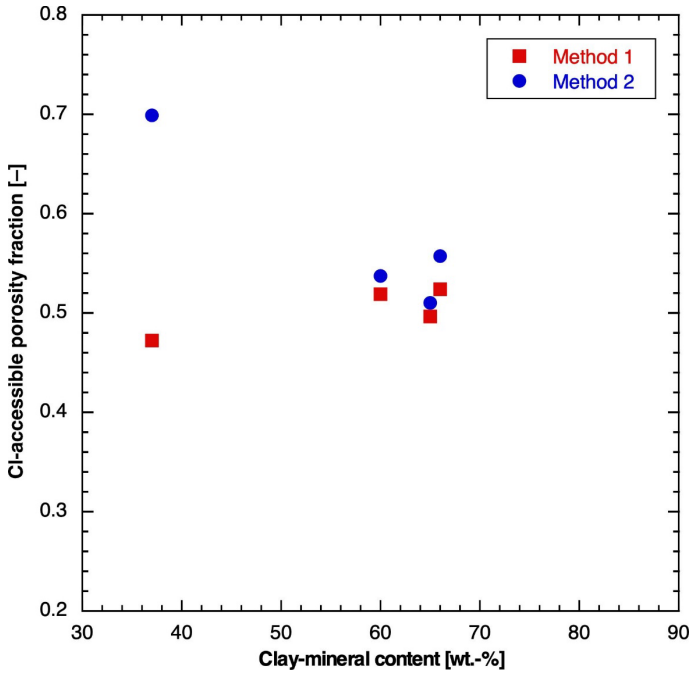

Fig. 4.6-6: Cl-accessible porosity fractions derived from squeezing experiments as a function of the clay-mineral content

See text for explanations regarding the two methods.

4.6.7 Stable isotopic composition of squeezed water

Results of stable water-isotope analyses are listed in Tab. 4.6-10 and shown as a function of depth in Fig. 4.6-7. The following observations can be made:

- Within any sample, the variation of the δ-values with squeezing pressure is small (within analytical error).
- $\delta^{18}O$ shows a distinct trend of values decreasing downwards, whereas $\delta^{2}H$ shows no depth trend in the Dogger but a more negative value in the Staffelegg Formation.
- In a plot $\delta^{18}O$ vs. $\delta^{2}H$ (Fig. 4.6-8), the shallower samples are located far on the right side of the global ($\delta^{2}H = 8\ \delta^{18}O + 10$, Craig 1961) and the local ($\delta^{2}H = 7.55\ \delta^{18}O + 4.8$, Kullin & Schmassmann 1991) meteoric water lines. The deeper samples come closer to these lines.
- The same information is illustrated in Fig. 4.6-9 by the depth trend of deuterium excess ($\delta^{18}O - 8\ \delta^{2}H$), which increases systematically with depth.

Tab. 4.6-10: Stable isotopic composition of squeezed waters

The aliquots selected for interpretation are shown in bold.

Depth [m]	**Formation**	**Pressure** [MPa]	**$\delta^{18}O$** [‰ VSMOW]	**$\delta^{2}H$** [‰ VSMOW]	**D excess** [‰]
732.74	Variansm. Fm.	**200**	**–3.56**	**–38.2**	**–9.7**
		300	–3.64	–38.3	–9.2
792.72	«Murchisonae-Ool. Fm.»	**200**	**–4.04**	**–38.0**	**–5.7**
		300	–4.08	–38.3	–5.6
850.29	Opalinus Clay	**200**	**–4.51**	**–38.9**	**–2.8**
		300	–4.39	–38.3	–3.2
911.28	Staffelegg Fm.	**300**	**–5.18**	**–40.6**	**0.8**
		400	–5.22	–41.3	0.5

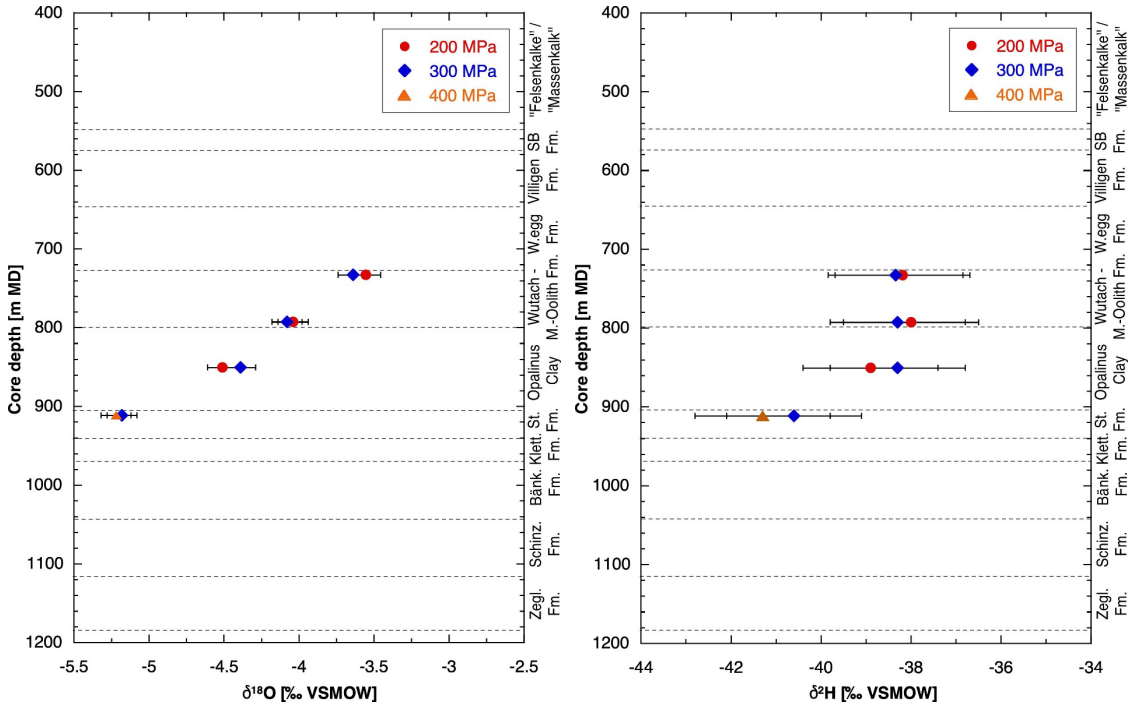

Fig. 4.6-7: Depth trends of $\delta^{18}O$ and $\delta^{2}H$ in squeezed waters

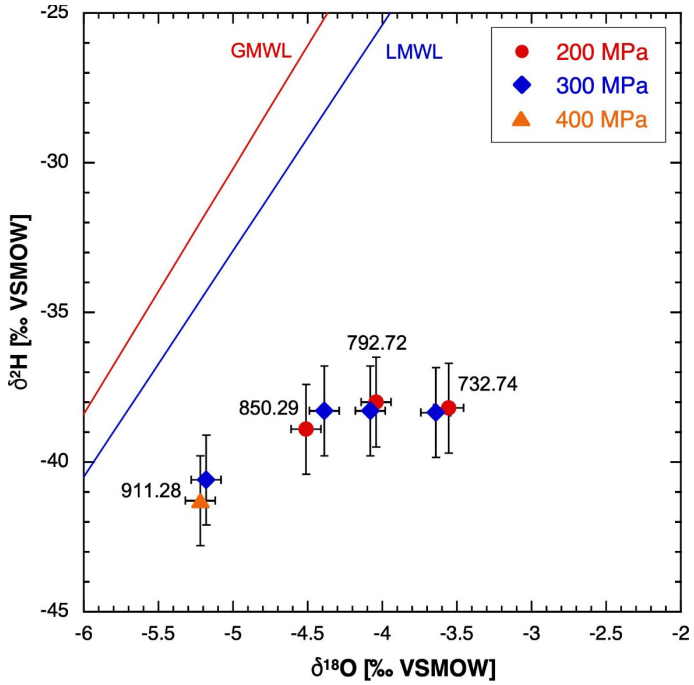

Fig. 4.6-8: Plot of $\delta^{18}O$ vs. $\delta^{2}H$ for squeezed waters
GMWL = Global Meteoric Water Line, LMWL = Local Meteoric Water Line. Numbers indicate sample depths in m.

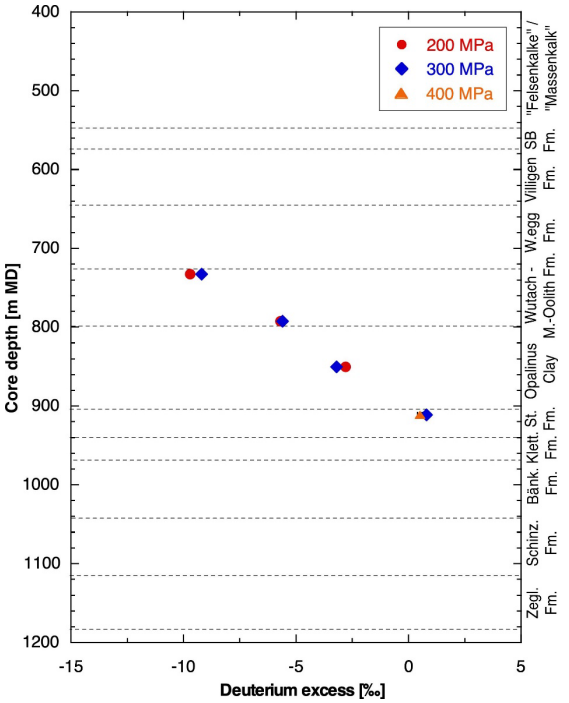

Fig. 4.6-9: Depth trend of deuterium excess in squeezed waters

4.7 Data from advective displacement experiments

Andreas Jenni, Mirjam Kiczka, Carmen Zwahlen & Urs Mäder

Advective displacement (AD) experiments are a methodology for a comprehensive physico-chemical characterisation, including porewater chemistry and certain transport properties (details in method report, Waber ed. 2020). This section presents a data summary, more details where important, and short discussions where appropriate. The full data sets are provided in Appendix B. Integration of the data into context and depth profiles are included in Chapter 5.

Initially three samples from the Opalinus Clay and the clay-rich confining units were processed. These experiments were successful from a technical point of view, subjected to a similar analytical program, with differences mainly related to the duration of each experiment (numbers of sampled fluid aliquots). However, during data processing, it became clear that the high nitrate concentrations – an experimental artefact – in all three experiments disturbed the chemical system in the cores to an extent that did not allow for the characterisation of the in-situ porewater and initial anion accessible porosity fractions (discussed in Section 4.7.5.4). In addition, Ag filters replaced the PEEK filters used in earlier experiments, with the intention to suppress microbial activity. But this led to lower Br concentrations in early aliquots, attributed to surface complexation/precipitates on the filters. All information about these compromised experiments is written in italics. An additional experiment with a sample from the Opalinus Clay was started at a later time, for which sample preparation was improved as detailed in Section 4.7.2. This experiment was subjected to a shorter duration. The extent of pre- and post-mortem characterisation of core material was optimised based on gained experience from former boreholes BUL1-1, TRU1-1, MAR1-1, BOZ1-1, and BOZ2-1 investigations. The program fulfilled the planned work, but partially provided longer durations of advective displacement than requested. The duration of the percolation period was 56 – 380 days, transporting 0.3 – 2.5 pore volumes of fluid.

The salinity in this borehole is in the range of BUL1-1, TRU1-1 and MAR1-1 boreholes, but significantly higher than in BOZ1-1 and BOZ2-1 (neglecting the nitrate contribution; see Section 4.7.5.4).

4.7.1 Sample material and overview of analytical work

The four sample cores (Fig. 4.7-1) span 145 m of clay-rich confining and host rock units (778 – 923 m depth), from the «Humphriesioolith Formation» («Brauner Dogger») to the Staffelegg Formation, and include two samples from the Opalinus Clay, including the one processed at a later time.

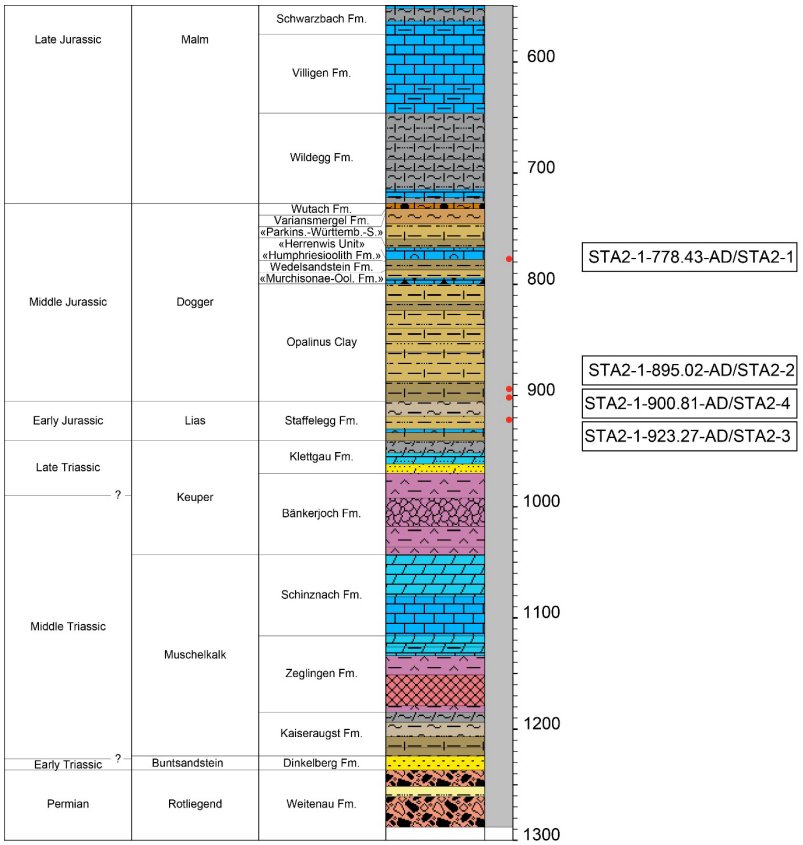

Fig. 4.7-1: Location of samples used for advective displacement experiments (red dots)
Short labels are consecutively numbered laboratory abbreviations. STA2-4 (Opalinus Clay) was processed at a later time.

X-ray computed tomography (CT) was performed on a medical scanner (Waber ed. 2020) for sample selection (Fig. 4.7-2) and detection of disturbing features (fractures, pyrite accumulations, macro-fossils, etc.). Dry cutting with a mitre saw was used for obtaining a central core segment for AD experiments (yellow in Fig. 4.7-2), and adjacent two discs for accompanying characterisation (green in Fig. 4.7-2). In case of STA2-4, disking during cutting only allowed for sampling two discs below the core segment for the AD experiment, and in case of STA2-2 only one disc from above the AD-core could be taken. The central core segment was machined on a lathe from 95 mm to 80 mm in diameter. Tab. 4.7-1 lists all analytical work performed on the four samples.

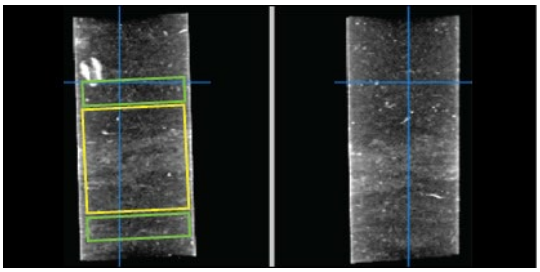

STA2-1-778.43-AD («Humphriesioolith Fm.»)

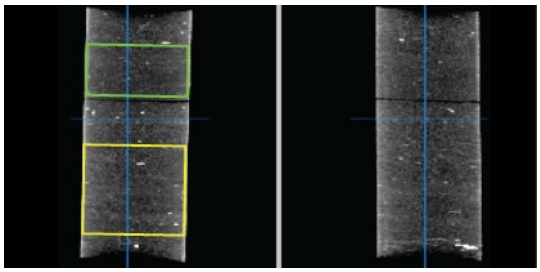

STA2-1-895.02-AD (Opalinus Clay)

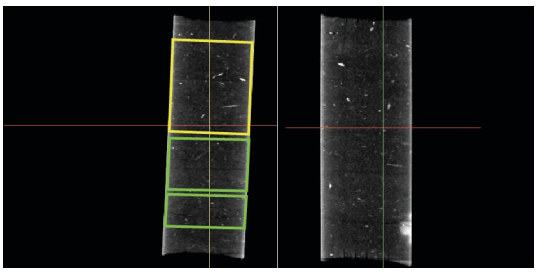

STA2-1-900.81-AD (Opalinus Clay)

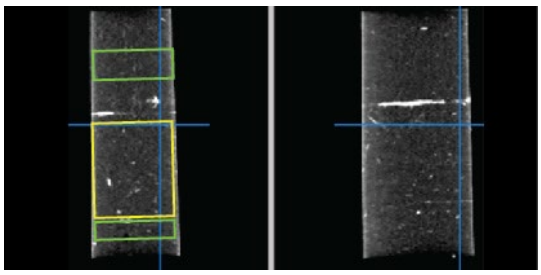

STA2-1-923.27-AD (Staffelegg Fm.)

Fig. 4.7-2: X-ray CT images of AD samples

Central sections parallel to core axis at right angle. Grey scale range setting is 1'700 – 2'500 HU. Yellow segments are used for advective displacement, green segments for pre-characterisation. Low X-ray absorbance represents clay/quartz-rich sections (darker grey), slightly lighter grey indicates carbonate-richer parts, siderite is brighter, and pyrite is white (strongest absorbance). Black lines/gaps represent fractures. Image base is downhole direction.

Tab. 4.7-1: Summary of analytical work performed on samples for advective displacement experiments

y = yes = done; n = no = not done; integer numbers refer to the number of samples processed; +: samples from above (left number) and below (right number) the core were processed, or the sum of both samples (ave); 'above' and 'below' refer to the orientation in the infiltration apparatus, which is reversed in case of STA2-4 compared to Fig. 4.7-2 (see section below); Pre: sample pre-characterisation; Post: post-mortem characterisation; WC: water content; M: mass; V,A,L: core volume, sectional area and length; Min: mineralogy; Clay: clay mineralogy; AqEx: aqueous extracts; Ni-en: cation selectivity with Ni-en method; Post_WC: post-mortem water content determined along a profile with 5 segments; AD_exp: complete analysis of fluid sample aliquots collected during advective displacement.

Parameter	**STA2-1**	**STA2-2**	**STA2-4**	**STA2-3**
Sample ID RWI	STA2-1-778.43-AD	STA2-1-895.02-AD	STA2-1-900.81-AD	STA2-1-923.27-AD
Lab sample ID	STA2-1xx-AD	STA2-2xx-AD	STA2-4xx-AD	STA2-3xx-AD
Depth [m]	778.43	895.02	900.81	923.27
Geol. unit	«Humphriesioolith Fm.»	Opalinus Clay	Opalinus Clay	Staffelegg Fm.
Member		Clay-rich sub-unit'		Frick Mb.
AD_exp	y	y	y	y
Pre_WC	1+1	1+0	2+0	1+1
Pre_M	y	y	y	y
Pre_V,A,L	y	y	y	y
Pre_Min	1	1	1	1
Pre_Clay	1	1	1	1
Pre_AqEx	1+1	1+0	2+0	1+1
Pre_Ni-en	ave	1+0	n	ave
Post_WC	5	2	4	5
Post_M	y	n	y	y
Post_V,A,L	y	n	y	y
Post_AqEx	1+1	0+1	1+1	1+1
Post_Ni-en	n	n	n	n

4.7.2 Conditions of advective displacement experiments

Sample preparation was performed according to Waber (ed.) (2020). In addition to the description therein, the STA2-4 core was fully wrapped with elastic electric tape on top of the latex sleeves (tape was only applied to the ends of the latex rubber sleeves in previous sample preparations). Then, a cold-shrink tube (3M Kaltschrumpfschlauch 8430.9, EPDM, 93.7/42.6/229) was applied, overlapping the edges of the Ti head pieces. The ends of the cold-shrink sleeve were sealed with clear silicone sealant, as done with the latex rubber sleeves. Cores were infiltrated from the base upwards (Fig. 4.7-2), i.e., against downhole direction, except STA2-4: this core was flipped by 180° and was infiltrated parallel to the downhole direction. Therefore, the aqueous extracts from the top of the core segment as mounted in the apparatus can be compared with the early exfiltrating chemistry to estimate the anion accessible porosity. All figures or sample names refer to the orientation in the infiltration apparatus.

Ag membrane filters replaced the PEEK filters used in earlier experiments as a measure to reduce any potential microbial activity in all cores except STA2-4. However, the first measured aliquots were significantly lower in Br compared to later aliquots and had a lower Br/Cl ratio as obtained from aqueous extracts. This reduction of Br concentration was attributed to surface complexation on the Ag filters to form AgBr. Ag filters were abandoned after STA2-3 preparation, as was done for STA2-4 for which PEEK filters were used as for earlier experiments.

The overview table (Tab. 4.7-2) presents some experiment specific parameters such as variation in sample preparation, sample processing dates, storage time and other characteristic times like arrival of the first fluid drop and its electric conductivity. Numbers of samples taken and analysed are listed as well as average pressures for confining and injection. The number of percolated pore volumes is based on the water content determined from pre-characterisation. Infiltration pressure of the artificial porewater (APW) was on average 46 bar, pressurised by He. The hydraulic gradients are large, 5'000 – 6'000 m_{H2O}/m (sample dimensions are in Tab. 4.7-4). Experiments were started within 3 days of sample delivery and 2 weeks after drilling, but the second OPA sample STA2-4 was started almost 14 months after drilling. The time until arrival of a first fluid drop at the electric conductivity cell (outflow, before sampling syringe) was 7 – 17 days after start of infiltration.

Confining pressure was on average 62 – 66 bar, pressurised by a piston pump and controlled by diaphragm accumulators, where a membrane separates the confining fluid from the pre-pressurised gas (Membranspeicher MBSP 050-210/60 S ST NBR). There is no gas-water interface in this set-up, and no gas is expected to dissolve in the confining fluid. In the previous set-up, Ar or Kr was used to pressurise the confining fluid, but these gases were detected in the syringes that collected the exfiltrate owing to a small gas-permeability of the latex membranes.

Tab. 4.7-2: Conditions of advective displacement experiments

Parameter	**STA2-1**	**STA2-2**	**STA2-4**	**STA2-3**
Depth [m]	778.43	895.02	900.81	923.27
Geol. unit	«Humphriesioolith Fm.»	Opalinus Clay	Opalinus Clay	Staffelegg Fm.
Drilled	04.03.2021	11.03.2021	11.03.2021	12.03.2021
Delivered	08.03.2021	22.03.2021	14.02.2022	22.03.2021
Prep_AD	11.03.2021	25.03.2021	25.04.2022	25.03.2021
Injection	12.03.2021	26.03.2021	26.04.2022	26.03.2021
First drop	29.03.2021	08.04.2021	07.05.2022	01.04.2021
Days to first drop	17.3	12.4	11.3	6.5
Initial gas [mL]	3.4	13.6	0.1	10.7
End_AD	26.08.2021	11.4.2022	21.06.2022	25.08.2021
Duration [d]	166.8	380.4	55.9	151.9
Pore-volumes	0.8	1.1	0.3	2.5
EC_initial (25°C) [mS/cm]	24.4	23.4	27.3	20.5
Filter	Ag-Filter	Ag-Filter	PEEK fabric	Ag-Filter
Core packing	Teflon tape, 2 latex sleeves	Teflon tape, 2 latex sleeves	Teflon tape, 2 latex sleeves, adhesive tape, cold-shrink tube	Teflon tape, 2 latex sleeves
Confining pressure	Piston pump on water, diaphragm accumulator	Piston pump on water, diaphragm accumulator	Piston pump on water, diaphragm accumulator	Piston pump on water, diaphragm accumulator
AD-samples	13	13	7	20
AD-samp_chem	10	10	3	14
AD-samp_isotopes	10	10	4	14
in-line pH	8	7	3	11
P_Conf [bar]	66	62	62	60
P_Inf [bar]	46	47	46	46
Gradient [mH_2O/m]	5'375	5'738	6'087	5'706

4.7.3 Mineralogy and petrophysical properties

For each core, the mineralogy was determined on the sum of subsamples cut adjacent to the core segment used for the AD experiments (Tab. 4.7-1). Results are summarised in Tab. 4.7-3 and plotted in Section 4.2. Samples cover a range of clay-mineral contents of 39 – 70 wt.-%, calcite contents of 6 – 17 wt.-%, and quartz contents of 16 – 44 wt.-%. The clay-mineral fraction is composed of variable amounts of illite (13 – 22 wt.-%), illite/smectite mixed layers (15 – 32 wt.-%), and kaolinite (9 – 32 wt.-%). The clay-mineral content of sample STA2-4 is higher (70 wt.-%) than for most Opalinus Clay AD cores processed so far.

Carbon, sulphur and nitrogen analyses are also included. Pyrite contents are moderately low (0.3 – 1 wt.-%) because pyrite-rich lithologies were avoided based on X-ray CT characterisation (Fig. 4.7-2). More details, including end-member clays, are included in Appendix B.

A plethora of petrophysical parameters can be derived from sample dimensions, mass, water content, and changes in these parameters determined before and after an AD experiment (Tab. 4.7-4). These quantities include porosity, bulk density, grain density, water uptake during the experiments, and unsaturated porosity (saturation ratio). The relationships are given in Waber (ed.) (2020). Note that the water content determined for pre-characterisation is based on 2 sub-samples adjacent to the AD core segment, if sufficient material was available.

The corrected initial water content as well as any unsaturated (gas-filled) porosity fraction of the core used in the AD experiment can be derived from the post-mortem water content and the usually observed slight core volume expansion during the experiment. The core volume increases by 0.5 – 1.4% (Tab. 4.7-4), accompanied by a water uptake of 4.0 – 5.4 g. Accounting for volume expansion, there remains a small net water uptake of 0.6 – 2.9 g that must reflect an initially small volume of unsaturated porosity, ranging from 0.6 – 2.9 mL, corresponding to a saturation ratio in the range 0.95 – 0.99. This analysis is valid if significant drying of a sample core is avoided during sample preparation by minimising exposure times, as was done for AD experiments (Waber ed. 2020). In case of STA2-4, the core expansion exceeds the water uptake, which leads to an initial saturation slightly > 1. This is very likely due to the largest measurement uncertainty, associated with the measurement of the core dimensions using callipers. Although reading precision is in the order of 0.05 mm, using callipers on slightly uneven cores adds to the uncertainty, as do any small breakouts along edges. Assuming a practical accuracy of ± 0.1 mm for diameter and length, results in a typical error of approximately ± 1 mL in core volume (or ± 1 g in terms of porewater mass) for the core dimensions commonly used. Such an error would translate to a saturation ratio of 0.98 – 1.02 at porewater contents of 40 – 50 g. Thus, the initial state can be assumed saturated for samples STA2-2 and STA2-4. STA2-1 and STA2-3 yield saturation ratios of 0.95 and may thus have been initially marginally desaturated, indicative of the presence of a gas phase (already in situ or after core retrieval), if sample drying during core recovery and handling can be excluded. Note that these samples are still nearly saturated.

Tab. 4.7-3: Mineralogy of advective displacement samples, including C, S and N analyses
b.d.: below detection

Parameter	**Unit**	**STA2-1**	**STA2-2**	**STA2-4**	**STA2-3**
Depth	[m]	778.43	895.02	900.81	923.27
Geol. unit		«Humphr.ool. Fm.»	Opalinus Clay	Opalinus Clay	Staffelegg Fm.
S	[wt.-%]	0.4	0.5	0.4	0.1
C(inorg)	[wt.-%]	2.3	1.2	1.1	0.9
C(org)	[wt.-%]	0.8	1.0	0.9	0.8
N	[wt.-%]	0.0	0.1	b.d.	0.0
Quartz	[wt.-%]	19	17	15	44
K-feldspar	[wt.-%]	5	5	1	6
Plagioclase	[wt.-%]	3	3	2	4
Calcite	[wt.-%]	17	7	7	6
Dolomite / Ankerite	[wt.-%]	1	b.d.	b.d.	2
Siderite	[wt.-%]	b.d.	3	2	b.d.
Anhydrite	[wt.-%]	b.d.	b.d.	b.d.	b.d.
Celestite	[wt.-%]	b.d.	b.d.	b.d.	b.d.
Pyrite	[wt.-%]	1	1	0.7	0.3
Clay minerals	**[wt.-%]**	**54**	**63**	**70**	**39**
Illite	[wt.-%]	18	16	16	13
Illite/smectite ML (85-90)	[wt.-%]	7	7	16	7
Illite/smectite ML (75-80)	[wt.-%]	8	6	3	b.d.
Illite/smectite ML (50-70)	[wt.-%]	3	2	4	4
Illite/smectite ML (20-40)	[wt.-%]	b.d.	b.d.	b.d.	b.d.
Smectite	[wt.-%]	0.1	b.d.	b.d.	b.d.
Kaolinite	[wt.-%]	11.2	23.5	22.7	8.9
Chlorite	[wt.-%]	1.4	1.5	1.0	0.8
Chl/Sm ML (85-95)	[wt.-%]	5.2	6.3	7.7	5.0
Total illite/smectite	[wt.-%]	**18**	**15**	**23**	**17**
(tot_ill/sm+sm)/(total_clay)		0.34	0.24	0.33	0.45
(tot_ill+ill/sm+sm)/(total_clay)		0.67	0.50	0.55	0.78

Tab. 4.7-4: Core dimensions and derived petrophysical parameters

_L = length; _A = area; _V = volume; _M = mass; WD = wet density; GD = grain density; WCw = water content rel. to wet mass; _WL = water loss

Parameter	**Unit**	**STA2-1**	**STA2-2**	**STA2-4**	**STA2-3**
Depth	[m]	778.43	895.02	900.81	923.27
Geol. unit		«Humphr.ool. Fm.»	Opalinus Clay	Opalinus Clay	Staffelegg Fm.
Pre_Core_M	**[g]**	**1'069.92**	**1'024.14**	**958.10**	**1'030.41**
Pre_Core_DM	[cm]	8.00	8.01	8.00	8.01
Pre_Core_L	[cm]	8.49	8.09	7.60	8.08
Pre_Core_A	[cm^2]	50.27	50.37	50.24	50.39
Pre_Core_V	[cm^3]	427.01	407.61	381.74	407.21
Post_Core_M	**[g]**	**1'074.98**	**1'029.55**	**962.58**	**1'034.38**
Post_Core_DM	[cm]	8.01	8.02	8.02	8.02
Post_Core_L	[cm]	8.52	8.16	7.66	8.11
Post_Core_A	[cm^2]	50.35	50.52	50.52	50.48
Post_Core_V	[cm^3]	429.16	412.45	387.06	409.19
Delta_M	**[g]**	**5.06**	**5.41**	**4.48**	**3.96**
Delta_Core_DM	[cm]	0.006	0.011	0.022	0.007
Delta_Core_L	[cm]	0.029	0.073	0.064	0.026
Delta_Core_A	[cm^2]	0.079	0.145	0.277	0.085
Delta_Core_V	[cm^3]	**2.153**	**4.834**	**5.323**	**1.974**
Delta_Core_V-%	[%]	0.504	1.186	1.395	0.485
Pre_Bulk_WD	**[g/cm^3]**	**2.506**	**2.513**	**2.510**	**2.530**
Post_Bulk_WD	**[g/cm^3]**	**2.505**	**2.496**	**2.487**	**2.528**
Delta_Bulk_WD	[g/cm^3]	-0.001	-0.016	-0.023	-0.003
Delta_Bulk_WD-%	[%]	-0.031	-0.650	-0.914	-0.100
Pre_GD	**[g/cm^3]**	**2.751**	**2.718**	**2.735**	**2.690**
Post_GD	**[g/cm^3]**	**2.746**	**2.721**	**2.710**	**2.703**
Delta_GD	[g/cm^3]	-0.005	0.003	-0.025	0.013
Corr_Pre_GD	**[g/cm^3]**	**2.725**	**2.716**	**2.717**	**2.689**
Pre_WCw		**0.0559**	**0.0475**	**0.0517**	**0.0374**
Post_WCw		**0.0551**	**0.0523**	**0.0524**	**0.0407**
Delta_WCw		-0.0008	0.0047	0.0007	0.0033
Corr_Pre_WCw		**0.0507**	**0.0473**	**0.0480**	**0.0371**
Pre_H_2O_Core	**[g]**	**59.85**	**48.66**	**49.55**	**38.55**
Post_H_2O_Core	**[g]**	**59.28**	**53.80**	**50.46**	**42.15**
Delta_H_2O_Core	[g]	-0.57	5.14	0.91	3.60
Corr_Pre_H_2O_Core	**[g] or [mL]**	**54.21**	**48.39**	**45.98**	**38.19**
Unsat_Vol	[g] or [mL]	2.91	0.58	-0.84	1.99
Pore_Vol_tot	[mL]	57.12	48.97	45.14	40.18
Sat_ratio		**0.95**	**0.99**	**1.02**	**0.95**
Pre_Poro_WL		**0.1402**	**0.1194**	**0.1298**	**0.0947**
Post_Poro_WL		**0.1381**	**0.1305**	**0.1304**	**0.1030**
Delta_Poro_WL		-0.0020	0.0111	0.0006	0.0084
Delta_Poro_WL-%	[%]	-1.4495	9.2768	0.4449	8.8212
Corr_Pre_Poro_WL		**0.1270**	**0.1187**	**0.1205**	**0.0938**
Corr_Pre_Poro_tot		**0.1338**	**0.1201**	**0.1182**	**0.0987**
Delta_Corr_Poro_WL-%	[%]	-9.41	-0.55	-7.20	-0.93

There are significant differences in water content measured in adjacent samples (pre-characterisation) and in the core itself (post-mortem), the latter showing -1.5%$_{rel.}$ to +9.3%$_{rel.}$ higher values. It reduces to -9.4%$_{rel.}$ to -0.6%$_{rel.}$ if accounting for core expansion (Delta_Corr_Poro_WL-%). This leads to different values of bulk wet density, water-loss porosity and grain density (assuming saturated conditions) derived from pre-characterisation and post-mortem data (Fig. 4.7-3). This spread is larger than measurement uncertainties and illustrates that the largest contribution to uncertainty is sample heterogeneity for parameters that depend on water content. Differences in water content commonly correlate with differences in clay-mineral content, such that this heterogeneity is mainly an issue of lamination in fine-grained sediments. In case of STA2-1, a thin layer enriched in calcite at the middle of the AD core (visible as bright band/laminae on the CT image, Fig. 4.7-2) is suspected to cause this low water content.

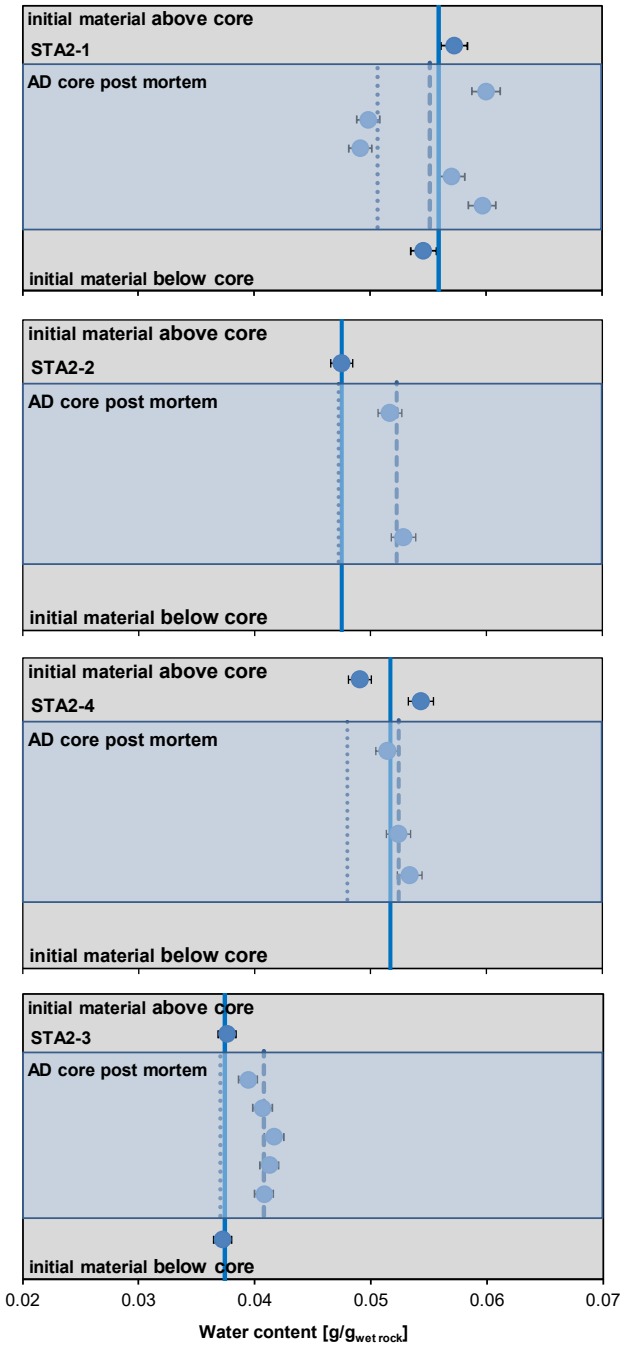

Fig. 4.7-3: Details of water content measurements before and after AD experiments

STA2-1 = STA2-1-778.43-AD («Humphriesioolith Fm.»); STA2-2 = STA2-1-895.02-AD (Opalinus Clay); STA2-4 = STA2-1-900.81-AD (Opalinus Clay); STA2-3 = STA2-1-923.27-AD (Staffelegg Fm.). Vertical lines indicate the average value for pre-characterisation (solid line), average of post-mortem characterisation (dashed line) and the calculated corrected initial water content (dotted line). Error bars refer to measurement uncertainty of 2%.

4.7.4 Aqueous extracts, CEC and cation selectivity of AD samples

Aqueous extracts, CEC and cation selectivity determinations were carried out within the pre-characterisation and post-mortem analysis. Detailed analyses are provided in Appendix B. Methods are the same as used for other core samples (Waber ed. 2020), with the exception of sample masses for water content that may have been smaller than used for regular core sample analysis. Averaged data – also used for integrative data plots – are presented in this section. Averaging refers to aqueous extraction measurements of pieces above and below the segment used for the AD experiments (indicated in Fig. 4.7-2 and Tab. 4.7-5). For CEC / cation selectivity, the pieces were combined in equal proportions and analysed as a single sample.

All averaged aqueous extract solutions (Tab. 4.7-5) from pre-characterisation processed at $S/L \approx 1$ (solid/liquid weight ratio) contain low concentrations of NH_4 (up to 1.5 mg/L) and NO_3 (up to 0.73 mg/L). *S/L* (S_d/(L+PW)) refers to the exact *S/L* of the aqueous extract accounting for the porewater of the wet solid sample with weight S_w (S_d: weight of dry solid). The factor ($1/WC_w \cdot L/S_w$) refers to the scaling factor required to scale aqueous concentrations for conservative components to porewater concentrations (i.e. at water content).

Characteristic molar ion ratios (Tab. 4.7-6) do not follow a systematic trend with depth. Tab. 4.7-7 shows that the aqueous extract solutions are at or very close to calcite saturation. Extracts are distinctly undersaturated with respect to sulphates and strontianite, and also undersaturated with respect to dolomite (ordered). TIC was used as input for the carbon system, because the titrated alkalinity would also include acetate. However, the calculated alkalinity agrees well with the measured one due to low relative acetate concentrations in samples from this borehole.

Tab. 4.7-5: Composition of aqueous extract solutions from pre-characterisation

Parameter	**Unit**	**STA2-1**	**STA2-2**	**STA2-4**	**STA2-3**
Depth	[m]	778.43	895.02	900.81	923.27
Geol. unit		«Humphr.ool. Fm.»	Opalinus Clay	Opalinus Clay	Staffelegg Fm.
Averaging		top+base (1+1)	Top (1)	top1+top2 (2+0)	top+base (1+1)
$1/WC_w*L/S_w$		19.13	22.03	20.68	28.04
Rock wet	[g]	30.02	30.47	29.39	30.15
Water	[g]	30.43	30.44	29.84	30.50
WC_w	[g/g_{wet}]	0.056	0.048	0.052	0.037
S/L (S_d/(L+PW))		0.883	0.910	0.889	0.918
pH at Titration		8.76	8.76	8.63	9.12
Na	[mg/L]	276	288	279	241
NH_4	[mg/L]	1.49	1.10	1.46	1.16
K	[mg/L]	6.84	6.95	9.44	6.26
Ca	[mg/L]	3.39	3.72	3.36	1.92
Mg	[mg/L]	0.737	0.727	0.655	0.320
Sr (OES)	[mg/L]	0.080	0.091	< 0.1	0.050
Ba (OES)	[mg/L]	< 0.025	< 0.025	< 0.025	0.030
F	[mg/L]	4.88	3.05	3.16	4.60
Cl	[mg/L]	173	142	148	118
Br	[mg/L]	0.56	0.48	0.41	0.26
NO_3	[mg/L]	0.64	0.73	0.42	0.46
SO_4	[mg/L]	235	231	219	205
I	[mg/L]	n.d.	n.d.	n.d.	n.d.
Alk (tit)	[meq/L]	2.91	3.95	3.71	2.99
Alk as HCO_3	[mg/L]	177.6	241.0	226.6	182.2
TOC	[mg/L]	< 5	5.19	1.81	4.47
TIC	[mg/L]	33.5	49.1	46.2	33.8
lactate	[mg/L]	< 0.2	< 0.2	< 2	< 0.2
acetate	[mg/L]	5.40	7.61	4.68	1.87
propionate	[mg/L]	< 0.2	< 0.2	< 2	0.392
formate	[mg/L]	0.256	0.391	< 2	0.277

Tab. 4.7-6: Cation ratios and details of carbon system in aqueous extract solutions from pre-characterisation

Parameter	**Unit**	**STA2-1**	**STA2-2**	**STA2-4**	**STA2-3**
Depth	[m]	778.43	895.02	900.81	923.27
Geol. unit		«Humphr.ool. Fm.»	Opalinus Clay	Opalinus Clay	Staffelegg Fm.
Br/Cl*1'000	[mol/mol]	1.43	1.49	1.22	1.00
SO_4/Cl	[mol/mol]	0.50	0.60	0.55	0.64
Ca/Mg	[mol/mol]	2.79	3.10	3.11	3.64
Ca/Sr	[mol/mol]	93	89	Sr < 0.1	85
(Ca+Mg)/(Na+K)	[eq/eq]	0.014	0.015	0.014	0.009
Alk (tit)	[meq/L]	2.91	3.95	3.71	2.99
TIC	[meq/L]	2.78	4.09	3.84	2.81
acetate	[meq/L]	0.091	0.129	0.079	0.032
TOC	[mg/L]	< 5	5.2	1.8	4.5
acetate (as C)	[mg/L]	2.20	3.10	1.90	0.76

Tab. 4.7-7: Saturation indices calculated for aqueous extract solutions from pre-characterisation

Nagra PSI 2012 thermodynamic data base, calculated in PHREEQC for 25°C, using ordered dolomite; kgw = kg water; charge = Σ(cation charge) – |Σ(anion charge)| ; %-error = 100*charge / (Σ(cation charge) + |Σ(anion charge)|).

Parameter	**Unit**	**STA2-1**	**STA2-2**	**STA2-4**	**STA2-3**
Depth	[m]	778.43	895.02	900.81	923.27
Geol. unit		«Humphr.ool. Fm.»	Opalinus Clay	Opalinus Clay	Staffelegg Fm.
Charge	[eq/kg_w]	-4.9E-04	-2.6E-04	-2.1E-04	-1.3E-04
%-error		-1.94	-0.99	-0.82	-0.59
Acetate	[eq/kg_w]	9.1E-05	1.3E-04	7.9E-05	3.2E-05
Ionic strength	[mol/kg_w]	1.51E-02	1.55E-02	1.50E-02	1.31E-02
tot_alk	[eq/kg]	2.94E-03	4.28E-03	3.98E-03	3.11E-03
pH		8.76	8.76	8.63	9.12
log pCO_2	[bar]	-3.57	-3.41	-3.30	-3.95
SI(calcite)		-0.11	0.08	-0.10	-0.02
SI(dolomite)		-0.53	-0.19	-0.55	-0.46
SI(gypsum)		-2.65	-2.63	-2.68	-2.95
SI(celestite)		-2.55	-2.51	-5.48	-2.79
SI(strontianite)		-1.27	-1.06	Sr < 0.1	-1.12
SI(anhydrite)		-2.87	-2.86	-2.91	-3.18

Aqueous extracts of all cores were also produced after termination of the experiments. A thin disc (13 – 19 mm) from the top and base of each core was processed according to the protocols used for pre-characterisation. The base of the core represents the inlet of the artificial porewater, whereas the top represents the outflow to sampling. The two may yield different results depending on the overall progress of fluid percolation (different concentrations in inlet sample compared to outlet), and averaging is therefore meaningless, unless a full breakthrough was achieved, including equilibration with the exchanger.

Results (Tab. 4.7-8) show that Br (not present in the APW) was effectively flushed out of each core, whereas other minor anionic components were buffered to some extent (e.g., F, NO_3). Ion-exchange processes must be considered to fully understand the changes in cation fractions. A more in-depth analysis will be required to reconcile differences between extracts from pre-characterisation and post-mortem analysis.

Calculation of speciation and saturation indices (Tab. 4.7-9) of the post-mortem aqueous extract solutions from Tab. 4.7-8 indicated no significant change compared to initial aqueous extracts: post-mortem extracts are close to calcite saturation, and distinctly undersaturated with respect to sulphates and strontianite. TIC was used as input for the carbon system.

Cores with excessive nitrate exfiltration (STA2-1, STA2-2, STA2-3) show high NO_3 concentrations in the aqueous extracts especially in the top of the core (post-mortem), which indicates NO_3 mobilisation in the core during infiltration. In addition, initially elevated TOC and acetate were only partly flushed out: the mobilisation of NO_3 seems to correlate with TOC mobilisation (both artefacts, discussed in Section 4.7.8).

Tab. 4.7-8: Composition of aqueous extract solutions from post-mortem characterisation
STA2-1, STA2-2, STA2-3 experiments are compromised by artefacts summarised in Section 4.7.8.

Parameter	**Unit**	**STA2-1**	**STA2-1**	**STA2-2**
Depth	[m]	778.43		895.02
Geol. unit		«Humphriesioolith Fm.»		Opalinus Clay
averaging		top post-mortem (outflow side)	base post-mortem (inflow side)	base post-mortem (inflow side)
$1/WC_w*L/Sw$		17.77	21.43	19.99
Rock wet	[g]	30.34	30.41	30.20
Water	[g]	30.52	30.55	30.31
WC_w	[g/g_{wet}]	0.06	0.05	0.05
S/L (S_d/(L+PW))		0.88	0.90	0.90
pH at Titration		8.74	8.90	8.68
Na	[mg/L]	239	244	232
NH_4	[mg/L]	1.41	1.53	1.26
K	[mg/L]	6.72	6.54	6.15
Ca	[mg/L]	2.84	2.66	2.58
Mg	[mg/L]	0.62	0.95	0.55
Sr (OES)	[mg/L]	0.07	0.06	< 0.1
Ba (OES)	[mg/L]	< 0.025	< 0.025	< 0.025
F	[mg/L]	5.59	5.54	3.02
Cl	[mg/L]	102	134	70.1
Br	[mg/L]	0.09	0.02	< 0.16
NO_3	[mg/L]	39.6	7.15	9.95
SO_4	[mg/L]	213	209	163
I	[mg/L]			n.m.
Alk (tit)	[meq/L]	2.76	2.64	4.48
Alk as HCO_3	[mg/L]	168	161	273
TOC	[mg/L]	15.16	7.72	0.97
TIC	[mg/L]	29.80	29.70	55.96
lactate	[mg/L]	0.91	0.32	< 2
acetate	[mg/L]	5.45	1.45	< 2
propionate	[mg/L]	< 0.2	< 0.2	< 2
formate	[mg/L]	0.40	< 0.2	< 2

Tab. 4.7-8: continued

Parameter	**Unit**	**STA2-4**		**STA2-3**	
Depth	[m]	900.81		923.27	
Geol. unit		Opalinus Clay		Staffelegg Fm.	
averaging		top post-mortem (outflow side)	base post-mortem (inflow side)	top post-mortem (outflow side)	base post-mortem (inflow side)
$1/WC_w$*L/Sw		20.03	19.56	26.71	25.72
Rock wet	[g]	30.64	30.41	30.07	30.12
Water	[g]	30.02	30.14	30.47	30.38
WC_w	[g/g_{wet}]	0.05	0.05	0.04	0.04
S/L (S_d/(L+PW))		0.92	0.91	0.91	0.91
pH at Titration		8.62	8.67	8.85	8.74
Na	[mg/L]	296	273	213	199
NH_4	[mg/L]	1.62	1.48	< 1	< 1
K	[mg/L]	12.12	10.65	6.12	5.56
Ca	[mg/L]	4.25	3.62	2.13	1.88
Mg	[mg/L]	0.70	0.62	0.35	0.43
Sr (OES)	[mg/L]	0.09	0.07	0.04	0.03
Ba (OES)	[mg/L]	< 0.025	< 0.025	< 0.025	< 0.025
F	[mg/L]	3.08	3.33	4.23	4.19
Cl	[mg/L]	163	138	104	106
Br	[mg/L]	0.22	< 0.16	< 0.016	< 0.016
NO_3	[mg/L]	0.54	0.28	9.54	2.55
SO_4	[mg/L]	229	208	147	131
I	[mg/L]	n.m.	n.m.	n.m.	n.m.
Alk (tit)	[meq/L]	3.90	3.99	3.24	3.10
Alk as HCO_3	[mg/L]	238	244	198	189
TOC	[mg/L]	4.52	1.52	9.90	5.50
TIC	[mg/L]	47.31	49.04	35.58	35.17
lactate	[mg/L]	< 2	< 2	0.34	< 0.2
acetate	[mg/L]	5.97	3.62	1.91	0.78
propionate	[mg/L]	< 2	< 2	< 0.2	< 0.2
formate	[mg/L]	< 2	< 2	0.31	< 0.2

Tab. 4.7-9: Saturation indices calculated for aqueous extract solutions obtained post-mortem

Nagra PSI 2012 thermodynamic data base, calculated in PHREEQC for 25°C, using ordered dolomite; kgw = kg water; charge = Σ(cation charge) – ׀Σ(anion charge)׀ ; %-error = 100*charge/ (Σ(cation charge) + ׀Σ(anion charge)׀); STA2-1, STA2-2, STA2-3 experiments are compromised by artefacts summarised in Section 4.7.8.

Parameter	**Unit**	**STA2-1**	**STA2-1**	**STA2-2**
Depth	[m]	778.43		895.02
Geol. unit		«Humphriesioolith Fm.»		Opalinus Clay
Position		top post-mortem (outflow side)	base post-mortem (inflow side)	base post-mortem (inflow side)
Charge	[eq/kg$_w$]	-1.9E-06	-1.0E-04	-2.8E-05
%-error		-0.01	-0.47	-0.14
Acetate	[eq/kg$_w$]	9.2E-05	2.5E-05	< 1.0E-07
Ionic strength	[mol/kg$_w$]	1.30E-02	1.33E-02	1.22E-02
tot_alk	[eq/kg]	2.60E-03	2.65E-03	4.84E-03
pH		8.74	8.90	8.68
log pCO_2	[bar]	-3.60	-3.77	-3.26
SI(calcite)		-0.23	-0.12	-0.06
SI(dolomite)		-0.78	-0.34	-0.43
SI(gypsum)		-2.74	-2.78	-2.89
SI(celestite)		-2.65	-2.71	-5.57
SI(strontianite)		-1.41	-1.30	-4.00
SI(anhydrite)		-2.96	-3.01	-3.11

Tab. 4.7-9: continued

Parameter	**Unit**	**STA2-4**	**STA2-4**	**STA2-3**	**STA2-3**
Depth	[m]	900.81		923.27	
Geol. unit		Opalinus Clay		Staffelegg Fm.	
Position		top post-mortem (outflow side)	base post-mortem (inflow side)	top post-mortem (outflow side)	base post-mortem (inflow side)
Charge	[eq/kg$_w$]	5.3E-05	-3.1E-05	7.6E-05	-9.0E-05
%-error		0.20	-0.13	0.40	-0.50
Acetate	[eq/kg$_w$]	1.0E-04	6.1E-05	3.2E-05	1.3E-05
Ionic strength	[mol/kg$_w$]	1.58E-02	1.46E-02	1.11E-02	1.04E-02
tot_alk	[eq/kg]	3.94E-03	4.09E-03	3.11E-03	3.04E-03
pH		8.62	8.67	8.85	8.74
log pCO_2	[bar]	-3.29	-3.33	-3.63	-3.52
SI(calcite)		0.00	0.00	-0.15	-0.30
SI(dolomite)		-0.44	-0.42	-0.74	-0.90
SI(gypsum)		-2.55	-2.65	-2.99	-3.07
SI(celestite)		-2.46	-2.60	-2.95	-3.09
SI(strontianite)		-1.20	-1.23	-1.37	-1.58
SI(anhydrite)		-2.86	-2.96	-3.22	-3.30

Cation exchange capacities and cation selectivities determined by the Ni-en method (Waber ed. 2020) were performed on one combined sample for each core from the two samples used for aqueous extracts. The results are also presented and interpreted in Section 4.5. Tab. 4.7-10 shows uncorrected (for porewater contribution and mineral dissolution/precipitation) capacities of 79 – 133 meq/kg (dry rock) with errors of up to ~ ± 5%. Ni consumptions agree well with the sum of cations. Ammonium was not measured but is expected to be present on the exchanger judged by the presence of up to 9 mg/L of NH_4 in the aqueous extracts performed at the same *S/L* ratio (Tab. 4.7-5). The high nitrate concentrations derive from the Ni-en solution. The negative charge balance arises from the lack of incorporating ethylendiamine complexes from the Ni-en solution into the calculation (Tab. 4.7-10). The low Br concentrations agree with the Br concentrations in aqueous extracts, as well as Br/Cl and SO_4/Cl ratios. The cation occupancies (selectivities) derived from Ni-en extracts, and applying a correction for the porewater contribution, are presented in Sections 4.5 and 5.6.

Tab. 4.7-10: Composition of Ni-en extract solutions and related parameters from pre-characterisation

kg_d = kg dry rock

Parameter	**Unit**	**STA2-1**	**STA2-2**	**STA2-4**	**STA2-3**
Depth	[m]	778.43	895.02	900.81	923.27
Geol. unit		«Humphr.ool. Fm.»	Opalinus Clay	Opalinus Clay	Staffelegg Fm.
Averaging		1 averaged sample	1 sample top	no sample	1 averaged sample
$1/WC_w*L/S_w$		19.33	22.87		27.73
Rock wet	[g]	30.14	29.83		30.95
Solution	[g]	30.91	30.99		30.95
WC_w	[g/g_{wet}]	0.06	0.05		0.04
S/L ($S_d/(L+PW)$)		0.87	0.88		0.93
pH (initial)		8.27	8.29		8.29
Ni (initial)	[mg/L]	5845	6187		6187
pH (final)		8.35	8.42		8.51
Na	[mg/L]	1285	1160		897
K	[mg/L]	225	183		183
Mg	[mg/L]	183	139		83
Ca	[mg/L]	776	719		439
Sr	[mg/L]	26.6	23.9		15.7
Ba	[mg/L]	0.137	0.696		0.435
Fe	[mg/L]	< 0.05	< 0.05		< 0.05
Ni	[mg/L]	2'027	2'525		3'596
F	[mg/L]	0.21	< 0.16		0.21
Cl	[mg/L]	153	129		112
Br	[mg/L]	0.47	0.40		0.24
NO_3	[mg/L]	12'171	12'457		12'510
SO_4	[mg/L]	155	146		141
TDS	[mg/L]	17'001	17'484		17'978
charge %-error	[%]	-4.82	-4.68		-3.10
Na	[meq/kg_d]	64.0	57.6		42.1
K	[meq/kg_d]	6.6	5.3		5.0
Mg	[meq/kg_d]	17.2	13.0		7.4
Ca	[meq/kg_d]	44.4	40.9		23.6
Sr	[meq/kg_d]	0.69	0.62		0.39
Ba	[meq/kg_d]	0.002	0.012		0.007
Fe	[meq/kg_d]	< 0.002	< 0.001		< 0.001
SumCat	[meq/kg_d]	132.9	117.5		78.5
SumCat_err	[meq/kg_d]	5.68	5.10		3.50
Ni_cons	[meq/kg_d]	137.2	131.8		86.9
Ni_cons_err	[meq/kg_d]	4.60	5.00		5.10
Br/Cl	[mol/mol*1'000]	1.36	1.38		0.95
SO_4/Cl	[mol/mol]	0.37	0.42		0.46

4.7.5 Chemical and isotopic evolution of displaced porewater aliquots

An artificial porewater (APW) was injected to force advective displacement. The outflow of each experiment was continuously sampled in small syringes (Waber ed. 2020). These syringe aliquots were analysed for chemical and water isotopic composition. Hydraulic conductivity was evaluated for each sampled aliquot (Darcy's law), and any expelled gas was also recorded. Although gas-tightness is commonly good, some gas loss cannot be excluded for a syringe sampling system. Most data for each experiment are included in tables and graphs in this section, and more details are provided in Appendix B.

According to the method of advective displacement (Mäder 2018), it is expected that the first few sampled aliquots are of similar composition and represent the displaced porewater from the sample core. After this, a gradual breakthrough of the injected APW should be observed, until full breakthrough of conservative components (e.g. Cl, Br), given enough time. This model behaviour is disturbed in the first three of four experiments due to artefacts that led to exceptionally large mobilisations of nitrate.

4.7.5.1 Artificial porewater used for advective displacement

In the absence of constraining data, an artificial porewater composition (Tab. 4.7-11, details in text below) was chosen that was based on work performed for the deep geothermal well in Schlattingen (advective displacement experiments detailed in Mäder & Waber 2017). The composition was calculated with PHREEQC for 25 °C, to be saturated with respect to calcite and dolomite, and a partial pressure of CO_2 of $10^{-2.2}$ bar. This partial pressure was imposed by bubbling with an Ar/CO_2 gas mixture during mixing and again when the fluid reservoir was filled before the experiments started. A recipe with the appropriate amounts of PA-grade chemicals is given in Tab. 4.7-12.

Deuterium was added as a water tracer for advective-diffusive transport, aiming for a δ^2H of approximately +100 ‰ (VSMOW). There is no Br contained in the APW and therefore bromide-breakout can be used as an anionic tracer in the case of significant Br concentrations in the porewater. If the Cl concentration in the APW is significantly different from the displaced early aliquots, Cl breakthrough forms an additional anionic tracer for transport.

All experiments were fed from PFA-coated fluid tanks containing the APW batch 3 (STA2-1, STA2-2, STA2-3) or batch 2 (STA2-4). After every tank opening, the headspace was pressurised with He after bubbling with the Ar/CO_2 gas mixture mentioned above. The compositions of the two APW batches were designed to be identical, and the analyses agree well within analytical uncertainties.

Tab. 4.7-11: Composition and recipe for the artificial porewater

* calculated from the weighed-in chemical compounds; pH measured; CO_2-Ar bubbling not taken into account; n.a.: not analysed.

			Batch 3 STA2-1 to STA2-3		**Batch 2 STA2-4**		
Parameter	**Unit**	**Recipe**	**Calc.***	**Meas.**	**Calc.***	**Meas.**	**Compounds**
pH		7.19		7.38		7.43	
Na	[mg/L]	3'989	3'988	4'059	3'988	4'009	$NaCl$; $NaHCO_3$; Na_2SO_4
NH4	[mg/L]			< 10		< 10	
K	[mg/L]	79.4	79.3	78.7	79.4	78.4	KCl
Ca	[mg/L]	503	504	506	503	488	$CaCl_2 \cdot 2H_2O$
Mg	[mg/L]	226	226	208	226	206	$MgCl_2 \cdot 6H2O$
Sr(OES)	[mg/L]			< 0.25		< 0.5	
Ba	[mg/L]			< 0.25		< 0.5	
Si	[mg/L]			< 2.5		9.04	
Al	[mg/L]			0.279		< 50	
F	[mg/L]			< 1.6		< 1.6	
Cl	[mg/L]	5'992	5'986	5'826	5'985	5'908	$CaCl_2 \cdot 2H_2O$; KCl; $MgCl_2 \cdot 6H_2O$
Br	[mg/L]			< 1.6		< 1.6	
NO_3	[mg/L]			5.25		1.94	
SO_4	[mg/L]	2'305	2'303	2'132	2'304	2'146	Na_2SO_4
I	[mg/L]			n.a.		n.a	
TOC	[mg/L]			7.4		< 5	
TIC	[mg/L]	29.3	29.32	28.0	29.33	33.9	$NaHCO_3$
lactate	[mg/L]			< 20		< 20	
acetate	[mg/L]			< 20		< 20	
propionate	[mg/L]			< 20		< 20	
formate	[mg/L]			< 20		< 20	
$\delta^{18}O$	[‰ VSMOW]		–11.43	–11.52	–11.43	–11.24	
$\delta^{2}H$	[‰ VSMOW]	100	91.9	90.8	110.9	113.3	D_2O

Tab. 4.7-12: Recipe for the artificial porewater for a 2-litre batch

			Recipe		**Batch 3 STA2-1 to STA2-3**	**Batch 2 STA2-4**
Chemical	**Manufacturer**	**Grade**	[g/kg_w]	[$g/2kg_w$]	**weighted in** [g/2L]	**weighted in** [g/2L]
$NaHCO_3$	Merck	p.a.	0.2051	0.4101	0.4102	0.4103
$CaCl_2 \cdot 2H_2O$	Merck	p.a.	1.8465	3.6930	3.6944	3.6922
KCl	Merck	p.a.	0.1514	0.3029	0.3026	0.3027
$MgCl_2 \cdot 6H_2O$	Merck	p.a.	1.8907	3.7814	3.7827	3.7812
$NaCl$	Merck	p.a.	7.1916	14.3831	14.3838	14.3837
Na_2SO4	AnalaR NORMAPUR	Ph.Eur.	3.4089	6.8177	6.8114	6.8121
D_2O (100%)	Roth	> 99.8% D	0.0318	0.0635	0.0607	0.0673

4.7.5.2 Physical conditions, hydraulic conductivity, sampling, and pore volume equivalents

All core samples were subjected to 62 – 66 bar hydraulic confining pressure, and an infiltration pressure of initially around 48 bar set by a He headspace. The infiltration pressure was gradually decreasing with time (displaced APW, and any small He leak), and was replenished repeatedly until the end of the last experiment. The pressure range covered 43 – 48 bar.

Temperature conditions were stable without diurnal fluctuations, ranging seasonally from 21.5 to 25.5 °C. Critical temperature-sensitive measurements, such as electric conductivity, pH and hydraulic conductivity, were temperature-compensated, either intrinsically or explicitly (details in Waber ed. 2020).

Hydraulic conductivity referenced to 25 °C was evaluated for all sampled aliquots based on sample mass and Darcy's law (detailed data in Appendix B, method in Waber ed. 2020) (Fig. 4.7-4). Observations in all AD experiments performed so far show initially lower apparent hydraulic conductivities due to the expulsion of gas from the dead volume in the outflow, and any small unsaturated volume in the sample core itself. Then, hydraulic conductivities increase, followed by a slight decrease to a steady-state value, if sufficient run-time was provided.

The early conductivities (after approximately 0.2 pore volumes, when gas exfiltration decreased and conductivity increases linearly) and those measured towards the end of the experiments (Tab. 4.7-13) span a narrow range from $1.1 – 2.7 \cdot 10^{-13}$ m/s (neglecting the late values attributed to clogging in the high nitrate core STA2-2). These conductivities refer to a direction perpendicular to bedding and a sample length of 8 – 9 cm, measured at very large hydraulic gradients (Tab. 4.7-2). A gradual but rather minor decrease after a maximum value (STA2-3) may be due to slow sample consolidation, and this was also observed in earlier work (Mäder 2018). These latter values are most representative for in-situ conditions, although the confining stress of 60 bar (6 MPa) in the experiments is still considerably less than the lithostatic stresses at 778 – 923 m depth.

STA2-2 shows a substantial conductivity drop after the expected increasing trend. The outflow contains large amounts of nitrate, and the Cl concentration in the outflow after 0.7 pore volumes drops below the concentration in the infiltrating APW (Section 4.7.5.4). Especially a relatively strong decrease of hydraulic conductivity and an increasing exfiltration of gas are observed. But also periods with low hydraulic conductivity and minor gas exfiltration occurred. All these unexpected observations are attributed to the interaction with the confining system and to microbial activity, which seems to affect conductivity. Also clogging in the filters or even in the inflow or outflow system cannot be ruled out. The STA2-2 outlier at an early time at 2.25×10^{-13} *m/s coincides with enormous gas outflow (three times the fluid volume), presumably from microbial activity in the bottom of the core, that may also have increased the fluid flow above. All related artefacts are discussed in Section 4.7.8.*

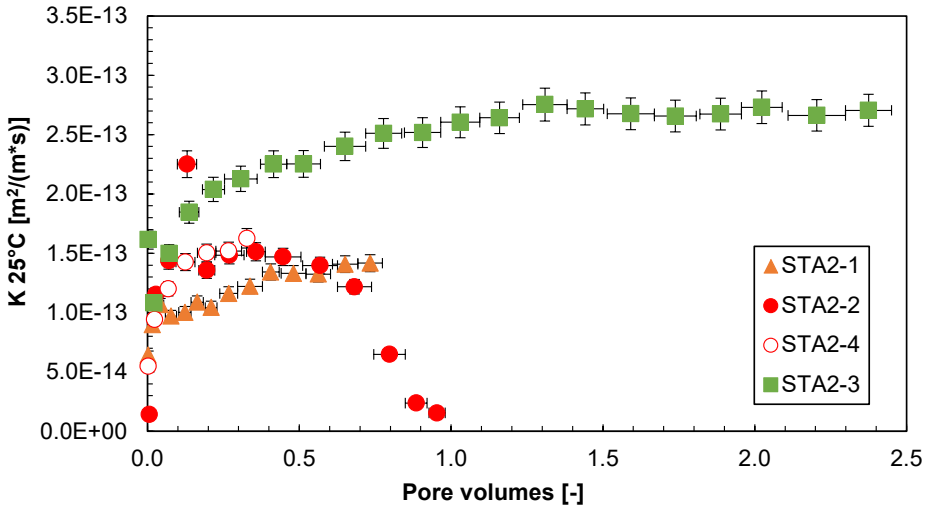

Fig. 4.7-4: Evolution of hydraulic conductivity during advective displacement experiments

STA2-1 = STA2-1-778.43-AD («Humphriesioolith Fm.»); STA2-2 = STA2-1-895.02-AD (Opalinus Clay); STA2-4 = STA2-1-900.81-AD (Opalinus Clay); STA2-3 = STA2-1-923.27-AD (Staffelegg Fm.). Pore volume fractions relate to transport time based on water content. Experiment duration is 56 – 257 days. Horizontal length of symbol bar covers the sampling interval, vertical bars are an estimate of combined uncertainties; STA2-1. STA2-2, STA2-3 experiments are compromised by artefacts summarised in Section 4.7.8.

Tab. 4.7-13: Hydraulic conductivity of AD samples

STA2-1, STA2-2, STA2-3 experiments are compromised by artefacts summarised in Section 4.7.8.

Parameter	**Unit**	**STA2-1**	**STA2-2**	**STA2-4**	**STA2-3**
Depth	[m]	778.43	895.02	900.81	923.27
Geol. unit		«Humphriesioolith Fm.»	Opalinus Clay	Opalinus Clay	Staffelegg Fm.
Early_K (25 °C)	[m/s]	1.09×10^{-13}	2.25×10^{-13}	1.50×10^{-13}	1.85×10^{-13}
Late_K (25 °C)	[m/s]	1.42×10^{-13}	1.51×10^{-13}	1.63×10^{-13}	2.70×10^{-13}

The time axis for all data representations of sequential fluid aliquots is converted to pore volume fractions by dividing the cumulative sample mass (volume) by the water content of the core. In this way, experiments with very different hydraulic conductivities or different water contents can be represented in a meaningful way for transport. There may be some minor ambiguities in case where water contents from pre-characterisation deviate from the true water content of a sample core, or if a significant initial unsaturated porosity fraction would be present. The chosen approximation is sufficient for a visual presentation of data.

Sampled aliquots (mass) plotted versus pore volume fraction (time) provides an overview of all syringe samples taken for all three AD experiments (Fig. 4.7-5). For each experiment 7 to 21 samples were collected.

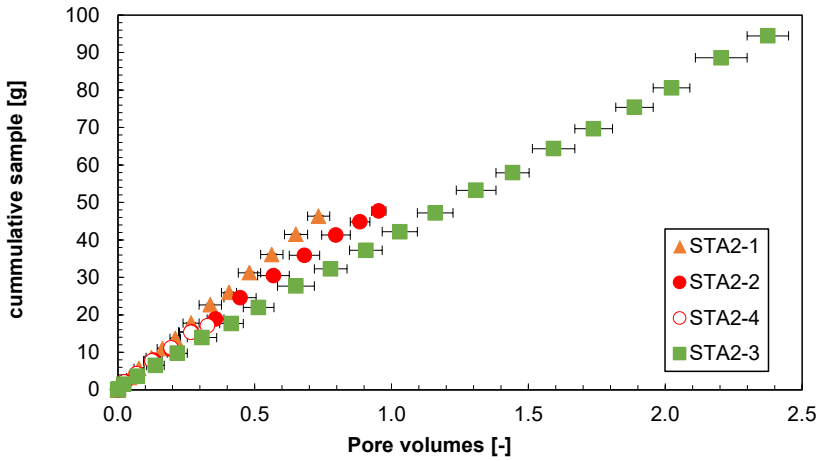

Fig. 4.7-5: Sampling schedule and sample volumes taken

STA2-1 = STA2-1-778.43-AD («Humphriesioolith Fm.»); STA2-2 = STA2-1-895.02-AD (Opalinus Clay); STA2-4 = STA2-1-900.81-AD (Opalinus Clay); STA2-3 = STA2-1-923.27-AD (Staffelegg Fm.). Each data point represents a syringe aliquot taken, with the horizontal bar indicating the duration for sampling, here converted to pore volume fraction percolated. Different slopes reflect different volumetric flow rates scaled by porosity.

4.7.5.3 Inline measurement of electric conductivity and pH

Electric conductivity (EC) was continuously monitored in all experiments (Fig. 4.7-6, Waber ed. 2020, for method). Conductivity cells were initially calibrated but may show a drift to varying extent over time due to electrode corrosion, commonly resulting in low apparent readings. Therefore, electric conductivity values are only meant to provide an indication of salinity but are not used quantitatively. The electric conductivities follow in principle the major electrolyte components.

The extremely high nitrate concentrations especially in the early outflow of the STA2-1, STA2-2, and STA2-3 lead to higher electric conductivities compared to those of STA2-4. The EC drop below the APW value of the outflows of the former cores coincides with the Cl concentrations dropping below the APW concentration, plus the decrease in nitrate. This indicates a major disturbance of the chemical system (Section 4.7.8).

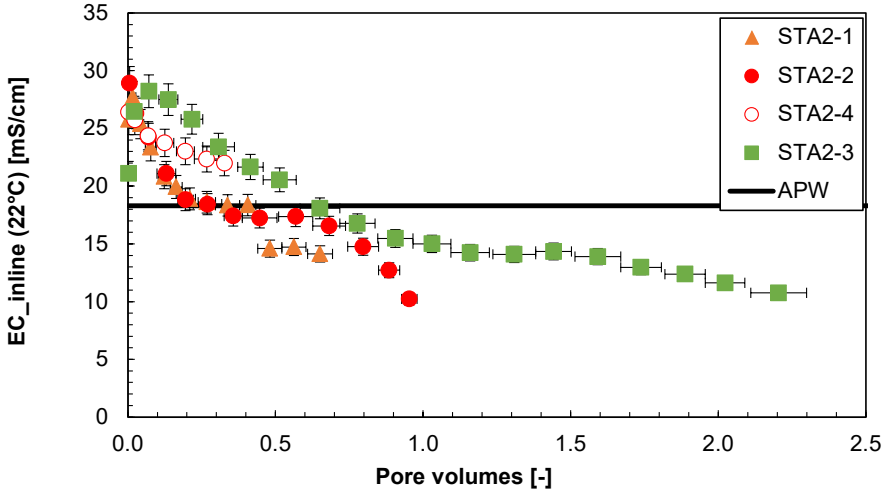

Fig. 4.7-6: Evolution of electric conductivity (22 °C) during advective displacement experiments

STA2-1 = STA2-1-778.43-AD («Humphriesioolith Fm.»); STA2-2 = STA2-1-895.02-AD (Opalinus Clay); STA2-4 = STA2-1-900.81-AD (Opalinus Clay); STA2-3 = STA2-1-923.27-AD (Staffelegg Fm.). Pore volume fractions relate to transport time based on water content. Experiment duration is 56 – 257 days. Horizontal length of symbol bar covers the sampling interval, vertical bars are an estimate of combined uncertainties; STA2-1. STA2-2, STA2-3 experiments are compromised by artefacts summarised in Section 4.7.8.

The aim was to measure pH inline three times before/after sampling of the first four aliquots, and less frequently at later times (method in Waber ed. 2020). Measurements took 12 – 24 hrs in most cases, to ensure that the dead volume of the very small flow-through pH cell was sufficiently flushed given the very slow flow rates of the experiments. The micro-electrode was left installed in the flow-through cell and was checked before and after each pH measurement period with a standard solution. The initial calibration was made at pH 7 and 9, and simple drift checks and corrections were made with a standard solution at pH 7. The electrode slope was checked from time to time and was found to remain remarkably stable. In most cases, drift corrections over 12 – 24 hrs were ≤ 0.1 pH units. The overall uncertainty is difficult to assess because these small electrodes may respond to manipulations at the flow-through cell (response to small strains) and

also small gas bubbles may temporarily affect readings. It is estimated that an error of ± 0.2 pH units is appropriate for most measurements. pH values of early aliquots are also tabulated below (Tab. 4.7-14).

These in-line pH measurements (Fig. 4.7-7) are rather tricky and require careful handling of equipment. Criteria to accept a value include a small drift and a reasonably well-defined pH-plateau, as well as a stable non-zero electric conductivity (no gas bubbles). It cannot be excluded that for long measurement durations some effect from outgassing or in-gassing of CO_2 may influence the readings. pH measurements on small aliquots taken from the syringes show slightly shifted relative to the inline measurements but show comparable evolutions with progress of percolation. pH evolutions are different for each core and interpretation is not straightforward.

The surprisingly high initial pH values of STA2-1 coincide with nitrate concentrations in the range of 10'000 mg/L, and with unexpected low Cl concentrations below 5'200 mg/L. The responsible processes are very likely artefacts (Section 4.7.8).

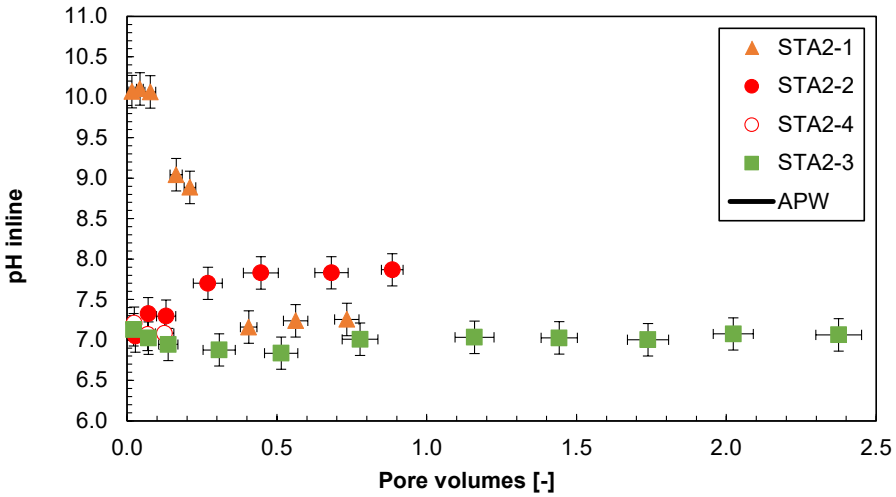

Fig. 4.7-7: Evolution of inline pH during advective displacement experiments

STA2-1 = STA2-1-778.43-AD («Humphriesioolith Fm.»); STA2-2 = STA2-1-895.02-AD (Opalinus Clay); STA2-4 = STA2-1-900.81-AD (Opalinus Clay); STA2-3 = STA2-1-923.27-AD (Staffelegg Fm.). Pore volume fractions relate to transport time based on water content. Experiment duration is 56 – 257 days. Horizontal length of symbol bar covers the sampling interval, vertical bars are an estimate of combined uncertainties; STA2-1. STA2-2, STA2-3 experiments are compromised by artefacts summarised in Section 4.7.8.

4.7.5.4 Evolution of major and minor components

Evolution of concentrations with progress of percolation are shown in Figs. 4.7-8 to 4.7-13. Select analytical data for the first two aliquots sampled are summarised in Tab. 4.7-14 further below, with full details in Appendix B. In case of the STA2-4 core (no nitrate-related artefacts), the compositions of the earliest aliquots displaced from the core samples are the most representative for the pore fluid extracted, and this is highlighted and interpreted in a separate Section 4.7.5.5.

The displaced **major components Cl and SO_4** from STA2-4 present a continuous decrease towards the APW as expected (Fig. 4.7-8). The **cations Na, Ca, Mg** are initially more concentrated in the outflow than in the injected APW and decrease steadily towards it. Major ion concentrations form an early plateau with an elevated first measurement, possibly due to minor

drying of the sample surface during preparation. A choice was made to use average compositions of the first two analysed aliquots to best represent the porewater composition. The resulting porefluid composition is summarised in Tab. 4.7-14 (Section 4.7.5.5) and is also used in the integrative plots in Chapter 5.

In case of cores STA2-1, STA2-2, and STA2-3 (outflows with high nitrate), Cl drops below the APW concentration (Fig. 4.7-9). This behaviour is only observed in cores with excessive nitrate exfiltration (also in previous AD experiments) and might be caused by an interaction of the confining fluid with the cores. Nitrate forms a major component and is a carrier for anionic charge along with chloride and sulphate. The evolution of SO_4 is different in each of the three experiments. Ca concentrations are higher than in STA2-4: they compensate for the exceptionally high nitrate, both decreasing with ongoing percolation (also see Fig. 4.7-10). The outflow chemistry of these cores is disturbed to such an extent that no porewater composition representative for in-situ conditions can be derived. Further details are given in Section 4.7.8.

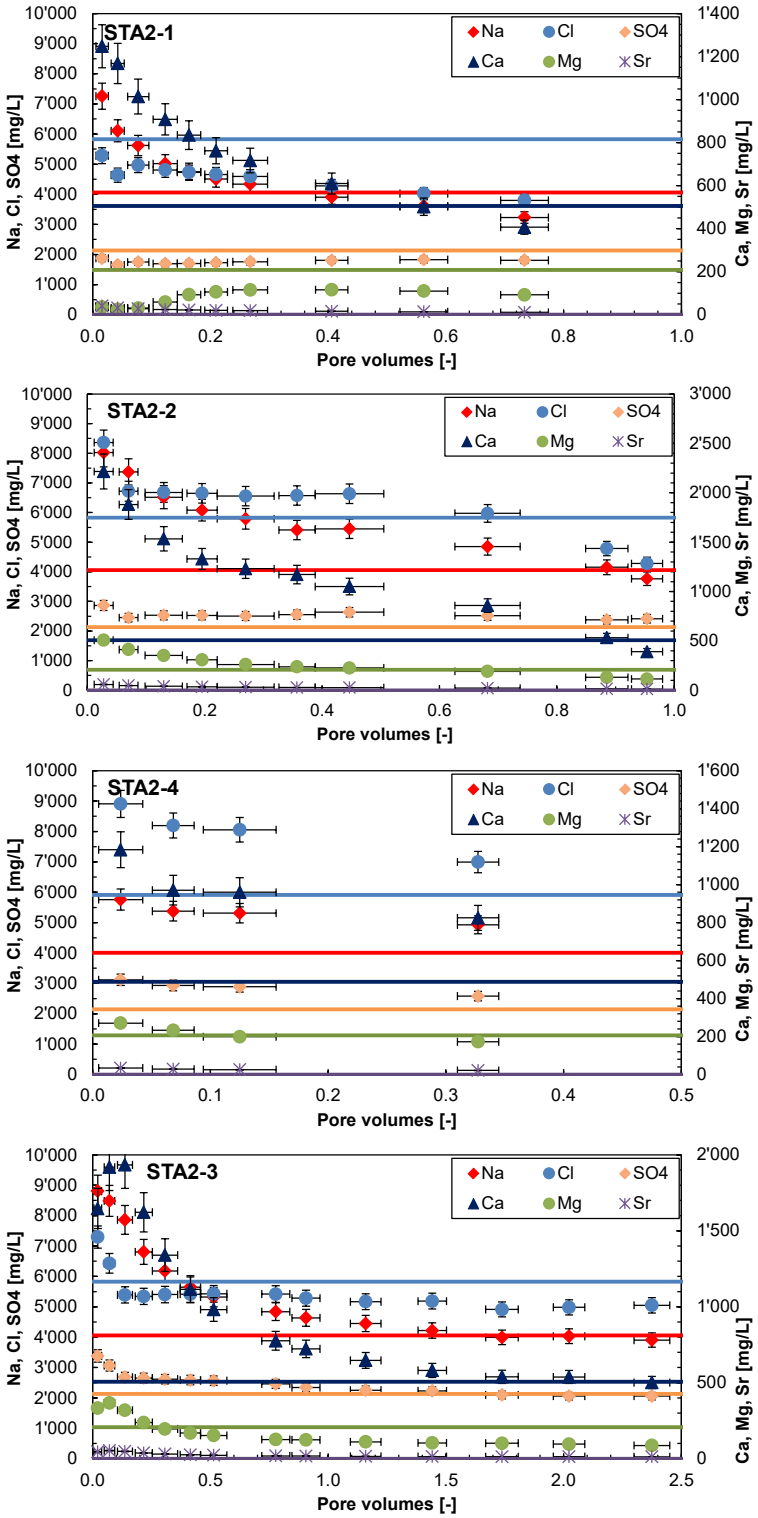

Fig. 4.7-8: Evolution of major components during advective displacement experiments

STA2-1 = STA2-1-778.43-AD («Humphriesioolith Fm.»); STA2-2 = STA2-1-895.02-AD (Opalinus Clay); STA2-4 = STA2-1-900.81-AD (Opalinus Clay); STA2-3 = STA2-1-923.27-AD (Staffelegg Fm.). Pore volume fractions relate to transport time based on water content. Experiment duration is 56 – 257 days. Horizontal length of symbol bar covers the sampling interval, vertical bars are an estimate of combined uncertainties. Horizontal lines represent the composition of the injected APW; STA2-1. STA2-2, STA2-3 experiments are compromised by artefacts summarised in Section 4.7.8.

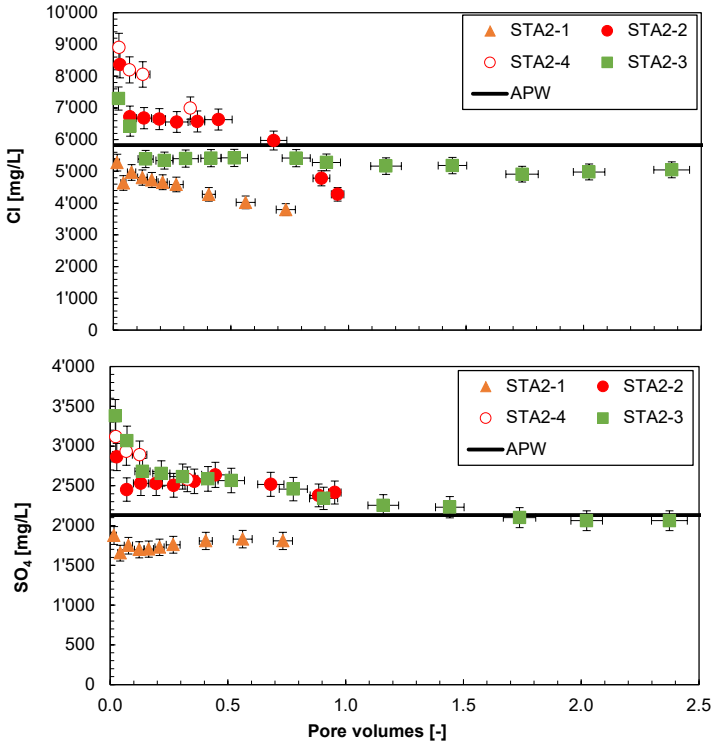

Fig. 4.7-9: Evolution of Cl and SO_4 during advective displacement experiments

STA2-1 = STA2-1-778.43-AD («Humphriesioolith Fm.»); STA2-2 = STA2-1-895.02-AD (Opalinus Clay); STA2-4 = STA2-1-900.81-AD (Opalinus Clay); STA2-3 = STA2-1-923.27-AD (Staffelegg Fm.). Pore volume fractions relate to transport time based on water content. Experiment duration is 56 – 257 days. Horizontal length of symbol bar covers the sampling interval, vertical bars are an estimate of combined uncertainties. Horizontal lines represent the composition of the injected APW; STA2-1. STA2-2, STA2-3 experiments are compromised by artefacts summarised in Section 4.7.8.

Of the **minor components (Br, NO_3, K, Sr, Si)**, only potassium is present in the injected APW. Its concentration pattern is influenced by cation exchange reactions, whereby the outflow concentration only matches the APW concentration when the entire exchanger in the core is in equilibrium with the APW (Fig. 4.7-10). During the limited run-time of experiment STA2-4, only the initial evolutions of concentrations of minor compounds are revealed, which agree with earlier AD experiments: Br and Sr decrease gradually, and dissolved silica elutes at approximately 5 mg/L. The initial STA2-4 outflow shows a nitrate value of 50 mg/L, decreasing to < 2 mg/L in the second sample and onwards. Ba and Al were measured by ICP-OES but remained below detection limits. The detection limits depend on dilution factors and were 0.25 mg/L for Ba, and 0.25 – 2.5 mg/L for Al.

In STA2-1, STA2-2, and STA2-3, bromide is low in the first measurements due to complexation with the silver filters. Nitrate is a major component in the early aliquots in experiments STA2-1, STA2-2, and STA2-3 (Fig. 4.7-11). For these samples, the maximum values reach up to 13 g/L in the first couple of aliquots, followed by a regular decrease, discussed in Section 4.7.8.

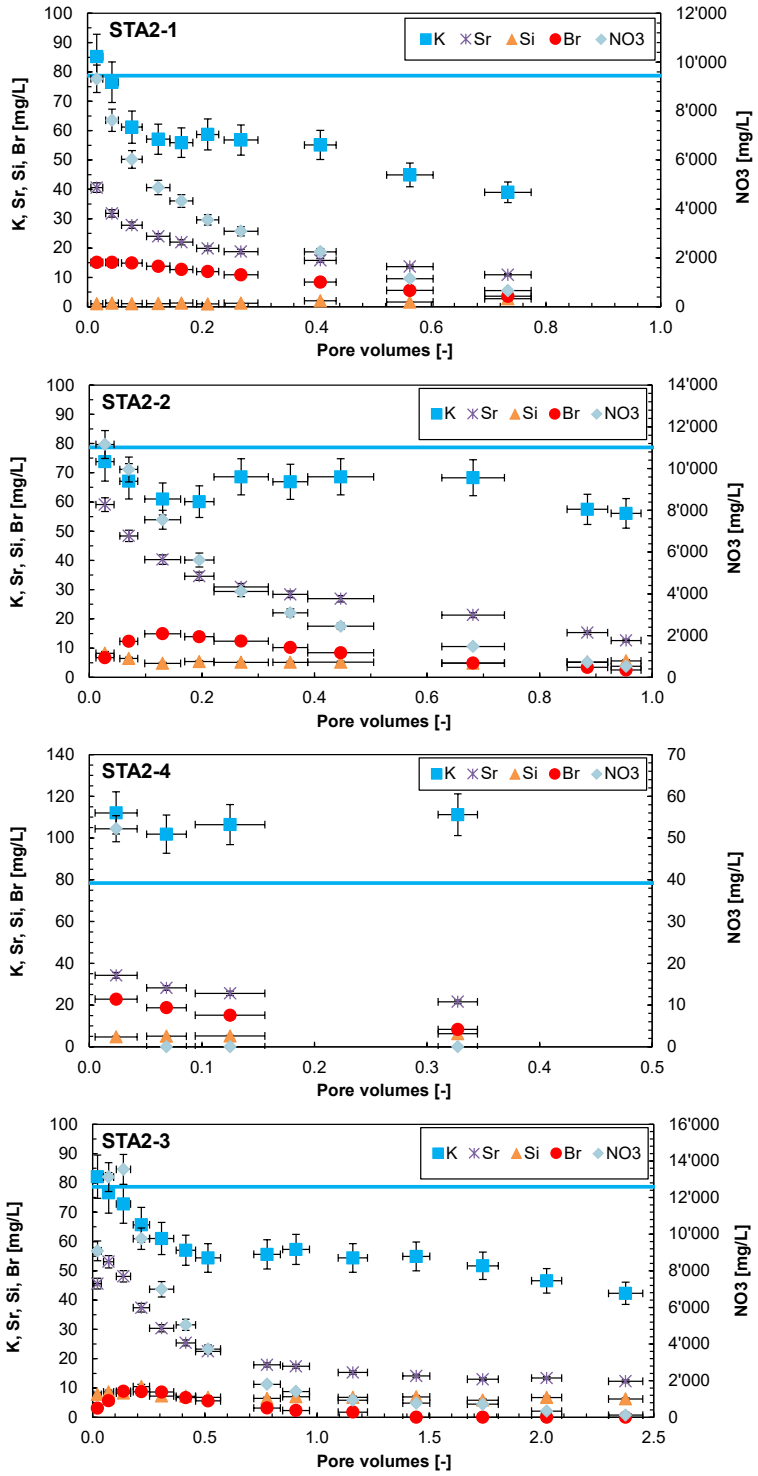

Fig. 4.7-10: Evolution of minor components during advective displacement experiments

STA2-1 = STA2-1-778.43-AD («Humphriesioolith Fm.»); STA2-2 = STA2-1-895.02-AD (Opalinus Clay); STA2-4 = STA2-1-900.81-AD (Opalinus Clay); STA2-3 = STA2-1-923.27-AD (Staffelegg Fm.). Pore volume fractions relate to transport time based on water content. Experiment duration is 56 – 257 days. Horizontal length of symbol bar covers the sampling interval, vertical bars are an estimate of combined uncertainties. Horizontal line represents the composition of the injected APW for K (0 for others); STA2-1. STA2-2, STA2-3 experiments are compromised by artefacts summarised in Section 4.7.8.

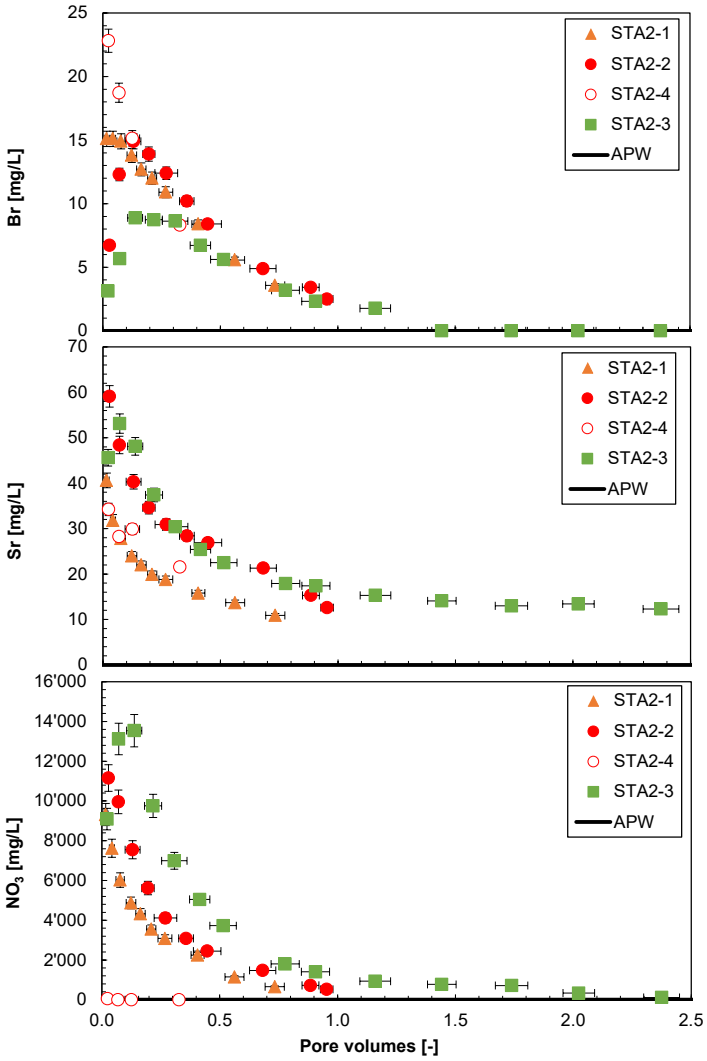

Fig. 4.7-11: Evolution of select minor components during advective displacement experiments

STA2-1 = STA2-1-778.43-AD («Humphriesioolith Fm.»); STA2-2 = STA2-1-895.02-AD (Opalinus Clay); STA2-4 = STA2-1-900.81-AD (Opalinus Clay); STA2-3 = STA2-1-923.27-AD (Staffelegg Fm.). Pore volume fractions relate to transport time based on water content. Experiment duration is 56 – 257 days. Horizontal length of symbol bar covers the sampling interval, vertical bars are an estimate of combined uncertainties. Br, Sr & NO_3 in the APW are 0. Br concentrations below detection are plotted at 0; STA2-1. STA2-2, STA2-3 experiments are compromised by artefacts summarised in Section 4.7.8.

The **carbon system (TIC, TOC, TC, LMWOA)** shares as the common feature with earlier AD experiments that relatively large TOC concentrations are eluted initially (230 mg/L, but > 1'000 mg/L for cores with high nitrate) that gradually decrease with progressive percolation (Fig. 4.7-12, Tab. 4.7-14 shows averages of first 2 aliquots). TOC clearly dominates the dissolved carbon inventory (TC) at early times. The TOC can partly be explained by low-molecular-weight organic acids (LMWOA), mainly acetate, in case of STA2-1 and STA2-4 (Fig. 4.7-13).

Aqueous extracts (Tab. 4.7-5) imply TOC values of 50 – 115 mg/L when scaled to porewater content, which partly cover the range observed in the early aliquots. In STA2-4, TOC in aqueous extracts of the post-mortem material at the in-flow side (base) are below the pre-characterisation

values. This observation is similar to previous work, with samples from the Schlattingen-1 geothermal well (Mäder & Waber 2017) and also TBO borehole BUL1-1 (Mazurek et al 2021), TRU1-1 (Aschwanden et al 2021), MAR1-1 (Mäder et al 2021) and BOZ1-1 (Wersin et al 2022).

TIC elutes initially at lower concentrations than TOC, covers a wide range of concentrations, but generally decreases to a close to constant concentration around 60 – 120 mg/L depending on the core (Figs. 4.7-12 and 4.7-13).

The carbon system correlates with the nitrate mobilisation: nitrate and TC initially elute at above 10 g/L and 1 g/L, respectively, and decrease in parallel with ongoing infiltration (cores STA2-1, STA2-2, STA2-3, artefact, discussed in Section 4.7.8).

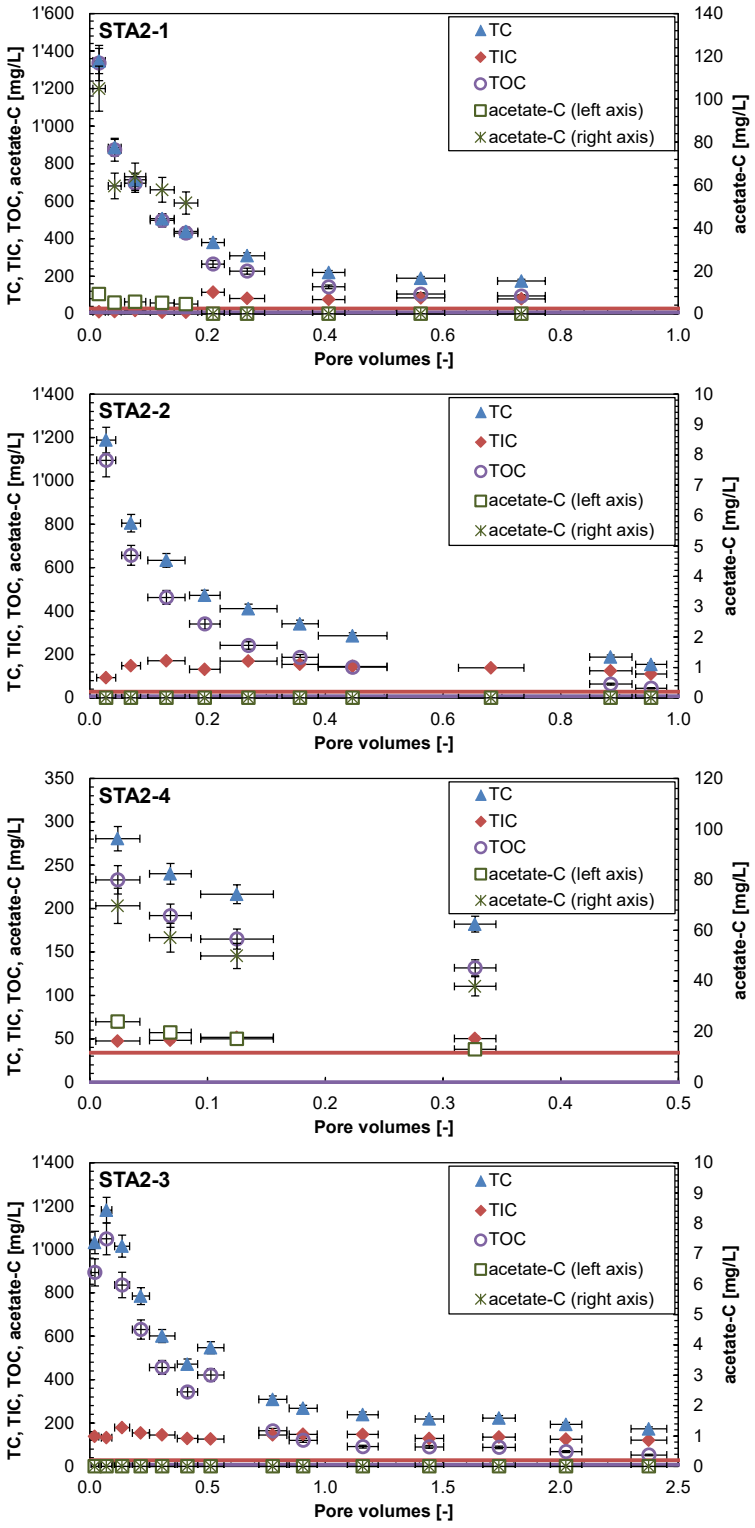

Fig. 4.7-12: Evolution of the carbon system during advective displacement experiments

STA2-1 = STA2-1-778.43-AD («Humphriesioolith Fm.»); STA2-2 = STA2-1-895.02-AD (Opalinus Clay); STA2-4 = STA2-1-900.81-AD (Opalinus Clay); STA2-3 = STA2-1-923.27-AD (Staffelegg Fm.). Pore volume fractions relate to transport time based on water content. Experiment duration is 56 – 257 days. Horizontal length of symbol bar covers the sampling interval, vertical bars are an estimate of combined uncertainties. Horizontal lines represent the composition of the injected APW; STA2-1. STA2-2, STA2-3 experiments are compromised by artefacts summarised in Section 4.7.8.

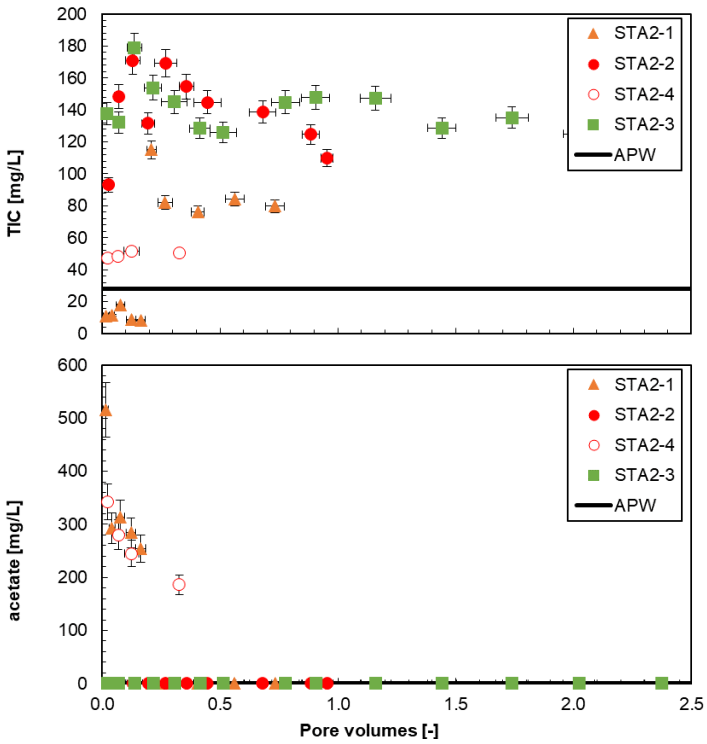

Fig. 4.7-13: Evolution of select carbon components during advective displacement experiments

STA2-1 = STA2-1-778.43-AD («Humphriesioolith Fm.»); STA2-2 = STA2-1-895.02-AD (Opalinus Clay); STA2-4 = STA2-1-900.81-AD (Opalinus Clay); STA2-3 = STA2-1-923.27-AD (Staffelegg Fm.). Pore volume fractions relate to transport time based on water content. Experiment duration is 56 – 257 days. Horizontal length of symbol bar covers the sampling interval, vertical bars are an estimate of combined uncertainties. Horizontal lines represent the composition of the injected APW. Concentrations below detection (acetate) are plotted at 0; STA2-1. STA2-2, STA2-3 experiments are compromised by artefacts summarised in Section 4.7.8.

The **measurement of pH** was performed in-line between some of the sampling intervals (setup in Waber ed. 2020) and in the laboratory when syringe aliquots were prepared/preserved for analysis. The latter was done in most cases very shortly after sampling (one to a few hours), or after a few days of storage. The total range covered for all samples, in-line and laboratory, is 6.9 – 7.8 (Fig. 4.7-14), both showing similar spreads. Exceptionally high pH up to 10.4 is measured in early aliquots from STA2-1. Values of both approaches either match within the error, or a close to constant offset between the in-line and laboratory measured pH is observed, with the in-line pH being systematically lower. This can be explained by outgassing of CO_2 during the laboratory measured pH leading to higher values.

The pH series define relatively smooth trends with percolation progress, but not a systematic behaviour in all experiments. The calculated partial pressure of CO_2 is larger than atmospheric in the aliquots, and this bears the potential for outgassing and resultant supersaturation with respect to calcite, and a possibility for some loss of Ca and TIC by precipitation.

It should be noted that in samples with the large initial nitrate concentrations (STA2-1, STA2-2, and STA2-3), there is some uncertainty regarding the generation of this dissolved nitrate. Depending on the processes, this could also affect pH values. While the pH may still be representative for the porewater of the experiment it may deviate from the undisturbed state (Section 4.7.8).

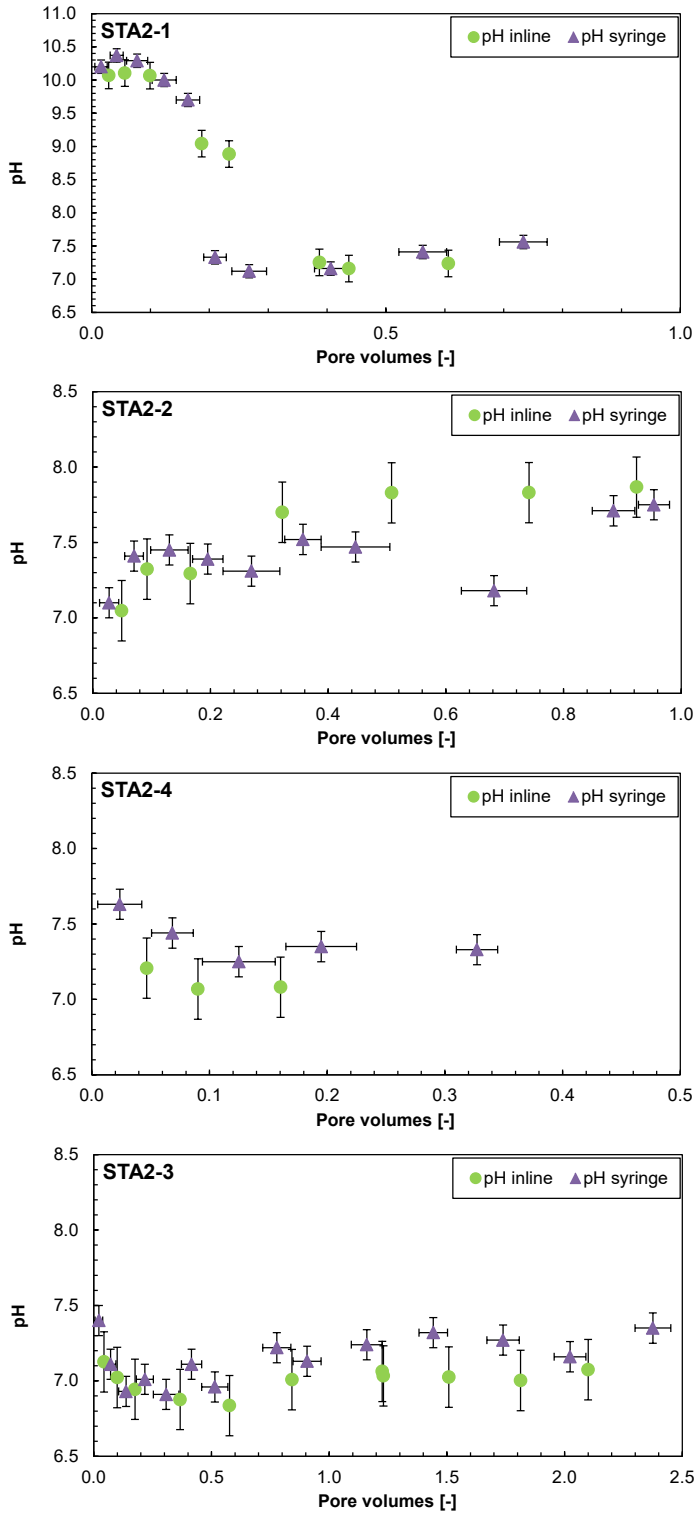

Fig. 4.7-14: Evolution of pH during advective displacement experiments

STA2-1 = STA2-1-778.43-AD («Humphriesioolith Fm.»); STA2-2 = STA2-1-895.02-AD (Opalinus Clay); STA2-4 = STA2-1-900.81-AD (Opalinus Clay); STA2-3 = STA2-1-923.27-AD (Staffelegg Fm.). Pore volume fractions relate to transport time based on water content. Experiment duration is 56 – 257 days. Horizontal length of symbol bar covers the sampling interval, vertical bars are an estimate of combined uncertainties; STA2-1. STA2-2, STA2-3 experiments are compromised by artefacts summarised in Section 4.7.8.

4.7.5.5 Early displaced aliquots representing the porewater composition

In case of the STA2-4 experiment, early displaced aliquots were obtained by averaging the first two measured samples (Tab. 4.7-14). Interpretation of these early displaced aliquots as being representative of the in-situ porewater, contained in the core at the time of the experiment, requires integration and interpretation of the entire data set supported with geochemical calculations. Comprehensive reactive transport simulations are expected to further constrain the initial porewater compositions, as well as the transport properties of the cores. Only speciation calculations are included in this data report for the early compositions. Speciation calculations for all individual syringes are provided in Appendix B. The laboratory pH values were used for the speciation calculations.

Initial outflow chemistry and its evolution with ongoing percolation indicate a fundamentally disturbed porewater in cores STA2-1, STA2-2, and STA2-3, as shown in the section above (discussed in Section 4.7.8). Therefore, no in-situ porewater chemistry can be derived and values in Tab. 4.7-14 have informative character for the experimental conditions only.

Tab. 4.7-14: Composition of earliest aliquots from advective displacement experiments, representing the in-situ porewater chemistry in case of STA2-4

italic: values compromised by artefacts (nitrate mobilisation); * only one syringe value (early maximum), due to initial AgBr formation on Ag-filter

Parameter	**Unit**	**STA2-1**	**STA2-2**	**STA2-4**	**STA2-3**
Depth	[m]	778.43	895.02	900.81	923.27
Sample ID RWI		BOZ2-1-425.69-AD	STA2-1-778.43-AD	STA2-1-895.02-AD	STA2-1-900.81-AD
Lab sample ID		BOZ2-1xx-AD	STA2-1xx-AD	STA2-2xx-AD	STA2-4xx-AD
Geol. unit		«Humphr.ool. Fm.»	Opalinus Clay	Opalinus Clay	Staffelegg Fm.
pH inline	[-]	*10.09*	*7.19*	7.14	*7.07*
pH lab	[-]	*10.29*	*7.26*	7.54	*7.26*
Na	[mg/L]	*6'682*	*7'697.5*	5'567	*8'644.5*
NH_4	[mg/L]	*54.1*	*18.9*	13.59	*16.2*
K	[mg/L]	*80.85*	*70.45*	106.9	*79.35*
Ca	[mg/L]	*1'208*	*2'048*	1'077	*1'783*
Mg	[mg/L]	*30.25*	*459.95*	252	*349.7*
Sr	[mg/L]	*36.2*	*53.75*	31.23	*49.35*
Ba	[mg/L]	*< 0.25*	*< 0.25*	< 0.25	*< 0.25*
Si	[mg/L]	*1.12*	*7.34*	4.91	*8.235*
Al	[mg/L]	*< 2.5*	*< 2.5*	< 2.5	*< 2.5*
F	[mg/L]	*3.86*	*9.195*	< 1.6	*7.765*
Cl	[mg/L]	*4'958*	*7'541.5*	8'552	*6'862*
Br	[mg/L]	*15.1**	*14.90**	20.8	*8.88**
NO_3	[mg/L]	*8'471*	*10'556.5*	52.23	*11'104*
SO_4	[mg/L]	*1'764*	*2'657.5*	3'026	*3'223.5*
TOC	[mg/L]	*1'105*	*876*	212	*971.5*
TIC	[mg/L]	*11.05*	*120.7*	47.9	*135*
lactate	[mg/L]	*143*	*< 20*	< 20	*< 20*
acetate	[mg/L]	*404.5*	*< 20*	312	*< 20*
propionate	[mg/L]	*< 20*	*< 20*	< 20	*< 20*
formate	[mg/L]	*69.55*	*< 20*	< 20	*< 20*
$\delta^{18}O$	[‰VSMOW]	*–5.54*	*–6.47*	–5.05	*–6.36*
$\delta^{2}H$	[‰VSMOW]	*–47.7*	*–48.4*	–39.3	*–47.3*

The speciation calculation (Tab. 4.7-15) reveals a cation charge surplus (positive 'Charge') that is not large and partially explained by significant TOC concentrations that were not included in the speciation. TIC was used as constraint for inorganic carbon. The aliquots are all significantly oversaturated with respect to calcite and also dolomite. Such oversaturation may result from shifts in pH linked to potential in-gassing or outgassing of CO_2 during sampling and storage. Alternatively, the large TOC (and TC) contents pose analytical difficulties to obtain TIC and associated errors may be larger than commonly assigned to TIC measurements.

Saturation is also reached or slightly exceeded for celestite, strontianite, and gypsum in most cores. The implication is that the ion-activity products ($[Sr]\cdot[SO_4]$) and ($[Ca]\cdot[SO_4]$) are controlling factors, but this does not necessarily mean that these minerals are also present in the core before the experiments. There are generally larger SO_4, Ca and Sr concentrations in the early aliquots than in the APW (Figs. 4.7-8 and 4.7-11). The high initial Ca concentrations in STA2-1, STA2-2, and STA2-4 can be explained by the high nitrate elution which either cause calcite dissolution and/or induce cation exchange reactions.

A more in-depth analysis and interpretation will have to be carried out, including reconstructions by geochemical modelling.

Tab. 4.7-15: Saturation state of earliest aliquots from advective displacement experiments

Nagra PSI 2012 thermodynamic data base, calculated in PHREEQC for 25 °C; dolomite-o: ordered dolomite; dolomite-d: disordered dolomite; charge = Σ(cation charge) – |Σ(anion charge)|; %-error = 100*charge / (Σ(cation charge) + |Σ(anion charge)|) ; STA2-1, STA2-2, STA2-3 experiments are compromised by artefacts summarised in Section 4.7.8.

Parameter	**Unit**	**STA2-1**	**STA2-2**	**STA2-4**	**STA2-3**
Depth	[m]	778.43	895.02	900.81	923.27
Geol. unit		«Humphriesiool. Fm.»	Opalinus Clay	Opalinus Clay	Staffelegg Fm.
Charge	[eq/kg_w]	*4.2E-02*	*3.1E-02*	1.2E-02	*4.8E-02*
%-error		*6.34*	*3.45*	2.01	*5.28*
Acetate	[eq/kg_w]	*6.9E-03*	*< 3.4E-04*	5.3E-03	*< 3.4E-04*
Ionic strength	[mol/kg_w]	*0.37*	*0.52*	0.34	*0.52*
tot_alk	[eq/kg_w]	*2.2E-03*	*9.9E-03*	4.0E-03	*1.1E-02*
pH (Lab)		*10.29*	*7.26*	7.54	*7.26*
log pCO_2		*-6.82*	*-1.71*	-2.34	*-1.65*
SI(calcite)		*1.96*	*1.24*	0.85	*1.21*
SI(dolomite-o)		*2.64*	*2.16*	1.40	*2.06*
SI(dolomite-d)		*2.09*	*1.61*	0.85	*1.51*
SI(gypsum)		*-0.10*	*0.18*	0.05	*0.21*
SI(celestite)		*0.10*	*0.32*	0.23	*0.38*
SI(strontianite)		*0.89*	*0.11*	-0.24	*0.11*
SI(anhydrite)		*-0.31*	*-0.03*	-0.17	*0.00*

4.7.5.6 Initial values and evolution of stable water isotope composition

The stable water isotope ratios δ^2H and $\delta^{18}O$ in the outflows of core STA2-4 show an initial plateau and start to evolve towards the APW values after 0.1 pore volumes (Fig. 4.7-15), as expected from theory and measured in AD experiments from borehole BAC1 (Gaucher et al. *in prep*.). The plateau values represent a reliable estimate for the in-situ porewater.

In theory, isotope ratios are expected to evolve in the δ^2H – $\delta^{18}O$ diagram (Fig. 4.7-16) on a straight line from the in-situ values to the APW values (e.g., compare with Gaucher et al. *in prep*.). This is already visible in case of STA2-4 despite a rather short run-time.

Isotope ratios in the δ^2H – $\delta^{18}O$ diagram in outflows from cores STA2-1, STA2-2, and STA2-3 behave very different from expectations and are discussed in Section 4.7.8.

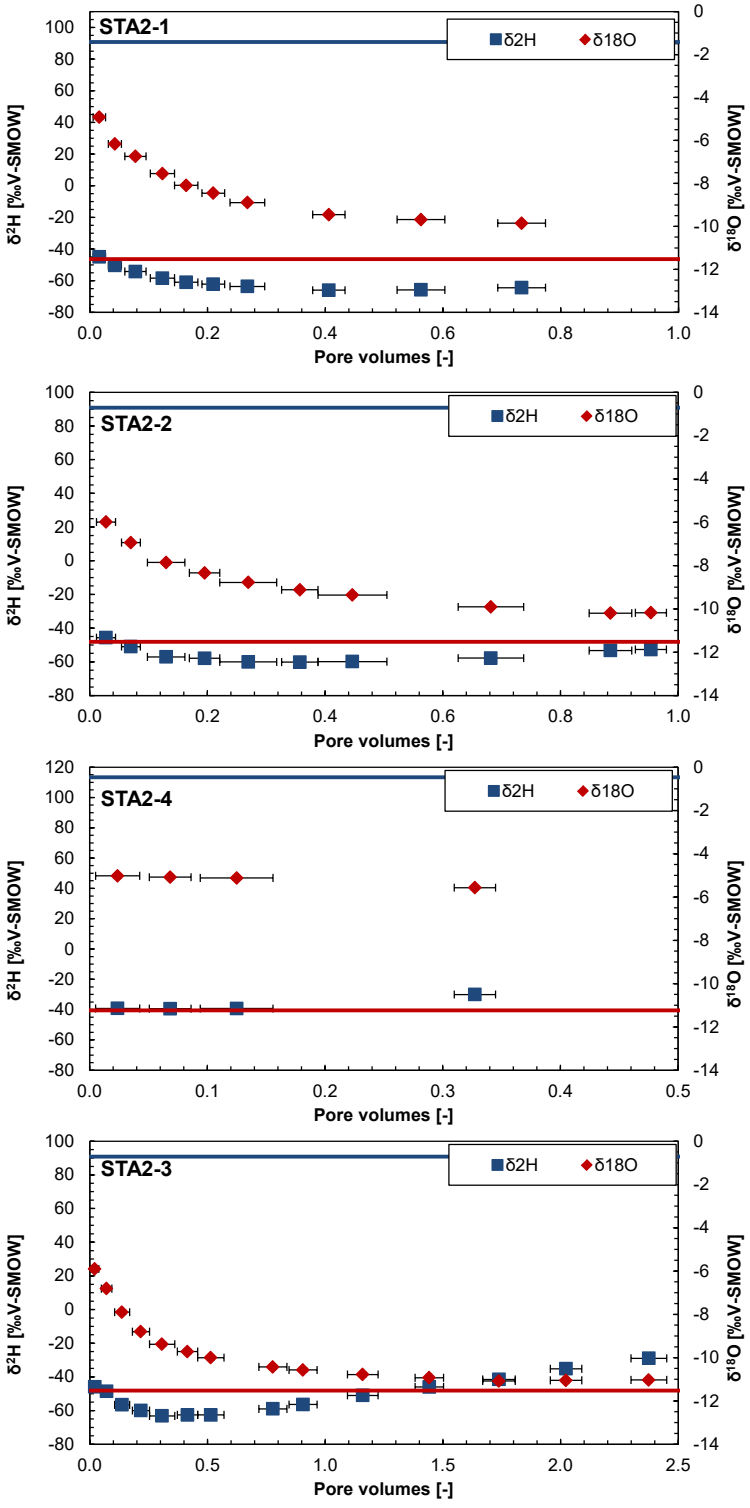

Fig. 4.7-15: Evolution of δ^2H and $\delta^{18}O$ during advective displacement experiments

STA2-1 = STA2-1-778.43-AD («Humphriesioolith Fm.»); STA2-2 = STA2-1-895.02-AD (Opalinus Clay); STA2-4 = STA2-1-900.81-AD (Opalinus Clay); STA2-3 = STA2-1-923.27-AD (Staffelegg Fm.). Pore volume fractions relate to transport time based on water content. Experiment duration is 56 – 257 days. Horizontal length of symbol bar covers the sampling interval. Measurement errors are 1.5 ‰ for δ^2H and 0.1 ‰ for $\delta^{18}O$; STA2-1. STA2-2, STA2-3 experiments are compromised by artefacts summarised in Section 4.7.8.

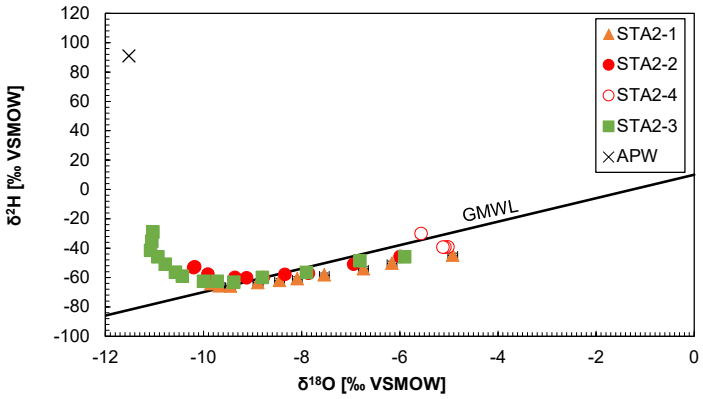

Fig. 4.7-16: Stable isotope composition of aliquots from advective displacement experiments
STA2-1 = STA2-1-778.43-AD («Humphriesioolith Fm.»); STA2-2 = STA2-1-895.02-AD (Opalinus Clay); STA2-4 = STA2-1-900.81-AD (Opalinus Clay); STA2-3 = STA2-1-923.27-AD (Staffelegg Fm.). Measurement errors are 1.5 ‰ for δ^2H and 0.1 ‰ for $\delta^{18}O$. GMWL is the global meteoric water line. 1st aliquots are located the furthest to the right and evolve towards the left; STA2-1. STA2-2, STA2-3 experiments are compromised by artefacts summarised in Section 4.7.8.

4.7.6 Derivation of anion-accessible porosity

There are several ways by which chloride and bromide accessible porosity fractions may be obtained. The principle is the same: namely the ratio between the anion concentration obtained from aqueous extracts up-scaled to porewater content divided by that obtained from earliest aliquots from the advective displacement experiments (discussion in Waber ed. 2020 and Mäder 2018). There are some variants depending on how water contents were measured and averaged, or how inferred water losses and volume changes may be corrected. In the case where a full or well-advanced breakthrough in chloride is captured, such a ratio may also be obtained by post-mortem aqueous extracts (top and base) and the latest aliquots sampled before the end of the experiments (for the outlet / top), or the injected APW (for the inlet / base). Normally, bromide drops below detection and only the chloride data can be evaluated for post-mortem datasets. The bromide data commonly is more 'noisy'.

The top two data lines (line 1 and 2 in Tab. 4.7-16) list the average concentrations (Cl, Br) for the first two displaced aliquots as shown in Tab. 4.7-14. Because Br complexation with the Ag filters massively decreased Br concentrations in the first aliquots, only the second value was used in experiments with Ag filters, which must be seen as a minimum value. Line 3 lists the concentration of Cl in the last syringe sampled (for post-mortem evaluation). The following three lines list different Cl concentrations in aqueous extracts, up-scaled to water content: for the sample from above the AD core (line 4), for the sample from below (line 5) and a corrected and averaged value (line 6). The correction compensates for a small amount of water loss (unsaturated volume) commonly observed and evaluated from a measured net water uptake. The net water uptake is the measured water uptake (mass gain of the core during the experiment) corrected for a commonly measured small volume increase during the experiment (Section 4.7.3 and Tab. 4.7-4). The correction hinges on the assumption that sample treatment for the AD core and the off-cuts share the same history (core handling, storage, sample preparation) and therefore also potentially underwent similar water losses. These corrections are rather small, with small net water uptakes. The following three lines (7 – 9) contain the same data for Br. The observed range in up-scaled concentrations is an indication of heterogeneity, mainly in clay-mineral content. A homogeneous sample with respect to the degree of anion-exclusion should yield the same up-scaled Cl and Br

concentrations, despite differences in water content. A consistent proportion of anion-accessible porosity would then be evaluated regardless of choosing a sample from the top or from the base as a reference for the early displaced aliquots. The two data lines for Cl suffixed with _p-m (lines 10 and 11) are the up-scaled chloride concentrations evaluated post-mortem from aqueous extracts from the top of the core (outlet to sampling) and the base of the core (APW inlet).

The final data block (lines 12 – 19 in Tab. 4.7-16) lists the accessible porosity fraction obtained by various combinations and averaging. The first four lines 12 – 15 list values that are derived without knowledge of the net water uptake. The next two lines 16 and 17, including the suffix _corr, indicate values obtained after applying a correction for net water uptake as mentioned above. The last two data lines represent the post-mortem evaluations of the top of the core (outlet, line 18) and the base of the core (inlet, line 19).

The pre-characterisation anion accessible porosity fractions derived for STA2-4 of 0.36 for Cl and 0.41 for Br are below the post-mortem value for Cl of 0.47. In the AD experiments from boreholes BOZ1 and BOZ2, Br shows a higher accessibility than Cl, which is also observed in case of STA2-4. The reason for this behaviour is not yet fully understood but might be connected to the difference in transport behaviour (Mäder 2018). However, differences are small considering the overall uncertainty of the approach. The corrected Cl accessibility fraction (line 16) of 0.36 is the preferred anion accessibility fraction of this core. This value is below the range of 0.42 to 0.51 determined previously for Opalinus Clay with the same approach in the TBO boreholes BUL1-1 (Mazurek et al 2021), MAR1-1 (Mäder et al 2021) and BOZ1-1 (Wersin et al 2022) but agrees well with the low accessibility of 0.35 in the core STA3-4 (Aschwanden et al 2022). Both cores show an exceptionally high clay-mineral content of 70 wt.-% (STA2-4) and 65 wt.-% (STA3-4). The AD experiment TRU1-4 (Aschwanden et al. 2021) resulted in a comparable Cl accessibility fraction (0.37), also associated with a high CEC that is indicative of a high clay content (neighbouring samples show clay-mineral contents of 65 wt.-%). An in-depth interpretation of anion accessibility goes beyond the scope of this data report and must consider all data from other boreholes as well.

Due to the disturbed chemistry measured in the outflows of cores STA2-1, STA2-2, and STA2-3, the derived values cannot be trusted. However, nitrate values are low in the last outflows of the experiments, and the possible interaction of the confining fluid with the core at the very base of the cores might be limited. Assuming a good equilibration at the core base with the adjacently inflowing APW permits an evaluation of the chloride post-mortem accessible porosity fraction for chloride (STA2-1 & STA2-3). In STA2-2 the hydraulic conductivity decreases strongly at the end of the experiment, indicating an alteration of the pore size distribution (e.g. partial clogging) somewhere in the core. Hence, chloride post-mortem accessibility fractions are omitted.

Tab. 4.7-16: Chloride and bromide-accessible porosity fractions

Preferred values are shaded in blue; values in italics are unreliable due to interferences with nitrate or formation of AgBr on the Ag-filters.

Line	Parameter	Unit	STA2-1	STA2-2	STA2-4	STA2-3
	Depth	[m]	778.43	895.02	900.81	923.27
	Geol unit		«Humphriesi-oolith Fm.»	Opalinus Clay	Opalinus Clay	Staffelegg Fm.
1	Cl-AD_ave (1-2)	[mg/L]	*4'958*	*7'542*	8'552	*6'862*
2	Br-AD_ave (1-2) or *(max)	[mg/L]	*15.10**	*14.90**	20.77	*8.88**
3	Cl_AD_last	[mg/L]	*3'797*	*4'279*	6'995	*5'050*
4	Cl-AqEx-upscaled_top	[mg/L]	3'309	3'128	3'033	3'370
5	Cl-AqEx-upscaled_base	[mg/L]	3'288	n.m.	n.m.	3'217
6	Cl-AqEx-upscaled_ave_corr	[mg/L]	3'132	3'091	3'111	3'131
7	Br-AqEx-upscaled_top	[mg/L]	10.6	10.5	8.5	7.4
8	Br-AqEx-upscaled_base	[mg/L]	10.6	n.m.	n.m.	7.4
9	Br-AqEx-upscaled_ave_corr	[mg/L]	10.1	10.4	8.5	7.0
10	Cl-AqEx-upscaled_top_p-m	[mg/L]	1'812	n.m.	3'271	2'778
11	Cl-AqEx-upscaled_base_p-m	[mg/L]	2'872	1'402	2'696	2'727
12	Cl-AqEx_top / Cl-AD_ave		*0.67*	*0.41*	0.35	*0.49*
13	Br-AqEx_top / Br-AD_ave		*0.70*	*0.70*	0.41	*0.84*
14	Cl-AqEx_ave / Cl-AD_ave		*0.67*	*0.41*	0.35	*0.48*
15	Br-AqEx_ave / Br-AD_ave		*0.70*	*0.70*	0.41	*0.83*
16	Cl-AqEx_ave_corr / Cl-AD_ave		*0.63*	*0.41*	0.36	*0.46*
17	Br-AqEx_ave_corr / Br-AD_ave		*0.67*	*0.70*	0.41	*0.79*
18	Cl_AqEx_p-m_top / Cl_last_AD		*0.48*	*n.m.*	0.47	0.55
19	Cl_AqEx_p-m_base / Cl_APW		0.49	*0.24*	0.46	0.47

4.7.7 Transport properties marked by breakthrough of δ^2H, $\delta^{18}O$, Cl and Br

There are four components that can be used to elucidate on transport properties by their breakthrough behaviour, namely Cl, Br, and the water isotope ratios δ^2H and $\delta^{18}O$. Chloride is a good tracer in the STA2-4 experiment, because the APW has a distinctly lower Cl concentration than the in-situ porewater. In theory, the resolution towards a full breakthrough is diminished because small differences between large concentrations can no longer be resolved. Bromide is a break-out tracer that is gradually flushed out of the core (no Br in the APW). Again, if a full break-out is approached, bromide concentrations tend to fall below the detection limit. Water tracers also feature a considerable contrast between the in-situ porewater (Tab. 4.7-14) and the APW and are therefore suitable to trace the APW breakthrough. However, the run-time of the STA2-4 experiment is not sufficient to even approach full breakthrough.

For comparison (Fig. 4.7-17) STA2-4 breakthrough data are normalised to 1 and inverted in case of decreasing trends to mimic a breakthrough behaviour. The normalised breakthrough of chloride, for example, is given by $1-(Cl-Cl_{APW})/(Cl_{PW}-Cl_{APW})$, where Cl_{PW} refers to the value of the early aliquots representing the in-situ porewater composition (Tab. 4-7.14). The average of the first and second aliquot was taken to represent the in-situ porewater. A slightly elevated first value (possibly due to a potential drying of the surface) leads to a negative value for the first sample.

In case of STA2-4, δ^2H and $\delta^{18}O$ breakthroughs agree well. A small but significant difference between Br and Cl breakthrough behaviour can be observed. This same behaviour was illustrated in earlier work by Mäder (2018). The faster Br breakthrough contradicts the larger Br accessibile porosity compared to Cl (Tab. 4.7-16), which indicates that transport in clay-rich media is not yet fully understood, although in this case differences are rather subtle.

$\delta^{18}O$ and δ^2H break through more slowly compared to the anions Br and Cl, as expected in the presence of an anion-depleted porosity fraction and under advective conditions. In STA2-4, and in all later AD experiments using an additional cold-shrink tube (BAC1 borehole), $\delta^{18}O$ and δ^2H breakthroughs match perfectly. Any mismatch observed in earlier AD experiments may indicate artefacts, to be further elaborated on during synthesis work.

The disturbed chemistry and its evolution with ongoing percolation (Section 4.7.5.4 and 4.7.5.6) in case of the STA2-1, STA2-2, and STA2-3 experiments lead to unexpected breakthrough curves for all four tracers (Section 4.7.8), and no transport properties can be derived. The corresponding breakthrough curves are not shown.

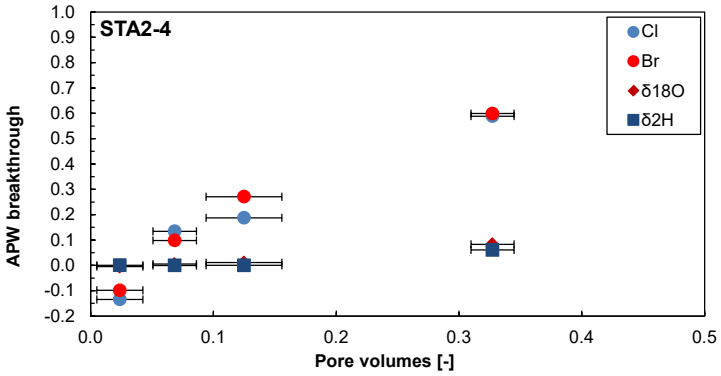

Fig. 4.7-17: Breakthrough of Cl, Br, δ^2H and $\delta^{18}O$ during the advective displacement experiment

STA2-4 = STA2-1-900.81-AD (Opalinus Clay). Pore volume fractions relate to transport time based on water content. Experiment duration is 56 days. Horizontal length of symbol bar covers the sampling duration.

4.7.8 Discussion of artefacts: interaction of core sample and its porewater with the confining fluid

This discussion pertains to experiments that were carried out before applying cold-shrink tubing as additional isolation layer above the Teflon tape and latex rubber sleeves, as a barrier between the confining water and the core sample (Waber ed. 2020). These include STA2-1, STA2-2 and STA2-3 in this report, but not ST2-4 that was carried out with the improved design, as were later experiments for the Bachs-1-1 borehole.

Artefacts are related to (selective) permeation of components in the confining water across the latex rubber sleeves and Teflon tape to the core sample. This is known to have occurred for dissolved Ar (and Kr when Ar was replaced by Kr; Mäder et al. 2021), but likely also involved a water component as evidenced by disturbed signatures in the breakthrough of the water stable isotopes. If the water permeation is small, it may only noteably affect the isotope ratios, but if it is significant relative to the overall fluid transport, it may also become visible in measurements of dissolved chemical constituents.

Some of the permeated components are expected to trigger bio-geochemical processes. They involve the production of elevated nitrate concentrations together with the mobilisation and production of dissolved organic carbon in some samples, and may possibly also affect stable isotope compositions, depending on the exact (but unknown) reaction pathways for these coupled geochemical redox reactions that are most likely microbially induced.

Because the above processes are interdependent, it is not straightforward to identify simple cause-and-effect type of processes. The experiments of the past have been affected to various degrees by the above processes, but there is no clear-cut systematics readily evident, and a more detailed analysis (e.g. supported by reactive transport modelling) may be required for a more complete understanding. These artefacts had been identified and discussed for the past experiments in the respective reports, and some of the data evaluation had been declared as not reliable. This had mainly concerned water stable isotope compositions of some early aliquots, cation concentrations and a few evaluations of the chloride and/or bromide-accessible porosity fraction.

There is apparently a progressive increase in the extent of artefacts with time as cores were processed for TBO boreholes. Early experiments (BUL1-1, TRU1-1) were affected by a limited disturbance in the water stable isotope ratios. The first elevated nitrate concentrations were observed in three cores from MAR1-1 (Staffelegg Formation, Klettgau Formation), apart from

disturbed stable water isotope ratios. Only one core (Hauptrogenstein) was affected by high nitrate for BOZ1 samples, others by disturbed water isotope ratios. Two samples from BOZ2 were affected by high nitrate concentrations (Opalinus Clay, Staffelegg Formation), and all showed disturbed stable isotope ratios. Two cores from STA3-1 were affected by high nitrate concentrations (Opalinus Clay, Staffelegg Formation) but a sample from the Wedelsandstein Formation showed no nitrate production and apparently did not suffer any notable disturbance of the stable isotope ratios (latex sleeves, no cold-shrink tube).

Argon permeation

A common feature for cores wrapped only with latex sleeves is the penetration of some Ar from the confining fluid that is then observed in the gas phase primarily in sampling syringes of the early aliquots (along with gas from the initial dead volume in the head space, and any He that dissolves in the He-pressurised APW and gets transported across the core). Gas permeation (and other components) across latex membranes is documented in literature but is not well understood. Apparently, dissolved gases can get transferred across the membrane interface into the latex emulsion, and then again released at the other interface. It is unclear to which degree this is decoupled from water transport and transport of other solutes. The boundary condition for Ar at the latex interface in experiments without cold-shrink tubing as additional isolation layer is evolving from no Ar present when filling the pressure vessel with a mixture of tap water and distilled water until the solubility limit at the confining pressure. This increase in dissolved Ar is via minor initial advection and diffusion through a steel tube (1.6 mm ID) of 40 – 60 cm length that connects an Ar-pressurised reservoir filled originally with tap/distilled water. Because this tank was usually not cleaned or filled with fresh lab water, there may have been an accumulation of solutes that diffuse back from the pressure vessel, such as DOC arising from greased O-rings, although it is uncertain if this is a factor for the observed artefacts.

The dissolution of Ar in the confining water was avoided in case of all cores from the STA2-1 borehole by the installation of diaphragm accumulators, where a membrane separates the confining water from the pre-pressurised gas, and the use of a piston pump for pressure generation (Section 4.7.2). There is no gas-water interface present in the entire confining system. The installation of the diaphragm accumulators substantially decreased the gas content in the outflow.

Water stable isotope ratios

In many past experiments of TBO (and also some earlier ones) we observed a disturbance in the early aliquots of the δ^2H ratio, and a difference in breakthrough behaviour between δ^2H and $\delta^{18}O$, with the former being delayed relative to the latter (only seen in experiments of sufficient duration). This disturbance comprised an initial slight decrease in the δ^2H ratios (more negative) followed by a reversal caused by the breakthrough increasingly dominated by the large positive value of 100 ‰ of the APW. We argued that such a behaviour may be caused by a limited degree of evaporation at the core surface (during dry-cutting) producing an isotopically heavier residuum near the core surface that disturbed the earliest aliquots (of porewater composition) to slightly less negative ratios. We now also consider that a small leakage of the confining water may induce a similar affect, because the confining water composition is distinctly more negative for δ^2H (–80 ‰, approximately) compared to the in-situ porewater (between –50 and –40 ‰). Such ingress must initially be small as it is reversed by the onset of breakthrough of the APW signature after some fractions of pore volumes transported (approx. 0.1 – 0.4). The effect is different for $\delta^{18}O$ because the APW and the confining water have a similar isotopic ratio (–11.5 ‰, approximately) that is distinctly more negative than that in the porewater (–6 ‰, approximately). Therefore, the APW $\delta^{18}O$ breakthrough may appear to be enhanced by any admixture of a component of confining water. In contrast, it appears that a full breakthrough of APW is not achieved for δ^2H

for some of the long-lasting experiments. This may be an indication of a continuous admixture of a component of confining water. The rate of permeation through the latex membrane may not be constant, and the fluid pathway after the passage through the latex is not known. It may be that this is along the latex – Teflon interface to the low-pressure outflow side. In this case, the penetrated water does not pass through the sample core but just along the wetted surface in contact with the PEEK filter that is confined between rock material and a titanium coupling piece. It can be seen in δ^2H – $\delta^{18}O$ cross-plots of the isotopic evolution of aliquots in disturbed experiments that earliest data plot towards a tap water / laboratory water composition (component from confining water) and later bend towards the APW composition, but still with a tap water component persisting (Fig. 4.7-16).

It appears that stable water isotope ratios have been affected to various degrees in all experiments except for one (STA3-1, Wedelsandstein Formation). No such artefacts were observed in experiments where cold-shrink tubing was applied as an additional isolation barrier for the confining water, although some of the data series were rather short (e.g., STA3-4, STA2-4). While there appears to be a link between the confining water and artefacts that disturb the isotope ratios, the exact nature of permeation through latex membranes remains unclear at present.

Nitrate production

The early outflows of cores STA2-1, STA2-2, and STA2-3 from different formations show nitrate concentrations in the range of 9 – 13 g/L, gradually decreasing at later sampling times. In contrast, STA2-4 outflow shows an initial nitrate value of 50 mg/L decreasing to < 2 mg/L in the second sample and onwards (Fig. 4.7-10 & 4.7-11, Tab. 4.7-14, Appendix B). The nitrate charge is mainly balanced by Ca, and to a lesser extent by Na. The origin of the extremely high nitrate concentrations is in detail still unknown but must be related to a reactive nitrogen phase in the cores (associated with kerogenous solid organic matter, that may also be a source for the mobilised and measured DOC in all early aliquots, Fig. 7.7-12). This phase is not reactive during comparably short and anaerobic aqueous extracts, and neither during long-term aerobic extracts. Such long-term extracts were conducted on original rock material mixed with ultra-pure Milli-Q water and left to react for more than 4 weeks, while opening the lid every few days to allow equilibration with oxygen. These aqueous extracts remained at low nitrogen concentrations of < 10 mg/L (colorimetric measurement with test strips, MQuant Supelco 1.10020.0001, Merck). Aqueous extracts of post-mortem samples from the nitrate-releasing cores show nitrate concentrations up to 40 mg/L (Tab. 4.7-8), generally higher at the outlet side than at the inlet of the core. This indicates a nitrogen mobilisation during certain AD experiments. Other possible sources in the experimental set-up (APW tank, confining fluid, various materials in contact with the core) were analysed, but no nitrogen species were detected. Redox reactions may produce nitrate from more reduced nitrogen in the kerogen, possibly coupled to reduction of readily available sulphate from porewater. However, reduced sulphur was not measured. The processes that produce the added ionic strength for the nitrate contribution, i.e. the charge-balancing cationic component, possibly involve mineral dissolution, and cation exchange complicates the interpretation. In one case (STA2-1, «Humphriesioolith Formation»), strongly elevated early pH values (10 to 10.5) are associated with a sample that contains high nitrate (approx. 10'000 mg/L), and this may also be coupled to the redox processes. Core samples that have so far been affected by early very high nitrate concentrations originate from the following Formations: Hauptrogenstein (BOZ1-1), «Humphriesioolith Formation» (STA3-1), Opalinus Clay (BOZ2-1, STA3-1, STA2-1), Staffelegg Formation (MAR1-1, BOZ2-1, STA3-1, STA2-1), Klettgau Formation (MAR1-1). There are multiple experiments with moderate early nitrate production (a few 100's of mg/L), but 70% of all TBO AD experiments are not affected (10 – 100 mg/L in very early outflow only). It is unclear what triggers nitrate oxidation from kerogen in some experiments but not in others. Because the additional cold-shrink tube did suppress excessive nitrate production

(Opalinus Clay from STA2-1 and STA3-1, and all samples from the BAC1-1 borehole), there appears to be a connection to permeation of some components from the confining fluid to trigger these redox processes.

There is some indication that in cores with early high nitrate concentrations also the breakthrough behaviour of other major components like Cl is affected. In the extreme cases of STA2-1, the Cl concentrations in the outflow drop below the APW concentration (Fig. 4.7-9) after some time (Cl in the APW is distinctly less concentrated than in the porewater of the core samples). In agreement, the electric conductivity drops below the APW value (Fig. 4.7-6). This may be an indication for a dilution effect caused by the ingress of a significant proportion of confining water (contains almost no Cl) that is persistently diluting the outflow aliquots and accordingly also affects the stable isotope composition of water. Some of these severely affected cores also show an anomalous evolution of hydraulic conductivity (STA2-2, Opalinus Clay) that is very likely related to the overall geochemical disturbance.

It is evident that such experiments cannot be used to define the composition of the porewater (early aliquots) or the anion-accessible porosity fraction for Cl or Br. Two of the affected STA2 cores (STA2-1, STA2-3) performed under stable hydraulic conditions but remained in chloride concentrations slightly (STA2-3) or distinctly (STA2-1) below the APW, as said perhaps due to admixture of confining fluid at the outflow end of the core sample. These two samples are being flushed with APW at the inflow end for 2.4 (STA2-3) or 0.75 (STA2-1) pore volumes. This end of the core sample was therefore used to derive the Cl-accessible porosity fraction from the post-mortem aqueous extract of the lower end of the core, and the inflow concentration of Cl (APW). Similarly, certain data from previous experiments that were affected by early geochemical disturbances are considered as reliable (documented in the respective reports).

While the afore discussed artefacts have compromised the affected experiments and delivered in some cases only an incomplete dataset, they may be useful for process understanding of disturbed systems, e.g., the generation of high nitrate and DOC concentrations, presumably by microbially induced redox reactions. The exact mechanisms are presently not fully understood but land itself to a more quantitative treatment supported by transport modelling simulations.

4.7.9 Concluding remarks and open issues

Four advective displacement experiments were conducted on samples from the clay-rich Dogger units and Liassic, focussing on the derivation of constraints for a representative porewater composition, anion accessible porosity fractions, and transport properties. A systematic and consistent dataset on petrophysical and geochemical properties was obtained for one core sample only. This sample from the Opalinus Clay (STA2-4) was processed one year after the initially performed experiments, using an improved set-up with an additional sealing layer consisting of a cold-shrink tube, also used for later experiments (Bachs-1-1 borehole). The STA2-4 experiment resulted in a full characterisation of the in-situ porewater, and of the anion-accessible porosity fractions.

The evolutions of the outflow chemistry of STA2-1, STA2-2, and STA2-3 experiments, as well as derived in-situ porewater chemistries, and derived anion accessibility fractions, disagree with values from alternative approaches, or cannot be explained without considering severe artefacts (e.g. nitrate production, possible leakage by components from the confining water). But the pre-characterisation data of the three cores affected by artefacts during infiltration are a valuable contribution to the mineralogy, water content, aqueous extracts, and cation exchange properties data sets from this borehole. At the end of two experiments that produced early elevated nitrate («Humphriesioolith Formation», Staffelegg Formation), the in-flow ends of the core samples are

likely in equilibrium with the infiltrating APW, and disturbances by any artefacts still affecting the outflow are small. Therefore, the derived post-mortem chloride accessible porosity fractions are considered reliable (Tab. 4.7-16) for these two samples.

The sulphate system in all aliquots appears to be controlled by celestite equilibrium. This either implies that such a control is imposed by this mineral being initially present, or that a disturbance causes to reach such a solubility-product control. In the latter case, the reconstruction of the porewater sulphate concentration is more challenging, and also influences the carbonate system and clay-exchanger complex by ways of interdependent thermodynamic mass-action equilibria.

Like in all earlier work, there are unusually high concentrations of TOC mobilised in the earliest aliquots, decreasing gradually to values more in line with aqueous extracts, but still at significant concentrations.

The implementation of Ag filters (very thin, made of very fine-grained precipitated silver with very large specific surface area) at the base and top of the cores STA2-1, STA2-2, and STA2-3 aimed at decreasing microbial activity. As a side effect, this significantly decreased Br concentrations in at least the first aliquot by formation of AgBr at the filter surface. Therefore, PEEK filters were used again in STA2-4 and later AD experiments, as was done earlier.

The data of this study, in combination with data from boreholes STA3-1 and BAC1-1, imply that the use of an additional separation layer (between the confining water and the core sample) in core packing in form of a cold shrink tube is a definitive improvement in reducing artefacts. The mechanical, hydraulic and electrochemical sensor aspects of the experimental setup reliably performed for the duration of the experiments. The analytical procedures were already optimised and adequate, intrinsically limited by very small sample volumes in some cases.

4.8 Water-isotope data from diffusive-exchange experiments

Lukas Aschwanden & Thomas Gimmi

The porewater isotope composition ($\delta^{18}O$, $\delta^{2}H$) was derived by isotope diffusive-exchange experiments conducted on core material of 80 samples collected across an interval of 476.5 – 1'109.2 m depth. The obtained highly resolved profiles for $\delta^{18}O$ and $\delta^{2}H$ cover the lithologies from the «Felsenkalke» + «Massenkalk» of the Malm to the Triassic Schinznach Formation.

Isotope diffusive-exchange experiments were conducted in two different laboratories for reasons of quality assurance and optimisation of data production time. Hydroisotop GmbH conducted experiments and analyses on 33 samples between 731.4 and 925.7 m, whereas 47 samples were investigated by the University of Bern (Rock-Water Interaction Group) in the interval of 476.5 – 781.7 m and 928.9 – 1'109.2 m, respectively as part of the standard program plus 8 additional samples in the interval 732.9 – 894.8 m (*cf.* Section 4.8.1.1).

The data set of Hydroisotop GmbH is provided in their data report in Appendix C. The relevant data produced at the University of Bern are summarised in Appendix A.

4.8.1 Data evaluation

4.8.1.1 Experimental and analytical data

All the isotope diffusive-exchange experiments followed the experimental and analytical protocol given in Waber (ed.) (2020). The evaluation of the experimental and analytical data underlying the derivation of the water stable isotope composition of the in situ porewater followed a standardised procedure as detailed below.

In order to qualify for a successful isotope diffusive-exchange experiment the following criteria had to be met (within the propagated analytical uncertainties) by the two experiments (so-called LAB[9] and NGW or ICE[10] experiments) conducted for one core sample:

- No severe leakage (evaporation). In most cases, the mass of experiment container including rock and test water before and after experiment remained constant (± 0.04 g). If the loss of mass was > 0.04 g, corrections were applied to the measured isotope value of the equilibrated test water by Rayleigh-distillation calculations before calculating the porewater isotope ratio, assigning the mass loss to evaporation of the initial test water. If the correction of the $\delta^{18}O$ value for evaporation was > 0.5 ‰ VSMOW (typically meaning that the mass loss of test water was > 5% of the initial mass of test water), the porewater isotope value was marked as less reliable.
- Reasonable mass ratio of porewater to test water yielding a change in the isotope signal of the test water after equilibration outside the propagated analytical uncertainty. Porewater to test water ratios as low as 0.1 – 0.2 were accepted but the calculated isotope composition of the porewater was marked as less reliable, whereas ratios < 0.1 lead to unreliable results that were rejected. The mass of porewater in an experiment is defined by the mass of rock and its gravimetric water content. The latter is not known when starting an experiment.
- Limited mass transfer between rock and test water, i.e., 1) limited transfer of test water to rock (< 0.5 $m_{\text{test water}}$) caused either by high salinity of porewater compared to test water or hydrating mineral phases (e.g. anhydrite, halite), or 2) limited transfer of porewater to test water (< 0.02 g) caused by high salinity of test water compared to porewater. Such mass transfer between rock and test water may lead to isotope fractionation processes whose impacts on the experiments are poorly understood. Porewater isotope data not fulfilling these criteria are kept but classified as less reliable provided that the experiments do not show any further unconformities and that the calculated porewater isotope data and water contents derived from isotope mass balance agree well with those of neighbouring samples (i.e. within the propagated analytical uncertainty). If this is not the case (i.e. the data constitute outliers), the experiments are considered as failed.
- Analyses of stable isotopes of test water solutions within the required accuracy.

Of the 88 investigated samples (176 individual experiments) only two experiment couples did not pass these criteria, owing to strong desiccation during sample preparation (STA2-1-522.23-PW and STA2-1-576.22-PW). Porewater isotope compositions calculated from these experiments are unreliable and will not be shown in the following graphs. For 18 samples the experimental data resulted in an elevated uncertainty of the calculated isotope composition of the in situ porewater (Tab. 4.8-1 and Section 4.8.1.2). These data are shown but marked with open symbols in the following graphs.

---

9 LAB: Experiments with laboratory tap water used as test water (same terminology for experiments performed at the University of Bern and Hydroisotop GmbH).

10 NGW and ICE: Experiments using test water depleted in ^{18}O and ^{2}H (melt water of Antarctic ice cores). Different terminology for experiments performed at the University of Bern (NGW) and Hydroisotop GmbH (ICE).

Tab. 4.8-1: Summary of samples showing experimental artefacts

Porewater isotope compositions calculated from these experiments are afflicted by somewhat larger uncertainties. * Samples show discrepancies for multiple quality criteria.

Elevated uncertainty of calculated porewater isotope composition owing to:	**Sample ID**
Minor evaporation of test water (5 – 10%; corrected by Rayleigh-distillation calculations)	STA2-1-476.47-PW *
Low porewater to test water ratios (0.1 – 0.2)	STA2-1-1022.28-PW * STA2-1-1099.98-PW
Transfer of porewater to test water (> 0.02 g)	STA2-1-960.43-PW * STA2-1-966.63-PW STA2-1-1060.82-PW STA2-1-1068.55-PW
Transfer of test water to porewater (> 0.5 $m_{\text{test water}}$)	STA2-1-821.37-RP STA2-1-890.41-RP STA2-1-904.24-RP
Tiny rock fragments in test water	STA2-1-599.95-PW STA2-1-770.22-PW
Sample material contained few fragments of rim material of the drill core (potentially dessiccated and/or contaminated with drilling fluid).	STA2-1-622.13-PW STA2-1-725.76-PW
Relative difference of more than 20% between water contents calculated from $\delta^{18}O$ and $\delta^{2}H$ data (criterion 1 in Section 4.8.1.2)	STA2-1-476.47-PW * STA2-1-563.09-PW * STA2-1-960.43-PW *
Relative difference of more than 20% between water contents from isotope mass balance and gravimetry (criterion 2 in Section 4.8.1.2)	STA2-1-476.47-PW * STA2-1-484.06-PW STA2-1-563.09-PW * STA2-1-610.73-PW STA2-1-960.43-PW * STA2-1-999.10-PW STA2-1-1022.28-PW *

4.8.1.2 Calculation of porewater composition and water contents

Porewater $\delta^{18}O$ and $\delta^{2}H$-values were calculated using equation 76 in Appendix A in Waber (ed.) (2020) considering the ratio q of the gravimetric water contents of the individual subsamples used in the experiments (for details see Appendix A in Waber ed. 2020). Water contents could then also be calculated by mass balance from the porewater isotope values. The robustness of the calculated porewater $\delta^{18}O$ and $\delta^{2}H$-values was further tested according to the following criteria:

1. A relative difference of less than 20% between the water contents calculated from $\delta^{18}O$ and $\delta^{2}H$ data derived from the experiments with test water depleted in ^{18}O and ^{2}H (NGW or ICE subsamples).
2. A relative difference of less than 20% between the average water content calculated by isotope mass balance from $\delta^{18}O$ and $\delta^{2}H$ data and the average of the gravimetric water content of the two subsamples used in the experiments.

If the relative difference in the different water contents is larger than 20% the calculated porewater $\delta^{18}O$ and $\delta^{2}H$-values are considered less reliable. Such data may still be used for further interpretation by accepting the larger propagated uncertainty; they are marked with open symbols in the following graphs.

Of the 83 samples that passed the experimental quality criteria (*cf.* Section 4.8.1.1; including samples with elevated experimental uncertainties) three samples show larger discrepancies according to both criteria above (Tab. 4.8-1 and Figs. 4.8-1 and 4.8-2) and four samples according to criterion 2 only. Four of these samples are afflicted by larger uncertainties from the experiments themselves (*cf.* Section 4.8.1.1). In these cases, the larger discrepancies in the water contents are due to experimental artefacts. The remaining three samples that show larger discrepancies in the water contents (criterion 2 only) do not show any experimental irregularities. In these cases, the differences between the average of the water contents derived by isotope mass balance and the average of the gravimetric water content of the two subsamples likely reflect lithological heterogeneity of the different subsamples used in the two experiments. Note that in anhydrite-bearing lithologies hydration of anhydrite during the isotope diffusive-exchange experiments also plays a role, although its extent and effect is unknown at this stage.

All samples that pass the above criterion 2 display a consistent, previously observed relationship between the average water content derived by isotope mass balance and the average of the gravimetric water content of the subsamples used in the experiments, the former being around 8% larger than the latter (Fig. 4.8-2). As the water content is generally well correlated with the clay-mineral content of the rocks (*cf.* Section 4.3), it was postulated that this difference might be associated with minor exchange with water of different isotope composition adsorbed on clay minerals (e.g. Pearson et al. 2003). However, no stringent explanation exists at this stage.

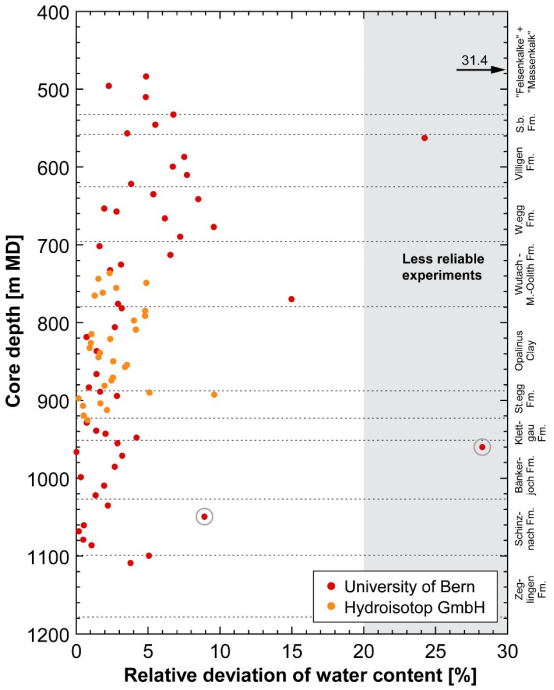

Fig. 4.8-1: Relative deviation of water contents obtained from $\delta^{18}O$ and $\delta^{2}H$ mass balance

The relative deviation is defined as the absolute difference between the water contents calculated from the $\delta^{18}O$ and $\delta^{2}H$ mass balance, divided by the latter (using data from the NGW experiment only; Waber ed. 2020). Grey area: Relative deviation of water contents obtained from $\delta^{18}O$ and $\delta^{2}H$ mass balance is > 20%. For samples within this area the calculated porewater $\delta^{18}O$ and $\delta^{2}H$ values are considered less reliable. Samples with a grey circle show some signs of contamination by drilling fluid (*cf.* Section 4.4).

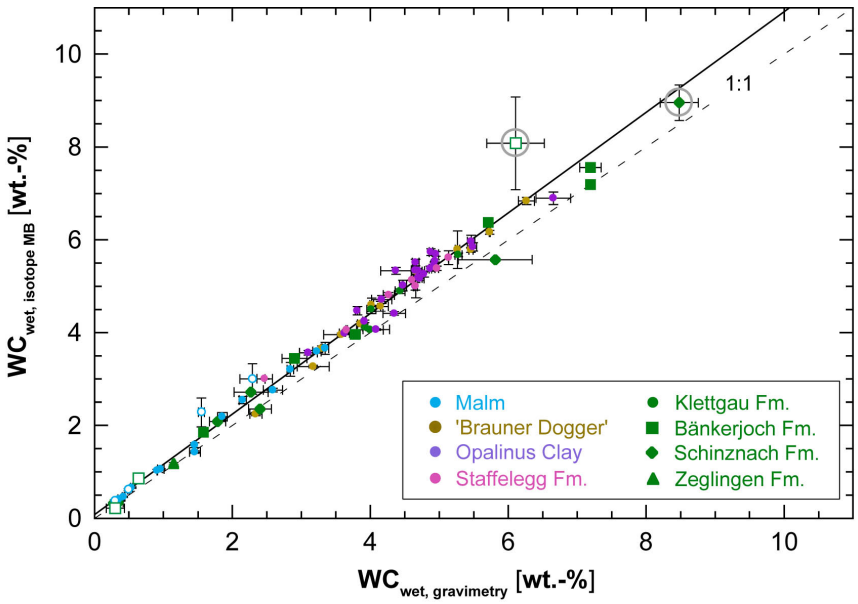

Fig. 4.8-2: Average water content obtained by water-loss at 105 °C ($WC_{wet,\ gravimetry}$) of subsamples LAB and NGW vs. average water content calculated from $\delta^{18}O$ and $\delta^{2}H$ mass balance from NGW diffusive-exchange experiments ($WC_{wet,\ isotope\ MB}$)

Open symbols refer to samples showing differences larger than 20% between the average water content derived by isotope mass balance and the average gravimetric water content of the two subsamples used in the experiment. These samples are excluded from the linear regression (solid black line), which has a slope of 1.08. Samples with a grey circle show signs of contamination by drilling fluid (*cf.* Section 4.4).

4.8.1.3 Contamination by drilling fluid

Contamination of some samples by drilling fluid – even in the central parts of the core material – was identified on the basis of aqueous extract solutions (*cf.* Section 4.4). This concerns an argillaceous sandstone sample from the Klettgau Formation (STA2-1-960.43-PW) and a dolomite-rich sample from the Schinznach Formation (STA2-1049.83-PW). These samples show a rather high porosity (17 vol.-% and 21 vol.-%, respectively) and likely elevated permeability allowing percolation of the drilling fluid to central parts of the drill core sample, which affected the porewater isotope composition derived from the isotope diffusive-exchange experiments to some degree. These samples are not excluded from the following graphs but marked with a grey circle being less reliable data.

4.8.2 $\delta^{18}O$- and $\delta^{2}H$-values of porewater

4.8.2.1 Data comparison University of Bern – Hydroisotop GmbH

All the porewater isotope data that pass the various quality criteria are illustrated in Fig. 4.8-3 as a function of depth. A new phenomenon in the dataset obtained by Hydroisotop GmbH was identified for STA2-1, resulting in a three-part segmented, curved pattern in the isotope data. Each segment shows the same general bell-shaped trend with – relatively – depleted isotope values at the top and (less distinct) at the bottom of each segment. This segmentation is observed for both isotope tracers but is somewhat less pronounced for $\delta^{18}O$. Each segment corresponds to a series of experiments that were terminated at the same day. Accordingly, the observed segmentation

seems to reflect an experimental artefact, probably caused by diurnal fluctuations of a parameter to which the termination of isotope diffusive-exchange experiments is sensitive, such as, e.g., the temperature. In order to better assess these trends, additional experiments were performed at the University of Bern using samples of more or less similar depth where the most depleted isotope values are observed in the profile of Hydroisotop GmbH. These additional experiments could not reproduce the questionable segmentation and they suggest an overall smoother profile. Thus, the most depleted values at the top of each of the three segments of the Hydroisotop dataset are considered unreliable, although they pass the quality control criteria above. For illustration purposes these values are shown in Fig. 4.8-3 (marked with a black circle), however, they are excluded from all other graphics that include data from isotope-diffusive exchange experiments. When ignoring these three data points, good agreement (within the propagated uncertainty) with the dataset of the University of Bern is obtained.

4.8.2.2 Depth profiles of porewater isotope composition

In the uppermost part of the investigated sequence in the «Felsenkalke» + «Massenkalk» and the Schwarzbach Formation no clear trends are indicated owing to the large scatter of the data. This is mainly related to experimental difficulties associated with these lithologies, e.g. low water contents. Across the interval Villigen Formation – Schinznach Formation both $\delta^{18}O$ and $\delta^{2}H$ values of the porewater show well defined, curved profiles. Although both tracers indicate the same general trends, some differences exist. In the Villigen Formation the oxygen isotope signature of the porewater evolves towards slightly more enriched values (from -3.2 ‰ VSMOW to -2.5 ‰ VSMOW) at the base of the Formation from where $\delta^{18}O$ increasingly becomes more negative across the interval Wildegg Formation – Staffelegg Formation approaching a local minimum of -7.0 ‰ VSMOW at around 960 m depth in the Klettgau Formation. The $\delta^{2}H$ values of the porewater also slightly increase in the Villigen Formation (from -40 ‰ VSMOW to -35 ‰ VSMOW), however, across the interval Wildegg Formation – Opalinus Clay they remain constant (neglecting the segmentation observed for the dataset of Hydroisotop GmbH, which is considered an experimental artefact; *cf.* Section 4.8.1.1.). In the Staffelegg Formation the $\delta^{2}H$ values of the porewater sharply evolve towards a local minimum in the Klettgau Formation (-52 ‰ VSMOW) as observed for the oxygen isotopes.

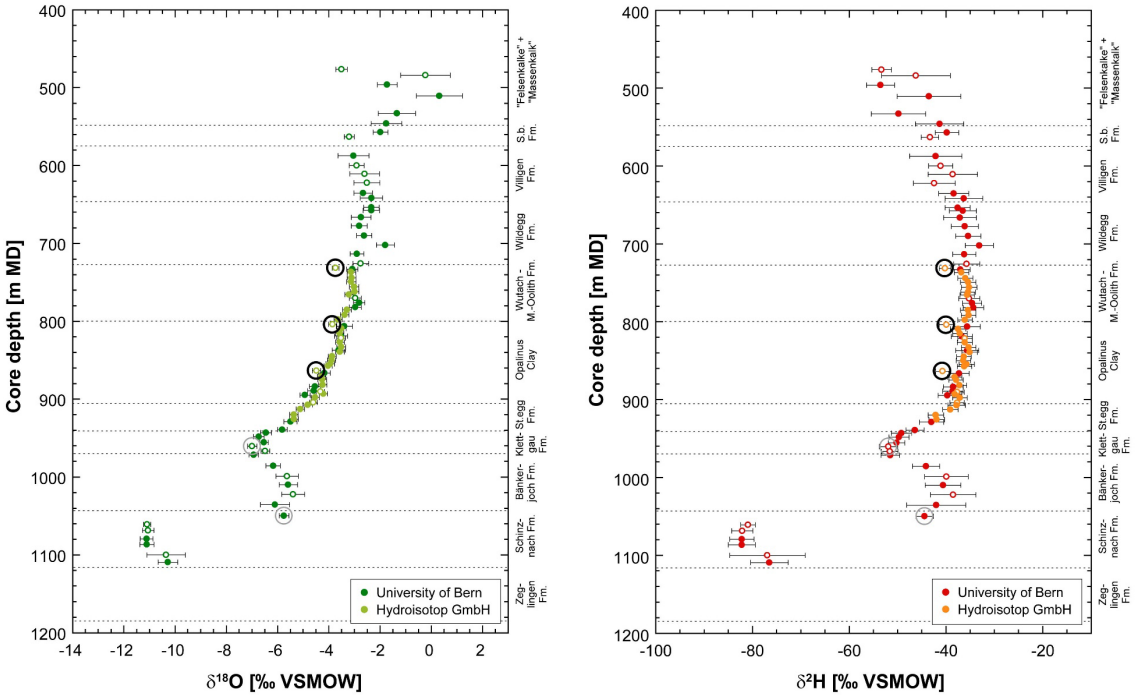

Fig. 4.8-3: Depth distribution of porewater $\delta^{18}O$ and $\delta^{2}H$ values obtained from isotope diffusive-exchange experiments

Open symbols refer to porewater isotope values which are less reliable owing to experimental artefacts (see text). Open symbols with additional black circles relate to samples where experimental artefacts render the calculated porewater isotope composition unreliable (see text). These data are shown here for illustration purposes, but they are excluded from all other graphs. Samples with a grey circle show signs of contamination by drilling fluid (*cf.* Section 4.4).

The different shapes of the $\delta^{18}O$ and $\delta^{2}H$ profiles are also illustrated in Fig. 4.8-4, which shows the depth profile of deuterium excess (defined as $\delta^{2}H - 8\times\delta^{18}O$; deuterium excess is +10 ‰ for a sample that lies on the GMWL, lower values of deuterium excess reflect sample positions to the right of the GMWL in a plot of $\delta^{18}O$ vs. $\delta^{2}H$; note that the deuterium excess as used at this stage carries no direct implications about the palaeoclimate at the time of infiltration). D-excess shows generally very negative values of around –42 ‰ in the «Felsenkalke» + «Massenkalk» and increases to values of around –21 ‰ in the underlying Schwarzbach Formation. In the Villigen Formation D-excess remains constant, whereas the interval Wildegg Formation – Klettgau Formation is characterised by constantly increasing deuterium excess (from around –18 ‰ to 4 ‰).

From the local minimum in the Klettgau Formation $\delta^{18}O$ and $\delta^{2}H$ values of the porewater evolve towards a local maximum in the Bänkerjoch Formation at around 1'022 m depth. Just below the top of the Schinznach Formation both tracers sharply decrease towards most negative values in the water conducting zone of the Formation only a few tens of meters below ($\delta^{18}O$ = –10.8 ‰ VSMOW; $\delta^{2}H$ = –80.1 ‰ VSMOW; *cf.* Section 5.7). Deuterium excess shows constant values of around 5.5 ‰ across the Bänkerjoch Formation and the Schinznach Formation.

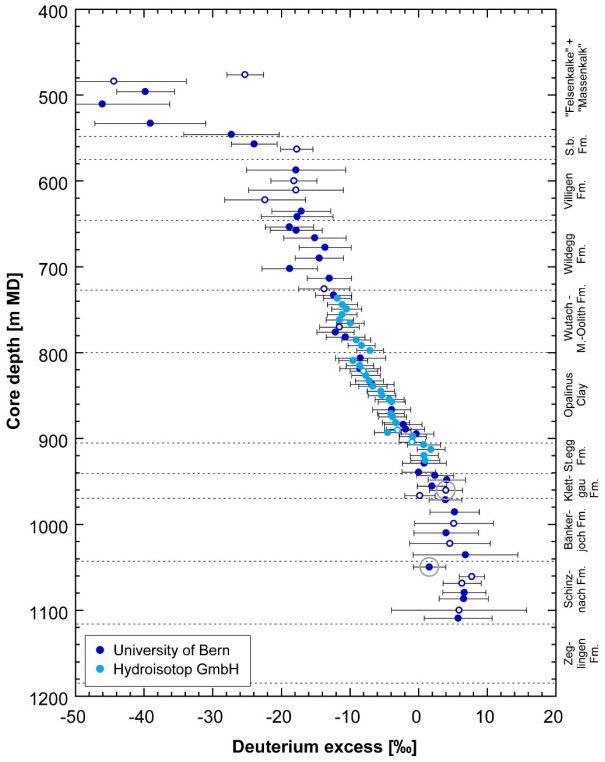

Fig. 4.8-4: Depth trend of deuterium excess in porewater based on the isotope diffusive exchange technique

Deuterium excess is +10 ‰ for a sample that lies on the GMWL. Lower values of deuterium excess reflect sample positions to the right of the GMWL in a plot of δ^2H vs. $\delta^{18}O$. Note that the deuterium excess as used at this stage carries no genetic implications about the origin of H_2O, e.g. on palaeo-climate at the time of infiltration. Open symbols refer to samples which are less reliable owing to experimental artefacts (see text). Samples with a grey circle show signs of contamination by drilling fluid (*cf.* Section 4.4).

4.8.2.2 δ^2H versus $\delta^{18}O$ and comparison with Global Meteoric Water Line

In the $\delta^2H - \delta^{18}O$-diagramm (Fig. 4.8-5) some remarkably regular and linear trends can be observed. Porewater isotope signatures in the Malm fall to the right of the Global Meteoric Water Line (GMWL). From the «Brauner Dogger» across the Opalinus Clay the porewater isotope composition continuously evolves towards values depleted in ^{18}O and approaching the GMWL, indicating a meteoric component in the latter porewaters. In the interval Staffelegg Formation – Klettgau Formation the porewater isotope composition evolves along a trajectory parallel to the GMWL towards values depleted in both ^{18}O and ^{2}H. The underlying Bänkerjoch Formation again shows enriched porewater isotope signatures before a sharp drop to distinctly more negative values across the water-conducting zone of the Muschelkalk (*cf.* Section 5.8 for further discussion) located on or slightly to the right of the GMWL.

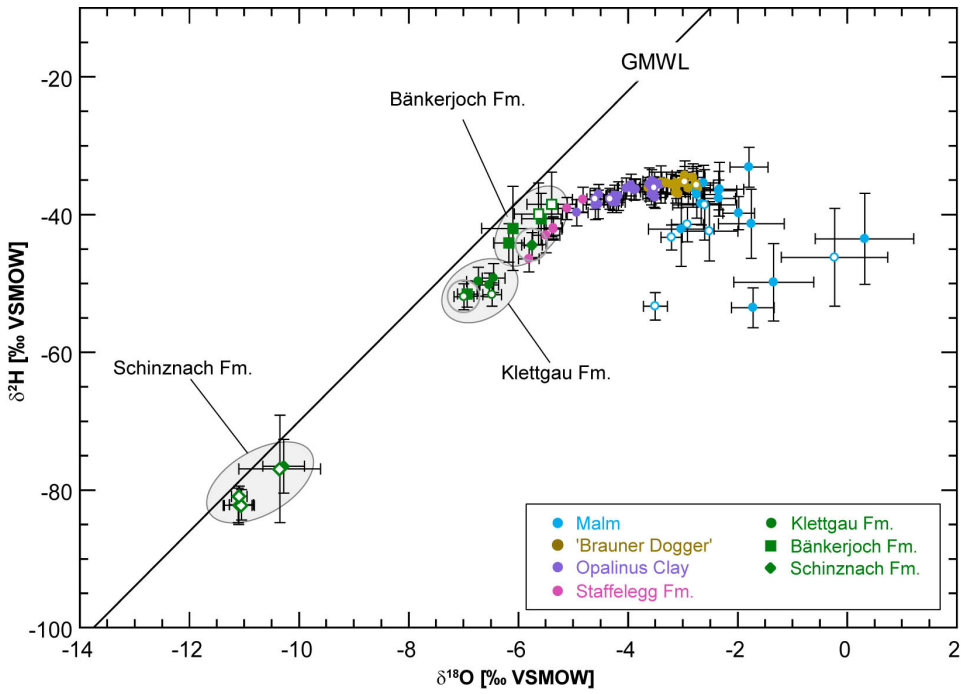

Fig. 4.8-5: δ^2H vs. $\delta^{18}O$ values of porewater obtained from isotope diffusive-exchange experiments

GMWL = Global Meteoric Water Line ($\delta^2H = 8 \times \delta^{18}O + 10$ ‰ VSMOW; Craig 1961), open symbols refer to porewater isotope values which are less reliable owing to experimental artefacts (see text). Samples with a grey circle show signs of contamination by drilling fluid (*cf.* Section 4.4).

5 Discussion of porewater data

5.1 Chloride data and estimation of Cl^- and Br^--accessible porosity

Paul Wersin, Carmen Zwahlen, Martin Mazurek, Thomas Gimmi

Chloride, a major component in the porewater, has been determined by squeezing (Section 4.6), advective displacement (Section 4.7) and aqueous extraction (Section 4.4). This anion is considered to behave as a conservative species with no or very limited interaction with the minerals. The same can be said for bromide, which occurs at much lower concentrations in the porewater. In argillaceous rocks, anions are repelled from the negative structural charge of the clay-mineral surfaces and are thus affected by ion exclusion. In other words, they only 'see' part of the total water-filled porosity, the fraction of which is often termed anion-accessible porosity (Pearson 1999, Pearson et al. 2003) or also 'free' porosity. Ion exclusion is not complete according to theory and depends on distance from charged surfaces, but here this simplifying assumption is made for adopting a simplest possible model.

Knowing the concentration of Cl per bulk (total) porewater in a sample from aqueous extraction ($C_{Cl\ in\ bulk\ porewater}$), the Cl-accessible porosity fraction, f_{Cl}, can be estimated from Cl measurements in squeezing ($C_{Cl\ in\ squeezed\ water}$) or advective displacement ($C_{Cl\ in\ adv.\ displaced\ water}$) experiments, assuming that the latter represent the composition of the 'free' porewater:

$$f_{Cl} = \frac{n_{anion-accessible}}{n_{total}} = \frac{C_{Cl\ in\ bulk\ pore\ water}}{C_{Cl\ in\ squeezed\ or\ adv.displaced\ water}}$$

$C_{Cl\ in\ bulk\ porewater}$ is calculated from:

$$C_{Cl\ in\ bulk\ pore\ water} = \frac{C_{Cl\ in\ aq.extract}}{WC_{dry}\ {}^{S}/_{L}}$$

with C = concentration [mg/L], n = porosity [–], WC_{dry} = water content relative to dry rock mass [g/g], S/L = solid/liquid ratio of aqueous extraction experiment [g/g]. The Br-accessible porosities are derived in an analogous fashion.

The anion-accessible porosity fractions have been derived according to the above equation for squeezed and advectively displaced porewaters (Tabs. 4.6-8, 4.6-9 and 4.7-16). Both methods enable to mobilise porewater that is thought to be a proxy of the so-called 'free' porewater (not affected by the negatively charged clay surface). It should be noted, however, that the two methods operate by entirely different mechanisms. Whereas porewater is mobilised by mechanical compaction implying a deformation of the porespace in the squeezing method, this is achieved by a strong hydraulic pressure gradient imposed by an artificial porewater in the advective displacement method. Thus, method-specific artefacts may be expected and likely not the same volume of the porespace is sampled by the two methods. In the case of non-reactive Cl, experimental artefacts appear to be minor as suggested from previous studies (e.g., Mazurek et al. 2021). In the case of the squeezed waters, it is generally assumed that the waters squeezed at the lowest pressure best reflect the in situ porewater (Mazurek et al. 2015, Wersin et al. 2016). For the advectively displaced waters, the first two measured aliquots are assumed to be the most representative of the in situ porewater (Section 4.7). It should be noted that three out of the four AD experiments of STA2-1 were strongly affected by microbial perturbation leading to high nitrate porewater concentrations. Thus, only data from one sample at 900.81 m is deemed to yield reliable porewater data (Section 4.7.5). Regarding estimation of anion-acessible porosity fractions, however, also two of the perturbed AD samples were considered, based on the data from post-mortem analysis of the cores Section 4.7.6).

The derived values of the Cl-accessible porosity fraction (f_{Cl}) for the two datasets are shown as a function of the clay-mineral content in Fig. 5.1-1, with the SQ values derived according to the preferred method 1 (from POST data, see Section 4.6, Tab. 4.6-8). Note that the SQ sample from the Staffelegg Formation shows a large difference between method 1 & 2 (f_{Cl} 0.47 or 0.70). Porosity fractions obtained from AD and SQ experiments range between 0.47 and 0.52 except for AD sample 900.81 m from the Opalinus Clay which shows a value of 0.36. The corresponding mean value from both methods is 0.476 ± 0.055[11]. This value is in the same range as the corresponding ones from previous boreholes, such as TRU1-1 (0.45 ± 0.05), Aschwanden et al. 2022) and MAR1-1 (0.46 ± 0.08, Mäder et al. 2022) and STA3-1 (0.45 ± 0.05, Aschwanden et al. 2022), but slightly above BOZ1-1 (0.42 ± 0.08, Wersin et al. 2022a), BOZ2-1 (0.42 ± 0.07, Gimmi et al. 2022), and slightly below the estimated value for BUL1-1 (0.52 ± 0.06).

There is no clear trend with clay-mineral content above 35 wt.-% as also noted in many of the other boreholes (see below). There are no data available from STA2-1 at lower clay-mineral content where a dependency on this parameter would be expected, as indicated for example for the BUL1-1 data (also depicted in Fig. 5.1-1). It would be important to know the anion accessibility because within the sampled interval the lithologies in the STA2-1 profile vary substantially. In order to derive a porewater profile for Cl, the anion accessibility in these lithologies must be known or assumed. In BUL1-1, which also lies in the Nördlich Lägern siting region, an increasing trend of f_{Cl} with decreasing clay-mineral content was suggested below a clay-mineral content of 20 wt.-% (even though the precise relationship could not be discerned) (Fig. 5.1-1). In other boreholes, such as TRU1-1, the increasing trend of f_{Cl} seems to start already at 40 wt.-% clay-mineral content, whereas in BOZ1-1 this "threshold" seems to occur at about 25 wt.-%. Given these premises, we consider a uniform f_{Cl} value of 0.47 for clay mineral contents > 20 wt.-% as "reference" for deriving the Cl profile for the entire sequence, but also explore the effect when assuming a "threshold" clay-mineral content of 40 wt.-% (Section 5.2). Below these "threshold" clay-mineral contents, a linear increase of f_{Cl} to a value of 1 at a clay-mineral content of zero is assumed.

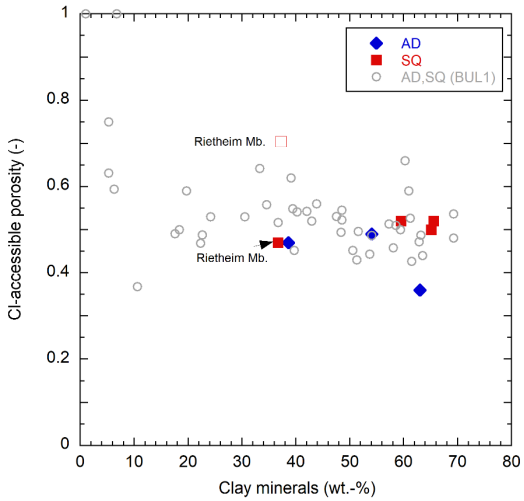

Fig. 5.1-1: Cl-accessible porosity fraction as a function of the clay-mineral content from AD and SQ data as well as data from BUL1-1 borehole

BUL1-1 data comprises AD, SQ and through-diffusion data (Mazurek et al. 2021). The SQ data are derived from method 1 (See section 4.6). Note that the SQ sample from the Rietheim Member (Staffelegg Formation) shows a large difference between method 1 (f_{Cl} 0.47) and method 2 (f_{Cl} 0.7), shown as open squares.

[11] Note that the mean is pulled down by one AD sample at 900.81 m from the footwall of the Opalinus Clay.

The fact that f_{Cl} shows considerable scatter when plotted against the clay-mineral content suggests that the latter is not the only parameter that determines the anion accessibility. Mineralogical composition of the clay fraction, mean pore size, grain-size distribution, fabric and other factors are expected to affect the anion accessibility as well. Note that the negative structural charge of the clays is predominately carried by the smectite and illite components. Furthermore, according to theory, the anion accessibility also varies with the salinity and the composition of the porewater, i.e., it is not just a material property. All these partly interdependent effects cannot be properly quantified at this stage, which severely limits the application of theoretical models.

An uncertainty range of ± 20% is considered for f_{Cl}, which is probably sufficient for clay-rich lithologies but may still be an underestimation for clay-poor rocks. This uncertainty propagates into the calculated Cl concentrations in the anion-accessible porewater, i.e., an error of ± 20% must be considered in addition to the propagated analytical error.

For Br, fewer data are available, including one AD and four SQ samples. Note that for the latter, estimation of Br accessible porosity fractions was only deemed possible with method 2 (based on AqEx data from adjacent cores, see Section 4.6) due to methodological reasons. The derived f_{Br} values as a function of the clay-mineral content show f_{Br} values between 0.4 and 0.6, except for the SQ sample at 911.28 m from the Rietheim Member with a f_{Br} of 0.76. Such a high value appears plausible when considering the Cl and Br profiles (Section 5.2); it is possibly related to the high amount of organic carbon (~ 5 wt.-%) in this lithology. Disregarding this sample, the mean value is ≈ 0.5, i.e. somewhat higher than obtained for f_{Cl}.

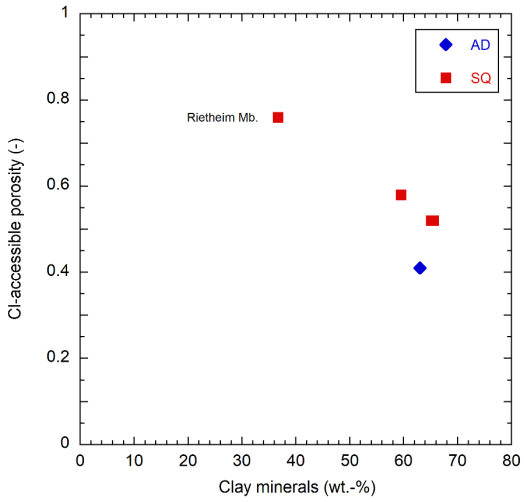

Fig. 5.1-2: Br-accessible porosity fraction as a function of the clay-mineral content derived from SQ (method 2) and AD data

Fig. 5.1-3 illustrates the Cl-accessible porosity fraction as a function of depth. No clear trend for the sampled interval («Brauner Dogger» – Staffelegg Formation) can be discerned.

In this figure, also SQ data obtained by method 2 (i.e. Cl concentration in bulk water derived from AqEx of a subsample of the SQ core) are shown. These illustrate similar (but slightly higher) values relative to those of method 1 for three out four samples. As mentioned above, one sample at 911.28 m from the Rietheim Member («Posidonienschiefer»), shows a significantly higher f_{Cl} value with method 2. Such a high value appears plausible for this organic-rich lithology when looking at the Cl profile obtained from AqEx (see below). The reason for the differing values is not clear at this stage.

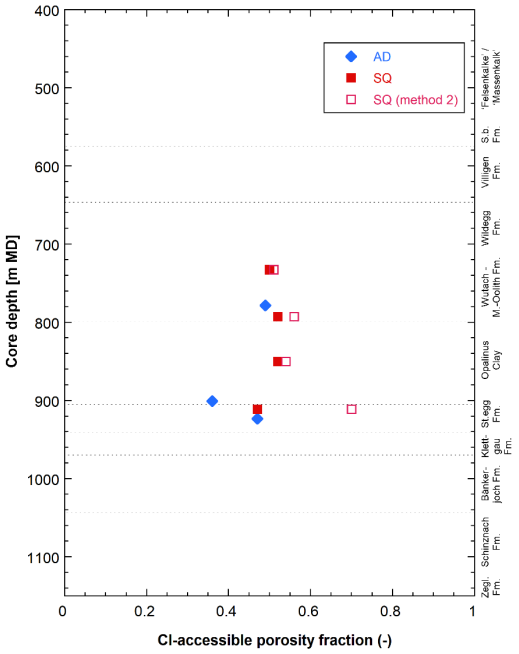

Fig. 5.1-3: Cl-accessible porosity fraction as a function of depth

5.2 Chloride, bromide and Br/Cl profiles

Paul Wersin, Carmen Zwahlen, Martin Mazurek, Thomas Gimmi

The chloride profile depicted in Fig. 5.2-1 includes aqueous extraction data re-calculated to in-situ conditions assuming the relationship between clay-mineral content and f_{Cl} (with clay-mineral content of 20 wt.-% as "threshold" value) as discussed in Section 5.1. The Cl concentrations obtained from squeezing and advective displacement, as well as those for the groundwaters in the Malm and the Muschelkalk (Table 2.2, Lorenz, 2023), are also shown in Fig. 5.2-1. The error bars include the propagated analytical uncertainty and, for aqueous extraction data, an additional 20% that reflect the uncertainty related to f_{Cl} (see Section 5.1, Fig. 5.1-1). It should be pointed out that for samples from the uppermost formations («Felsenkalke» + «Massenkalk», Schwarzbach Formation, Villigen Formation) no mineralogy data were acquired and thus only crude estimates on clay-mineral content could be made.

Data from all three methods are consistent within the extended error bars[12]. The Cl profile is reasonably well constrained and supported by the dense sampling, in particular in the Opalinus Clay. In some lithologies in the upper and lower confining units, however, Cl concentrations show considerable variations (Fig. 5.2-1). In general, the Cl profile indicates a curved profile between the Malm and Muschelkalk aquifers with maximum Cl concentrations of 7 – 8.5 g/L as illustrated in Fig. 5.2-1 (left). In that figure, porosity determined from water-loss is considered to re-calculate Cl in aqueous extracts. Considering pycnometer porosity (Section 4.3.4) instead leads to a similar profile, but a shift to slightly higher concentrations for the re-calculated AqEx data (Fig. 5.2-1 right) can be discerned. This difference is because of the slightly lower pycnometer porosities (deduced from grain and bulk wet density measurements). Also, the scatter in the Opalinus Clay

[12] It should be noted that only one AD sample is considered because of the strong nitrate perturbation in the other samples.

and the «Brauner Dogger» appears somewhat larger and the profile slightly more curved towards the Malm aquifer with the latter choice. The reasons for these slight differences are not known at this stage.

Looking at the Cl profile from the Malm aquifer down to the Muschelkalk aquifer in more detail, one can note:

- A slight general increase with depth is suggested in the Malm units (down to ~ 730 m depth) from the profile based on water-loss porosity, but this is less obvious when pycnometer porosity is considered instead.

- The Cl profile in the «Brauner Dogger» is flat with variations within the estimated uncertainty ranges. An exception is the outlier at 729.13 m which represents iron-oolitic horizon with 39 wt.-% goethite and 44 wt.-% clay minerals. The Cl-accessible porosity fraction is likely underestimated for this type of sediment, as indicated from previous boreholes. Using an accessibility of 1 instead of 0.47 would lead to a concentration of ~ 7 g/L, a value similar to those of neighbouring samples.

- From the top to the centre of the Opalinus Clay the Cl profile remains flat, but subsequently concentrations seem to decrease slightly towards the top of the Staffelegg Formation according to AqEx data re-calculated from water-loss porosity. This trend is less clear when AqEx data based on pycnometer porosity is considered. A strongly decreasing trend towards the Keuper aquifer is observed in the Staffelegg and Klettgau Formations with considerable scatter. Note also the outliers at 911.03 and 911.28 m from the Rietheim Member with high C_{org} contents of 4 – 5 wt.-%. For these samples, a higher anion-accessible porosity is likely more appropriate than the one applied with the simple relationship detailed in the previous section. In fact, a higher f_{Cl} value for the SQ sample 911.28 m was derived when considering method 2 (Section 4.6.6) as discussed in the section above.

- From the Keuper aquifer, a general decreasing trend towards the Muschelkalk can be inferred. The large variations noted in the Bänkerjoch Formation may be at least partly due to the considerable uncertainites regarding the water content and the anion-accessibility in these anhydrite bearing rocks. The porewaters exhibit minimum concentrations < 1 g/L at 1'070 – 1'080 m depth, which are similar to the groundwater concentrations from the packer interval at 1'058 – 1'117 m depth. Porewater concentrations indicate a strong increase with depth from ~ 1'080 m depth to the last sample at 1'109 m depth. Note that the rock salt layer is located at about 1'150 – 1'170 m depth (Zeglingen Formation).

As mentioned above, the relationship used to derive the Cl-accessible porosity fraction for the samples with low and intermediate clay-mineral content is based on the assumption of a linear relationship with the clay-mineral content < 20 wt.-% (towards a value of 1 for clay-free rock). Fig. 5.2-2 compares the profiles obtained for a "threshold" value of 20 wt.-% (left) with those using a "threshold" value of 40 wt.-%. Both profiles are similar in the lower part up to the «Brauner Dogger», but the profile based on 40 wt.-% threshold appears to be closer to the line connecting the Muschelkalk and Keuper groundwaters. In the Malm units, however, the profile based on < 20 wt.-% threshold appears somewhat smoother than that based on < 40 wt.-% threshold.

In summary, a broadly consistent and well-defined Cl profile for the Opalinus Clay and confining units is obtained from squeezing, advective displacement and aqueous extraction data. The observed scatter is related predominantly to the uncertainty in the anion-accessible porosity (which may not only vary as a function of the clay-mineral content), and to a lesser extent to the uncertainty in the water content. In this analysis, a simple relationship of the anion-accessible porosity with the clay-mineral content (as proxy of surface charge) based on squeezing and

advective displacement data was used. Other relationships with the clay-mineral content (e.g., linear extrapolation from clay-mineral content <40 wt.-%) do not result in a less scattered profile. The lower part of the Cl profile is influenced by the Keuper and Muschelkalk aquifers.

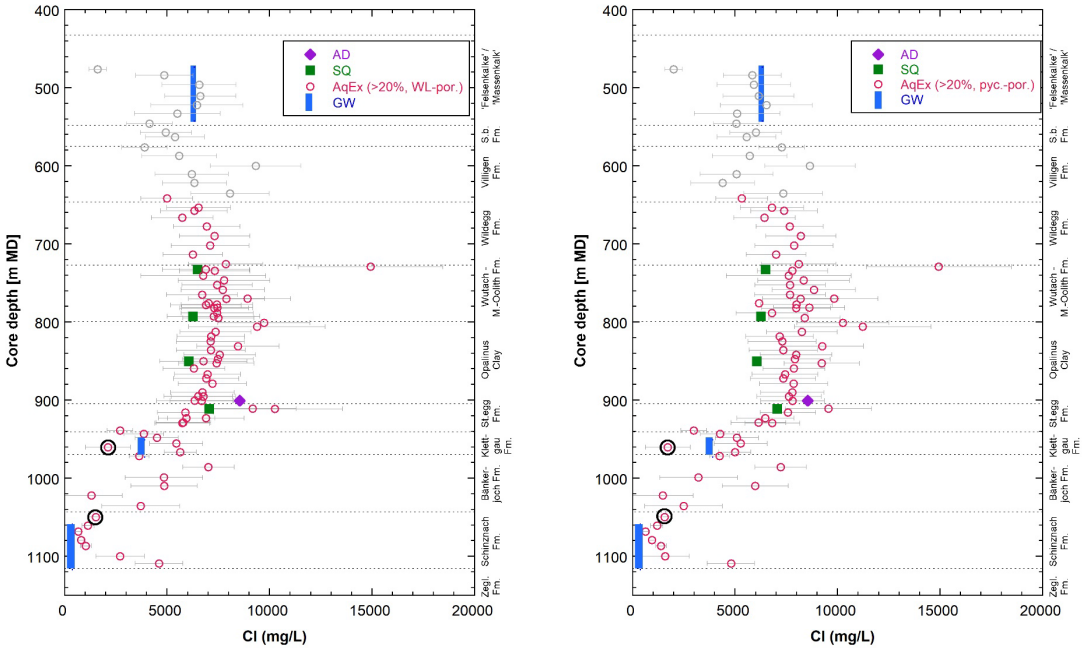

Fig. 5.2-1: Cl profile based on data from squeezing, advective displacement, aqueous extraction, and groundwater samples; AqEx data recalculated from water-loss porosity (left) and pycnometer porosity (right) and assuming 20 wt.-% clay-mineral content as threshold for linear extrapolation of f_{Cl} values (see text)

Aqueous extraction data in the Br profile re-calculated to Br-accessible porosity assuming the relationship between accessibility and clay-mineral content for Cl as discussed in Section 5.1. Grey symbols: no mineralogical analysis available for these data points; clay-mineral contents were roughly estimated as: 0 wt.-% for «Felsenkalke» + «Massenkalk», 10 wt.-% for Schwarzbach Formation and Villigen Formation. Error bars of Br data from aqueous extraction include propagated analytical uncertainty plus another 20% that reflect the uncertainty related to f_{Cl}. Note that the groundwater data are not corrected for drilling fluid contamination.

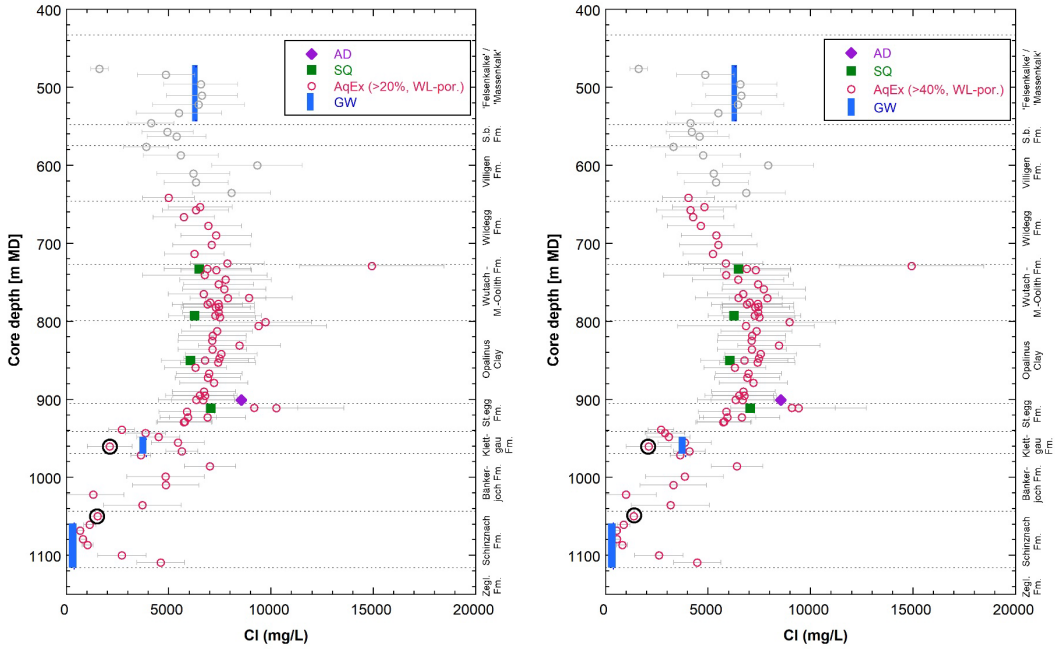

Fig. 5.2-2: Cl profile with data from squeezing, advective displacement, aqueous extraction, and groundwater samples; AqEx data recalculated from water-loss porosity assuming 20 wt.-% clay-mineral content (left) and 40 wt.-% (right) and as threshold for linear extrapolation of f_{Cl} values (see text)

Aqueous extraction data re-calculated to Cl-accessible porosity assuming the relationship between accessibility and clay-mineral content as discussed in Section 5.1. Error bars on the data from aqueous extraction include propagated analytical uncertainty plus another 20% that reflect the uncertainty related to f_{Cl}. Grey symbols: no mineralogical analysis available for these data points; clay-mineral contents were roughly estimated as: 0 wt.-% for «Felsenkalke» + «Massenkalk», 10 wt.-% for Schwarzbach Formation and Villigen Formation. Black encircled points: affected by drilling fluid contamination.

The Br profile (Fig. 5.2-3) reveals a similar shape as the one of Cl in the upper part (Malm-Staffelegg Formation), albeit with somewhat more scatter, which is likely related to the larger analytical uncertainty of this minor element. Using the pycnometer porosity (Fig. 5.2-3 right) instead of the water-loss porosity (Fig. 5.2-3 left) to calculate porewater concentrations from aqueous extracts leads to somewhat more scatter besides the slightly increased concentrations in the centre of the sequence.

From the Malm aquifer down to the Keuper aquifer, the Br profile shows considerable scatter with average values of about 20 – 30 mg/L. The curvature towards the Malm aquifer is less pronounced than in the case of the Cl profile. Below the Keuper aquifer, the Br profile diverges from that of Cl. Thus, an increase of Br concentrations is noted across the Bänkerjoch Formation, below which a sudden decrease to low values, slightly higher than in the sampled Muschelkalk groundwater, is indicated.

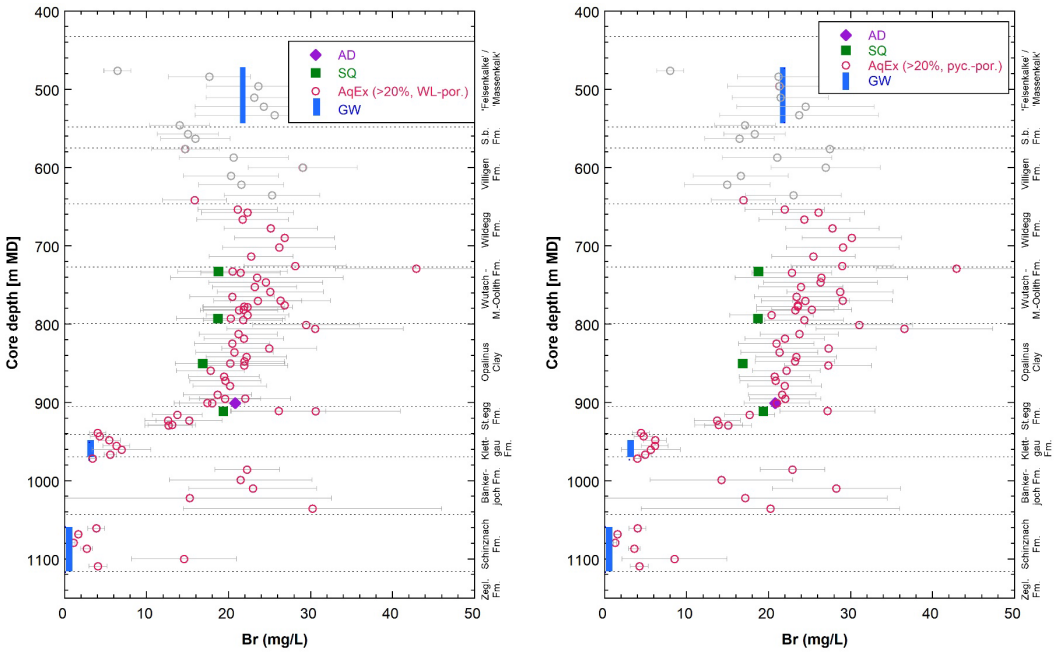

Fig. 5.2-3: Br profile with data from squeezing, advective displacement, aqueous extraction, and groundwater samples; AqEx data recalculated from water-loss porosity (left) and pycnometer porosity (right) and assuming 20 wt.-% clay-mineral content as threshold (see text)

Aqueous extraction data in the Br profile re-calculated to Br-accessible porosity assuming the relationship between accessibility and clay-mineral content for Cl as discussed in Section 5.1. Error bars of Br data from aqueous extraction include propagated analytical uncertainty plus another 20% that reflect the uncertainty related to f_{Cl}. Note that the groundwater data are not corrected for drilling fluid contamination.

The Br/Cl profile (Fig. 5.2-4) shows less scatter than the individual Cl and Br profiles. This is mainly because uncertainty related to anion-accessibility and water content does not affect the Br/Cl ratio, contrary to the individual concentrations. AqEx, SQ, AD and groundwater data show consistent datasets.

Constant 1'000*Br/Cl ratios of about 1.5 are depicted in the Malm units. Below, a slightly decreasing trend in the «Brauner Dogger» and Opalinus Clay, followed by a strong drop towards the Keuper aquifer is observed. The Br/Cl ratios rise strongly to high values in the Bänkerjoch Formation, but decrease again in Muschelkalk units, reaching low values at the level of the aquifer, but somewhat above the ratio of the sampled groundwater (0.11). The halite-rich layer at about 1'160 m depth exhibits an even lower ratio of ~ 0.01.

It is interesting to note that the Br/Cl ratios in the Dogger units are higher than what was observed in BUL-1-1 and the boreholes from ZNO (TRU-1-1 and MAR-1-1). However, the boreholes STA3-1, BOZ1-1 and BOZ2-1 from JO display similar ratios. The positive excursion in the Bänkerjoch Formation was also observed the STA3-1 borehole as well as in the BOZ1-1 and BOZ2-1 boreholes.

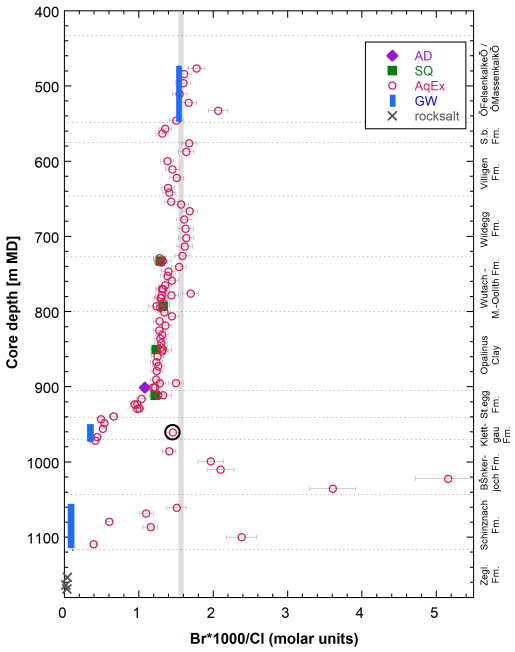

Fig. 5.2-4 1'000*Br/Cl (molar units) profile with data from squeezing, advective displacement, aqueous extraction, groundwater and halite samples

Grey bar: range in modern seawater. The propagated uncertainty for SQ data assumes the same analytical uncertainty as for the other samples (4% for Br). Black encircled point: affected by drilling fluid contamination.

5.3 Sulphate and SO_4/Cl profiles

Paul Wersin, Martin Mazurek, Thomas Gimmi

Sulphate data from squeezing, advective displacement, aqueous extraction and groundwaters are illustrated in Fig. 5.3-1. Data from aqueous extraction were re-calculated to concentrations in bulk porewater (Fig. 5.3-1 left) or to concentrations in anion-accessible porewater (using the same accessibility as for Cl, Fig. 5.3-1 right), assuming conservative behaviour of sulphate. This assumption is not true at least in anhydrite-bearing lithologies in the Bänkerjoch Formation where mineral dissolution contributed to SO_4 concentrations in the extracts, as is evident from the AqEx samples with re-calculated unrealistically high SO_4 concentrations of more than 50 g/L, way above the solubility of gypsum or anhydrite (not shown in Fig. 5.3-1).

SO_4 concentrations based on squeezing and advective displacement yield distinctly lower values in comparison with the aqueous extraction concentrations per bulk water or per accessible porewater re-calculated from aqueous extraction. The advective displacement sample (900.81 m) is consistent with the SQ sample located just below (911.28 m). The AD/SQ datasets suggest a constant profile with concentrations of ~ 2.4 g/L followed by a slightly increasing trend with depth in the lowest part of the sampled sequence, The concentration in the Keuper groundwater is rather high (5.6 g/L) and lies within the trend indicated for the porewater data from AD/SQ above. The Muschelkalk groundwater exhibits a lower concentration (~ 1.7 g/L) than the Keuper groundwater and the AD and SQ porewaters above. The sampled Malm groundwater displays a much lower concentration of 0.009 g/L.

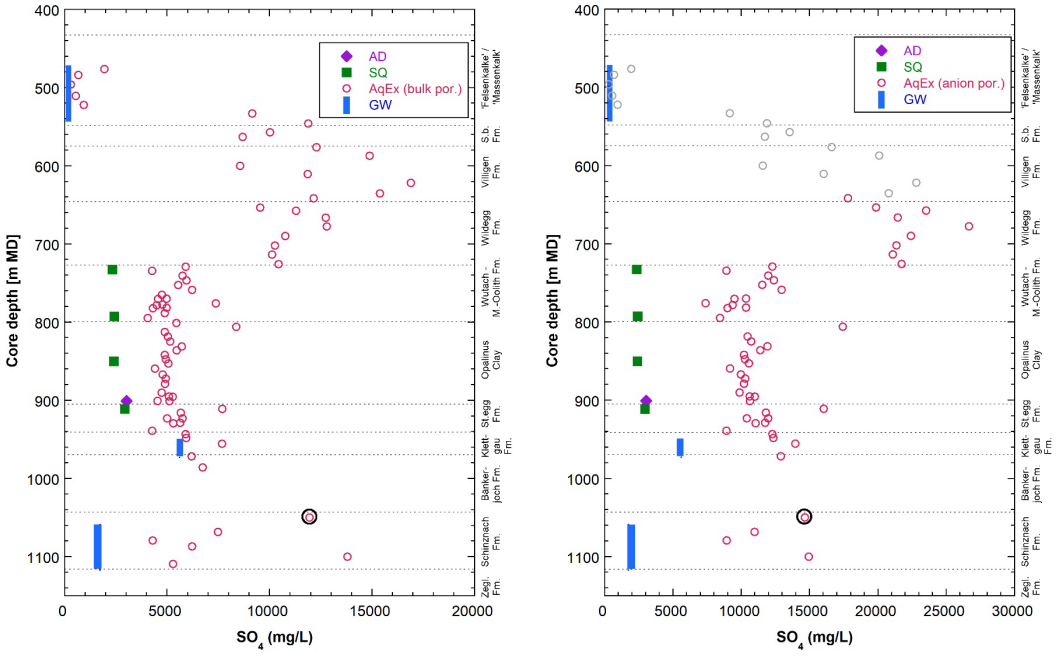

Fig. 5.3-1: SO_4 profiles with data from squeezing, advective displacement, aqueous extraction, and groundwater samples; left: AqEx data re-calculated to bulk porosity; right: AqEx data re-calculated to anion-acessible porosity

Aqueous extraction data re-calculated to contents in bulk porewater using water content. Aqueous data re-calculated to SO_4-accessible porosity assuming the same relationship between accessibility and clay-mineral content as applied above for Cl. Grey symbols: no mineralogical analysis available for these data points; clay-mineral contents were roughly estimated as: 0 wt.-% for «Felsenkalke» + «Massenkalk», 10 wt.-% for Schwarzbach and Villigen Formations. Black encircled points: affected by drilling fluid contamination. Note that the groundwater data are not corrected for drilling fluid contamination.

The re-calculated aqueous extraction concentrations exhibit systematically higher and more variable concentrations than the SQ and AD data. The discrepancy between aqueous extraction and squeezing/advective displacement data becomes even larger when anion exclusion is considered, e.g., by assuming the same relationship between anion-accessible porosity and clay-mineral content as that applied for Cl (Fig. 5.3-1 right). However, it should be noted that the anion-exclusion effect of SO_4 in the considered rocks is not well known. From double layer theory, the exclusion of SO_4 in clayrocks is predicted to be higher because of its higher charge (Gimmi & Alt-Epping 2018). On the other hand, SO_4 has a larger tendency to form weak complexes, such as with alkaline earths, thus partly compensating the charge effect. Also, data for selenate in Opalinus Clay from Mont Terri suggest a similar diffusion regime as for Cl (Gimmi et al. 2014), even though no exact values for anion accessibility are available. A similar discrepancy between squeezing or advective displacement data on the one hand and aqueous extraction data on the other hand has been observed for other boreholes, such as Schlattingen-1 (Wersin et al. 2013), the BUL1-1 borehole (Mazurek et al. 2021), the TRU1-1 borehole (Aschwanden et al. 2021), The MAR1-1 borehole (Mäder et al. 2021), the BOZ1-1 borehole (Wersin et al. 2022a), the BOZ2-1 borehole (Gimmi et al. 2022) or the STA3-1 borehole (Aschwanden et al. 2022) as well as in the Mont Terri Rock Laboratory (Wersin et al. 2020). In the latter case, waters sampled from packed-off boreholes exhibited similar sulphate concentrations and SO_4/Cl ratios as waters squeezed from nearby drillcores. The reason for the higher sulphate levels derived from aqueous extraction compared to squeezing or advective displacement

data is not understood at this stage, despite recent systematic aqueous extraction studies on Opalinus Clay including Mont Terri and BUL1-1 samples (Debure & Gailhanou 2019, Aschwanden & Wersin 2020).

The porewaters from squeezed samples are close to saturation with respect to celestite (SI: -0.08 to +0.1), while the AD sample is slightly oversaturated (SI: +0.24). Celestite could be identified in some samples of the rock matrix of the Opalinus Clay and overlying formation at Mont Terri and Schlattingen-1 by a combined SEM/microprobe study (Jenni et al. 2019). Samples from advective displacement and squeezing are generally undersaturated with regard to gypsum, and gypsum is not thought to play a role in this issue.

The depth profile of SO_4/Cl ratios (Fig. 5.3-2) shows a similar trend as the SO_4 profile. The general discrepancy between AD and SQ data on the one hand and AqEx data on the other are clearly evident and not discussed further.

In the «Brauner Dogger» – top Staffelegg Formation sequence, the SO_4/Cl ratios of AD and SQ data are constant at a value of ~ 0.14, much higher than that of the overlying Malm groundwater ($\sim 5 \times 10^{-4}$). The underlying Keuper and Muschelkalk groundwaters display higher values of 0.5 and 1.7, respectively. Note that almost all SO_4/Cl ratios are generally higher than that of modern seawater (0.052) (dashed red line in Fig. 5.3-2 right).

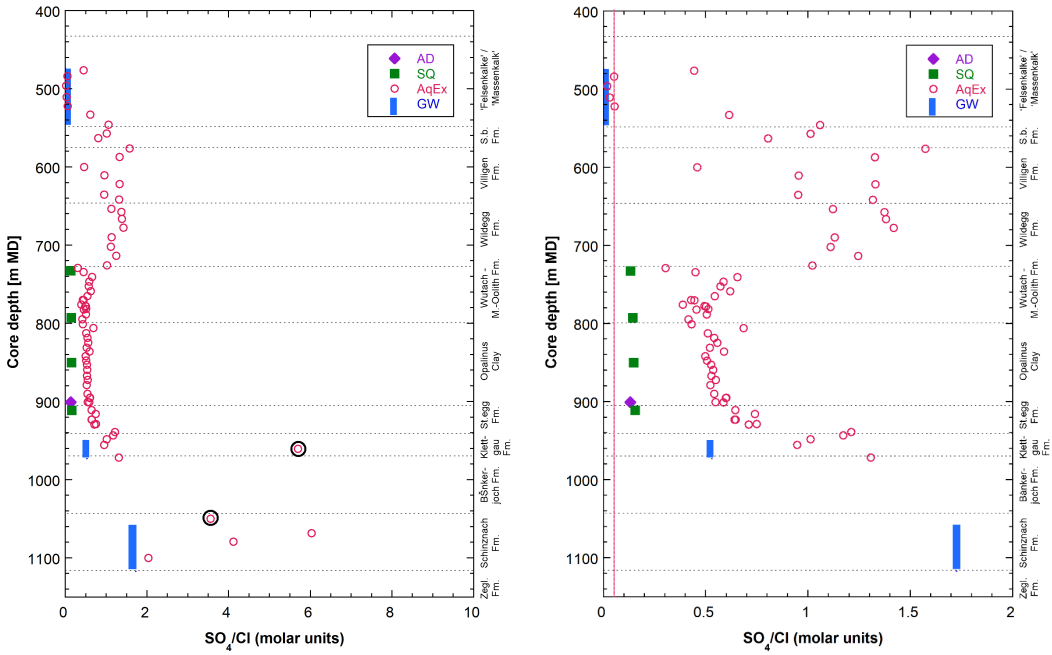

Fig. 5.3-2: Profiles showing molar SO_4/Cl ratios obtained from different methods at different scales

Dashed red line: seawater ratio. Dashed line: modern seawater ratio. Black encircled points: affected by drilling fluid contamination. Note that the groundwater data are not corrected for drilling fluid contamination.

5.4 Cation concentrations in porewaters

Paul Wersin, Eric Gaucher, Thomas Gimmi

Squeezing and advective displacement are the two methods that yield direct information on the cation concentrations in the porewater. Moreover, these can be estimated by simple modelling from the cation exchange data, notably from the cation occupancies on the exchanger. Aqueous extraction data, on the other hand, do not enable straightforward determination of porewater cations because of their modification via cation exchange and mineral reactions during the extraction process.

Both the squeezing and advective displacement method may potentially induce changes in porewater composition, thus also affecting cation composition and distribution. Data from previous boreholes and the Mont Terri rock laboratory, however, suggest that using not too high squeezing pressures and very early samples in the case of squeezing and advective displacement, respectively, experimental artefacts are relatively minor (e.g., Wersin et al. 2016, Wersin et al. 2020, 2022b), or at least some level of consistency between AD and SQ data is obtained (Mazurek et al. 2021, Aschwanden et al. 2021, Mäder et al. 2021, Wersin et al. 2022a, Gimmi et al. 2022). It should be pointed out that because of microbially-induced high nitrate levels in three of the four AD experiments only one AD experiment with an improved setup is considered here (Section 4.7).

Depth profiles for Na, Ca, Mg and K in porewater are illustrated in Fig. 5.4-1. The data from the AD sample is comparable with data from the nearby SQ sample. Na is the main cation, followed by Ca, Mg and K. The Na and Ca profiles are very similar as also illustrated by the constant molar Ca/Na ratio (~ 0.11) (Fig. 5.4-2). Both cations show a slight increase for the lowest samples in the Opalinus Clay/Staffelegg Formation. Mg shows a decreasing trend with depth across the «Brauner Dogger» and Opalinus Clay but, like Na and Ca, an increase in the lowermost sample in the Staffelegg Formation. K concentrations are constant along the sampled sequence. A flat profile is also indicated for Sr, but the AD sample shows a clearly higher concentration than the nearby squeezing sample (Sr data not shown).

Groundwater data from the Malm and Keuper aquifer are in line with porewater trends regarding Na and K. For divalent cations Ca and Mg and Sr, groundwater concentrations of these bounding aquifers are lower than those of the porewaters in-between.

The porewater composition in Dogger and Liassic is Na-Cl dominated with little variations as indicated from the available samples. According to the classification of Jäckli (1970)[13] the porewaters are of Na-(Ca)-Cl-(SO_4) type, showing slightly increased SO_4 levels in the lowest sample from the Staffelegg Formation. The relationships of cations and their consistency with exchangeable cation populations are further discussed in Section 5.6.

[13] Ions with > 50 eq.-% are underlined; ions with 20 – 50 eq.-% are not underlined, ions with 10 – 20 eq.-% are put in brackets.

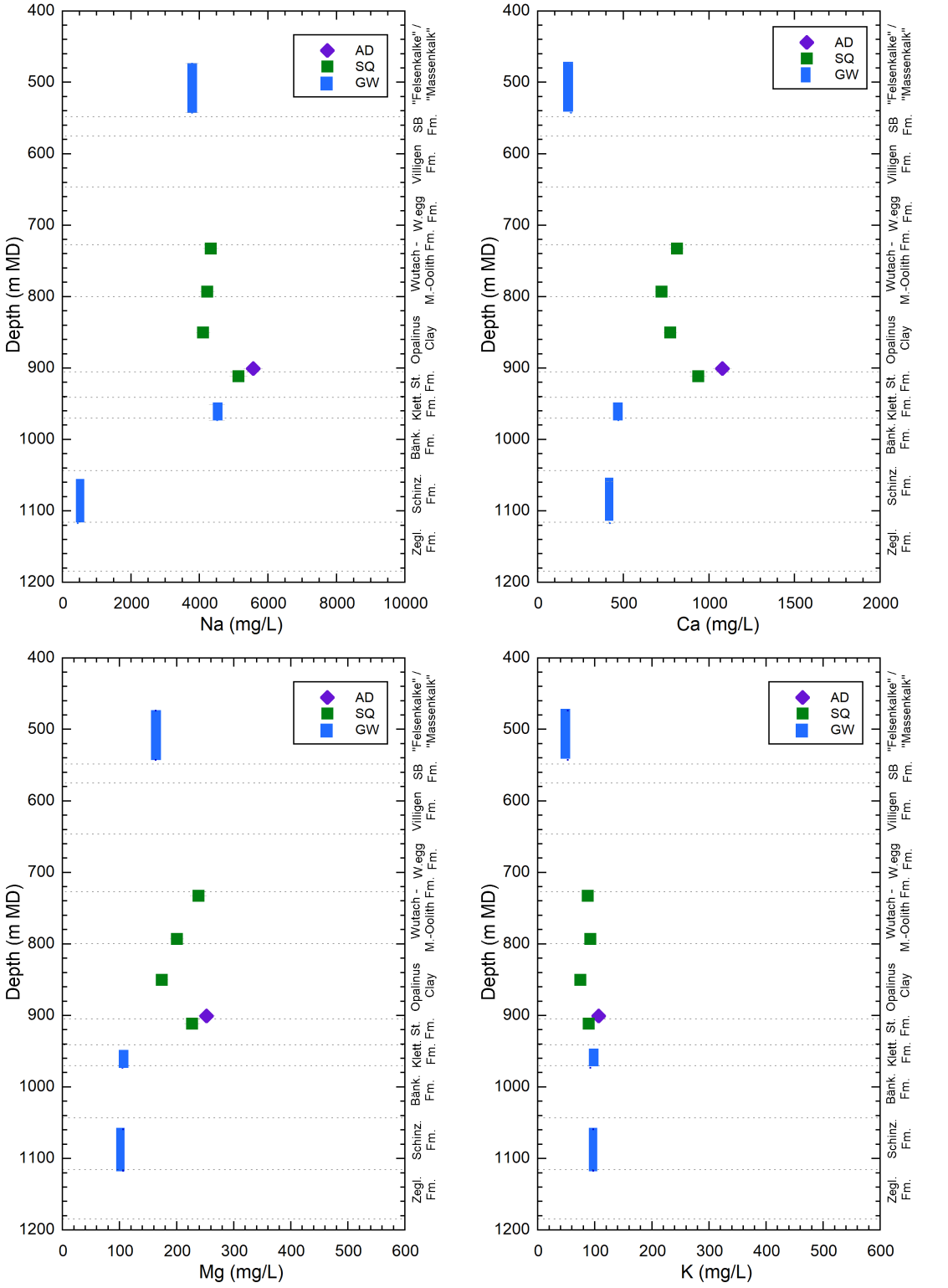

Fig. 5.4-1: Depth profiles for Na, Ca, Mg and K in porewater with data from squeezing, advective displacement and groundwater samples

Note that the groundwater data are not corrected for drilling fluid contamination.

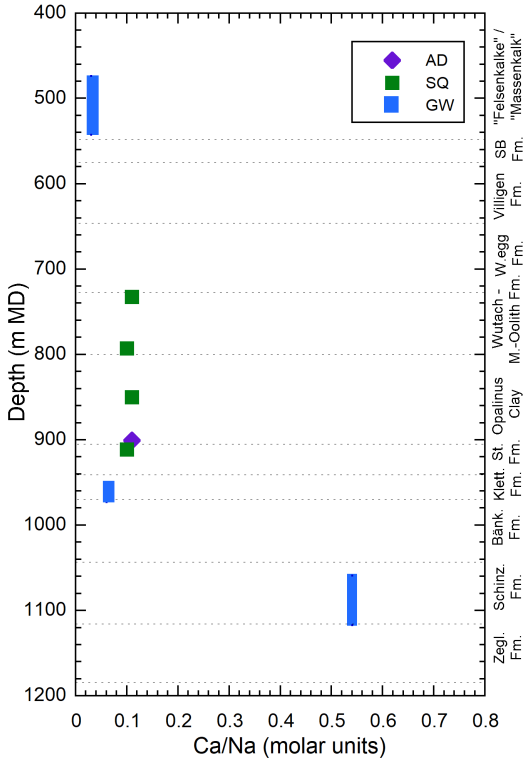

Fig. 5.4-2: Ca/Na ratio (molar units) for SQ and AD samples and groundwater
Note that the groundwater data are not corrected for drilling fluid contamination.

5.5 Dissolved carbon species (inorganic, organic), alkalinity, pH and pCO_2

Paul Wersin, Eric Gaucher, Thomas Gimmi

5.5.1 Dissolved inorganic carbon, alkalinity, pH and pCO_2

The two methods yielding information on the carbonate system of the porewater are squeezing and advective displacement. Notably, with these two methods, TIC, alkalinity (determined by titration) and pH can be measured. The alkalinity may include other compounds (e.g. low-molecular organic acids) than the carbonate species (HCO_3^-, CO_3^{2-}) and thus TIC is considered to be a more reliable parameter for constraining the carbonate system of the porewaters (Wersin et al. 2020).

Knowing pH and TIC, the (dissolved) carbonate system is entirely constrained (at constant temperature and pressure) according to Gibbs phase rule and the CO_2 partial pressure can be calculated. It should be noted that it is not straightforward to obtain reliable measurements on these parameters, which are prone to perturbations. For example, degassing of CO_2 during the squeezing process may alter pH and TIC parameters[14] (Tournassat et al. 2015, Wersin et al. 2020). In the case of advective displacement, an important perturbation related to microbial activity inducing high nitrate levels was observed in some experiments and for this reason these were discarded (Section 4.7.5). Equilibrium with calcite, omnipresent in the sedimentary sequence,

[14] But alkalinity is not affected by changes in CO_2 partial pressures as long as no dissolution/precipitation reaction occurs.

may help to further constraint on pH/pCO_2. Thus, from the measured Ca, TIC and pH, the saturation state with regard to calcite can be calculated, providing a plausibility test regarding the carbonate system. It is worth noting, however, that calculated saturation indices for calcite close to zero do not a priori confirm that measured parameters, such as pH and TIC, reflect in-situ conditions. In fact, perturbations during the experimental procedure might lead to a new equilibrium with calcite at different pH/pCO_2 conditions.

Tab. 5.5-1 shows the measured pH and TIC data together with the derived pCO_2 and saturation index for calcite from speciation calculations with PHREEQC. Note that for the AD sample, pH from in-line and lab (after sampling) measurements are considered here. Measured pH values for the AD sample are 7.1 and 7.5, whereas those for SQ are much higher, in the range of 8.3-8.6, as also illustrated in Fig. 5.5-1 (left, closed symbols). Conversely, TIC values are twice as high for the AD sample (~ 4 mM) compared to SQ (~ 2 mM). Regarding pCO_2, measured AD data indicate values of -2.0 to -2.3 bar in log units, whereas much lower values (-3.4 to -3.7) are derived for SQ data, as also illustrated in Fig. 5.5-1 (right, closed symbols). All samples are oversaturated with regard to calcite, but oversaturation is higher in SQ samples.

The pCO_2 data obtained for the AD sample lie within the expected values (about -2 to -3 log(bar); Wersin et al. 2020), but as noted above, the AD water is oversaturated with respect to calcite. The oversaturation is more pronounced when considering lab pH, suggesting that this value is less reliable than the in-line pH value, probably due to CO_2 out-gassing during sampling and storage.

Regarding SQ data, pCO_2 appear clearly too low, a feature that has been systematically observed and explained by CO_2 degassing occurring during the squeezing process (Tournassat et al. 2015, Wersin et al. 2020). This process in turn leads to high pH and an increase in HCO_3^- and thus CO_3^{2-} activity (leading to calcite oversaturation), schematically represented by the two reactions (where "-" represents degassing):

$$HCO_3^- \rightarrow CO_2(g)^- + OH^-$$

$$2\ HCO_3^- \rightarrow CO_2(g) + CO_3^{2-} + H_2O$$

Tab. 5.5-1: Measured pH and TIC as well as calculated pCO_2, $SI_{calcite}$ from AD and SQ experiments

Calculated pCO_2 and pH assuming calcite equilibrium for SQ data (see text).

		From measured parameters				Calculated	
Method	**Depth** [m]	**pH** (lab)	**TIC** [mmol/L]	**log pCO_2** [bar]	**SI calcite** [-]	**log pCO_2** [bar]	**pH** [-]
AD in-line pH	900.81	7.14	4.06	-1.96	0.43		
AD lab pH	900.81	7.54	4.06	-2.34	0.85		
SQ	732.74	8.61	2.13	-3.73	1.48	-1.98	6.99
SQ	792.72	8.38	1.94	-3.51	1.21	-2.15	7.09
SQ	850.29	8.33	2.05	-3.43	1.23	-2.08	7.04
SQ	911.28	8.55	1.89	-3.73	1.41	-2.07	7.02

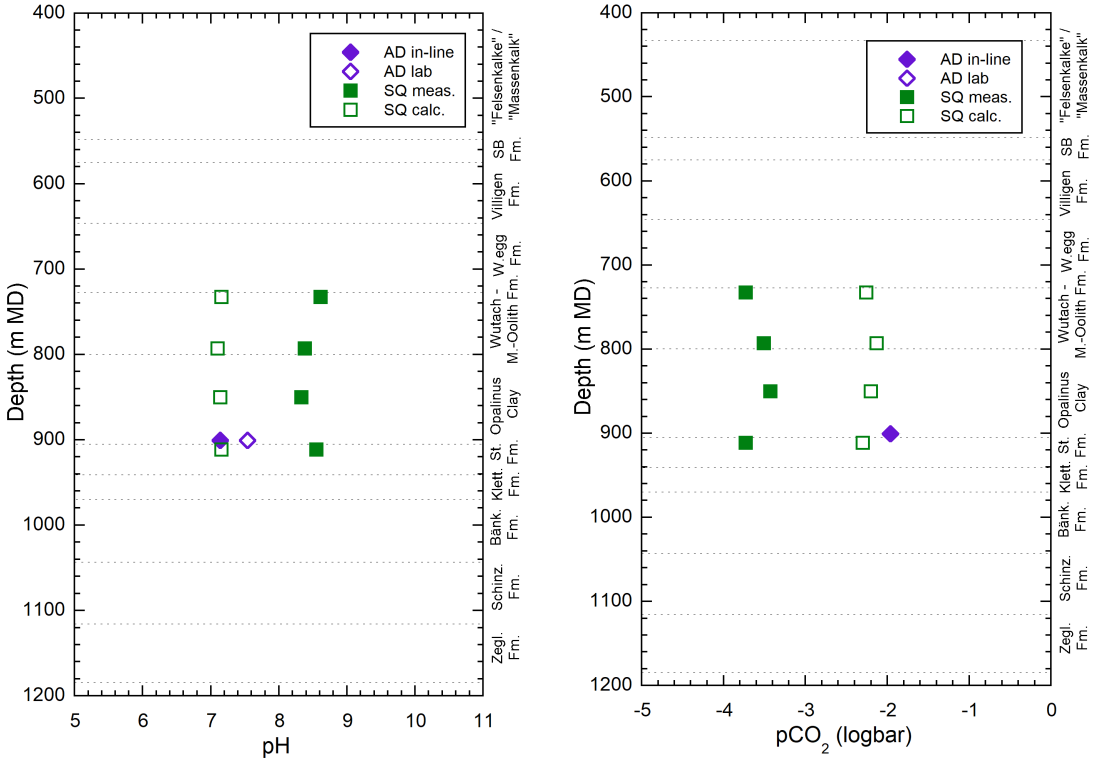

Fig. 5.5-1: pH (left) and pCO_2 values (right) from AD and SQ (see text)
Solid symbols: measured pH, pCO_2: calc. from measured pH and TIC
Open symbols: models based on calcite equilibrium (see text)

Under the assumption that SQ samples were affected by CO_2 degassing during the experimental procedure, CO_2 was added until calcite saturation was reached by using PHREEQC. This results in lower pH and higher pCO_2 values, depicted as open symbols in Fig. 5.5-1. These calculated pH/pCO_2 values seem to be in a reasonable range (pH 7.0 – 7.1, log pCO_2 -2.0 to -2.2) and more consistent with previous pH/pCO_2 data in Opalinus Clay (Wersin et al. 2020). This supports the hypothesis that the carbonate system was mainly affected by CO_2 degassing and much less by carbonate dissolution during the squeezing procedure.

In summary, the AD sample displays reasonable pH/pCO_2 data in spite of the oversaturation with regard to calcite. The oversaturation is likely related to a too high measured TIC, the reason of which, however, is not known at this stage. In the case of SQ, re-calculating pCO_2 and pH assuming calcite equilibrium seems to yield reasonable values.

5.5.2 Dissolved organic carbon

Information on dissolved organic carbon is available from advective displacement (AD) and squeezing (SQ) data as well as from aqueous extracts of AD cores (AqEx-AD):

- SQ: TOC
- AD: TOC, low molecular-weight organic acids (LMWOA)
- AqEx-AD: low molecular-weight organic acids (LMWOA)

Moreover, the (solid) organic carbon content (C_{org}) from the corresponding SQ and AD samples is available besides those from PW, RP and DI samples.

Before discussing the dissolved organic carbon data it is worth mentioning some general points: The organic carbon in the sedimentary rock consists of refractory kerogen and only a small fraction is extractable by solvents (< 1%) (Deniau et al. 2008). Comparison of the bulk geochemical features and thermal reactivity of kerogens from Mol (Boom Clay), Bure (Callovo–Oxfordian argillite) and Tournemire (Toarcian shales) underground research laboratories. The water-soluble organic carbon is even smaller, thus for example reaching a few mg C/L in the porewater of Opalinus Clay at Mont Terri or in the Callovo-Oxfordian Formation sampled from seepage boreholes (Courdouan Merz 2008; Courdouan et al. 2007a & b). Higher concentrations (several tens to hundreds of mg C/L) are generally measured in porewaters extracted from core samples, such as from squeezing or advective displacement (Wersin et al. 2013, Wersin et al. 2020). In case of the aqueous extracts, significant amounts of organic carbon are released to the solution. This indicates that a fraction of the "solid" carbon is mobilised during the extraction process. It also suggests the preferential release of loosely bound small organic molecules.

The TOC porewater concentrations from AD and SQ data are illustrated in Fig. 5.5-2 (left). These show consistent values of 150 – 230 mg/L. The increasing trend from the 'Brauner Dogger' into the Opalinus Clay is in qualitative agreement with the (total) organic C profile, which depicts higher C_{org} amounts in Opalinus Clay compared to the over and underlying formations (Fig. 5.5-2 right). The high C_{org} obtained for the SQ core from the Rietheim Member is not reflected in the corresponding TOC porewater concentration. Note that the AD sample contains a high concentration of acetate, making up 60% of the TOC. The other measured LMWOA are below detection for this sample. Note that no LMWOA data are available for squeezed samples.

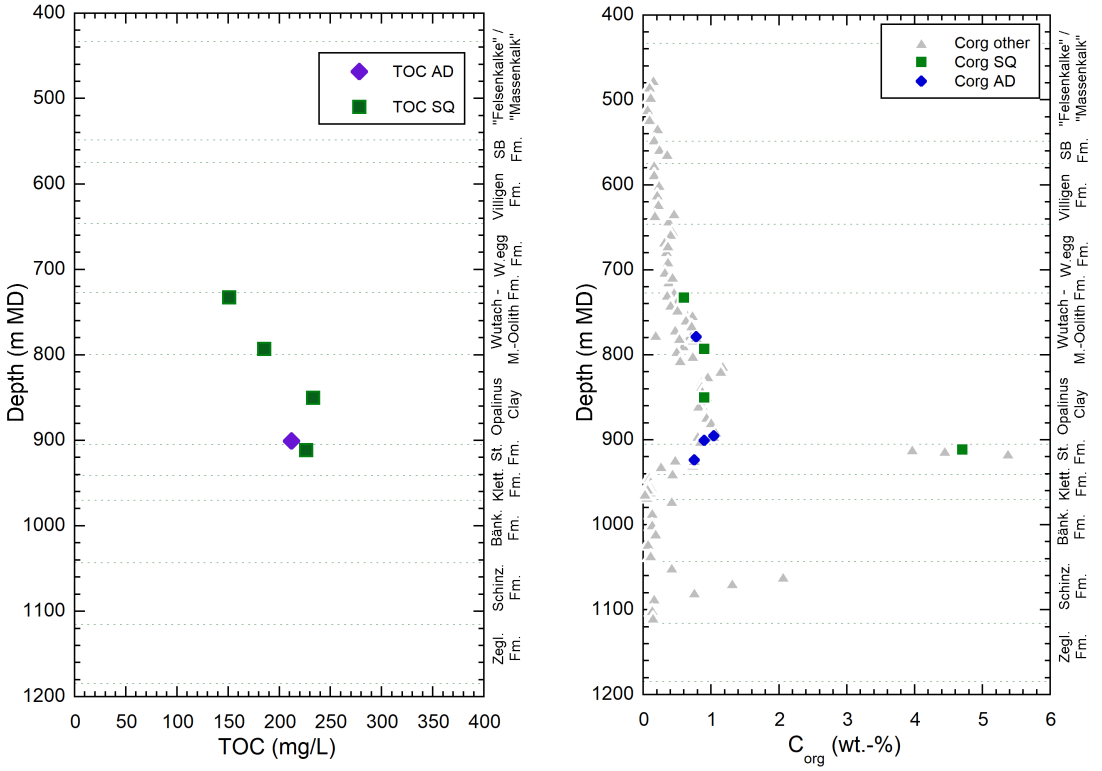

Fig. 5.5-2: TOC concentrations (left) from AD and SQ and organic carbon content in rock samples from AD, SQ and other cores (right)

5.6 Cation exchange capacity and exchangeable cation population

Paul Wersin

5.6.1 Corrected exchangeable cation data

As mentioned in Section 4.5, in order to obtain the exchangeable cation concentrations, the extracted cation data need to be corrected for cations dissolved in the porewater and the cations released from (potential) mineral dissolution. As shown from previous work (e.g., Hadi et al. 2019) and also indicated from speciation calculations presented in Section 4.5 (Tab. 4.5-4), carbonate mineral dissolution is minimised with the appropriate *S/L* ratio, extraction time and pH conditions. Such conditions were applied to the Uni Bern dataset.

Two correction methods for cations dissolved in the porewater were applied based on the concentrations of the main anions chloride and sulphate (Bradbury & Baeyens 1998, Hadi et al. 2019). The first correction method ($NaCl/Na_2SO_4$) attributes dissolved Cl and SO_4 from the Ni-extracts to Na and leaves the other cations unchanged. The second method ($NaCl/CaSO_4$) attributes Cl to Na and SO_4 to Ca, leaving the other cations unchanged. In both methods, the CEC is calculated from the sum of cations (SCAT) minus the concentrations (normalised to meq/kg_{dry_rock}) of Cl and SO_4. The corresponding data are shown in Tab. 5.6-1. The relative difference between the uncorrected and corrected sums of extracted cations (SCAT) is 6-8% for the three samples.

The values for the corrected SCAT are close to those of Ni consumption, albeit generally somewhat lower by -9% to -17%. The match between the two datasets supports the validity of the correction procedure for deriving the CEC based on the sum of cations.

Fig. 5.6-1 shows the CEC parameters as function of the clay-mineral content. It illustrates the expected increasing trend with clay-mineral content but note that this trend is based on only three samples. Further correlations are discussed in the following section where data from PSI are included.

The exchangeable cations are expressed as cation fractional occupancies (in equivalent fractions) in Tab. 5.6-1. Na and Ca are the main exchangeable cations, followed by Mg and K. The Sr occupancies are considerably lower (0.5 – 0.6% of the CEC).

Tab. 5.6-1: Sum of cations and cation occupancies obtained from Ni-en extraction after correction (Uni Bern data)

First line for each sample indicates fractional cation occupancies (in equivalent units) obtained by the $NaCl/Na_2SO_4$ correction method, the second line those obtained by the $NaCl/CaSO_4$ method.

Type	Depth [m]	Formation	Clay mineral content [wt.-%]	Ni-cons. [meq/kg$_{rock}$]	Sum CAT raw [meq/kg$_{rock}$]	Sum CAT corr. [meq/kg$_{rock}$]	Na [fr.oc.]	K [fr.oc.]	Ca [fr.oc.]	Mg [fr.oc.]	Sr [fr.oc.]
AD	744.88	Wedel-sandst.	23	137.2	121.1	113.8	0.47 0.49	0.05	0.35 0.32	0.12	0.005
AD	827.93	Opalinus Clay	50	131.8	108.5	100.1	0.52 0.55	0.05	0.31 0.28	0.11	0.005
AD	903.38	Staffelegg Fm.	33	86.9	72.7	65.3	0.49 0.53	0.06	0.33 0.29	0.11	0.006

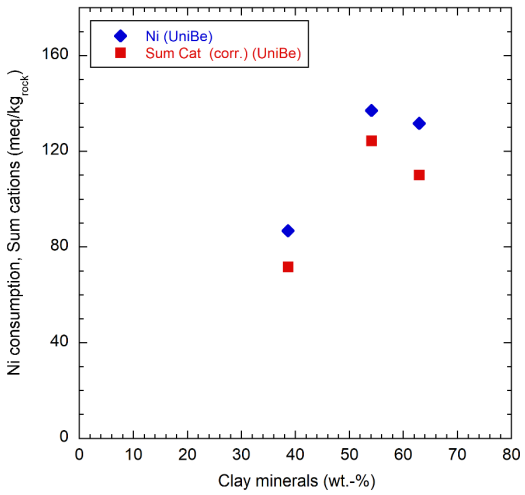

Fig. 5.6-1: Ni consumption and sum of (corr.) cations as a function of the clay-mineral content (data of Uni Bern)

5.6.2 Comparison with data from PSI

A dataset including 20 samples from the STA2-1 borehole was elaborated by PSI (Marques Fernandes & Baeyens, 2023). Samples originated from the top of the «Brauner Dogger» down to the Klettgau Formation. In a first step, the CEC at PSI was estimated for all samples from Ni consumption with the Ni-en extraction method. Subsequently, the main dataset was generated via CsCl extraction, from which the CEC and the exchanger population were obtained. The CEC was derived by subtracting the anion equivalents (Cl, SO_4, HCO_3/CO_3) from those of the cations (Na, Ca, Mg, K, NH_4, Sr). The exchanger population was derived by two correction methods: (1) attributing Cl and SO_4 to Na and TIC to Ca, and (2) attributing Cl to Na and SO_4 and TIC to Ca. Note that these two methods are analogue to the ones used for the Uni Bern samples presented above, except for the additional consideration of TIC. The contribution of the latter is less relevant

in the case of the Uni Bern data (see Tab. 4.5-4) because of much higher solid/liquid ratios and thus a lower contribution of mineral dissolution to the measured cation concentrations.

One dolostone sample with essentially zero clay-mineral content at 960.43 m was not included in the following analysis because data was deemed unreliable, leaving 19 PSI samples.

The conditions applied in the different extraction methods of PSI and Uni Bern are compared in Tab. 5.6-2. Important differences of the PSI methods relative to that of the Uni Bern are (i) the lower solid/liquid ratios, (ii) the smaller amount of solid mass and (iii) the more variable concentration of the index cation depending on the expected CEC.

Tab. 5.6-2: Extraction conditions applied by Uni Bern and PSI

	University of Bern	**PSI**	**PSI**
Extraction method	Ni-ethylenediamine	Ni-ethylenediamine	CsCl
Initial extract solution concentration	100 – 105 mmol/L	3.3 mmol/L	4 – 33 mmol/L
Solid/liquid ratio	~ 0.9 kg/L	~ 0.03 kg/L	~ 0.05 – 0.2 kg/L
Amount of solid used	~ 30 g	~ 1 g	~ 1 – 7 [a)] g
Extraction time	24 h	24 h	24 h
Final pH	8.4 – 8.5	8.3 –8.5	8.6 – 9.5
Sample disaggregation	Disintegration by hand to a few mm^3 pieces	Milled and passed through 1 mm sieve	Milled and passed through 1 mm sieve
Sample storage time prior to preparation	1 – 14 days	Several months [b)]	Several months [b)]
Extraction in glovebox	Yes	No	Yes

[a)] *S/L* ratio adjusted to obtain the expected index cation consumption-to-CEC ratio.

[b)] In glovebox

Cation exchange capacity and corrected sum of extracted cations

The Ni-en consumption and the corrected ΣCAT data (the latter from Ni-en extraction in the case of Uni Bern and CsCl extraction in the case of PSI) are shown in Fig. 5.6-2. From the comparison of these two datasets, the following findings can be derived:

- The CEC values obtained from Ni consumption exhibit consistent values for both datasets (to the degree the small number of samples permits a comparison; Fig.5.6-2 left). In this context, it should be noted that the two datasets were not performed on the same samples, thus CEC variations at similar depths due to mineralogical variation can be expected.
- The CEC values obtained from the corrected sum of cations also indicates consistency between Uni Bern and PSI datasets (Fig. 5.6-2 right).
- In the case of Uni Bern data, the corrected ΣCAT data are generally slightly lower than those of Ni consumption (by -17 to -9%), whereas the PSI data rather show the opposite (-8 to +30%).
- In general, the expected positive trend between clay-mineral content and CEC, both for Ni consumption and corrected sum of cations is illustrated (Fig. 5.6-3).
- The trend improves when illite content or smectite content is considered instead of clay-mineral content (not shown). In fact, the CEC is primarily induced by the structural negative

charge of these minerals, whereby the negative charge carried by smectite is about four times larger than that of illite. The correlation between the sum of illite and 4x smectite content and the CEC is superior to that exhibited by the clay-mineral content, as illustrated in Fig. 5.6-4. Note, however, that only for part of the samples data on illite and smectite contents are available.

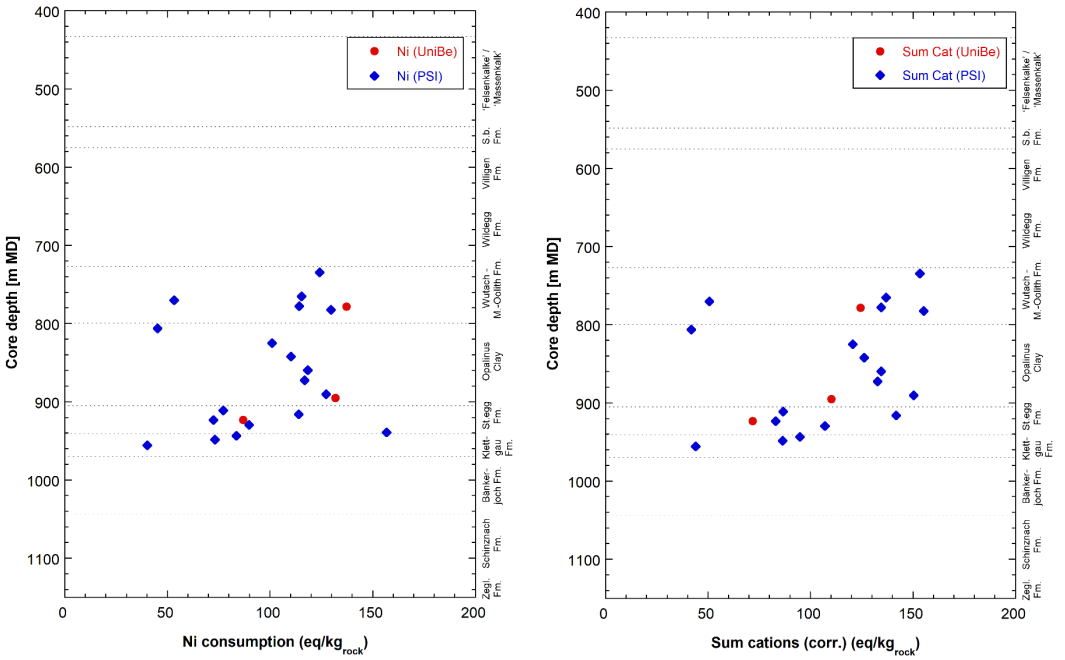

Fig. 5.6-2: Comparison of CEC data from Uni Bern and from PSI; Ni consumption data (left) and corrected sum of cations data (right)

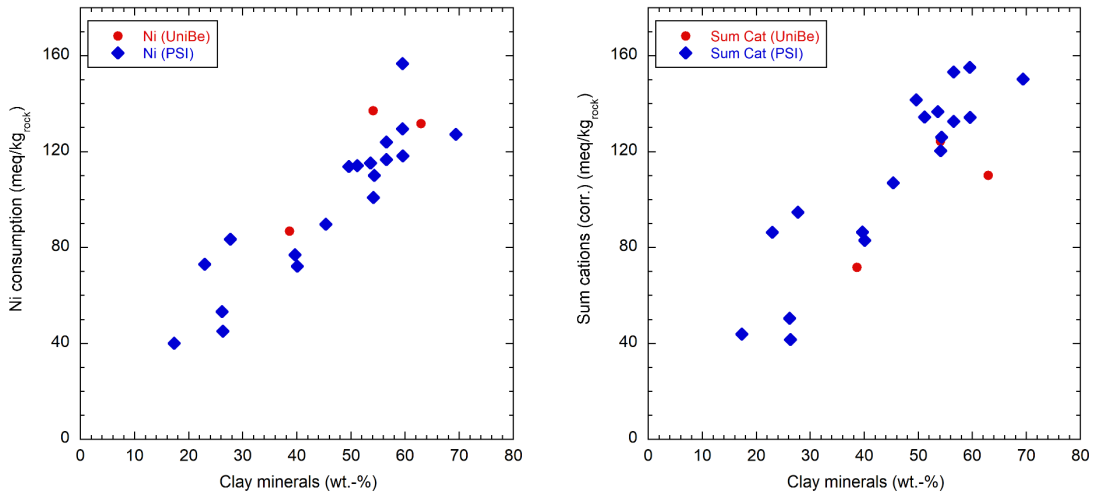

Fig. 5.6-3: CEC data as function of the clay-mineral content; left: Ni consumption data; right: Corrected sum of cations

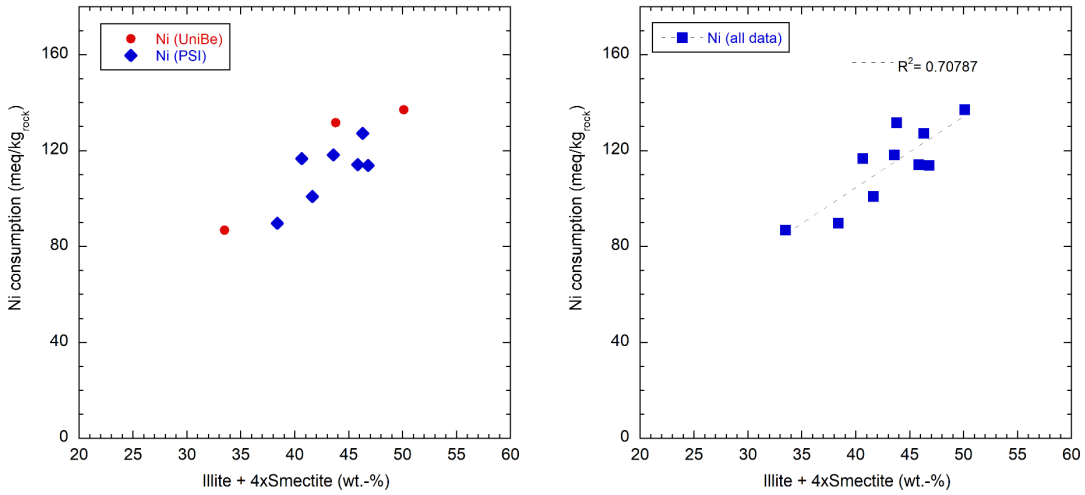

Fig. 5.6-4: Ni consumption as function of the sum of illite end-member content and 4× smectite end-member content

Note that illite and smectite contents were not measured for all samples.

Exchangeable cation occupancies

The advantage of comparing fractional cation occupancies rather than the extracted cation concentrations is that they are normalised to the sum of cations (as proxy for the CEC) and do not directly depend on the clay-mineral content of the sample.

Fig. 5.6-5 shows the Na and Ca occupancies derived from the two correction methods. Note that in method 1 Cl and SO_4 are attributed to Na (and TIC to Ca for PSI data), whereas in method 2, SO_4 and, in the case of PSI data, also TIC is attributed to Ca. Thus, the Na fraction is minimised in method 1 and maximised in method 2, while the opposite is true for Ca. Besides the two datasets, the calculated occupancies from the SQ and AD porewater data are shown. The calculations were done with the PHREEQC simulator and the well-established single-site cation exchange model for Opalinus Clay (Pearson et al. 2011; Wersin et al. 2016).

Comparison of "measured" Uni Bern and PSI exchangeable cation data illustrates more or less consistent trends for all measured exchangeable cations, except for K, as illustrated in Figs. 5.6-5 to 5.6-7. The "back calculated" exchangeable AD/SQ data generally support the overall trends. For K, PSI data display systematically higher occupancies, which is related to the extraction by CsCl mobilising a larger pool of K present in the illite fraction. The same mismatch was already observed in previous boreholes (Mazurek et al. 2021, Aschwanden et al. 2021 & 2022, Mäder et al. 2021, Wersin et al. 2022, Gimmi et al. 2022). The higher K occupancies of the PSI data can explain the somewhat lower corresponding Na occupancies relative to the Uni Bern and the "back calculated" exchangeable AD/SQ data. This is illustrated by the consistent behaviour of the ΣNa+K for all three datasets (Fig. 5.6-5 right). Monovalent cation data suggest constant ratios in the upper part of the sampled profile down to the footwall of the Opalinus Clay. Further down an increase with depth is indicated.

There are two outliers in the PSI data at 777.85 m and 806.13 m depth when considering method 2 for the correction of Na (but not by method 1). Conversely, sample 911.03 m displays seemingly too low values when the correction method 1 is applied. The reasons for these variations are not clear at this stage.

The Ca occupancies also suggest a flat profile in the upper part, followed by a decrease from the Staffelegg Formation into the Klettgau Formation. On the other hand, Mg occupancies display a slightly decreasing trend with depth in the upper part of the sequence, followed by a marked increase with depth (Fig. 5.6-6). Consistency between the "measured" and "back-calculated" data-sets is improved considering Ca occupancies corrected by method 2 relative to method 1.

Ca/Na and Ca/(Na+K) profiles suggest a constant trend in the «Brauner Dogger» and the Opalinus Clay, but the scatter reflected by the PSI data is considerable. At the footwall of the latter formation, these ratios exhibit a marked decrease down to the bottom of the sampled sequence.

The Mg/Ca ratios show constant values across most of the profile but rise sharply in the Klettgau Formation. The Sr/Ca ratios suggest a similar trend but show more scatter.

Exchangeable ammonium (only measured by PSI) displays low fractional occupancies of 0.014 – 0.020.

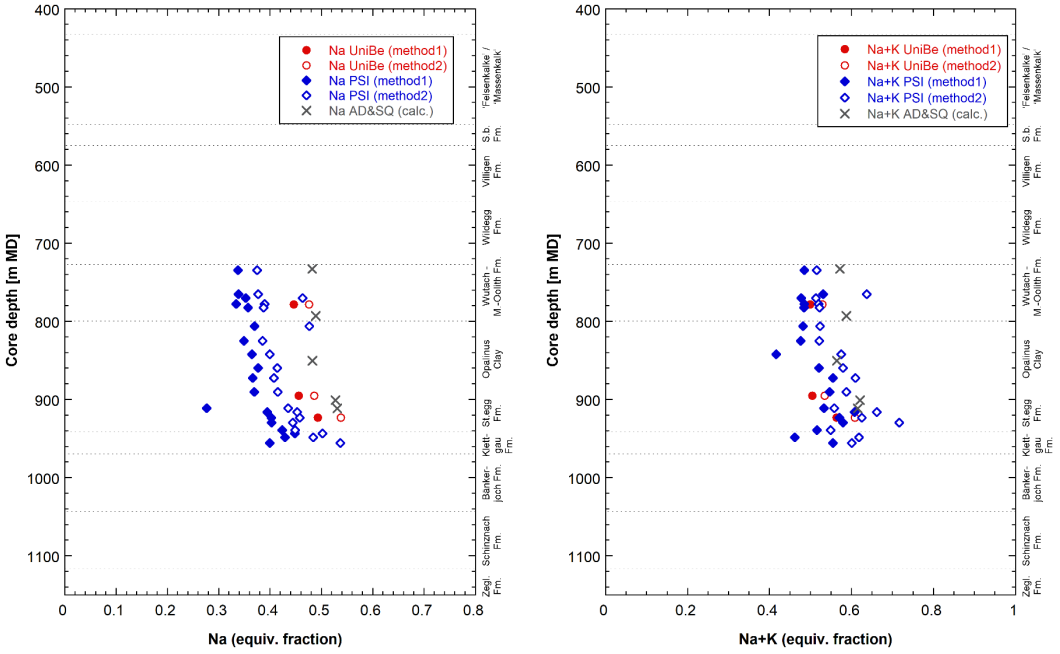

Fig. 5.6-5: Na (left) and Na+K (right) occupancies according to Uni Bern and PSI data and re-calculated from AD/SQ data

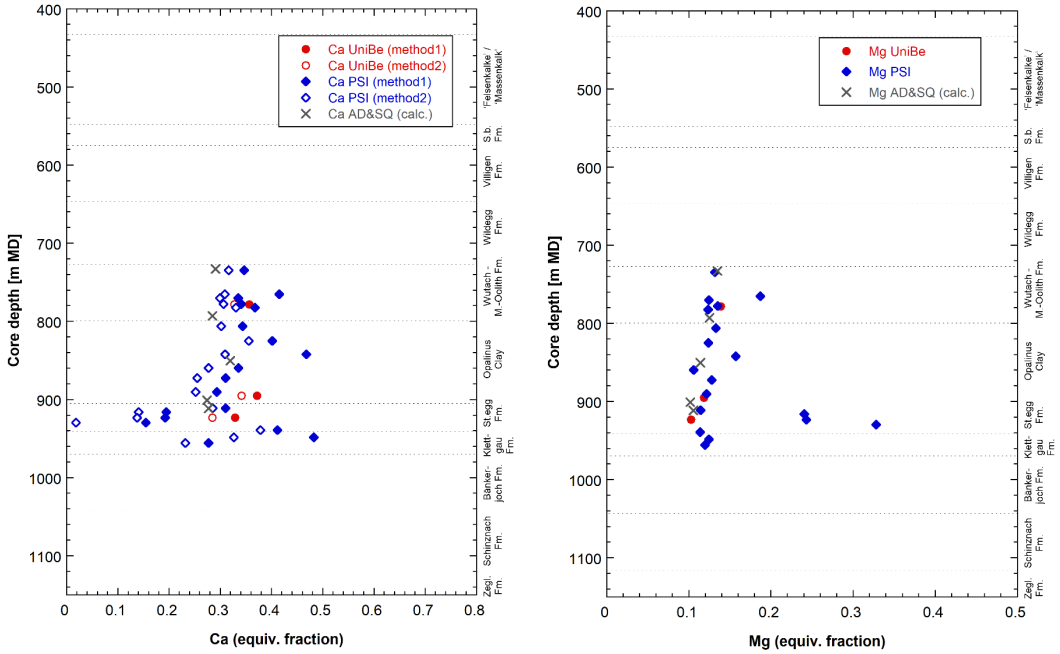

Fig. 5.6-6: Ca (left) and Mg (right) occupancies according to Uni Bern and PSI data and re-calculated from AD/SQ data

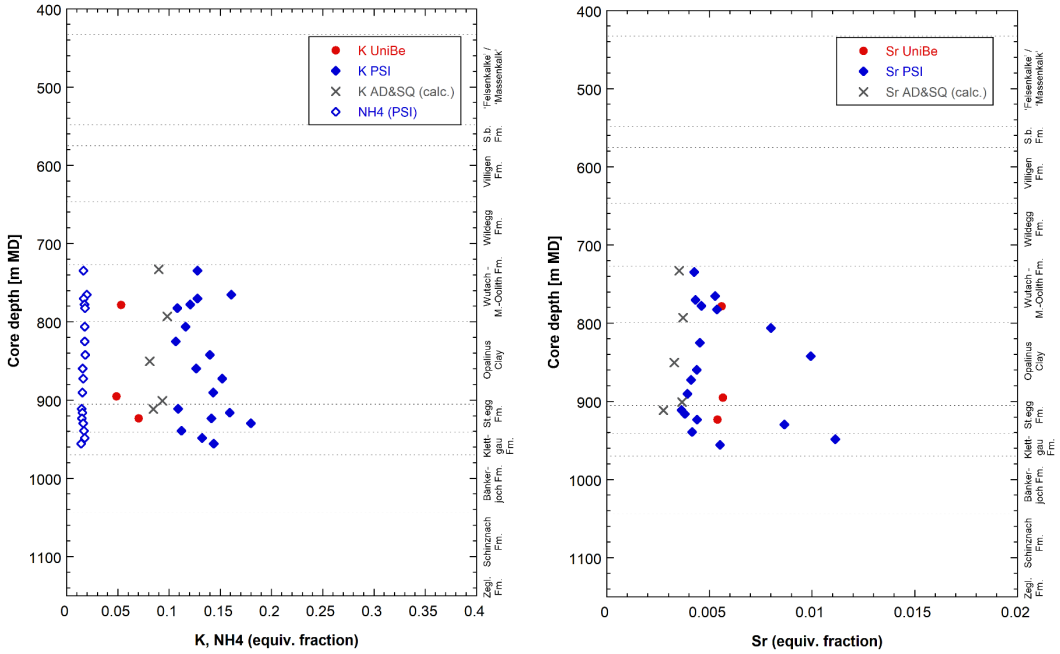

Fig. 5.6-7: K, NH_4 (left) and Sr occupancies (right) according to Uni Bern and PSI data and calculated from AD/SQ data

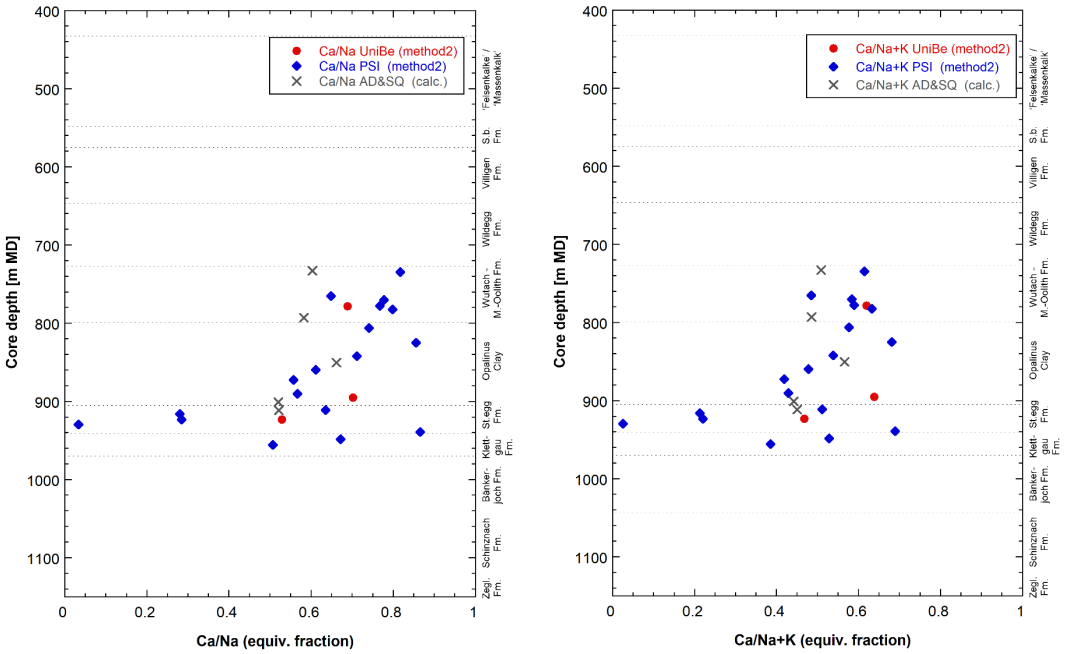

Fig. 5.6-8: Ca/Na ratios (left) and (Ca+Mg/Na) (right) according to Uni Bern and PSI data and re-calculated from AD/SQ data

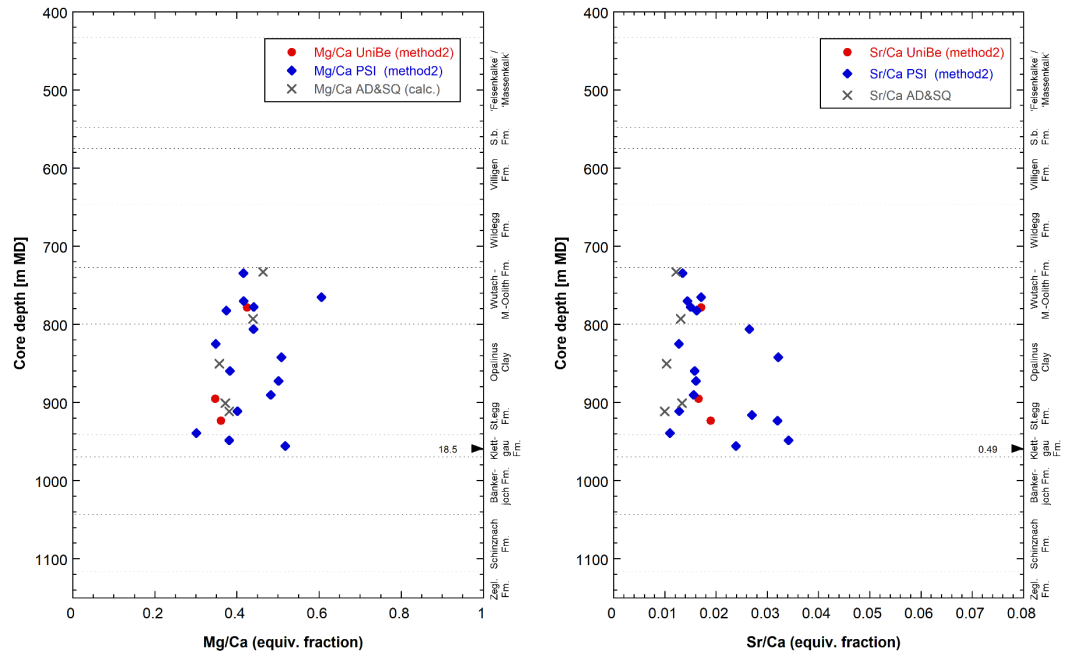

Fig. 5.6-9: Mg/Ca ratios (left) and Sr/Ca ratios (right) according to Uni Bern and PSI data and re-calculated from AD/SQ data

Extracted anions

The amounts of extracted Cl and SO_4 are illustrated in Fig. 5.6-10. Note that for PSI data, Cl data from aqueous extraction are shown, because CsCl was used for extraction of exchangeable cations. These Cl data compare well with those analysed in the Ni-en extracts of Uni Bern. Both these datasets agree with the (larger) AqEx dataset of Uni Bern which is also illustrated in Fig. 5.6-10 (left). Regarding SO_4, also broad agreement between the datasets is depicted in Fig. 5.6-10 (right), but data from Ni-en extracts (Uni Bern) display slightly lower levels than the two other datasets.

The Cl concentrations (in eq/kg_{rock}) show increasing levels with depth in the Malm units. This trend continues within the «Brauner Dogger» but with a large scatter. Rather constant levels are noted in the Opalinus Clay, below a clear decrease with depth is evident. The Cl profile is discussed in more detail in Sections 4.4.4 and 5.2.

The extracted SO_4 levels are generally in the same range (on an equivalent basis) as the Cl levels. They show a rather similar profile as Cl in most part of the profile but show more scatter. From the Staffelegg Formation downwards, an increase with depth is suggested.

Total inorganic carbon (TIC) measured in the PSI extracts is 4 – 9 $mmol/kg_{dry\ rock}$. This is higher than expected from Uni Bern extracts. TIC was not measured in the latter but calculated to be below 1 $mmol/kg_{dry\ rock}$ based on the assumption of calcite equilibrium (Tab. 4.5-4). The higher TIC in the PSI extracts is explained by the lower *S/L* ratio, which induces a higher proportion of dissolved carbonate from dissolving carbonate minerals.

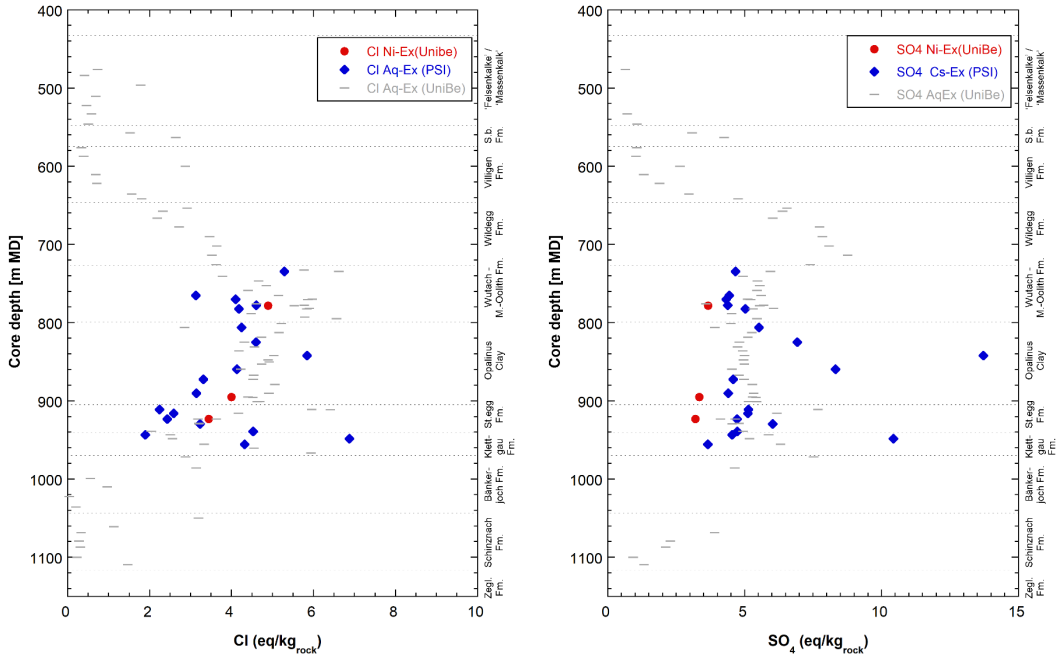

Fig. 5.6-10: Extracted Cl (left) and SO_4 (right) according to Uni Bern and PSI data

5.7 Stable water isotopes

Lukas Aschwanden & Thomas Gimmi

5.7.1 Comparison between different methods for the determination of stable porewater isotope compositions

The porewater oxygen and hydrogen isotope compositions were determined using three different methods including isotope diffusive-exchange (Section 4.8), advective displacement (Section 4.7) and high-pressure squeezing (Section 4.6). Data of the three techniques are available for the section 730 – 930 m where clay-rich rocks dominate and all methods can be applied. For the clay-poor rocks of the Malm and the Muschelkalk only data from isotope diffusive-exchange experiments are available. For the advective displacement technique, the average of the first two displaced solution aliquots is considered as being most representative for the in situ porewater. For the squeezed water, the one obtained at the lowest squeezing pressure (200 MPa or 300 MPa) is considered as being most representative for the in situ porewater.

All the porewater isotope data, together with those for the groundwater samples from the aquifers in the Malm, Keuper and the Muschelkalk (*cf.* Section 2.3), are shown in Fig. 5.7-1 as a function of depth. For isotope data from isotope-diffusive exchange experiments, the error bars reflect the propagated experimental and analytical uncertainty. For isotope data from advective displacement and high-pressure squeezing experiments, only the analytical error is illustrated. Note that for advective displacement three experiments were affected by extensive microbially-induced nitrate production, which biased also the water isotopes. The data of these experiments are not reliable (*cf.* Section 4.7) and thus, they are not shown in the following graphs. In a fourth experiment with an improved set-up, nitrate production was successfully suppressed. The porewater isotope data obtained from this experiment is reliable and is shown in the following graphs. For δ^2H, there is good agreement (within the uncertainty) between the data derived from the advective displacement experiment and those from neighbouring samples investigated by the isotope diffusive-exchange technique. However, for $\delta^{18}O$ the advective displacement experiment shows a slightly depleted value. A similar behaviour is also observed for high-pressure squeezing for which both isotope tracers show slightly depleted values compared to the data derived from diffusive-exchange experiments, however, somewhat more pronounced for $\delta^{18}O$ and less for δ^2H. The reason for this is not known at this stage.

5.7.2 Comparison with groundwater data and depth profiles

In the «Felsenkalke» + «Massenkalk» where the Malm groundwater was sampled the scatter and the uncertainties of the porewater isotope data are large. This is mainly owing to experimental difficulties associated with these lithologies (*cf.* Section 4.8). Thus, the agreement between the isotope composition of porewater and groundwater is poor: Within the packed-off interval only 2 and 3 – for $\delta^{18}O$ and δ^2H, respectively – of totally 5 investigated samples agree (within uncertainty) with the isotopic composition of the groundwater. In contrast, for the Keuper aquifer the agreement between groundwater and adjacent porewater is reasonably good. Between the two aquifers, the porewater isotope profiles show well-defined, bell-shaped curves, however, with somewhat different shapes for $\delta^{18}O$ and δ^2H. The former increasingly becomes more negative across the interval Wildegg Formation – Staffelegg Formation approaching a local minimum in the water-conducting zone of the Klettgau Formation, whereas the latter remains at constant values down to the base of the Opalinus Clay before sharply evolving towards the same local minimum in the water-conducting zone of the Klettgau Formation. This different behaviour likely reflects inherited trends from the initial porewater isotope profiles (i.e., before the isotope signatures in the confining aquifers changed to present-day values) with rather constant δ^2H but

decreasing $\delta^{18}O$ values across the Jurassic sequence. Interestingly, similar differences, partly less pronounced, were observed in data from other TBO boreholes (Mazurek et al. 2021, Aschwanden et al. 2021 & 2022, Mäder et al. 2021, Wersin et al. 2022, Gimmi et al. 2022) and also in the older data from Benken (Gimmi & Waber 2004; Gimmi et al. 2007). Note that none of the isotope tracers shows any irregularities or excursions in the deformed interval (883.78 – 890.19 m) of the Opalinus Clay (*cf.* Section 2.2) and neither do the anionic tracers Cl and Br (*cf.* Section 5.2). Thus, based on the tracer profiles there are no indications for recent advective flow in this interval.

From the local minimum in the Klettgau Formation $\delta^{18}O$ and $\delta^{2}H$ values of the porewater evolve towards a local maximum in the Bänkerjoch Formation at around 1022 m depth where the trend reverses. In the top of the Schinznach Formation both tracers sharply decrease towards most negative values in the water-conducting zone of the Formation only a few tens of meters below. The $\delta^{2}H$ values of groundwater from the Muschelkalk aquifer agree well (i.e. within the propagated uncertainty) with those of the porewater obtained from samples in the packed-off interval (except for the lowermost samples), but porewater $\delta^{18}O$ values are slightly enriched. The Muschelkalk groundwater appears to represent minima of $\delta^{18}O$ and $\delta^{2}H$ and the adjacent porewaters in the top of the Schinznach Formation and the Bänkerjoch Formation indicate remarkably steep gradients towards heavier values upwards. Note that the sample in the top of the Schinznach Formation (STA2-1049.83-PW) is contaminated with drilling fluid (*cf.* Section 4.4). The drilling fluid used in this section of the borehole shows $\delta^{18}O$ and $\delta^{2}H$ values of -7.15 ‰ VSMOW and -48.8‰ VSMOW, respectively (Lorenz, 2023), thus, slightly depleted in ^{18}O and ^{2}H compared to the calculated porewater of the contaminated sample in the top of the Schinznach Formation but distinctly enriched compared to the groundwater in the Muschelkalk and its porewater in the packed-off interval. It follows that – unlike as in previous boreholes – the remarkable steep gradients of porewater isotope composition towards the water-conducting zone in the Muschelkalk are mainly located in the Stamberg Member in the top of the Schinznach Formation and less pronounced across the overlying Bänkerjoch Formation. Such steep gradients indicate either that the change in the isotope signal of the groundwater towards present-day values is geologically young (as also indicated by the residence time of the groundwater of a few kyrs; REF), and/or the diffusion coefficients are very low in this section of the borehole. The latter is, however, considered less plausible, as the Schinznach Formation – especially its dolomitic top (Stamberg Member) – generally shows rather high porosity (*cf.* Section 4.3) and likely permeability.

It can be concluded that the continuous, bell-shaped profiles of porewater isotope composition between the Malm aquifer and the Keuper aquifer, as well as between the Keuper aquifer and the Muschelkalk aquifer, indicate that the evolution of the porewater isotope signatures in these intervals are clearly dominated by diffusive exchange with the confining water-conducting zones.

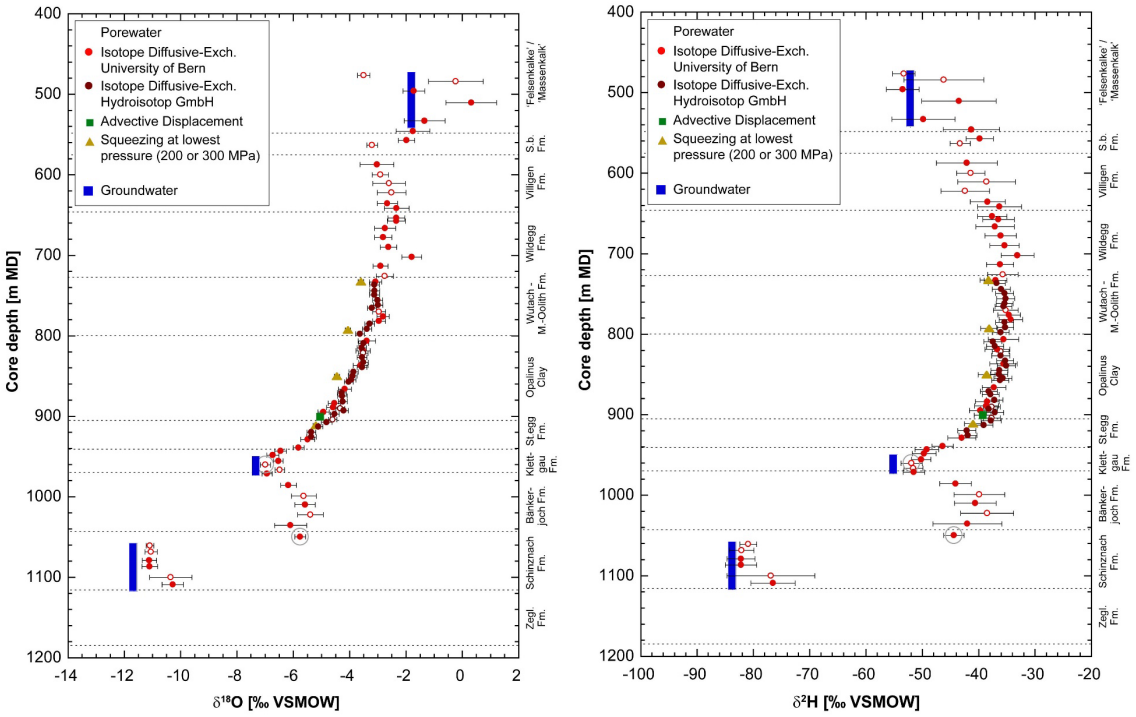

Fig. 5.7-1: Depth trends of $\delta^{18}O$ and $\delta^{2}H$ in groundwater and porewater derived by all techniques

Bars indicate propagated analytical errors (diffusive exchange) or simple analytical errors (squeezing, advective displacement). Groundwater data are from Lorenz (2023). Open symbols refer to porewater isotope values which are less reliable owing to experimental artefacts (*cf.* Section 4.8). The sample with a grey circle shows signs of contamination by drilling fluid (*cf.* Section 4.4).

5.7.3 $\delta^{2}H$ versus $\delta^{18}O$ and comparison with Global Meteoric Water Line

Fig. 5.7-2 illustrates all data in a $\delta^{18}O$ vs. $\delta^{2}H$ diagram. Such diagrams provide information on e.g., climatic conditions during recharge, on water-rock interactions, and/or on mixing of different water components.

Porewater isotope signatures in the Malm plot far to the right of the Global Meteoric Water Line (GMWL), like porewaters in the underlying «Brauner Dogger», however, the latter being enriched in ^{2}H. From the «Brauner Dogger» to the base of the Opalinus Clay the porewater isotope composition continuously evolves towards values less enriched in ^{18}O, as shown by the solid red arrow 1 in Fig. 5.7-2, and approaching the GMWL, indicating a meteoric component in the latter porewaters. The pronounced deviation of the porewater $\delta^{18}O$ – $\delta^{2}H$ signatures with respect to the Global Meteoric Water Line at the top of the section in the Malm and the «Brauner Dogger» indicates long residence times of these porewaters, with values affected by exchange with groundwater in the Malm aquifer, and possibly by water-rock interactions. Across the Staffelegg Formation down to the water-conducting zone in the Klettgau Formation the porewater isotope composition evolves along a trajectory parallel to the GMWL towards more depleted signatures but still enriched relative to modern recharge (solid red arrow 2 in Fig. 5.7-2). Note that modern recharge does not only refer to recent or post-glacial recharge but also recharge under climatic conditions similar to recent conditions (e.g. during an interglacial period in the Quaternary). The deviation of the Keuper groundwater from the GMWL is likely due to mixing with isotopically

different water components and/or water-rock interactions. The Bänkerjoch Formation shows somewhat less negative porewater $\delta^{18}O$ and $\delta^{2}H$ values also located slightly to the right of the GMWL (solid red arrow 3 in Fig. 5.7-2). In the top of the Schinznach Formation the porewater isotope composition sharply evolves to distinctly more negative values in the water-conducting zone of the Muschelkalk located on the GMWL and slightly depleted relative to modern recharge (solid red arrow 4 in Fig. 5.7-2), indicative for infiltration under colder-climate conditions.

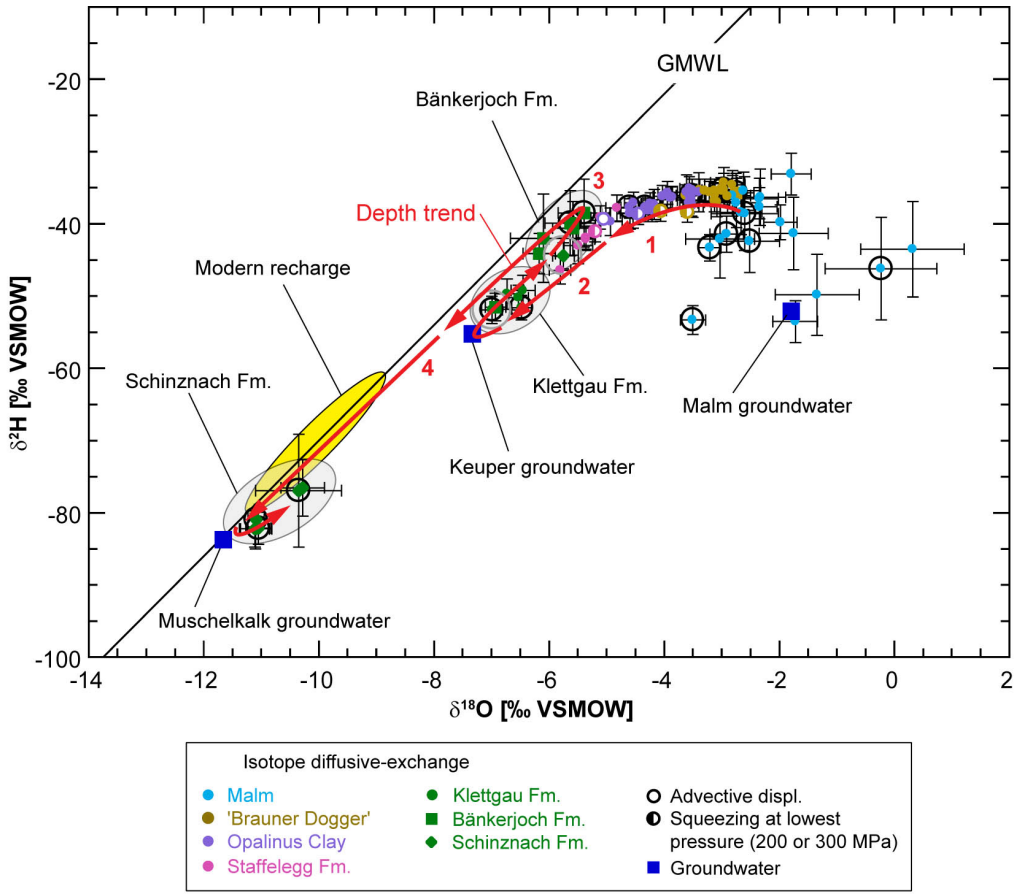

Fig. 5.7-2: $\delta^{2}H$ vs. $\delta^{18}O$ for groundwater and porewater derived by all techniques

Bars indicate propagated analytical errors (diffusive exchange) or simple analytical errors (squeezing, advective displacement). Groundwater data are from Lorenz (2023). GMWL = Global Meteoric Water Line (defined as $\delta^{2}H = 8\ \delta^{18}O + 10$; Craig 1961). Range of modern recharge from Kullin & Schmassmann (1991). Samples in circles are less reliable owing to experimental artefacts (black circles; *cf.* Section 4.8) and/or possible contamination by drilling fluid (grey circles; *cf.* Section 4.4). See text for details on the numbering of red arrows (depth trend).

6 Final remarks and main conclusions

RWI team

High-quality cores were extracted from the STA2-1 borehole between the top of the «Felsenkalke» + «Massenkalk» and the top of the Zeglingen Formation. Groundwater was sampled from the «Felsenkalke» + «Massenkalk» (Malm aquifer), the Klettgau Formation (Keuper aquifer) and the Schinznach Formation (Muschelkalk aquifer). The drill core samples enabled to acquire high quality mineralogical, petrophysical and porewater data using a well-established procedure. Drilling operations proceeded without major problems down to a maximum depth of 1288 m (Weitenau Formation, Permian). No significant quantities of drilling mud were lost during the drilling of STA2-1.

In general terms, the mineralogical composition is similar to that in the neighbouring boreholes. However, systematic trends of quartz, calcite or clay-mineral contents with depth as observed in borehole STA3-1 and even more so in BUL1-1 are less well developed, except in parts of the «Brauner Dogger». This is most probably related to the depositional environment. The composition of the clay fraction is similar to that in the other boreholes, including the typical and sharp upward increase of the illite/kaolinite ratio at the base of the Opalinus Clay. Within the Opalinus Clay, this ratio systematically decreases upwards, more so than in the neighbouring boreholes.

The depth trends of mineral contents (if present) correlate well with those of petrophysical parameters and can be even clearer (e.g. water content). Water content and porosity correlate positively with clay-mineral content, even though the correlation is far from perfect. This indicates that apart from clay-mineral content, other rock characteristics have an influence on porosity, which are probably related to the depositional environment and diagenesis.

Nitrogen adsorption data were obtained for 17 samples from the upper and lower confining units. The samples are lithologically very different, but the general trends match with those observed for the larger data set including the Bülach-1-1 and the STA-3-1 boreholes. There is a broadly positive correlation of the external specific surface area (BET, N_2 adsorption) with clay-mineral contents (or with illite and smectite end-member contents) and a weaker correlation with water contents. Average radii of external pores (assuming negligible interlayer water) tend to decrease with increasing water content or with clay-mineral content, but with larger differences notably for limestone samples with low water content or low clay-mineral content.

Drilling fluid contamination was identified in three aqueous extraction samples from the Klettgau and Schinznach Formation. It was noticed that aqueous extraction on dried rock yielded substantially lower Br and in the case of the Rietheim Member sample lower Cl concentrations compared to extracts conducted on wet rock. This might be related to complexation with transformed organic matter during the heating to 105 °C, but further investigations would be needed to test this hypothesis.

Between the Malm aquifer and the Keuper aquifer, as well as between the Keuper aquifer and the Muschelkalk aquifer the depth profiles of porewater $\delta^{18}O$ and $\delta^{2}H$ values are well defined, continuous and bell-shaped indicating that the porewater isotope signatures in these intervals are dominated by diffusive exchange with the confining water-conducting zones. Note that neither chemical nor isotope tracers show any irregularities or excursions in the deformed interval (883.78 – 890.19 m) of the Opalinus Clay. Porewaters in the Malm and the «Brauner Dogger» are enriched in ^{18}O and ^{2}H and plot far to the right of the Global Meteoric Water Line (GMWL) indicating long residence times. From the «Brauner Dogger» to the base of the Opalinus Clay the porewater isotope composition continuously evolves towards values less enriched in ^{18}O and approaching the GMWL, indicating a meteoric component in the latter porewaters. Somewhat different shapes of the profiles between the Malm and the Keuper are noted for $\delta^{18}O$ and $\delta^{2}H$, with a more or less steady decrease of the $\delta^{18}O$ values but a slight increase of the $\delta^{2}H$ values in

the upper part and a decrease only in the lower parts. The different trends of $\delta^{18}O$ and $\delta^{2}H$ values in this section of the borehole may be inherited from an earlier evolution (i.e., before the isotope signatures in the confining aquifers changed to present-day values) with rather constant $\delta^{2}H$ but $\delta^{18}O$ values decreasing with depth across the low-permeability formations of the Dogger. Across the Staffelegg Formation down to the water-conducting zone in the Klettgau Formation the porewater isotope composition evolves along a trajectory parallel to the GMWL towards more depleted signatures but still enriched relative to modern recharge. The Bänkerjoch Formation shows somewhat less negative porewater $\delta^{18}O$ and $\delta^{2}H$ values. Porewaters in the top of the Schinznach Formation indicate remarkably steep gradients towards general minima of $\delta^{18}O$ and $\delta^{2}H$ in the water-conducting zone of the Muschelkalk. The steep gradients of porewater isotope composition indicate that the Muschelkalk groundwater is geologically young (unless diffusion coefficients are very low). This is consistent with its position on the GWML, however, it is slightly depleted relative to modern recharge, indicative for infiltration under colder-climate conditions.

Anion-accessible porosities could be derived from squeezed (SQ) and advectively displaced (AD) porewaters from the interval «Brauner Dogger» – Staffelegg Formation. These yielded Cl-accessible porosity fractions (f_{Cl}) with a mean value of ~ 0.48 ± 0.06. This is in a comparable range as derived for previous boreholes from the TBO program. The same linear relationship of f_{Cl} with clay-mineral content as for the two other boreholes from the Nördlich Lägern siting region (BUL1-1, STA3-1) was used to derive Cl and Br concentrations per accessible porewater from aqueous extraction.

Broadly consistent Cl and Br profiles are revealed from squeezing, advective displacement and re-calculated aqueous extraction data. Using pycnometer porosities instead of water-loss porosities when scaling the aqueous extract data to concentrations per bulk porewater or accessible porewater leads to a similar profile but with slightly more scatter. The Cl profile exhibits a curved shape between the main aquifers in the Malm and Muschelkalk with a very weak excursion at the level of the Keuper aquifer, indicating the highest Cl concentrations of 7 – 8 g/L in the upper Opalinus Clay and «Brauner Dogger». The Br profile is comparable with that of Cl but shows a flatter shape in the Malm units and a stronger bend towards the Keuper aquifer. Overall, analogous profiles were derived for $\delta^{18}O$ and $\delta^{2}H$, which show clear excursions towards the Keuper aquifer.

The depth profile of the Br/Cl ratio reveals consistency between AqEx and SQ and AD data. The Br/Cl profile shows less scatter than that of Cl or Br due to the fact that no assumptions on anion accessibility need to be made and the uncertainty regarding re-calculation to the rock porosity cancels out. Constant Br/Cl ratios close to modern seawater are found in the upper part of the profile and decrease in the Staffelegg formation towards the Keuper aquifer. Below, the ratios exhibit larger scatter, suggesting a positive excursion in the Bänkerjoch Formation, followed by a strong decrease towards the Muschelkalk aquifer.

The sulphate profile obtained from SQ and AD, which covers the sequence Variansmergel Formation – Staffelegg Formation, indicates constant concentrations across the «Brauner Dogger» and Opalinus Clay and a slight rise in the Staffelegg Formation. Conversely, AqEx data yield systematically higher and more variable concentrations, as has been observed in the previous boreholes and the Mont Terri Rock Laboratory. SO_4/Cl ratios deduced from SQ and AD exhibit a similar shape as the SO_4 profile with values of ~0.14 (molar units) in the «Brauner Dogger» and Opalinus Clay.

Cation data representative of the porewater could be obtained from SQ and AD experiments. These generally indicate flat profiles for the major cations Na and Ca across the «Brauner Dogger» – Opalinus Clay sequence, followed by an increase in the Staffelegg Formation. Conversely, Mg shows a decreasing trend with depth, but also an increase in the Staffelegg Formation.

The cation exchange capacity (CEC) correlates positively with the clay-mineral content. An even better correlation can be deduced with the sum of illite and smectite end-member mineral contents, the main carriers of the CEC. The main exchangeable cations are Na and Ca, followed by Mg and K. The exchanger composition (cation occupancies) is approximately constant across the «Brauner Dogger» – Opalinus Clay but indicates a clear shift towards enrichment of Na and Mg at the expense of Ca in the Staffelegg-Klettgau sequence. The exchanger composition determined from extraction methods exhibits the same trends as the "back-calculated" exchanger composition obtained from modelling of the SQ and AD porewater data.

The porewaters in the Opalinus Clay and bounding formations display moderate salinities and ionic strengths with Cl concentrations of about 6 – 8.5 g/L over large parts of the profile. These chloride levels are somewhat lower than the ones of BUL1-1 from the same siting area (~ 12 g/L). The porewaters are of Na-(Ca)-Cl-(SO_4) type (according to the nomenclature of Jäckli 1970) in the interval sampled for SQ and AD (Variansmergel Formation – Staffelegg Formation).

The pH/pCO_2 conditions deduced for the SQ and AD data indicate a reasonable range based on current knowledge, with values ~ 7 and ~ -2 log(bar) for pH and pCO_2, respectively. For SQ data, however, a correction procedure by geochemical modelling was necessary to account for CO_2 degassing that had occurred during the squeezing process.

SQ and AD data yield TOC concentrations of about 200 mg C/L in the Opalinus Clay and Staffelegg Formation and slightly lower ones in the «Brauner Dogger». These concentrations are not thought to fully reflect in-situ porewater conditions, but rather the easily mobilisable fraction from the solid organic matter.

7 References

Allison, J.D., Brown, D.S. & Novo-Gradac, K.J. (1991): MINTEQA2/PRODEFA2, a geochemical assessment model for environmental systems: Version 3.0 user's manual. Environmental Research Laboratory, Office of Research and Development, U.S. Environmental Protection Agency, 106 p.

Aschwanden, L. & Wersin, P. (2020): Experimental study of sulphate in the Opalinus Clay: Results from extraction tests. Nagra Arbeitsbericht NAB 20-17.

Aschwanden, L., Camesi, L., Gimmi, T., Jenni, A., Kiczka, M., Mäder, U., Mazurek, M., Rufer, D., Waber, H.N., Wersin, P., Zwahlen, C. & Traber, D. (2021). TBO Trüllikon-1-1: Data report Dossier VIII. Rock properties, porewater characterisation and natural tracer profiles. Nagra Arbeitsbericht NAB 20-09.

Aschwanden, L., Camesi, L., Gaucher, E., Gimmi, T., Jenni, A., Kiczka, M., Mäder, U., Mazurek, M., Rufer, D., Waber, H.N., Wersin, P., Zwahlen, C. & Traber, D. (2022). TBO Stadel-3-1: Data report Dossier VIII. Rock properties, porewater characterisation and natural tracer profiles. Nagra Arbeitsbericht NAB 22-01.

Bradbury, M.H. & Baeyens, B. (1998): A physicochemical characterisation and geochemical modelling approach for determining porewater chemistries in argillaceous rocks. Geochim. Cosmochim. Acta 62, 783-795.

Courdouan Merz, A. (2008): Nature and reacivity of dissolved organic matter in clay formations evaluated for the storage of radioactive waste. PhD thesis. ETH Zurich.

Courdouan, A., Christl, I., Meylan, S., Wersin, P. & Kretzschmar, R. (2007a): Characterization of dissolved organic matter in anoxic rock extracts and in situ pore water of the Opalinus Clay. Applied Geochemistry 22, 2926-2939.

Courdouan, A., Christl, I., Meylan, S., Wersin, P. & Kretzschmar, R. (2007b): Isolation and characterization of dissolved organic matter from the Callovo-Oxfordian formation. Applied Geochemistry 22, 1537-1548.

Craig, H. (1961). Isotopic variations in meteoric waters. Science 133, 1702–1703.

Debure, M. & Gailhanou, H. (2019): GD experiment: Experimental study of sulphate in Opalinus Clay. Unpubl. Mont Terri Technical Note. Mont Terri Project, Switzerland.

Deniau, I., Devol-Brown, I., Derenne, S., Behar, F. & Largeau, C. (2008). Comparison of the bulk geochemical features and thermal reactivity of kerogens from Mol (Boom Clay), Bure (Callovo–Oxfordian argillite) and tournemire (Toarcian Shales) underground research laboratories. Science of the Total environment 389, 475-485.

Gaucher, E., Aschwanden, L., Camesi, L., Gimmi, T., Jenni, A., Kiczka, M., Mäder, U., Mazurek, M., Rufer, D., Waber, H.N., Wersin, P., Zwahlen, C. & Traber, D. (in prep.): TBO Bachs-1-1: Data report Dossier VIII. Rock properties, porewater characterisation and natural tracer profiles. Nagra Arbeitsbericht.

Gimmi, T. & Waber, H.N. (2004): Modelling of tracer profiles in porewater of argillaceous rock in the Benken borehole: Stable water isotopes, chloride and chlorine isotopes. Nagra Technical Report NTB 04-05.

Gimmi, T. & Alt-Epping, P. (2018): Simulating Donnan equilibria based on the Nernst-Planck equation. Geochim. Cosmochim. Acta 232, 1-13.

Gimmi, T., Waber, H. N., Gautschi, A., & Rübel, A. (2007). Stable water isotopes in pore water of Jurassic argillaceous rocks as tracers for solute transport over large spatial and temporal scales. Water Resources Research, 43.

Gimmi, T., Leupin, O.X., Eikenberg, J., Glaus, M., Van Loon, L.R., Waber, H.N., Wersin, P., Wang, H.A.O., Grolimund, D., Borca, C.N., Dewonck, S., Wittebroodt, C. (2014): Anisotropic diffusion at the field scale in a four-year multi-tracer diffusion and retention experiment - I: Insights from the experimental data. Geochimica et Cosmochimica Acta, 2014, 125, 373-393.

Gimmi, T., Aschwanden, L., Camesi, L., Gaucher, E.C., Jenni, A., Kiczka, M., Mäder, U., Mazurek, M., Rufer, D., Waber, H.N., Wersin, P., Zwahlen, C. & Traber, D. (2022). TBO Bözberg-2-1: Data report Dossier VIII. Rock properties, porewater characterisation and natural tracer profiles. Nagra Arbeitsbericht NAB 21-22.

Hadi, J., Wersin, P., Mazurek, M., Waber, H.N., Marques Fernandes, M., Baeyens, B., Honty, M., De Craen, M., Frederickx, L., Dohrmann, R. & Fernandez, A.M. (2019): Intercomparison of CEC method within the GD project. Mont Terri Technical Report TR 2017-06. Mont Terri Project, Switzerland.

Jäckli, H. (1970): Kriterien zur Klassifikation von Grundwasservorkommen. Eclogae geol. Helv. 63/2, 389-434.

Jenni, A., Aschwanden, L., Lanari, P., de Haller, A. & Wersin, P. (2019): Spectroscopic investigation of sulphur-containing minerals in Opalinus Clay. Nagra Arbeitsbericht NAB 19-23.

Kullin, M. & Schmassmann, H. (1991): Isotopic composition of modern recharge. *In:* Pearson F.J., Balderer, W., Loosli, H.H., Lehmann, B.E., Matter, A., Peters, Tj., Schmassmann, H.-J. & Gautschi, A. (1991): Applied Isotope Hydrogeology – A Case Study in Northern Switzerland. Studies in Environmental Science 43, Elsevier, Amsterdam, 65-89.

Lorenz, G.D. (*in prep.*): Borehole STA2-1 (Stadel-2-1): Fluid sampling and analytical hydrochemical data report. Unpubl. Nagra Interner Bericht.

Mäder, U. (2018): Advective displacement method for the characterisation of porewater chemistry and transport properties in claystone. Geofluids 2018, Article ID 8198762, doi.org/10.1155/2018/8198762

Mäder, U. & Waber, H.N. (2017): Results of advective displacement / multi-component transport experiments from claystone samples of the Schlattingen borehole. Nagra Arbeitsbericht NAB 17-16.

Mäder, U., Aschwanden, L., Camesi, L., Gimmi, T., Jenni, A., Kiczka, M., Mazurek, M., Rufer, D., Waber, H.N., Wersin, P., Zwahlen, C. & Traber, D. (2021). TBO Marthalen-1-1: Data report Dossier VIII. Rock properties, porewater characterisation and natural tracer profiles. Nagra Arbeitsbericht NAB 21-20.

Marques Fernandes, M. & Baeyens. B. (*in prep.*): Sorption measurements of Cs, Ni, Eu, Th and U on rock samples of Opalinus Clay and confining geological units from deep boreholes at the potential siting regions for a deep geological repository for radioactive waste in Switzerland: Jura Ost, Nördlich Lägern and Zürich Nordost. Nagra Technical Report NTB 22-02.

Mazurek, M. (2017): Gesteinsparameter-Datenbank Nordschweiz – Version 2. Nagra Arbeitsbericht NAB 17-56.

Mazurek, M. & Aschwanden, L. (2020): Multi-scale petrographic and structural characterisation of the Opalinus Clay. Nagra Arbeitsbericht NAB 19-44.

Mazurek, M., Oyama, T., Wersin, P. & Alt-Epping, P. (2015): Pore-water squeezing from indurated shales. Chemical Geology 400, 106-121.

Mazurek, M., Aschwanden, L., Camesi, L., Gimmi, T., Jenni, A., Kiczka, M., Mäder, U., Rufer, D., Waber, H.N., Wanner, P., Wersin, P. & Traber, D. (2021): TBO Bülach-1-1: Data Report Dossier VIII. Rock properties, porewater characterisation and natural tracer profiles. Nagra Arbeitsbericht NAB 20-08.

Naef, H., Büchi, M., Bläsi, H.R., Deplazes, G. & Gysi, M. (2019): Lithology Manual – Lithological description of drill cores and cuttings in Northern Switzerland. Nagra Arbeitsbericht NAB 19-11.

Nagra (2008): Vorschlag geologischer Standortgebiete für das SMA- und das HAA-Lager. Geologische Grundlagen. Nagra Technischer Bericht NTB 08-04.

Nagra (2014): SGT Etappe 2: Vorschlag weiter zu untersuchender geologischer Standortgebiete mit zugehörigen Standortarealen für die Oberflächenanlage. Geologische Grundlagen. Dossier II: Sedimentologische und tektonische Verhältnisse. Nagra Technischer Bericht NTB 14-02.

Parkhurst, D.L. & Appelo, C.A.J. (2013): Description of input and examples for PHREEQC Version 3: A computer program for speciation, batch-reaction, one-dimensional transport, and inverse geochemical calculations. No. 6-A43. US Geological Survey.

Pearson, F.J. (1999): What is the porosity of a mudrock? In *Muds and Mudstones: Physical and Fluid Flow Properties*; Aplin, A.C.; Fleet A.J.; Macquaker, J.H.S. (Eds.); Geological Society: London; Special Publications 158, pp 9-21.

Pearson, F.J., Arcos, D., Bath, A., Boisson, J.Y., Fernandez, A.M., Gäbler, H.E., Gaucher, E., Gautschi, A., Griffault, L., Hernan, P. & Waber, H.N. (2003): Mont Terri project – geochemistry of water in the Opalinus Clay formation at the Mont Terri rock laboratory. Federal Office for Water and Geology Rep. 5, Bern, Switzerland.

Pearson, F.J., Tournassat, C. & Gaucher, E.C. (2011): Biogeochemical processes in a clay formation in situ experiment: Part E – Equilibrium controls on chemistry of pore water from the Opalinus Clay, Mont Terri underground research laboratory, Switzerland. Applied Geochemistry 26, 990-1008.

Rufer, D. & Stockhecke, M. (2019). Field Manual: Drill Core Sampling for Analytical Purposes. Nagra Arbeitsbericht NAB 19-13, Nagra, Switzerland.

Rufer, D. & Mazurek, M. (2018): Pore-water extraction and characterization: Benchmarking of the squeezing and adapted isotope diffusive exchange methods. NWMO Technical Report NWMO-TR-2018-14. Nuclear Waste Management Organization, Toronto, Canada.

Thoenen, T., Hummel, W., Berner, U. & Curti, E. (2014): The PSI/Nagra Chemical Thermodynamic Database 12/07. PSI Bericht Nr. 14-04, Paul Scherrer Institut, Villigen, Switzerland.

Thommes, M., Kaneko, K., Neimark, A.V., Olivier, J.P., Rodriguez-Reinoso, F., Rouquerol, J., Sing, K.S. (2015). Physisorption of gases, with special reference to the evaluation of surface area and pore size distribution (IUPAC Technical Report). Pure and Applied Chemistry 87, 1051–1069.

Tournassat, C., Vinsot, A., Gaucher, E.C. & Altmann, S. (2015): Chemical conditions in clay-rocks. *In:* Tournassat, C., Steefel, C.I., Bourg, I.C. & Berrgaya, F. (eds.): Natural and engineered clay barriers. Developments in Clay Science 6, Chapter 3, 71-100. Elsevier.

Van Loon, L.R. & Glaus, M. A. (in prep.): Diffusion measurements of HTO, 36Cl- and 22Na+ on rock samples of Opalinus Clay and confining geological units from deep boreholes at the potential siting regions for a deep geological repository for radioactive waste in Switzerland: Jura Ost, Nördlich Lägern and Zürich Nordost. Nagra Working Report NAB 23-26.

Waber, H.N. (ed.) (2020): SGT-E3 deep drilling campaign (TBO): Experiment procedures and analytical methods at RWI, University of Bern (Version 1.0, April 2020). Nagra Arbeitsbericht NAB 20-13.

Wersin, P., Mazurek, M., Waber, H.N., Mäder, U.K., Gimmi, T., Rufer, D. & de Haller, A. (2013): Rock and porewater characterisation on drillcores from the Schlattingen borehole. Nagra Arbeitsbericht NAB 12-54.

Wersin, P., Mazurek, M., Mäder, U.K., Gimmi, T., Rufer, D., Lerouge, C. & Traber, D. (2016): Constraining porewater chemistry in a 250 m thick argillaceous rock sequence. Chemical Geology 434, 43-61.

Wersin, P., Pekala, M., Mazurek, M., Gimmi, T., Mäder, U.K., Jenni, A., Rufer, D. & Aschwanden, L. (2020): Porewater chemistry of Opalinus Clay: Methods, modelling & buffering capacity. Nagra Technical Report NTB 18-01.

Wersin, P., Aschwanden, L., Camesi, L., Gaucher, E.C., Gimmi, T., Jenni, A., Kiczka, M., Mäder, U., Mazurek, M., Rufer, D., Waber, H.N., Zwahlen, C. & Traber, D. (2022a). TBO Bözberg-1-1: Data report Dossier VIII. Rock properties, porewater characterisation and natural tracer profiles. Nagra Arbeitsbericht NAB 21-21.

Wersin, P., Mazurek, M. & Gimmi, T. (2022b). Porewater chemistry of Opalinus Clay revisited: Findings from 25 years of data collection at the Mont Terri Rock Laboratory. Applied Geochemistry, 138.